

**AFRL-VA-WP-TR-2001-3052**

**AERODYNAMIC ANALYSIS FOR THE  
DESIGN ENVIRONMENT (AANDE)  
VOLUME 1: THEORETICAL AND APPLICATIONS  
STUDY MANUAL**



**M. H. LOVE  
D. D. EGLE**

**LOCKHEED MARTIN TACTICAL AIRCRAFT SYSTEMS  
AIRFRAME AND INSTALLATION  
P.O. BOX 748, MAIL ZONE 2824  
FORT WORTH, TX 76101-0748**

**NOVEMBER 1999**

**FINAL REPORT FOR PERIOD OF 30 SEPTEMBER 1995 – 30 JUNE 1998**

**Approved for public release; distribution unlimited.**

**20011130 007**

**AIR VEHICLES DIRECTORATE  
AIR FORCE RESEARCH LABORATORY  
AIR FORCE MATERIEL COMMAND  
WRIGHT-PATTERSON AIR FORCE BASE, OH 45433-7542**

## NOTICE

USING GOVERNMENT DRAWINGS, SPECIFICATIONS, OR OTHER DATA INCLUDED IN THIS DOCUMENT FOR ANY PURPOSE OTHER THAN GOVERNMENT PROCUREMENT DOES NOT IN ANY WAY OBLIGATE THE UNITED STATES GOVERNMENT. THE FACT THAT THE GOVERNMENT FORMULATED OR SUPPLIED THE DRAWINGS, SPECIFICATIONS, OR OTHER DATA DOES NOT LICENSE THE HOLDER OR ANY OTHER PERSON OR CORPORATION; OR CONVEY ANY RIGHTS OR PERMISSION TO MANUFACTURE, USE, OR SELL ANY PATENTED INVENTION THAT MAY BE RELATED TO THEM.

THIS REPORT IS RELEASEABLE TO THE NATIONAL TECHNICAL INFORMATION SERVICE (NTIS). AT NTIS, IT WILL BE AVAILABLE TO THE GENERAL PUBLIC, INCLUDING FOREIGN NATIONS.

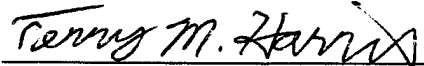
THIS TECHNICAL REPORT HAS BEEN REVIEWED AND IS APPROVED FOR PUBLICATION.



VICTORIA A. TISCHLER

Aerospace Engineer

Structural Design and Development Branch



TERRY M. HARRIS, Chief

Structural Design and Development Branch

Structures Division



DAVID M. PRATT, Technical Advisor

Structures Division

Air Vehicles Directorate

Do not return copies of this report unless contractual obligations or notice on a specific document require its return

**REPORT DOCUMENTATION PAGE**Form Approved  
OMB No. 074-0188

Public reporting burden for this collection of information is estimated to average 1 hour per response, including the time for reviewing instructions, searching existing data sources, gathering and maintaining the data needed, and completing and reviewing this collection of information. Send comments regarding this burden estimate or any other aspect of this collection of information, including suggestions for reducing this burden to Washington Headquarters Services, Directorate for Information Operations and Reports, 1215 Jefferson Davis Highway, Suite 1204, Arlington, VA 22202-4302, and to the Office of Management and Budget, Paperwork Reduction Project (0704-0188), Washington, DC 20503

<b>1. AGENCY USE ONLY (Leave blank)</b>		<b>2. REPORT DATE</b> NOVEMBER 1999		<b>3. REPORT TYPE AND DATES COVERED</b> Final, 09/30/1995 – 06/30/1998	
<b>4. TITLE AND SUBTITLE</b>  AERODYNAMIC ANALYSIS FOR THE DESIGN ENVIRONMENT (AANDE) VOLUME 1: THEORETICAL AND APPLICATIONS STUDY MANUAL				<b>5. FUNDING NUMBERS</b> C: F33615-95-C-3224 PE: 62201F PR: 2401 TA: TI WU: 05	
<b>6. AUTHOR(S)</b> M. H. LOVE D. D. EGLE					
<b>7. PERFORMING ORGANIZATION NAME(S) AND ADDRESS(ES)</b> LOCKHEED MARTIN TACTICAL AIRCRAFT SYSTEMS AIRFRAME AND INSTALLATION P.O. BOX 748, MAIL ZONE 2824 FORT WORTH, TX 76101-0748				<b>8. PERFORMING ORGANIZATION REPORT NUMBER</b>  FZM-8536	
<b>9. SPONSORING / MONITORING AGENCY NAME(S) AND ADDRESS(ES)</b> AIR VEHICLES DIRECTORATE AIR FORCE RESEARCH LABORATORY AIR FORCE MATERIEL COMMAND WRIGHT-PATTERSON AIR FORCE BASE, OH 45433-7542 POC: Victoria A. Tischler, AFRL/VASD, (937) 255-9729				<b>10. SPONSORING / MONITORING AGENCY REPORT NUMBER</b>  AFRL-VA-WP-TR-2001-3052	
<b>11. SUPPLEMENTARY NOTES</b>					
<b>12a. DISTRIBUTION / AVAILABILITY STATEMENT</b> Approved for public release; distribution unlimited.					<b>12b. DISTRIBUTION CODE</b>
<p>This report is part of the documentations that describe the complete development of the "Aerodynamic ANalysis for the Design Environment (AANDE)." It is one of the three manuals that comprise the final report. The remaining reports consist of the AANDE User's Manual (Volume II) and the AANDE Programmer's Manual (Volume III).</p> <p>The objective of the AANDE effort was to establish high quality reliable airloads for multidisciplinary design in ASTROS. This was accomplished by providing: a new steady linear aerodynamic procedure, alternate paths for the import of aerodynamic influence coefficient matrices and nonlinear pressure data, and a general asymmetric maneuver trim procedure.</p> <p>This manual details the capabilities integrated into ASTROS: ASTROS multi-database environment enabled, aerodynamic model architecture enables model integration, static load parameters implemented, 3-D aerodynamics in QUADPAN implemented, 3-D spline developed, Substructuring in Structures and Aerodynamics implemented, 6 DOF trim for steady aeroelastic analysis enabled, general control surface scheduling implemented and trim optimization developed for redundant controllers.</p>					
<b>14. SUBJECT TERMS</b> Aerodynamics, Analysis, Multidisciplinary Design, airloads, ASTROS, trim, asymmetric, multi-database, QUADPAN, spline, substructuring, control surface, optimization					<b>15. NUMBER OF PAGES</b> 160
					<b>16. PRICE CODE</b>
<b>17. SECURITY CLASSIFICATION OF REPORT</b> Unclassified	<b>18. SECURITY CLASSIFICATION OF THIS PAGE</b> Unclassified	<b>19. SECURITY CLASSIFICATION OF ABSTRACT</b> Unclassified		<b>20. LIMITATION OF ABSTRACT</b> SAR	
NSN 7540-01-280-5500				Standard Form 298 (Rev. 2-89) Prescribed by ANSI Std. Z39-18	

**THIS PAGE INTENTIONALLY LEFT BLANK**



# TABLE OF CONTENTS

<b>1. INTRODUCTION .....</b>	<b>1</b>
1.1 AANDE MOTIVATION.....	1
1.2 AANDE CONCEPTS.....	3
1.2.1 AANDE Aerodynamic Modeling.....	4
1.2.2 Three-dimensional Aerodynamics .....	6
1.2.3 Specification of Control Laws.....	8
1.3 AANDE CAPABILITIES .....	8
1.4 AANDE DOCUMENTATION .....	10
<b>2. ENHANCEMENTS TO SYSTEM ARCHITECTURE .....</b>	<b>11</b>
2.1 THE SYSTEM GENERATION PROGRAM.....	11
2.2 INPUT PACKET DEFINITION .....	12
2.3 THE FILE FORMAT .....	12
2.4 THE STANDARD ASTROS PACKET DEFINITION .....	13
2.5 MAPOL MODIFICATIONS .....	14
<b>3. ENHANCEMENTS TO ENGINEERING DISCIPLINES AND MODULES .....</b>	<b>15</b>
3.1 SOLUTION CONTROL ENHANCEMENTS.....	15
3.1.1 Analysis Model Concepts.....	15
3.1.2 New Steady Aeroelastic Analysis Disciplines .....	16
3.2 AERODYNAMIC AND AEROELASTIC MODEL ASSEMBLY .....	17
3.2.1 GROUP Entity Concepts .....	17
3.2.2 Aerodynamic and Aeroelastic Data Groups .....	17
3.2.3 Model Assembly Concepts .....	23
3.3 STEADY AERODYNAMIC DATA .....	26
3.3.1 Steady Aerodynamic Data Structures .....	26
3.3.2 QUADPAN Aerodynamic Method .....	28
3.3.3 Alternate Steady Aerodynamic Data.....	70
3.4 STEADY AERODYNAMIC SPLINES.....	72
3.4.1 Assembly of the Three-Dimensional Force Spline.....	73
3.4.2 Derivation of the Three-Dimensional Slope Spline .....	74
3.5 ASSEMBLY AND SOLUTIONS OF AEROELASTIC EQUATIONS.....	77
3.5.1 Rigid Loads.....	78
3.5.2 Aeroelastic Equations With Substructuring.....	81
3.5.3 Flexible Loads .....	83
3.5.4 BMST Component Load Computations .....	90
3.5.5 Generalized Trim .....	92
3.5.6 Control Surface Scheduling.....	94
3.5.7 Trim Optimization.....	95
3.5.8 Drag Analysis .....	101
<b>4. INTEGRATED TESTS AND APPLICATIONS.....</b>	<b>102</b>
4.1 AERODYNAMIC MODELING.....	104
4.1.1 Theory.....	104
4.1.2 Aerodynamic Codes .....	105
4.1.3 Models .....	105
4.1.4 Matrix Cases .....	107
4.1.5 Aeroelastic Model Comparisons - Flat Models .....	108
4.1.6 Aeroelastic Model Comparisons - Test Models .....	116
4.1.7 F-16XL Comparisons - Flat Models .....	123
4.1.8 Conclusions and Recommendations .....	123

4.2	SMALL SCALE APPLICATIONS .....	125
4.2.1	<i>Use of Substructuring</i> .....	126
4.2.2	<i>Instantiation of QUADPAN-Image For Centerline Symmetric Structure and Asymmetric Analysis</i> .....	130
4.2.3	<i>User-Defined Loads Simulating Adaptive Structures</i> .....	131
4.2.4	<i>Trim Optimization With Response Parameters</i> .....	132
4.3	VALIDATION OF AEROELASTIC TAILORING .....	133
4.4	F-16 WITH QUADPAN AERODYNAMICS .....	135
4.4.1	<i>QUADPAN With Control Surface Scheduling</i> .....	136
4.4.2	<i>QUADPAN Augmented With Nonlinear Aerodynamic Pressure Data</i> .....	139
4.4.3	<i>QUADPAN Five Degree of Freedom Trim</i> .....	141
4.5	DESIGN OPTIMIZATION WITH ALTERNATE LINEAR AERODYNAMICS .....	143
5.	REFERENCES .....	146

## LIST OF FIGURES

Figure 1-1	ASTROS Uses Maneuver Load Simulations In Design Optimization Studies .....	2
Figure 1-2	Aerodynamic Data For Maneuver Simulation Is Derived From Many Sources .....	3
Figure 1-3	Groups Enable the Assembly of Aerodynamic and Aeroelastic Models from Multiple Sources .....	5
Figure 1-4	Archetypical QUADPAN Model.....	7
Figure 1-5	Summary of Added Capabilities Providing ASTROS Versatile Modeling of Air-Loads In A Multidisciplinary Design Environment .....	8
Figure 3-1	Steady Aerodynamic and Steady Aeroelastic Model Groups .....	19
Figure 3-2	STDYGEOM - Model Geometry & Connectivity .....	19
Figure 3-3	Overlay Base Aerodynamics, CFD, Wind Tunnel As Best Aerodynamics Using Type RIGDALOD .....	20
Figure 3-4	RIGDALOD - Rigid Aerodynamic Loads .....	21
Figure 3-5	RIGDSLOD - Rigid Structural Loads .....	22
Figure 3-6	FLEXLOAD Group Computed At Each Subcase .....	22
Figure 3-7	Assembly And Trim Solutions of Aeroelastic Equations .....	25
Figure 3-8	Formulation of QUADPAN .....	32
Figure 3-9	Use of Vortex Wake on Lifting Configurations .....	35
Figure 3-10	Breakdown of Kutta Condition .....	37
Figure 3-11	Global Coordinate System.....	40
Figure 3-12	Contiguous and Non-Contiguous Elements.....	43
Figure 3-13	A Control Surface Sweep Computed For Each Onset Parameter .....	46
Figure 3-14	Initial Data in QUADPAN Packet.....	47
Figure 3-15	QUADPAN Geometry and Connectivity.....	48
Figure 3-16	QUADPAN Control Surface Hinge Axes Definition .....	49
Figure 3-17	Model of Jet Aircraft - Forward Lower View.....	50
Figure 3-18	Model of Jet Aircraft - Aft Upper View.....	51
Figure 3-19	Model of Jet Aircraft - Forward Upper View.....	51
Figure 3-20	Use of Panel Boundaries or Spacing Intervals to Control Mesh .....	52
Figure 3-21	Model of Transport Aircraft.....	54
Figure 3-22	Model of P-3C With Wing Stores and Nacelle Exhaust.....	56
Figure 3-23	P-3C With Vortex Wakes.....	57
Figure 3-24	The Importance of Wake Side Edge Modeling .....	59
Figure 3-25	Print Flag Options .....	62
Figure 3-26	Model Geometry Information Provided For Input Checking .....	63
Figure 3-27	Abutment Checks Are Critical To Model Debugging .....	64
Figure 3-28	Equation Mapping Section Indicates Order of Matrices In The Solution.....	65
Figure 3-29	QUADPAN Body Axes.....	66
Figure 3-30	QUADPAN Stability Axes.....	67
Figure 3-31	QUADPAN Wind Axes .....	68
Figure 3-32	Forward Swept Wing Sample Forces and Moments In The Body Axis .....	69
Figure 3-33	Strip Chord.....	70
Figure 3-34	Steady Aerodynamic and Steady Aeroelastic Model Groups.....	71
Figure 3-35	Control Surface Scheduling Flowchart.....	95
Figure 3-36	Structural Optimization Sequential To Trim Optimization. ....	100
Figure 4-1	Aeroelastic Tailoring Model (QUADPAN Grid) .....	106
Figure 4-2	F-16XL Model (Carmichael Grid) .....	107
Figure 4-3	Aeroelastic Tailoring Model (Vorlax Grid) .....	108
Figure 4-4	CL vs Alpha on Flat Aeroelastic Model - Mach 0.6 - Baseline Grid .....	109
Figure 4-5	CL vs Alpha on Flat Aeroelastic Model - Mach 0.6 - Fine Span Grid .....	110
Figure 4-6	CL vs CM on Flat Aeroelastic Model - Mach 0.6 - Baseline Grid.....	111
Figure 4-7	CL vs CM on Flat Aeroelastic Model - Mach 0.6 - Fine Chord Grid.....	111
Figure 4-8	CL vs CD on Flat Aeroelastic Model - Mach 0.6 - Baseline Grid.....	112

Figure 4-9	Mid-Span Cp on Flat Aeroelastic Model - Mach 0.6 - Baseline Grid .....	114
Figure 4-10	Mid-Span Cp on Flat Aeroelastic Model - Mach 0.6 - Baseline Grid .....	114
Figure 4-11	Mid-Span Cp on Flat Aeroelastic Model - Mach 0.6 - Fine Chord Grid .....	115
Figure 4-12	Mid-Span Cp on Flat Aeroelastic Model - Mach 0.6 - Fine Chord Grid .....	115
Figure 4-13	CL vs CM on Test Aeroelastic Model - Mach 0.6 - Baseline Grid .....	117
Figure 4-14	CL vs CD on Test Aeroelastic Model - Mach 0.6 - Baseline Grid .....	117
Figure 4-15	Mid-Span Cp on Test Aeroelastic Model - Mach 0.6 - Baseline Grid .....	118
Figure 4-16	Mid-Span Cp on Test Aeroelastic Model - Mach 0.6 - Baseline Grid .....	118
Figure 4-17	CL vs alpha on Test Aeroelastic Model - Mach 0.9 - Baseline Grid .....	120
Figure 4-18	CL vs CM on Test Aeroelastic Model - Mach 0.9 - Baseline Grid .....	120
Figure 4-19	CL vs alpha on Test Aeroelastic Model - Mach 1.2 - Baseline Grid .....	121
Figure 4-20	CL vs CM on Test Aeroelastic Model - Mach 1.2 - Baseline Grid .....	121
Figure 4-21	CL vs CD on Test Aeroelastic Model - Mach 1.2 - Baseline Grid .....	122
Figure 4-22	Mid-Span Cp on Test Aeroelastic Model - Mach 1.2 - Baseline Grid .....	122
Figure 4-23	CL vs alpha on Flat F-16XL Model - Mach 0.6 - Baseline Grid .....	124
Figure 4-24	Near Strake Cp on Flat F-16XL Model - Mach 0.6 - Baseline Grid .....	124
Figure 4-25	Small Scale Application Models Used in Unit and Integrated Testing .....	126
Figure 4-26	Example of Rectangular Wing With Substructuring .....	127
Figure 4-27	Rectangular Wing Unrestrained Longitudinal and Lateral Stability Derivatives .....	128
Figure 4-28	Rectangular Wing Restrained Longitudinal and Lateral Stability Derivatives .....	129
Figure 4-29	Asymmetric Trim Solution for Rectangular Wing .....	130
Figure 4-30	Static Load Parameters Used To Simulate Adaptive Structures .....	131
Figure 4-31	Input for Torsion Actuation On FSW Wing Spar .....	131
Figure 4-32	Trim Solution for TWI WING = 1.0 .....	132
Figure 4-33	Input For Function Based Trim Optimization .....	133
Figure 4-34	QUADPAN Used In Evaluation of Basis Vector Concept .....	133
Figure 4-35	Modeling For Fixed Boundary Condition .....	134
Figure 4-36	Modeling and Results for QUADPAN Reference = 8.9 Degrees .....	135
Figure 4-37	F-16 Structural and Aerodynamic Models Used in QUADPAN Based Simulations .....	136
Figure 4-38	LEF Schedules As Function of ALPHA And QDP .....	137
Figure 4-39	Sample Results from The F-16 QUADPAN Application .....	138
Figure 4-40	Wind Tunnel Pressures Were Transformed To The QUADPAN Model .....	139
Figure 4-41	Euler Computation Fluid Dynamics Pressures Were Transformed To The QUADPAN Model .....	140
Figure 4-42	Solution Control For RIGDALOD Import .....	140
Figure 4-43	Comparison of Pure QUADPAN and Two Alternate Nonlinear Aerodynamic Cases .....	141
Figure 4-44	TRIM Specification for Five Degree of Freedom Rolling Pull-Out Maneuver .....	141
Figure 4-45	Trim Results .....	142
Figure 4-46	Behavioral Results for Rolling Pull-Out Case .....	142
Figure 4-47	Design Optimization Studies Performed With Alternate Linear Aerodynamics Data .....	143
Figure 4-48	Solution Control With Alternate Aerodynamic Database .....	144
Figure 4-49	Weight History For Strength Optimization .....	145
Figure 4-50	Problem Set-Up For Trim Optimization With BMST Constraints .....	145

## LIST OF TABLES

Table 2-1	New Entity Name Types For MAPOL Character Variables .....	14
Table 3-1	Options for AIC Boundary Conditions in QUADPAN.....	16
Table 3-2	ASTROS Aeroelastic Solution is Assembled From Aerodynamic and Aeroelastic Data Groups .....	18
Table 3-3	Definition of Control Surfaces in QUADPAN.....	48
Table 3-4	Trim Optimization Constraint Coefficients.....	97
Table 4-1	Multi-Database, Aerodynamic Modeling, and Structural Modeling Capabilities Tested.....	102
Table 4-2	Static Aeroelastic Component Capabilities Tested .....	103
Table 4-3	Maneuver Trim Simulation Capabilities Tested .....	103
Table 4-4	Selected Cases to Evaluate Aerodynamic Cases .....	107

## FOREWORD

The Air Force Research Laboratory initiated development of ASTROS in 1983. Further development work was conducted and completed in 1987. This document presents the analytical foundations for the enhancements to the Automated Structural Optimization System (ASTROS) developed under the Aerodynamic Analysis for the Design Environment (AANDE) contract F33615-95-C-3224. This contract has been conducted by the Lockheed Martin Tactical Aircraft Systems (LMTAS) and their subcontractor Universal Analytics Inc.. Lockheed Martin Aeronautical Systems has also provided assistance to LMTAS in the AANDE program. Major contributors to the AANDE program include M.H. Love, the Program Manager, D.D. Egle, and D.K. Barker from LMTAS and R. Coopersmith from LMAS. From Universal Analytics, the major contributors were D.J. Neill, T. Shimko, S. Chen, and J. San Marco.

This report constitutes both theoretical developments and application guidelines. It is one of four documents generated under the AANDE program.

Dr. Ray Kolonay has been the primary Air Force program engineer. Dr. V.B. Venkayya initiated the program and has provided much of the overall program direction.

# 1. INTRODUCTION

The unique attributes of ASTROS (Ref. 1) hold great potential by savings in design time, improvements in vehicle performance, and reductions in structural weight in aerospace vehicles. This potential has been limited with regard to modeling and simulation of maneuver loads for design. The overall objective of the Aerodynamic Analysis for the Design Environment contract (F33615-95-C-3224) is to establish high quality, reliable loads simulation in ASTROS. The Lockheed Martin Tactical Aircraft team including Universal Analytics Inc. and Lockheed Martin Aeronautical Systems accomplished this objective by providing a new steady linear aerodynamic procedure, alternate paths for import of aerodynamic influence coefficient matrices and nonlinear pressure data, and a general asymmetric maneuver trim procedure.

The program encompassed three main tasks:

- 1.0 Phase I - System Specifications
- 2.0 Phase II - Module Development and Prototyping
- 3.0 Phase III - "Seamless" Integration and Verification.

In Phase I, changes to the ASTROS modules, paradigms, and data structures were identified, modeled, and tested against realistic scenarios of fighters, bombers, and transport aircraft. The results of these exercises formulated the plans for the software development and verification and are documented in the Software Design Guide (Ref. 2).

In Phase II, individual modules were developed and tested with realistic test cases as well as simple cases used for development. In Phase III, the modules were integrated into ASTROS through the memory manager, database, and MAPOL. Verification studies were performed simulating usage in a preliminary design scenario.

## 1.1 AANDE MOTIVATION

The ASTROS program is a finite element based system developed around a multi-schematic database and open architecture. It includes linear steady and unsteady aerodynamic methods that can be coupled with the structural finite elements for aeroelastic solutions. It also includes optimization techniques to allow the simultaneous sizing of structure to strength and aeroelastic requirements. Its evolving usage is providing lessons learned (Refs. 3-8). As a catalyst for "what if" studies in vehicle design and support, it provides means to acquire sensitivity of structural weight to configuration level criteria such as roll effectiveness and structural weight to detailed structural member criteria such as strength allowables. Figure 1-1 illustrates the utility of maneuver loads in such studies. Critical conditions are selected that typify maximum combinations of integrated load parameters such as rolling moment and pitching moment. A number of these conditions are simulated in the course of the design optimization. Listed in the figure are sample conditions and their criteria. The results of design optimization studies such as the configuration parameters weight and roll effectiveness summarized in the figure are dependent on the maneuver simulations in the study.

Successful implementation of a multidisciplinary design (MD) tool is dependent on the accuracy of the discipline simulations involved. Maneuver airloads within airframe sizing is integral to the structural flexibility, aerodynamics, and control schemes. Control schemes are the way an aircraft control effector suite (e.g. control surfaces, thrust vectoring) is used to trim the aircraft. They are designed to meet performance goals, while responding to available structural flexibility and aerodynamic effectiveness. Aerodynamic performance is a function of aerodynamic shape, structural flexibility and control schemes. ASTROS's objective is to provide

guidance in sizing airframe in an integrated system level environment and enhance communication of airframe input in its interaction with aerodynamics and controls at the system level.

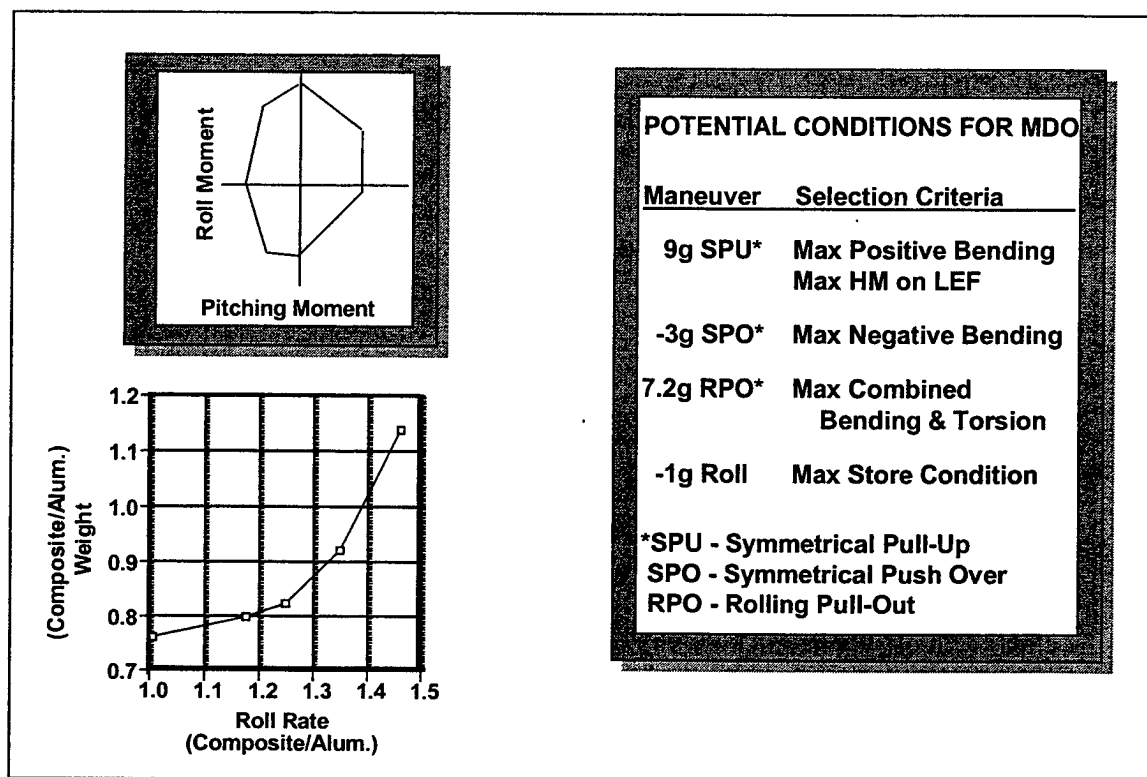


Figure 1-1 ASTROS Uses Maneuver Load Simulations In Design Optimization Studies

Growing requirements for the maneuver airloads discipline in ASTROS have led to the development work described in this document. In one ASTROS study (Ref. 4), many trials with USSAERO failed in the representation of the desired configurations either due to modeling limitations or due to unacceptable computational aerodynamic results. The limitations in capability led to surrogate approaches to simulate design critical loads.

In studying general solutions to these limitations, it is apparent that each analyst has preferred aerodynamics procedures and that general access to alternate aerodynamic methods is desirable; thus allowing acceptable levels of accuracy and skilled usage of aerodynamic models. Further, since aircraft design loads often lie in regions of discontinuous or separated aerodynamic flow, an ability to import nonlinear pressure data into ASTROS' linear aeroelastic paradigm would promote integration of computational fluid dynamics. In such cases, three-dimensional linear aerodynamic geometry allows distinction of surface data that is critical for thick aerodynamic bodies.

To integrate varying sources of data such as aerodynamic influence coefficient matrices from a linear panel method and nonlinear pressure data from a Navier Stokes method, ASTROS would require use of multiple databases of aerodynamic models. Each model (as illustrated in Figure 1-2) may require a separate discretization to accommodate the particular needs of the method (e.g., Mach-dependent or flight condition dependent mathematical models) and each model might contain geometry, pressure data and flexibility correction data. The creation, management and use of these aerodynamic databases require a substantial change to the ASTROS aeroelastic paradigm.



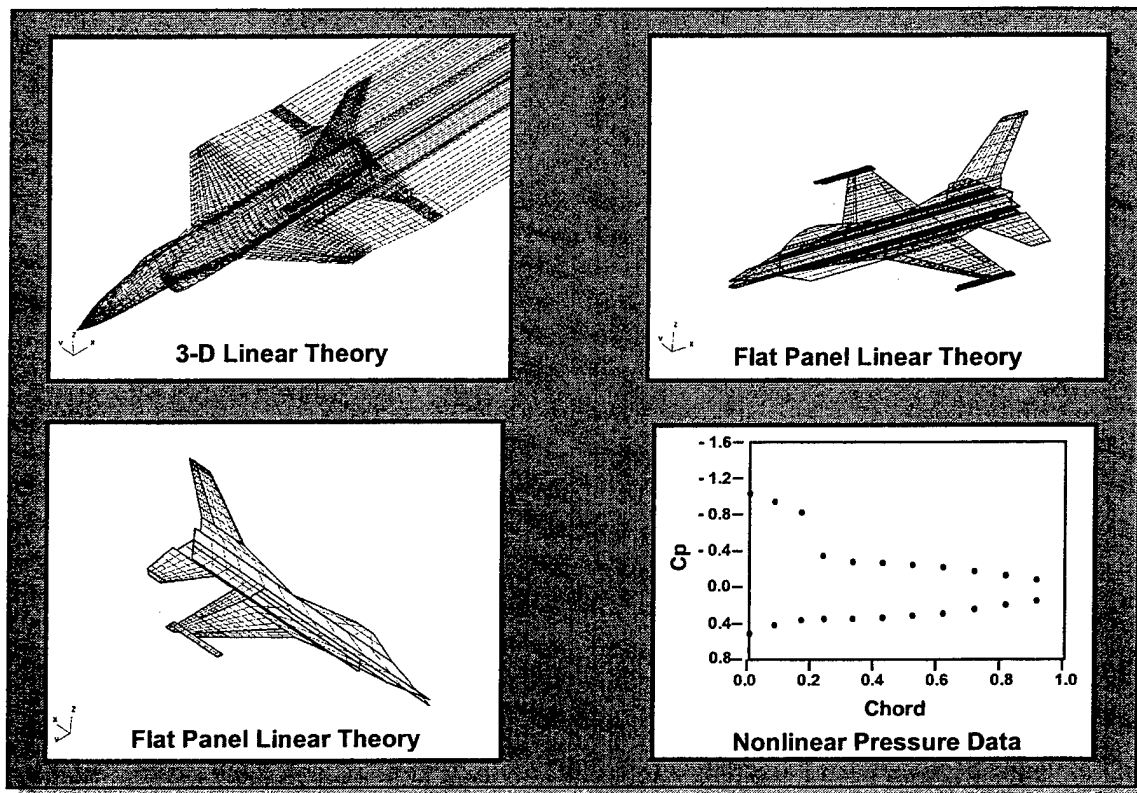


Figure 1-2 Aerodynamic Data For Maneuver Simulation Is Derived From Many Sources

While symmetric load requirements may drive the design for significant portions of wings, the fuselage and empennage structures designs are driven by asymmetric loads. Air vehicle trim analysis needs to be sufficiently robust to accurately predict aeroelastic criteria for control effectiveness and aerodynamic performance throughout the flight envelope during the course of preliminary design. In keeping with the original intent of ASTROS, these analysis conditions and their attendant design criteria need to be concurrently imposed as part of the structural optimization problem. As was shown in Ref. 8, the maneuver trim analysis must and can account for the lack of definition in the control law.

Further, the ASTROS models (both structural and aerodynamic) are seen to evolve during the design process. Initially, simple models may be adequate, but very soon, more sophisticated analyses are needed to accurately perform trade studies using automated design as an evaluator of vehicle design philosophies and a guarantor of interdisciplinary integrity. The enhancements described here are intended to allow the ASTROS tool to play such a role in aeroelastic synthesis of flight vehicles, from concept through structural layout. These enhancements are not limited to individual modeling features, but to a revamped paradigm for model creation and use that enables the evolution of the automated design problem statement as understanding of the vehicle grows.

## 1.2 AANDE CONCEPTS

The fundamental concepts developed and implemented in this contract involve the creation and use of aerodynamic data. The developed concepts enable a variety of constituent data to be computed and/or assembled in order to define an aerodynamic model. Inclusive in this development, the ASTROS paradigm of "flat panel" aerodynamics was augmented to include three-dimensional aerodynamic data. Besides the assembly of aerodynamic models, concepts were developed to enhance maneuver simulations. These simulations are performed through the combination of specified aerodynamic states, rigid body

accelerations, and control laws (e.g. control surface scheduling or trim optimization functions for redundant surfaces).

### 1.2.1 AANDE Aerodynamic Modeling

Under this enhancement to ASTROS, the creation of the aerodynamic model is separated from its use. This fundamental change enables ASTROS' archival re-use of aerodynamic models and, as a natural fallout, allows the creation of more than one aerodynamic model associated with a single configuration. While aerodynamic data can become voluminous (leading to multiple databases for separate disk storage), the real issue is to accurately simulate loads over a broad spectrum of flight conditions and trim states. To accomplish this, a plethora of aerodynamic methods are used to accurately predict pressure distributions on complex configurations. Each method will typically bring its own unique requirements to the mathematical (or discretized) model.

As an example, at high angle of attack flight conditions, not only are the rigid pressures computed by linearized panel methods inaccurate, but the flexible corrections (AIC's) are also inadequate. To assemble a reasonable model for predicting aeroelastic loads in this regime, the analyst might choose to bring Navier-Stokes or wind tunnel pressures together with a local, proprietary predictor of flexibility effects. On the other hand, a simple flat plate panel model may be perfectly adequate in certain other regimes for the same vehicle and, to require the overhead of the former model's generality in the creation of the latter model will make the tool too difficult to use.

The creation of an aerodynamic model of sufficient generality that ASTROS can bring to bear its MDO capabilities requires that the geometry, pressure data and flexibility data *can* be controlled separately, but also can be managed together as a *group* of entities that comprise a single model. The concept that has been implemented is that any number of static aerodynamic model *groups* can be created, either in separate executions or in the same stream as the aeroelastic trim solution. The aeroelastic analyses then *use* the model group(s) in any number of aeroelastic cases.

The groups and models concepts developed under the AANDE contract are shown in Figure 1-3. The core Model for aeroelastic analyses is the Steady Aerodynamic Model. It comprises STDYGEOM, AICS, RIGDALOD, and RIGDSL0D for geometry, aerodynamic influence coefficients, aerodynamic state pressure vectors, and user defined state load vectors correspondingly. These groups correspond to aerodynamic states (aerodynamic loads integration *model*, aerodynamic influence coefficient *method*, *Mach* number). A major shift from the original ASTROS paradigm involves the storage and use of aerodynamic pressure data. In the original ASTROS paradigm, data is stored and used in incremental standard for linear aeroelasticity. For example, a pressure vector for an angle of attack is stored and used at a state of one-degree angle of attack. In the AANDE paradigm, the pressure vectors are stored at actual states and therefore may contain characteristics of the nonlinearity in that state. Therefore, the pressure vectors within a Steady Aerodynamic Model will be associated with a Basis condition. For example, a pressure vector may be stored at an angle of attack state of twelve degrees. A Basis vector is also stored that includes the aerodynamic pressures at zero degrees angle of attack.

The Steady Aeroelastic Model includes the Steady Aerodynamic Model with the FLEXLOAD, SPLINE, and FLEXTRIM groups. These groups correspond to specific aeroelastic states (i.e. dynamic pressure, Mach number, trim definitions). The FLEXLOAD group includes the incremental load distributions from the aeroelastic solution stored in the structural domain. The SPLINE group is usually defined by the ASTROS core capabilities, but allows unique splines for each aeroelastic solution given the unique requirements resulting from the Steady Aerodynamic Model. Under the AANDE contract, the static aeroelastic model groups were defined to include future developments (e.g., nonlinear iterative trim algorithms) and developed to allow for linear maneuver trim including nonlinear aerodynamics.

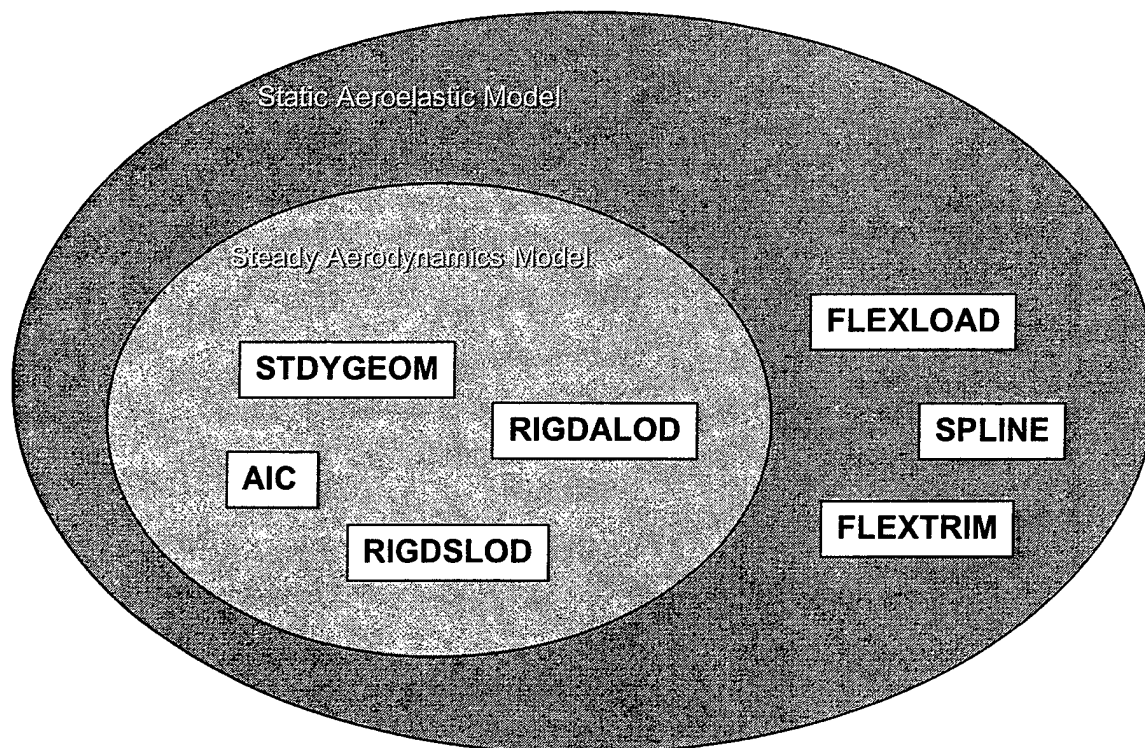


Figure 1-3 Groups Enable the Assembly of Aerodynamic and Aeroelastic Models from Multiple Sources

Sophisticated usage allows the disassembly of groups and their reassembly by **overlaying** parts of separate models to form new models. Thus, high order Navier-Stokes data can be incorporated into the low order basis of a model to extend its range of validity. As the design process progresses, models can grow in sophistication as the data become available from the more labor extensive modeling and/or wind tunnel test methods.

In a similar vein, the **aeroelastic** model is defined as the union of the aerodynamic model with the data required to attach it to a particular structural model. While the natural extension of the aerodynamic model concept is to embrace multiple structural models, ASTROS was not so enhanced under the effort described here. Instead, ASTROS execution was enabled to use numerous aeroelastic models that represent the attachment of multiple aerodynamic models to a single structural FE model. This development provides unlimited versatility in deriving the critical conditions to be treated simultaneously in the design process.

The steady aerodynamic capability is further expanded by development of a completely general approach to include user-specified alternate aerodynamic geometry, AIC matrices, and/or unit pressure distributions. This extension provides access to externally computed aerodynamic solutions, thereby providing a gateway to a variety of aerodynamic analyses and processes. Further, this extension provides access to wind tunnel and CFD pressure data as an alternative to the default ASTROS computed pressure data.

As indicated above, the implementation of this powerful capability is simply a natural usage of the model definition and management concept being implemented within the tool. Unlike the previous ASTROS concept of the USSAERO model, the current concept makes very few assumptions about the nature and source of the aerodynamic data. The way to conceptualize these changes is to understand that **all** aerodynamic models have equal status. There are no differences between so-called alternate aerodynamics and those data generated within the ASTROS tool.

### 1.2.2 Three-dimensional Aerodynamics

In addition to easy access to external, alternative aerodynamics, improvements to the basic steady aeroelastic capability include incorporation of the three-dimensional, true surface aerodynamic software, QUADrilateral PANel Method (QUADPAN - Refs. 9, 10). The new aerodynamic capability provides for three-dimensional linear aeroelastic solutions. The incorporation of three-dimensional aerodynamics necessitates changes in data handling as mentioned in the previous section and changes in solution strategies and thinking as described in the following.

QUADPAN is based on the linearized equation of inviscid, irrotational (potential) flow (Prandtl-Glauert equation) and requires a surface grid. It is applicable in the subsonic or supersonic speed regimes. It is limited to the analysis of attached flow, where the vorticity is confined to a wake sheet derived from the Kutta condition. The geometric representation is the actual airplane surface, yielding full thickness effects without any mean surface approximations.

Its capabilities as implemented include:

- Full or half model geometry
- Symmetric/antisymmetric or asymmetric capability
- Surface pressure distribution
- Force and moment coefficients
- Longitudinal/Lateral stability derivatives
- Transpiration methods for control surface deflection
- Propeller slipstream effects
- Engine inlet and exhaust simulation
- Aerodynamic Influence Coefficient (AIC) matrix

Pressure distributions are computed at the center of quadrilateral elements that represent the aerodynamic surface and are perpendicular to the true aircraft surface. The Aerodynamic Influence Coefficients (AIC) are computed to acquire the flexible increment to the rigid loads for the specified geometry and flight conditions. The local rotation axis for the AIC is the plane formed by the free-stream velocity vector and unit surface normal vector.

Figure 1-4 shows an archetypical fighter aircraft model. The model is made up of 60 QUADPAN panels comprising 6374 elements. A panel is the basic building block and consists of four corner points. Elements are defined within the panels, and the panels must satisfy various abutment rules (e.g. no gaps in the aerodynamic surfaces). A control surface is defined as a panel or group of panels. The model may be represented by centerline geometry if desired such that the user would define 30 panels and 3187 elements. QUADPAN will instantiate a reflection of its geometry if it recognizes asymmetric boundary conditions. Finally, to account for the Kutta condition, wake panels and elements are defined in the same manner as the true aerodynamic surface.

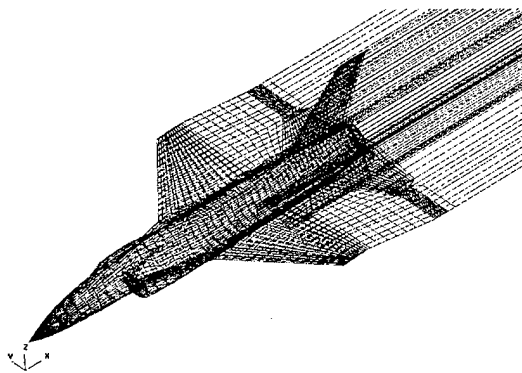


Figure 1-4 Archetypical QUADPAN Model

For a QUADPAN analysis within the ASTROS integration paradigm, parameter loads are acquired at a given Mach number for each control surface parameter defined plus a default group of onset parameters (e.g.  $\alpha$  and  $\beta$ ). The user may elect also to prescribe a set of basis onset flow parameters and deflected control surfaces for the incremental conditions to be perturbed about. Thus, because QUADPAN integrates a three-dimensional flow field, geometric-nonlinear integrated-aerodynamics is available to ASTROS. The resulting onset flow condition is treated as a thickness and camber basis (in the old ASTROS paradigm) and is used in the computation of incremental loads; requiring book-keeping of actual rather than incremental load vectors. This has downstream implications on aeroelastic solutions and trim such as the linearization of pressure data incremented from the basis load set.

An important distinction of three-dimensional aerodynamics in general is the nonexistence of antisymmetric aerodynamics. The flow is three-dimensional and thus an antisymmetric boundary condition is most likely to lead to an asymmetric flow condition. All such flow conditions are therefore referred to as asymmetric.

Solution resources for use of such typical models impose significant computational and storage requirements on the prospective ASTROS user. First, the AIC matrix is maintained in the database throughout the ASTROS run as a fully populated, often double precision dataset. Given that a typical run may contain independent AIC matrices and associated data for several Mach numbers, this will tax existing hardware; however, advances in hardware (memory and disk storage) will soon remedy this issue. Secondly, the computational costs of the AIC matrices and increment pressure data for all of the control parameters are relatively large with respect to the computational time of an optimization solution. A design optimization consisting of a structural model of 3000-4000 degrees of freedom with 200 design variables will require 6-8 CPU hours on a high-end workstation, while computation of the AIC and increment pressures could take one hour per Mach number on the same workstation. It will be beneficial to compute this database in a preprocessing environment and save the data on an ASTROS database that can be accessed at optimization run time, and this is provided for. Finally, the aeroelastic solution imposes greater numbers of degrees of freedom that are splined in the structural domain leading to longer decomposition times for the nonsymmetric aeroelastic stiffness matrix.

Integration of QUADPAN has been accomplished with the enhancement to ASTROS allowing it to recognize additional forms of data from the original NASTRAN Bulk type. A QUADPAN model is recognized through "BEGIN QUADPAN" in place of "BEGIN BULK." Therefore, minimum modification was required of QUADPAN for integration to ASTROS, and a methodology was implemented for integrating future codes in an open architecture.

### 1.2.3 Specification of Control Laws

Maneuver simulations require the specification of vehicle accelerations and control parameters that provide for the balance of forces and moments. Vertical acceleration,  $n_z$ , is an example of a typical vehicle acceleration. Examples of control parameters are angle of attack,  $\alpha$ , aileron deflection,  $\delta_a$ , and yaw,  $\beta$ . ASTROS allows the quasi-steady simulations, and this concept has been maintained. Under the AANDE contract, concepts have been developed to enhance ASTROS' use of redundant controllers. In general, treatment of accelerations and parameters is interchangeable as *control effectors*. The ASTROS user can specify through control effector scheduling or trim optimization functions a control law implementation. Scheduling is defined as a table "look-up" function that links one parameter with one or a set of other parameters. Thus, the number of redundant parameters is reduced through linking. Trim optimization allows the solution of optimal trim parameter settings in the case of multiple feasible solutions. In this case, an objective function such as minimum control surface energy or minimum wing-root-bending-moment is selected, and design variables such rigid body acceleration, control surface deflections, and maneuver response parameters are defined. In the AANDE program, a gradient based trim optimization routine was developed.

## 1.3 AANDE CAPABILITIES

Figure 1-5 lists the capabilities developed under the AANDE program. Each of these capabilities have been integrated in ASTROS version 12.5 providing a versatile, high quality tool for accurate air-loads in a multidisciplinary design environment.

- **ASTROS Multi-Database Environment Enabled**
- **Aerodynamic Model Architecture Enables Model Integration**
- **Static Load Parameters Implemented**
- **3-Dimensional Aerodynamics in QUADPAN Implemented**
- **3-Dimensional Spline Developed**
- **Substructuring In Structures & Aerodynamics Implemented**
- **6 DOF Trim For Steady Aeroelastic Analysis Enabled**
- **General Control Surface Scheduling Implemented**
- **Trim Optimization Developed For Redundant Controllers**

Figure 1-5 Summary of Added Capabilities Providing ASTROS Versatile Modeling of Air-Loads In A Multidisciplinary Design Environment

Implementation of the first two items, multiple databases and aerodynamic modeling architecture, provides the foundation of the aerodynamic modeling of ASTROS under this enhancement. The multiple database capability allows the ASTROS user access to aerodynamic data created from multiple sources in order to assemble his aerodynamic models for ensuing analyses. Enabling this capability required

modifications to ASTROS' system architecture (described in Section 2). For instance, the MAPOL executive language was modified to allow projection of data addresses across the multiple-databases. The aerodynamic modeling architecture was required to allow the ASTROS user ability to tag and organize the data in logical groups. An overview of the group concepts is described in the previous subsection. Details of the group concepts and their usage are described in Sections 3.1 through 3.3.3.

Static Load Parameters (SLPARM in the Bulk data) provide the ASTROS user the ability to define loads in the structural domain and include them in the aeroelastic analysis. This capability allows use of any load type available for the ASTROS STATIC analysis option (e.g. FORCE, MOMENT). Example uses of this capability include adaptive structures modeling through force-equivalent actuation and component aerodynamic load modeling from wind tunnel force models (e.g. weapon stores increments). Static Load Parameters are described in Subsection 3.5.1.2.

Three-dimensional aerodynamics analysis was implemented in ASTROS through the integration of the Lockheed Martin Aeronautical Systems Company QUADPAN code and the development of a three-dimensional spline. As was described in the previous subsection, use of a three-dimensional aerodynamics code ushers a new paradigm into aeroelastic analysis and multidisciplinary design optimization. Details of QUADPAN are provided in Subsection 3.3.2. Integrating QUADPAN into the aeroelastic analysis capability of ASTROS was allowed by enhancing the implementation of the infinite plate spline already imbedded in ASTROS. The mathematical derivation for this is included in Subsection 3.4.2. The aerodynamic modeling architecture that this capability was implemented through enables the ASTROS user to utilize three-dimensional linear aerodynamic codes other than QUADPAN as well.

Asymmetric aeroelastic maneuver simulation was enabled through the combination of implementing simplified substructuring techniques and full up six-degree of freedom solutions. The substructuring allows the ASTROS user to provide any of the following combinations of structural and aerodynamic models in asymmetric simulations:

1. Centerline symmetric structural model and centerline symmetric aerodynamic model.
2. Full-span definition structural model and full-span definition aerodynamic model.
3. Centerline symmetric structural model and full definition QUADPAN model.

The ASTROS user now has the options of the previous standard symmetric and antisymmetric trim solutions as well as the new asymmetric trim solution. The substructuring methodology is instantiated automatically from the solution requirements based on available models and minimal user input (described in Subsection 3.5.2). The new asymmetric trim capability is described in Subsection 3.5.5.

A general trim capability for multidisciplinary design requires the ability to deal with redundant control effectors (i.e. more control effectors than vehicle rigid body degrees of freedom). This capability was added through implementation of a control effector scheduling module and a trim optimization module. Scheduling implies that one control effector is dependent on a series of others through a combination of table look-ups. A versatile design of this function allows complex schedules for large numbers of control effectors as might be envisioned for adaptive structures applications (described in Subsection 3.5.6). In the case where the scheduling is unknown (as in early design), a trim optimization capability is required in which the ASTROS user may want to use the control effectors in a minimum energy approach or to specify a maneuver state that maximizes accelerations and control surface deflections within the specified maneuver. In this latter case, the user might be searching for a maximum within the design criteria. In the former case, the user might be searching for a likely control law for a minimum weight structure. Such a capability has been implemented (Subsection 3.5.7). A key constituent of the trim optimization is a generic bending moment, shear, torque computation (BMST). Through this definition, the user may compute any component load such as hinge moment or wing root bending moment (Subsection 3.5.4).

With the capabilities added to ASTROS under the AANDE contract, an ASTROS user has the tools to develop accurate aerodynamic models, conduct required maneuver simulations, and interface with

the multiple disciplines of airframe design throughout the course of the design process. These tools are available for analysis and design optimization studies.

## **1.4 AANDE DOCUMENTATION**

The AANDE contract is documented through four reports, Software Design Guide (Ref. 2), Theoretical and Application Studies Report (this report), the Programmer's Report (Ref. 11), and the User's Report (Ref. 12). The Software Design Guide (SDG) was developed at the end of Phase I of the AANDE program with the intention of developing requirements for ASTROS development beyond the original scope of AANDE but within the scope of air-loads in the design process. Many of the requirements in the SDG are implemented. The remaining documents are supplemental to the ASTROS version 12 documentation (Ref. 13). Areas of modification are documented fully. The Programmer's Report includes new and modified module descriptions and database entities. The User's Report includes new and modified ASTROS bulk data as well as user input requirements for QUADPAN. An appendix is provided on the User's document describing the construction of an ASTROS database for user developed aerodynamic data (data alternate to the ASTROS domain capability).



## 2. ENHANCEMENTS TO SYSTEM ARCHITECTURE

Early in the contractual effort, modifications to the ASTROS software infrastructure were performed in order to enable the new aerodynamic technologies. These modifications included:

- The ability to use multiple databases within ASTROS. This feature facilitated the use of alternate aerodynamic databases and allowed complete read/write support for any number of archival databases.
- The extension of database names, entity names, and relational attributes to 24 characters. This allows more descriptive names to be used.
- The extension of the MAPOL compiler to understand longer entity names as well as database logical names. (e.g. *dbname:entity\_name*) The latter feature was required for support of multiple databases.
- The definition and implementation of a new Group entity class. This class allows the definition of multi-level groups of aerodynamic data. Various operations on Group entities (ARCHIVE, ASSEMBLE, IMPORT and OVERLAY) allow the efficient manipulation of the collections of relations within the Groups. Additionally, Group entities themselves may be composed of other Groups thus allowing the multi-level data organization.

The changes support both the AANDE effort and provide a basis for additional extension of ASTROS features.

The following sections describe the changes to the system architecture and are also included in the Programmers Document (Ref. 11).

### 2.1 THE SYSTEM GENERATION PROGRAM

SYSGEN represents one of the most useful features of the ASTROS system architecture in that it provides for automated modification of many of the procedure's capabilities without requiring modification of any existing source code. The purpose of SYSGEN is to create a system database (SYSDB) defining system parameters through the interpretation of several input files. Also, a FORTRAN routine is written by SYSGEN that provides the link between the ASTROS executive system and the application modules that comprise the run-time library of the procedure. This program unit is then linked with the system during the assembly of the ASTROS executable image. The resultant procedure makes use of the system database as a pool of data that defines the system at run time. These data are

1. The contents of the ASTROS run-time library of MAPOL addressable modules including both utility and application modules, usually delivered as MODDEF.DAT or MODDEF.DATA;
2. The ASTROS standard executive sequence composed of MAPOL source code statements, usually delivered as MAPOLSEQ.DAT or MAPOLSEQ.DATA;
3. The set of bulk data entries interpretable by the system and defined through the specification of bulk data templates to be interpreted by the ASTROS Input File Processor (IFP), usually delivered as TEMPLATE.DAT or TEMPLATE.DATA;
4. The set of relational schemata used by the executive system to satisfy the declaration of relational variables in the MAPOL sequence without forcing the user to explicitly define each schema at run time, usually delivered as RELATION.DAT or RELATION.DATA;

5. The set of input packet definitions, usually delivered as **PACKET.DAT** or **PACKET.DATA**. These describe the general format of the MAPOL, Edit, Solution Control, Function, Bulk Data, and QUADPAN input packets;
6. The set of error message texts from which the UTMWRT system message writer utility builds error messages at run time, usually delivered as **SERRMSG.DAT** or **SERRMSG.DATA**.

Modifications of the AANDE contract created the sysgen data **PACKET.DAT**. This allowed the inclusion of QUADPAN without modifications of the QUADPAN user input formats. It also allows inclusion of other future codes such as QUADPAN.

## 2.2 INPUT PACKET DEFINITION

To allow for maximum generality in ASTROS input processing, there is a file called **PACKETS.DAT**. This file is organized as a sequence of specification entries that define different input packets. There is one group of entries for each input packet. New packets may be defined by adding new groups of entries to this file. Naturally, new software will be required to read any such new packets.

The format of the **PACKETS.DAT** file is given in the following section.

## 2.3 THE FILE FORMAT

Each packet has the general form:

<b>BEGINPACKET</b>	<i>Input Packet Name</i>
<b>STARTKEY</b>	<i>Keyword</i>
<b>ENDKEY</b>	<i>Keyword</i>
<b>FILENAME</b>	<i>Filename</i>
<b>CASE</b>	<b>UPPER, LOWER</b> or none
<b>BLANKLINE</b>	<b>KEEP, MIXED</b> or none
<b>ENDPACKET</b>	

where:

<b>STARTKEY</b>	indicates the beginning of the packet.
<b>ENDKEY</b>	indicates the end of the packet.
<b>FILENAME</b>	is the name of the file where the input contents are saved.
<b>BLANKLINE</b>	is the instruction to indicate whether blank lines in the input packet will be kept or deleted.
<b>CASE</b>	indicates the letter case type to be used to convert the input packet.

Both the entries for each packet, and the inputs within each entry, may be in any order. The **CASE** and **BLANKLINE** records are optional. These packets are processed by SYSGEN and the rules defined by the entries are saved in a relation named **PACKETRE** on the system database. These are later used by the PREPAS module of ASTROS. Note that the **FILENAME** is used by PREPAS to define a relation where the packet data is saved.

## 2.4 THE STANDARD ASTROS PACKET DEFINITION

The following is the **PACKETS.DAT** input for each of the standard system input data packets:

For the MAPOL Packet:

<b>BEGINPACKET</b>	<b>MAPOL</b>
<b>STARTKEY</b>	<b>MAPOL</b>
<b>ENDKEY</b>	<b>ENDMAPOL</b>
<b>FILENAME</b>	<b>MAPLPKT</b>
<b>BLANKLINE</b>	<b>KEEP</b>
<b>ENDPACKET</b>	

For the EDIT Packet:

<b>BEGINPACKET</b>	<b>EDIT</b>
<b>STARTKEY</b>	<b>EDIT</b>
<b>ENDKEY</b>	<b>ENEDIT</b>
<b>FILENAME</b>	<b>MAPLPKT</b>
<b>ENDPACKET</b>	

For the Solution Control Packet:

<b>BEGINPACKET</b>	<b>SOLUTION</b>
<b>STARTKEY</b>	<b>SOLUTION</b>
<b>ENDKEY</b>	<b>ENDSOLUTION</b>
<b>FILENAME</b>	<b>SOLNPKT</b>
<b>ENDPACKET</b>	

For the Function Packet:

<b>BEGINPACKET</b>	<b>FUNCTION</b>
<b>STARTKEY</b>	<b>FUNCTION</b>
<b>ENDKEY</b>	<b>ENDFUNC</b>
<b>FILENAME</b>	<b>FUNCPKT</b>
<b>ENDPACKET</b>	

For the Bulk Data Packet:

<b>BEGINPACKET</b>	<b>BULKDATA</b>
<b>STARTKEY</b>	<b>BEGIN BULK</b>
<b>ENDKEY</b>	<b>ENDDATA</b>
<b>FILENAME</b>	<b>BKDTPKT</b>
<b>ENDPACKET</b>	

For the QUADPAN Packet:

<b>BEGINPACKET</b>	<b>QUADPAN</b>
<b>STARTKEY</b>	<b>QUADPAN</b>
<b>ENDKEY</b>	<b>ENDQUADPAN</b>
<b>FILENAME</b>	<b>QDPANREL</b>
<b>BLANKLINE</b>	<b>KEEP</b>
<b>ENDPACKET</b>	

## 2.5 MAPOL MODIFICATIONS

MAPOL was modified to support the longer entity names implemented in CADDB changes. This was done to facilitate the creation of "indexed" entity names in the aerodynamic model groups. Also, the CHARACTER variable type is supported for the MAPOL language.

```
Declaration      :    CHARACTER A, B, C;

Assignment       :    A := "string";

Comparison       :    IF A = "QUADPAN" THEN
                      IF A "QUADPAN" THEN

Argument Passing :    CALL MODULE ( A );
```

CHARACTER data types may be set in a module and passed out to MAPOL with an updated value--just like other number variables.

Then, four new entity name types are created:

Table 2-1 New Entity Name Types For MAPOL Character Variables

<option>	Description
GGMEMBER	Group entity type
RGMEMBER	Relational group member
UGMEMBER	Unstructured group member
MGMEMBER	Matrix group member

These are basically entity name "variables" rather than entity name "symbols." The distinction is that the variables can be set in the module and passed through the MAPOL calling sequence. Regular entity names are static - once declared, they become a symbol rather than a variable name. The new feature is used in naming the members of a group. The GGMEMBER type is a RELATION on CADDB, but is denoted separately so that argument passing can perform the appropriate type checking. The other types are just like their non-group counterparts.

In MODDEF, these parameters are of type

```
CHARACTER      - 17
GGMEMBER       - 18
RGMEMBER       - 19
UGMEMBER       - 20
MGMEMBER       - 21
```

These values are specified on the parameter definition line in MODDEF.DAT (e.g., similar to RELATION which is a type 7 parameter).

### 3. ENHANCEMENTS TO ENGINEERING DISCIPLINES AND MODULES

#### 3.1 SOLUTION CONTROL ENHANCEMENTS

Solution Control enhancements were required to direct the use of multiple databases, new analysis disciplines and new options within the existing analysis disciplines.

##### 3.1.1 *Analysis Model Concepts*

A fundamental new approach was taken with respect to the aeroelastic and aerodynamic disciplines. The idea is that there are three kinds of models: aerodynamic, structural and aeroelastic. The aeroelastic model is a merging of one aerodynamic and one structural model. There are three kinds of analyses: aerodynamic analyses which operate on aerodynamic models; structural analyses which operate on the structural model; and aeroelastic analyses that use the aeroelastic model merged from the appropriate aerodynamic and structural models at some point.

The Solution Control syntax was revamped to illuminate this change in viewpoint. For example, the aerodynamic data is not (in general) computed due to the presence of an aeroelastic discipline. Instead, the user calls out the aerodynamic analyses that are required and the aeroelastic disciplines use these data along with the structural model.

NOTE: There is an inherent asymmetry in the design in that the structural model(s) should be generated in a similar way. However, it is beyond the scope of this effort to address this fundamental inadequacy of the NASTRAN paradigm. Nonetheless, it is important to see the symmetry that drives this new approach, although only the aerodynamic part will be implemented. For example, we can use modal structural models as an example of multiple structural models; for now, however, they must be associated with a single geometry (set of grids/degrees of freedom).

The structural model (of which there will be only one) comes into being in the usual manner--bulk data leading to structural degrees of freedom and stiffness and mass matrices. The aerodynamic and aeroelastic models (of which there will be an unlimited number) are created and named using Solution Control. To support the simplest cases (e.g., the original ASTROS approach) ASTROS continues to "automatically" generate THE aerodynamic model and automatically "use" it in the aeroelastic disciplines as a default. Thus, while the Solution Control syntax becomes verbose in the general case, the simple aeroelastic executions remain relatively simple to invoke.

The idea of model creation and the model management options that are available with the enhancements to CADDB, combined with the hierarchical nature of Solution Control, are used to allow the user to build the aeroelastic model for each subcase of the aeroelastic disciplines. That means, in general, that the structural and aerodynamic models are assembled and combined based on the user's Solution Control commands.

In each aeroelastic subcase, the user identifies the models and the condition(s) to be solved. The aerodynamic model needs to be built first using one of two approaches: an ASTROS SAERO discipline or some external process that creates a steady aerodynamic model on a CADDB database. The ASTROS SAERO discipline has as a general feature, the ability to archive the resulting model to a CADDB database. The aeroelastic discipline FTRIM has as a general feature, the ability to combine disjoint constituents of the steady aerodynamic model into a single whole for use in the current subcase. This addresses the "alternate" or "augmented" aerodynamic model.

### 3.1.2 New Steady Aeroelastic Analysis Disciplines

#### 3.1.2.1 SAERO, Static Aerodynamic Matrix Generation

SAERO <sym> ( METHOD=<meth>, MACH=<mach>, MODEL=<name> , AIC=<option>)

Defines the static aerodynamic matrix generation for an aerodynamic model. By default, the output is GROUPed with the MODEL name on the RUNDB. An ARCHIVE AERO command can store the model on another DB for later reuse.

<sym>: SYMMETRIC, ANTISYMMETRIC or ASYMMETRIC  
<option>: SYMMETRIC, ANTISYMMETRIC, ASYMMETRIC, or BOTH  
<meth>: USSAERO or QUADPAN  
<mach>: Mach Number  
<name>: PACKET name of the AERO model input Packet (this option allows multiple input streams in a single run!)

NOTE: METHOD controls the paths of integration with aerodynamic theories. At this time, USSAERO and QUADPAN are domain aerodynamic codes in ASTROS. However, METHOD really implies linear theory type-implementation. In the case of USSAERO, the implication of flat panel, centerline symmetric geometry with centerline-symmetry-type boundary conditions is assumed for capability integration. For the case of QUADPAN, the implication of three-dimensional geometry as well as symmetric or asymmetric model and boundary condition symmetry is assumed for capability integration.

A new option was added to the SAERO discipline. There is now an AIC option that directs the formation of AIC matrices:

SAERO ( ..., AIC - <OPTION>, ..., )

where <options> may be any ONE of:

Table 3-1 Options for AIC Boundary Conditions in QUADPAN

<option> >	Description
NONE	No AIC matrix
ANTI	Antisymmetric AIC (assuming model is laterally symmetric)
ASYM	Asymmetric AIC (assuming model is asymmetric)
SYMM	Symmetric AIC (assuming model is laterally symmetric)
BOTH	Both symmetric and antisymmetric AICs (assuming model is laterally symmetric)

BOTH is the default value. If the AIC option doesn't conform to the model's geometric symmetry, downstream processing must respond to the option to make sense. For example, if anything other than NONE is requested, and the model is asymmetric, the ASYM option will be coerced by QUADPAN or USSAERO. If ASYM is requested, and the model is laterally symmetric, the problem is more complex. In

USSAERO, ASYM is coerced to BOTH all the time. In QUADPAN, a full geometric model should be coerced (just like an asymmetric onset flow).

### 3.1.2.2 FTRIM, Flexible Static Aeroelastic Trim Solution

FTRIM <sym> ( TRIM=<sid>, MODEL=<name>, DCON=<sid> )

Defines the flexible static aeroelastic trim solution using the structural model's mass and stiffness matrix.

<name>:           group name of the aerodynamic model created by the model assembly commands.

FTRIM operates much in the same manner as SAERO did in the prior ASTROS paradigm with the constraint options, although DCON is the only option listed here. The only other option not listed in the above statement is for trim optimization. Trim optimization is implied when a TRIMOPT bulk data card is included with the same <sid> as the TRIM <sid> from case control.

## 3.2 AERODYNAMIC AND AEROELASTIC MODEL ASSEMBLY

### 3.2.1 GROUP Entity Concepts

The new discipline level solution control commands (discussed in Section 3.1) are used to develop the aeroelastic model in a piece-wise fashion from conveniently organized groups of aerodynamic and aeroelastic data. For instance, an aeroelastic solution requires computation of 1) basic aerodynamic data (SAERO discipline), 2) aeroelastic splines, 3) flexible stability coefficients and flexible load increments, and 4) the trim solution (FTRIM discipline). This building block approach for assembly of the aeroelastic model lends itself to a general methodology for replacing or combining run-time aerodynamic and/or aeroelastic data groups with archived data groups. This concept is previously discussed in an overview in Section 1.2.1.

### 3.2.2 Aerodynamic and Aeroelastic Data Groups

Aerodynamic and aeroelastic data are segregated into logical groupings as shown in Table 3-2. The first two group types (QUADPAN and USSAERO input packets) are inputs to the two available ASTROS aerodynamic methods of the SAERO discipline. The next three group types (STDYGEOM, RIGDALOD, and AIC) are either outputs of the available ASTROS aerodynamic methods (run-time or archived from previous runs) or *alternate* data created from some external method. In either case, the aerodynamic model is assembled from groups of aerodynamic data that exist on either the run-time database and/or alternate database(s) of archived data. The RIGDSLOD group is defined by the user through the new SLPARM and current static load bulk data cards. It may be archived from previous runs in similar function as the STDYGEOM, RIGDALOD, and AIC groups. The subsequent aeroelastic discipline, FTRIM, requires a combination of the assembled aerodynamic model and the SPLINES group and computes as output the FLEXLOAD group.

Table 3-2 ASTROS Aeroelastic Solution is Assembled From Aerodynamic and Aeroelastic Data Groups

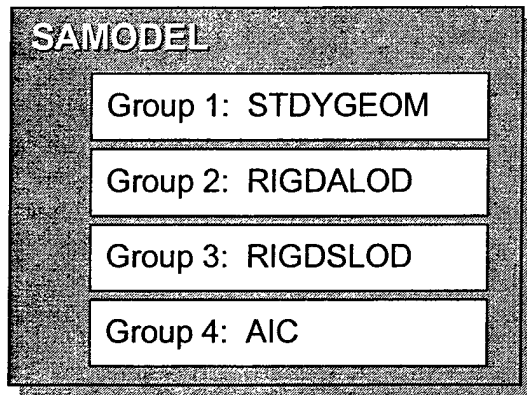
Group Type	Contents
QUADPAN Input Packet	<ul style="list-style-type: none"> <li>• geometry input</li> <li>• control surface definition</li> </ul>
USSAERO Input Packet	<ul style="list-style-type: none"> <li>• geometry input</li> <li>• control surface definition</li> </ul>
STDYGEOM	<ul style="list-style-type: none"> <li>• aerodynamic model geometry</li> </ul>
RIGDALOD	<ul style="list-style-type: none"> <li>• trim parameter rigid actual aerodynamic pressure vectors (not increment)</li> </ul>
AIC	<ul style="list-style-type: none"> <li>• symmetric AIC matrix</li> <li>• antisymmetric AIC matrix</li> <li>• asymmetric AIC matrix</li> </ul>
SPLINE	<ul style="list-style-type: none"> <li>• rigid load spline</li> <li>• slope spline</li> <li>• aeroelastic load increment spline</li> </ul>
RIGDSLOD	<ul style="list-style-type: none"> <li>• user defined rigid structural load (e.g. thrust load, distributed actuator load, ..)</li> </ul>
FLEXLOAD	<ul style="list-style-type: none"> <li>• trim parameter flexible load and deflection increment vectors</li> </ul>

For ASTROS discipline purposes, these groups are collected into a master group called a MODEL. For instance, ASTROS runtime FTRIM discipline subcases have associated with it a unique MODEL group that specifies the set of entities associated with the MODEL. However, members of a particular MODEL may also be members of other MODELS (i.e., the same STDYGEOM group may be used by more than one model). Two formalized MODEL groups have been established as depicted in Figure 3-1. A unique SAMODEL will be established for each SAERO subcase while a unique SAEMODEL will be established for each FTRIM subcase.

The steady aerodynamic model (SAMODEL) includes attributes traditionally thought of as aerodynamic with the exception of the RIGDSLOD group. The STDYGEOM, RIGDALOD, and RIGDSLOD groups will be discussed in the following paragraphs. The AIC group contains information on the aerodynamic influence coefficient matrices. A model may contain symmetric, antisymmetric and asymmetric AIC matrices, and it may contain matrices for multiple Mach numbers. Therefore in use, a model may appear in multiple boundary conditions and subcases once it is either imported or created at runtime.



### ***Steady Aerodynamic Model***



### ***Steady Aeroelastic Model***

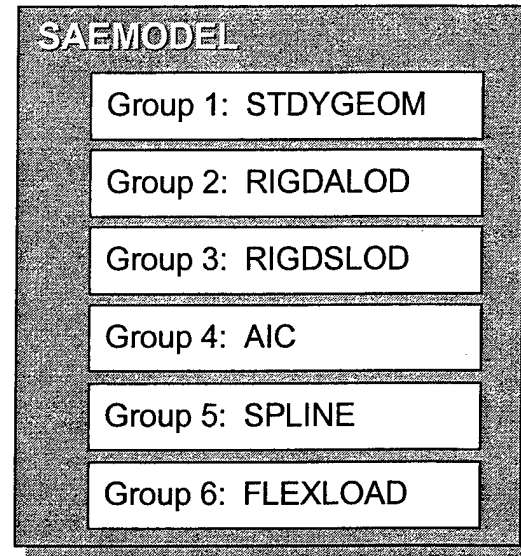
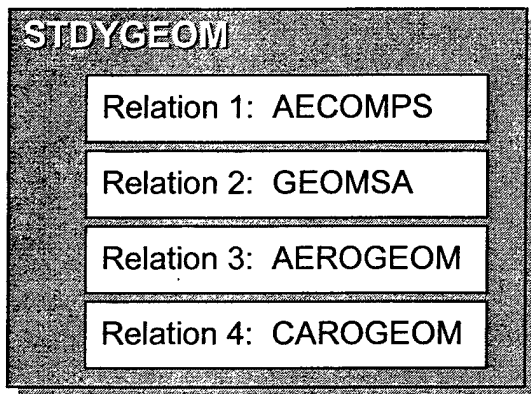


Figure 3-1 Steady Aerodynamic and Steady Aeroelastic Model Groups

The STDYGEOM group (illustrated in Figure 3-2) consists of the traditional ASTROS relations that define aerodynamic models. The addresses of these relations are stored in this group. By grouping the data, a single model geometry may be used with any RIGDALOD group to integrate rigid pressure data from many sources and at many Mach numbers. Future ASTROS enhancements could include using this geometry for both steady and unsteady aerodynamic analysis. Current restrictions however require separate definitions for steady versus unsteady discretizations.

### ***Steady Aerodynamic Model Geometry***



Aerodynamic Component Definition

Aerodynamic Panel Geometry ID

Aerodynamic Panel Corner Points

Aerodynamic Panel Connectivity

Figure 3-2 STDYGEOM - Model Geometry & Connectivity

The new SAERO and FTRIM solution control commands (discussed in Section 3.1) enable the user to execute aerodynamic and aeroelastic analyses that can take advantage of this formalized set of data groups (refer to Table 3-2). Aerodynamic and aeroelastic models are either assembled or modified (see Subsection 3.2.3) prior to these basic aerodynamic/aeroelastic discipline level commands. Models can be comprised of entirely run-time data, archived data, or some combination thereof. For instance, a trim

analysis scenario might include development of aerodynamic geometry and AIC matrices using the available ASTROS aerodynamic method, QUADPAN, and inclusion of archived CFD derived rigid pressure vectors and perhaps even wind tunnel derived pressure vectors. Figure 3-3 illustrates the final pressure vector that would be created for aeroelastic analysis. In this case, the user specifies 1) execution of the SAERO discipline to generate STDYGEOM, RIGDALOD, and AIC output groups from the QUADPAN input packet, 2) assembly of the modified aerodynamic model from run-time QUADPAN groups (STDYGEOM and AIC) and archived CFD group (RIGDALOD) and Wind Tunnel group (RIGDALOD), and 3) execution of subsequent aeroelastic disciplines.

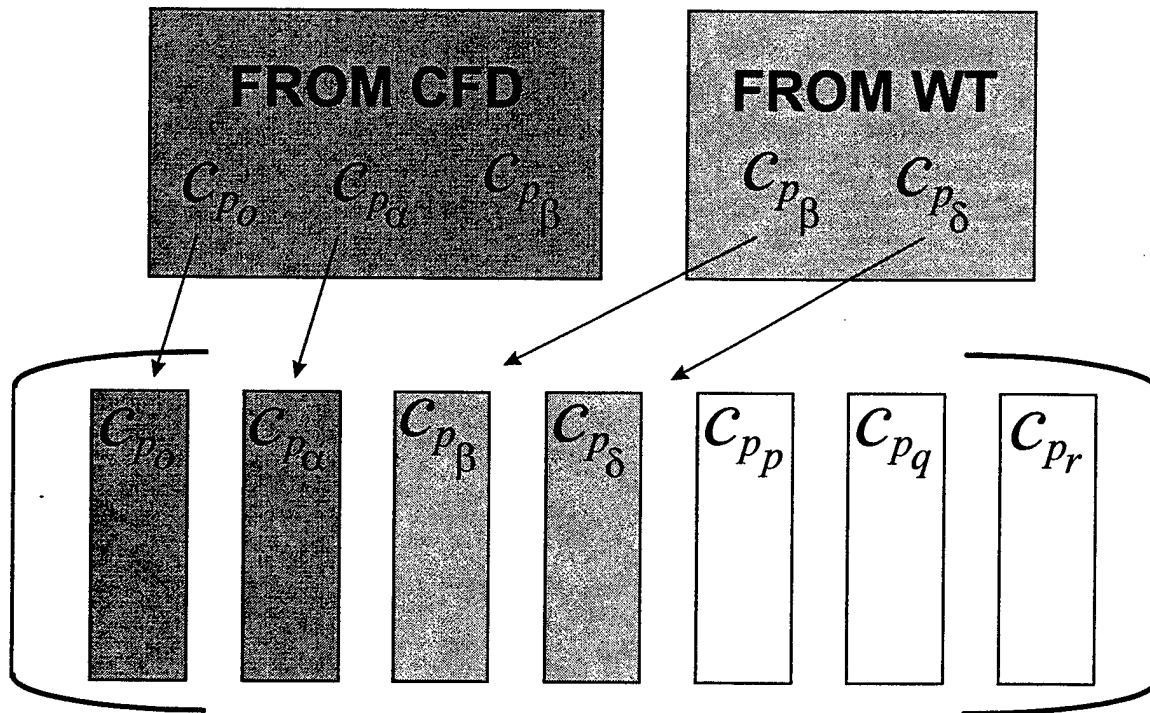


Figure 3-3 Overlay Base Aerodynamics, CFD, Wind Tunnel As Best Aerodynamics Using Type RIGDALOD

The RIGDALOD group is depicted in Figure 3-4. This group contains the table of contents of relations and matrices associated with actual full rigid aerodynamic pressure data. As such, this data is not restricted to linear theory (See Subsection 3.3.1). An important distinction in the AANDE paradigm from the original ASTROS paradigm is the database storage and usage of rigid aerodynamic pressure data. In the original ASTROS paradigm, pressure data was created and stored as increment (or unit) data for each control parameter (e.g.  $\alpha$ ,  $P$ ,  $\delta_a$ ). In the AANDE paradigm, rigid aerodynamic pressure data is stored as whole or *actual* data (e.g. pressure at  $\alpha = 12.5$  degrees, pressure at  $P = 200$  deg./sec, ..). A basis pressure vector is defined in each RIGDALOD group (see Subsection 3.3.1.1). The vector defines the pressure state at a specified set of angles and rates. This new paradigm allows the ASTROS user generality in defining pressure states from various sources. Ensuing logic in the model manipulation creates the necessary incremental pressure vectors ASTROS needs to perform linear aeroelastic analysis. This paradigm also allows for future growth in ASTROS including nonlinear iterative maneuver trim analysis.

The ASTROS user may modify individual data groups such as in Figure 3-3 by creating combinations from two or more existing run-time and/or archived data groups. Extending the analysis scenario of the previous paragraph, the analyst may also have an aerodynamic influence coefficient matrix created from a high order computation fluid dynamics basis. The AIC group from the CFD basis may be assembled with the new RIGDALOD group and the original STDYGEOM group. *The only requirement for group manipulations such as described is that the geometry of the combined groups must be compliant.*

## Rigid Aerodynamic Parameter Load Vectors

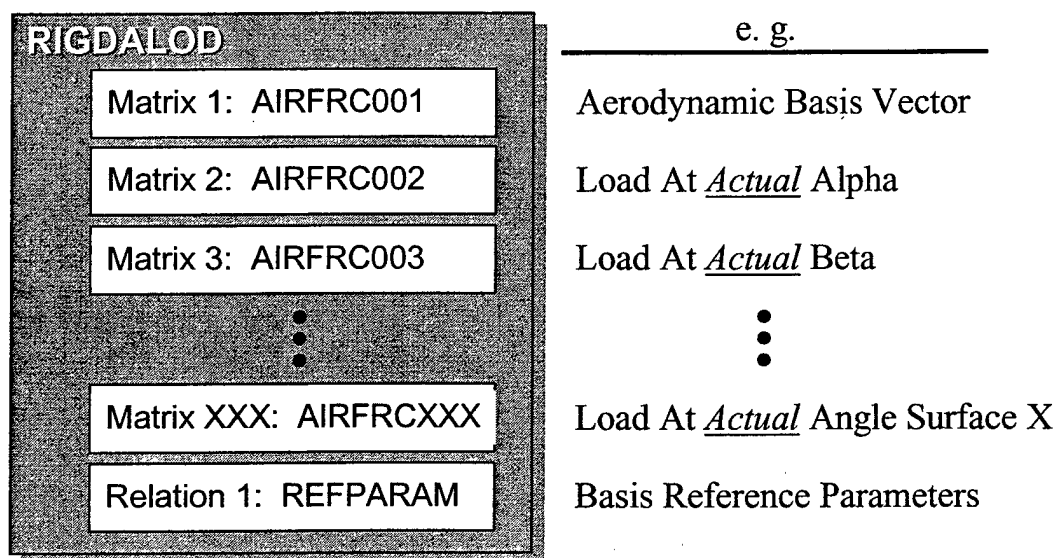
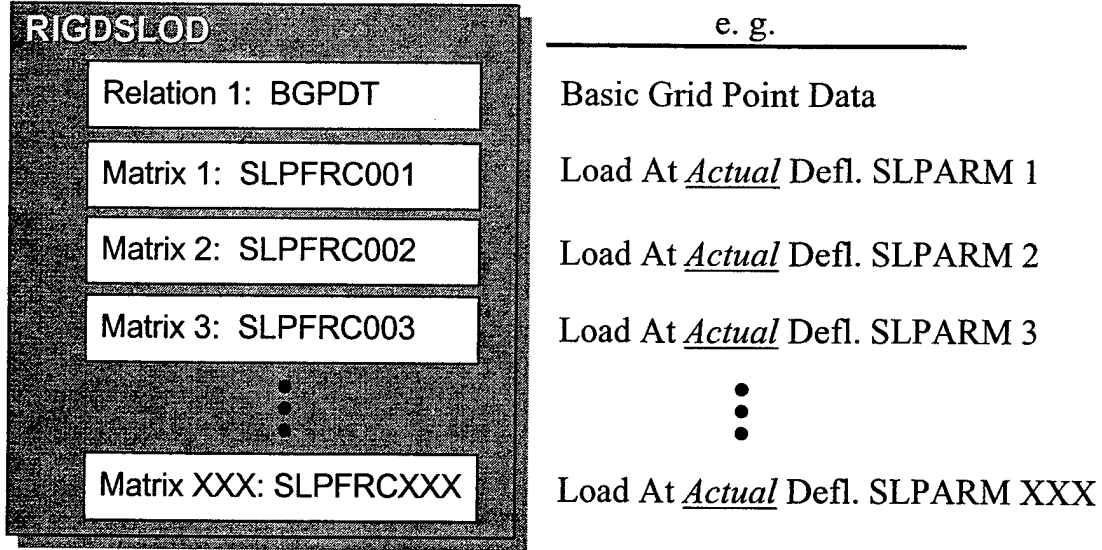


Figure 3-4 RIGDALOD - Rigid Aerodynamic Loads

The last group mentioned in the steady aerodynamic model is a new feature developed under the AANDE program. The RIGDSLOD group contains the addresses and table of contents of user defined loads (see Subsection 3.5.1.2). These loads are created from ASTROS' STATICS load parameters such as FORCE, MOMENT, GRAV, and TEMP. The loads are created in the structural domain, and they can be used to add augment the aerodynamic simulation. For instance, force increments from a wind tunnel model may be used to simulate aerodynamic store loads. Another example of this capability is the development of force actuation simulations typifying adaptive materials in smart structures. As shown in Figure 3-5, a new ASTROS Bulk data entry has been created called SLPARM. In like manner to the RIGDALOD group, the load vectors in RIGDSLOD are stored as actual loads referenced to a load parameter magnitude.

A steady aeroelastic model (SAEMODEL) is created by the user through model assembly commands or automatically from specification of steady aerodynamic model in an FTRIM discipline. Note that the steady aerodynamic model is a subset of the steady aeroelastic model. The two groups, SPLINE and FLEXLOAD are added to the aerodynamic model in the creation of the aeroelastic model. The SPLINE group is created during the processing of splines defined in the traditional fashion of ASTROS' bulk data entries. A SPLINE group is a permanent ASTROS entity. That is, once it is created, it is never purged from the ASTROS database and may be reused. The FLEXLOAD group, however, is recreated within each aeroelastic solution.

## Rigid Structural Parameter Load Vectors



(SLPARM : User-Defined Structural Load Parameter)

Figure 3-5 RIGDSLOD - Rigid Structural Loads

Design of the FLEXLOAD group (Figure 3-6) is discussed in the Software Design Guide (Ref. 2). The group contains addresses and a table of contents of results from unique linear aeroelastic solutions. The deflections and flexible aeroelastic loads are collected for incremental parameters and used in trim solutions to compute component loads (e.g. bending moments, shear, and torque - BMST).

## Flexible Aeroelastic Solution Vectors

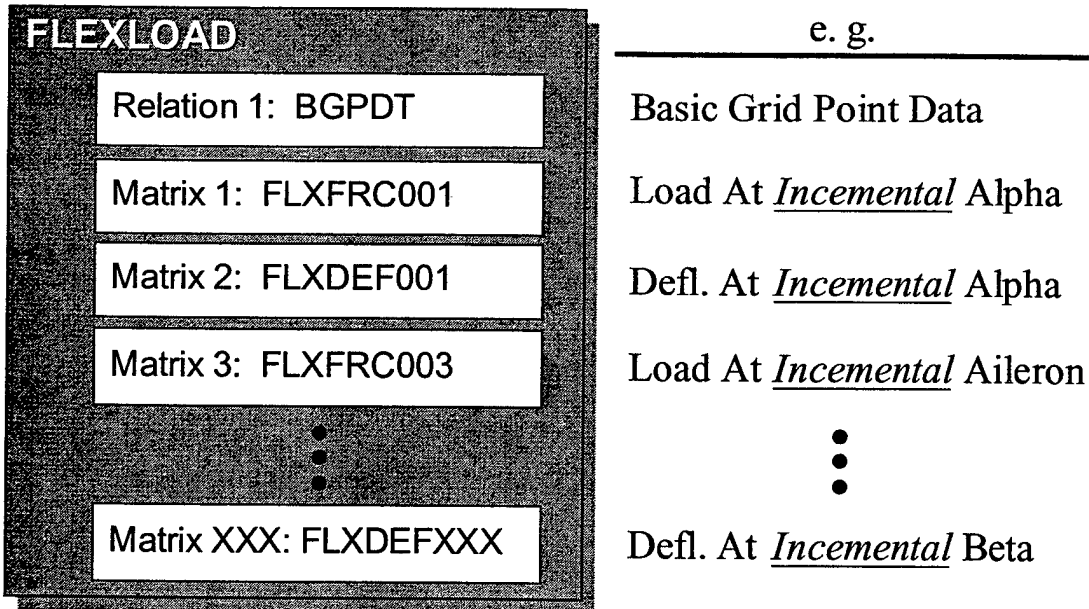


Figure 3-6 FLEXLOAD Group Computed At Each Subcase

When fully implemented, an ASTROS user will be able to create a steady aeroelastic model specifying a previously computed FLEXLOAD group and compute linear trim without re-computation of the aeroelastic solution. At the completion of AANDE, no option is provided to the ASTROS user to save a unique FLEXLOAD group. Only the FLEXLOAD group from the most recent aeroelastic solution will remain on the database.

Model assembly commands (to be discussed in Subsection 3.2.3) are used to IMPORT, ARCHIVE and OVERLAY any of the formalized data groups defined above (refer to Table 3-2). The ASTROS user is therefore provided with flexibility and generality to modify run-time data or provide alternate data to the aerodynamic/aeroelastic solution sequence. Some of the inherent capabilities and benefits of the model assembly solution control commands include:

- multiple aerodynamic models
- alternate methodologies
- combination of methodologies
- combination of run-time and archived data
- alternate or modified load data
- alternate AIC matrices
- alternate splines

The model assembly commands extend the aeroelastic analysis capability far beyond the original ASTROS methods and enable straightforward integration with external methodologies.

### ***3.2.3 Model Assembly Concepts***

Solution control model assembly commands were developed in order to assemble the aerodynamic and aeroelastic models for subsequent use by the discipline level commands. The aerodynamic and aeroelastic models are defined at the subcase level; therefore, a new hierarchical level was inserted in solution control between the BOUNDARY and DISCIPLINE levels.

```
SOLUTION
  OPTIMIZE/ANALYZE
  BOUNDARY
    MODEL_ASSEMBLY_COMMANDS
      DISCIPLINE MODEL=model_name
  END
```

Notice that each discipline level command requires the specification of only a single model\_name rather than a collection of model components. This removes redundant specification of model assembly commands for disciplines that use the same model. However, redundant model assembly commands are still required for the existing ASTROS paradigm of one model and multiple symmetric and antisymmetric boundary conditions (and even the case of both OPTIMIZE and ANALYZE sub-packets).

Four basic commands provide sufficient generality to assemble aeroelastic models from a combination of existing and archived data groups.

1. IMPORT
2. ARCHIVE
3. OVERLAY
4. ASSEMBLE

An example usage of these commands and the new discipline commands is provided in Subsection 3.2.3.4 after the description of the ASSEMBLE command.

### 3.2.3.1 Archiving & Importing

```
IMPORT <group_type group_name FROM logdb AS new_group_name  
ARCHIVE <group_type group_name TO logdb AS new_group_name
```

<group\_type> - defines type of GROUP and the rules for it's contents  
(SAMODEL, STDYGEOM, RIGDALOD, AIC, SPLINE ...)

<group\_name> - old or existing name of a GROUP to be imported or archived.

<logdb> - logical name of the source or target CADDDB database

<new\_group\_name> - name of the new GROUP output of the process.

The 'AS' part of the IMPORT command allows groups of the same name on disparate databases to be IMPORTed to the RUNDB database. The IMPORTed groups can then be OVERLAYed to form a new group for model assembly.

### 3.2.3.2 Overlaying

```
OVERLAY <group_type1 group_name1, group_type2 group_name2, ...,>  
AS <newgroup_name> USING TYPE group_type>
```

<group\_type> - defines type of GROUP the rules for it's contents  
(STDYGEOM, RIGDALOD, AIC, SPLINE)

<group\_name> - old or existing name of the GROUP to be imported or archived.

<new\_group\_name> - name of the new GROUP output of the process.

The OVERLAY command joins two or more GROUPs to form a new GROUP. GROUPs are OVERLAYed in pairs, starting with the first pair in the group\_list. The resulting OVERLAY group is then OVERLAYed with the next group\_name in the group\_list, and so on until the group\_list is exhausted. For a given pair, entities from the second group are added to those of the first group unless entities have duplicate identifiers. If duplicate entities and identifiers are encountered, the entity of the first group is replaced by the entity of the second group.

### 3.2.3.3 Assembling

```
ASSEMBLE <model_type>  
FROM <group_type1 group_name1, group_type2 group_name2, ...>  
AS <model_name>
```

<group\_type> - defines type of GROUP the rules on contents

(STDYGEOM, RIGDALOD, AIC, SPLINE)

<group\_name> - name of existing GROUP to be imported or archived.

<model\_name> - name of the new MODEL created by the process.

The ASSEMBLE command creates a model using the GROUP entity. The model is simply a collection of GROUPS that point to other database entities (GROUPS, RELATIONS, MATRICES, and UNSTRUCTURED entities).

### 3.2.3.4 Example Usage of the Model Assembly Commands

Presented in Figure 3-7 is a case where three databases are manipulated to assemble the aerodynamic model desired for a symmetrical flexible maneuver trim simulation. From the commands in this solution sequence, addresses of physical data are made known to the functional modules in ASTROS so that the physical data of a complete aerodynamic model may be assembled on the runtime database.

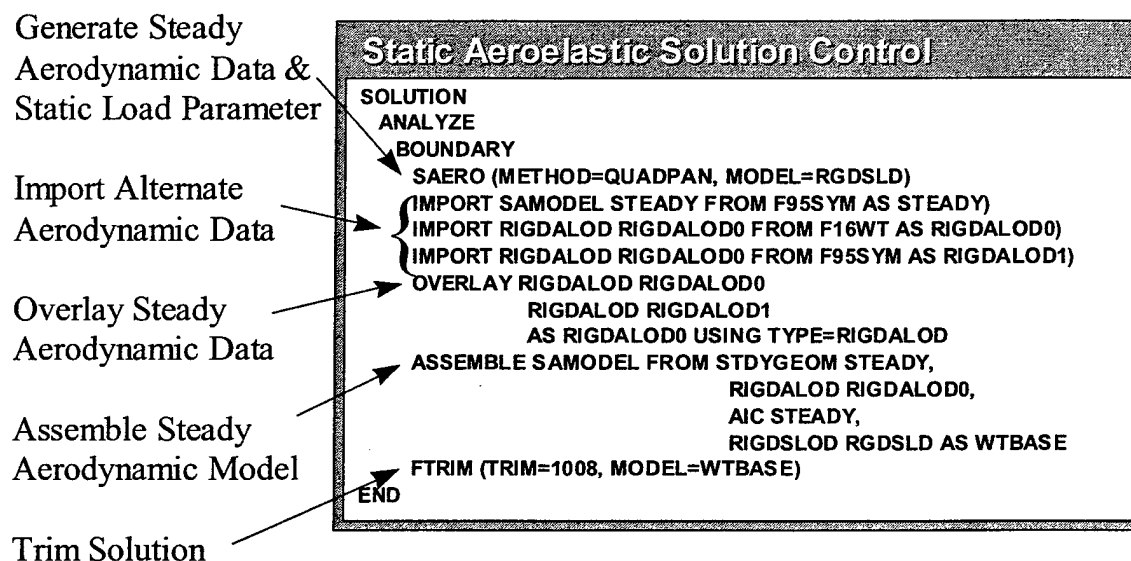


Figure 3-7 Assembly And Trim Solutions of Aeroelastic Equations

The SAERO command allows the generation of a user defined load from the static load parameter capability (discussed in Subsection 3.5.1.2). The data is stored in the ASTROS runtime database in the MODEL name RGDSLD. A steady aerodynamic MODEL named STEADY is imported from the database F95SYM. From that model, the RIGDALOD group - table of contents for rigid aerodynamic pressure data that is named RIGDALOD0 is imported and named RIGDALOD1. The physical aerodynamic data still lies out on the F95SYM database, but its address and table of contents are placed on the runtime database in RIGDALOD1. A third database RIGDALOD is also imported from F16WT and named RIGDALOD0. Similarly, the address and table of contents of the physical aerodynamic data associated with the model in F16WT is stored on the ASTROS runtime database.

The OVERLAY command is used in this case to acquire data from the F16WT database. This data is wind tunnel pressures, and by virtue of the ordering of the RIGDALOD groups and the intersection

of certain aerodynamic parameters in both RIGDALOD groups (e.g.  $\alpha$ ), certain addresses in the table of contents of RIGDALOD0 will be replaced with addresses from RIGDALOD1. Also, by virtue of a union, the new RIGDALOD0 group will contain items from both original groups.

Once these data are known to the runtime database, an aerodynamic model may be assembled. In this case, the geometry (identified by the group STDYGEOM) comes from the MODEL STEADY. The physical data is stored on the F95SYM database, and via the import of STEADY, the functional modules now have the address of all the geometry. Similarly, the AIC group is designated from STEADY. The new aerodynamic model is named WTBASE.

The FTRIM discipline identifies the aerodynamic model for use, and an AEROELASTIC MODEL is formed with this name. In the database, the AEROELASTIC MODEL name will be WTBASESAE. The AEROELASTIC MODEL will look for a SPLINE group named WTBASE since no group is identified in the FTRIM callout. However, a SPLINE group could be identified if the user chose to.

### 3.3 STEADY AERODYNAMIC DATA

Improvements to the basic steady aerodynamic capability occur in the preface segment and are accomplished by incorporating elements of the three-dimensional, true surface aerodynamic software, QUADPAN. The new steady aerodynamics capability generates aerodynamic pressure distributions for user defined control parameters, and matrices of aerodynamic influence coefficients for computation of pressure increments to unit pressure distributions. The USSAERO program was maintained as well under the AANDE program and therefore was modified to integrate the new aerodynamic data structures and group concepts. The QUADPAN aerodynamic solution is available as an option to the existing USSAERO aerodynamic solution and, therefore, serves to complement existing flat panel aerodynamic capability.

The steady aerodynamic as developed provides a completely general approach to include user-specified aerodynamic geometry, AIC matrices, and/ unit pressure distributions *alternate* to the domain ASTROS capabilities. This extension provides access to externally computed aerodynamic solutions, thereby providing the user community a gateway to other established aerodynamic analyses and processes. Further, this extension provides access to wind tunnel and computational fluid dynamics (CFD) pressure data as an alternative to the default ASTROS computed pressure data.

This section describes the basic data structures of all aerodynamics in ASTROS under the AANDE program. A discussion of the integration of QUADPAN and QUADPAN in general is provided. Finally, some discussion is provided on the development of an *alternate* steady aerodynamic database.

#### 3.3.1 Steady Aerodynamic Data Structures

The steady aerodynamic data structures were generalized to provide a common format for the import and archive of steady aerodynamic data. Two important concepts used in the generalization are aerodynamic basis vectors and provisions for nonlinear aerodynamic data. Aerodynamic basis vectors are pressure vectors representative of the nominal condition from which incremental pressure vectors will be computed. The basis vectors provide for the use of nonlinear aerodynamic data, and additional provisions were made that bound the degree of nonlinearity.



### 3.3.1.1 Aerodynamic Basis Vectors

The aerodynamic basis vector generalizes the thickness and camber (THKCAM) aerodynamic load vector in the previous ASTROS paradigm. The THKCAM load vector produced by the USSAERO (Unified Subsonic and Supersonic Aerodynamic Analysis) algorithm represents the aerodynamic loads produced at zero angle-of-attack with all other trim parameters at zero. Additionally, the aerodynamic influence coefficient (AIC) matrix produced by the USSAERO code provides pressure increments from that reference state. The QUADrilateral PANel Method (QUADPAN), on the other hand, is capable of producing a reference aerodynamic loading and corresponding AIC matrix at an arbitrary combination of onset flow conditions and control surface positions. In order to integrate QUADPAN and provide for import of alternate aerodynamic data, the aerodynamic basis vector concept was introduced.

Aerodynamic basis vectors represent the reference aerodynamic loading condition for the basis configuration. The basis, or nominal reference, configuration comprises a combination of onset flow and trim parameter deflections from a subset of all the trim parameters. The incremental aerodynamic loads due to each trim parameter are referenced to the basis aerodynamic load. For example, the aerodynamic loading due to a unit angle-of-attack would be calculated as follows.

$$\mathbf{P}_\alpha = \frac{\mathbf{P}((\alpha_{ref} + \alpha_{incr}), \beta_{ref}, P_{ref}, Q_{ref}, R_{ref}, \delta_{ref}) - \mathbf{P}(\alpha_{ref}, \beta_{ref}, P_{ref}, Q_{ref}, R_{ref}, \delta_{ref})}{\alpha_{incr}}$$

where

$$\mathbf{P}(\alpha_{ref}, \beta_{ref}, P_{ref}, Q_{ref}, R_{ref}, \delta_{ref}) = \text{aerodynamic basis vector}$$

In this manner, aerodynamic basis vectors provide a point of reference for the aerodynamic loads and stability derivatives as increments from the basis configuration.

The introduction of the aerodynamic basis vector concept requires that the aerodynamic data generated by the steady aerodynamic methods be provided to ASTROS as the actual aerodynamic loads for the specified parameter settings including the basis vector. This is a change from the previous ASTROS paradigm in which the aerodynamic load vectors represented the load *increment* from the THKCAM reference load vector rather than the *actual* load for the specified trim parameter settings. An additional requirement is that all non-zero trim parameters must be identified for the reference state. An important benefit of these enhancements is that aerodynamic data may be generated near the trimmed flight condition and thereby reduce errors due to extrapolation of unit data.

### 3.3.1.2 Nonlinear Aerodynamic Data

Provisions for nonlinear aerodynamic data have been incorporated into the AANDE version of ASTROS. Each rigid aerodynamic pressure vector is identified by Mach number and up to three trim parameters. Using these identifiers, a three-level hierarchy of nonlinear aerodynamic data can be created. In this hierarchy, the first parameter identifier is the primary parameter and the second and third parameter identifiers are secondary parameters. The primary parameter is responsible for first order effects and the secondary parameters are responsible for first and second order effects. Aircraft attitude parameters would be considered as primary parameters. Control surface deflection parameters would be considered as secondary parameters. Secondary parameters can produce first order effects when operating independently. Second order effects are the interaction effects of two secondary parameters acting together.

For linear analysis, only the first, or primary, parameter is used. An individual rigid aerodynamic load vector is present for each trim parameter contributing to the aerodynamics. The first parameter identifies the trim parameter and the second and third parameter identifiers are blank. First order

incremental aerodynamic loads due to each trim parameter are calculated as shown in the example in the previous section. This is the current implementation in the AANDE version of ASTROS.

This implementation, along with the alternate aerodynamic data import and aerodynamic basis vector capabilities, provides a mechanism by which nonlinear aerodynamic data can be used in the aeroelastic analysis. Aerodynamic data from nonlinear sources, such as wind tunnel or Computational Fluid Dynamics (CFD) data, can be incorporated in the enhanced ASTROS as alternate aerodynamic data. By providing alternate aerodynamic data at a reference state near the trimmed solution and at parameter perturbations about that reference state, a linearized solution may be obtained.

For nonlinear analysis, the secondary parameters would be used to calculate first and second order effects. For example, the change in control surface effectiveness for varying values of angle-of-attack and angle-of-sideslip could be included in the analysis through the aerodynamic data. One could even include the interference effects of two control surfaces acting together. Although this capability has not been implemented, it is envisioned to operate in the following manner.

Arbitrary nonlinear aerodynamic pressure vectors can be generated from the discrete nonlinear aerodynamic pressure vectors using a linear combination approach. Aerodynamic load vectors at the desired parameter values are interpolated from the discrete data. These data sets are combined to form an arbitrary data set as follows:

$$\begin{aligned}
 P(p_1, s_1, \dots, s_n) = & P(p_1) \\
 & + \sum_{i=1}^n [P(p_1, s_i) - P(p_1)] \\
 & + \sum_{i=1}^{n-1} \sum_{j=i+1}^n \left\langle \begin{array}{l} P(p_1, s_i, s_j) - P(p_1) \\ -[P(p_1, s_i) - P(p_1)] \\ -[P(p_1, s_j) - P(p_1)] \end{array} \right\rangle
 \end{aligned}$$

where  $p_1$  is a primary parameter and  $s_1, \dots, s_n$  are secondary parameters. The first term on the right hand side represents the primary parameter first order effect, the single summation term represents the secondary parameter first order effects, and the double summation term represents the secondary parameter second order effects.

Incremental aerodynamic loads due to each trim parameter can be calculated using a finite difference approach. These piece-wise linear incremental aerodynamic loads can be used in the aeroelastic equations in same manner as the existing system. An outer convergence loop will iterate until the aeroelastic solution converges.

### 3.3.2 QUADPAN Aerodynamic Method

QUADrilateral PANel Method (QUADPAN) is a surface panel code developed for the aerodynamic analysis of complete aircraft. It is based on the linearized equation of inviscid, irrotational (potential) flow (Prandtl-Glauert equation) and requires only a surface, rather than a volume grid. It is applicable in the subsonic or supersonic speed regimes (but not transonic or hypersonic). It is limited to the analysis of attached flow, where the vorticity is confined to a wake sheet derived from the Kutta condition.

Its capabilities include:

- Full or half model geometry
- Symmetric/antisymmetric or asymmetric capability
- Surface pressure distribution
- Force and moment coefficients
- Longitudinal/Lateral stability derivatives
- Simulated (transpiration) control surface deflection
- Propeller slipstream effects
- Engine inlet and exhaust simulation
- Aerodynamic Influence Coefficient (AIC) matrix

The rigid air loads are computed at the center of each quadrilateral element and are perpendicular to the true aircraft surface. The Aerodynamic Influence Coefficients (AIC) should be regarded as the flexible increment to the rigid loads for the specified geometry and flight conditions. The local rotation axis for the AIC is the plane formed by the free-stream velocity vector and unit surface normal vector.

The following paragraphs provide an overview of capabilities, theory, and modifications for integration in ASTROS, and guidelines for modeling in QUADPAN. Also provided is some description of QUADPAN input and output as integrated in ASTROS. Details of QUADPAN input are provided in User's Document for AANDE (Ref. 12).

### **3.3.2.1 An Introduction To QUADPAN**

QUADPAN is a computer program developed for the aerodynamic analysis of steady subsonic potential flow about arbitrary aircraft configurations.

- Surface pressure and velocity distributions.
- Force and moment coefficients.
- Longitudinal/lateral stability derivatives.
- Ground and wall (wind tunnel interference) effects.
- Simulated deflection of control surfaces.
- Flow field survey - pressure, velocity, and streamline direction at arbitrary points in the flow field.

The program is intended for detailed aerodynamic analysis of complete aircraft configurations with arbitrary onset flows in flight regimes where there are no strong viscous, transonic, or free-vortex effects.

### **BASIC OPERATION OF QUADPAN**

The code is an integrated program that performs three functions: input and geometry generation, calculation of the flow field, and output of the generated data.

#### **Input and Geometry Generation**

QUADPAN requires as input a complete geometric description of the external surface of the configuration. Onset flows are specified as a combination of angle of attack, angle of sideslip, and angular velocity of the configuration. Methods are also available for the simplified modeling of inlets, exhausts, and propeller slipstreams.

#### **Calculation of Flow Field**

QUADPAN generates a numerical solution to the Prandtl-Glauert equation (derived by linearizing the potential flow equation) with a panel method technique. The surface of the configuration is discretized

into a lattice of quadrilateral elements, on which source and doublet singularities are placed. Boundary conditions determined from the onset flow conditions are applied at points on the surface elements. The strengths of the sources and doublets are then determined as the solution to a linear system of equations. The velocities, pressures, and forces are determined from the resulting singularity strengths.

### **Program Output**

The output of the program consists of the total forces and moments on the vehicle and the surface velocities and pressures on the entire configuration. The velocity and pressure at arbitrary points away from the body may also be obtained. The output is available in two forms: the standard output designed for human readability, and the punch file designed for post-processing by user developed programs which plot results, calculate loads, perform boundary layer calculations, etc.

## **BASIC CHARACTERISTICS AND LIMITATIONS OF QUADPAN**

### **Geometry**

QUADPAN has virtually unlimited geometric modeling capability. The only strict requirement is that the geometry must consist of a collection of bodies that are closed. A closed body is wetted by the flow domain of interest on either its exterior or interior surface, but not both.

### **Viscosity**

QUADPAN is an inviscid code, with the only allowable viscous effect being the Kutta condition that is applied by attaching fixed vortex wakes to edges where this condition is appropriate. While QUADPAN will calculate the potential flow around any body for any incident flow, the results will be physically meaningful only when the flow remains attached to the body, and the boundary layer is thin compared to the dimensions of the body.

### **Compressibility**

QUADPAN solves the linearized equation for subsonic compressible flow. This equation is strictly valid only when the flow is subsonic everywhere. In practice it is possible to obtain reasonably accurate results as long as the areas of supersonic flow are small and do not have a gross impact on the rest of the flow. Generally, as long as the flow and the flow property of interest do not show strong transonic effects, the results obtained with QUADPAN will be acceptable.

The linearized equation excludes bodies which create large disturbances at high Mach numbers such as very thick shapes or wings at large angles of attack. Lower Mach numbers permit larger disturbances. For incompressible flows (Mach zero), the equation used in QUADPAN is exact and is not limited to small disturbances.

### **Free Vortex Effects**

Since QUADPAN is a linear potential method, it cannot calculate flow fields that are dominated by vorticity that is free to adjust itself to the surrounding flow. Obvious examples are the roll-up of the vortex structure behind wings, leading edge vortex flows, and free shear layers. A more subtle example is the flow associated with trailing edges of wings when large spanwise flows are present. This will be discussed later in more detail.

## **AREAS OF APPLICATION**

The use of QUADPAN is recommended when the following requirements are met:

- The flow conditions and geometry must satisfy the requirements described in the previous.
- The situation must be sufficiently demanding in terms of the complexity of the geometry, the need for detailed surface pressures, or the accuracy required of the answer, that an economical, easy to use flat panel method such as USSAERO is inadequate.
- The configuration must be sufficiently well developed that a complete definition of the surface geometry is available. The strength of QUADPAN is its ability to handle arbitrary 3-D geometries. If satisfactory answers can be obtained without having a full definition of the geometry, then QUADPAN is probably not the code to use. If, for example, the quantity of interest were judged to depend entirely on the platform of the configuration, it would be better to use USSAERO. If, however, the answer is judged to depend on thickness effects, or the interference of complex surfaces, QUADPAN should be used. For example, lateral forces and moments on thick configurations are predicted well by QUADPAN, and are generally not predicted well by flat panel methods.

### 3.3.2.2 User's Guide To The Theory Of QUADPAN

The section outlines the process used to calculate the potential flow field. The methods used to calculate lifting flows and compressible flows are described. Factors affecting the computational cost are discussed, followed by a discussion of the coordinate system used in the program and the basic concepts needed to develop a model. Finally, a summary of theoretical considerations necessary to use the program is provided.

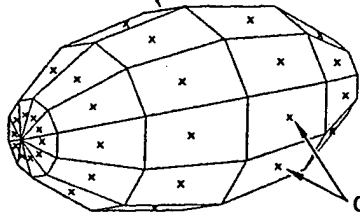
## FORMULATION OF POTENTIAL FLOW PROBLEM

### Basic Panel Method Concepts

QUADPAN belongs to a class of potential flow codes known as panel methods. These codes solve the Prandtl-Glauert equation for linearized compressible flow by subdividing surfaces into panels, or elements. Each element has associated with it singularities, such as sources or doublets, as shown in Figure 3-8. These singularities are solutions of the Laplace equation (or, more generally, the Prandtl-Glauert equation). Since the equation is linear, any combination of these elementary solutions is a solution of the equation. Furthermore, any solution of the equation can be produced by a suitable distribution of singularity strengths over the surface of the configuration being analyzed. In QUADPAN, each element consists of a uniform strength source and doublet distribution, making it a low order panel method.

The strength of the singularities on each element is calculated to make the fluid velocity normal to the surface equal to a prescribed value. This normal flow boundary condition is applied at a point in the middle of each element called a control point. For an impermeable surface, the normal velocity at each control point is zero. The user can prescribe a nonzero value for the normal velocity to simulate the flow into a inlet duct, or small deflections of a control surface.

SURFACE REPRESENTED WITH  
LATTICE OF ELEMENTS



CONTROL POINTS  
ON ELEMENTS

#### LINEAR SYSTEM

FOR  $n$  ELEMENTS, AT CONTROL POINT OF ELEMENT  $i$ :

$$\sum_{j=1}^n A_{ij} \mu_j = b_i$$

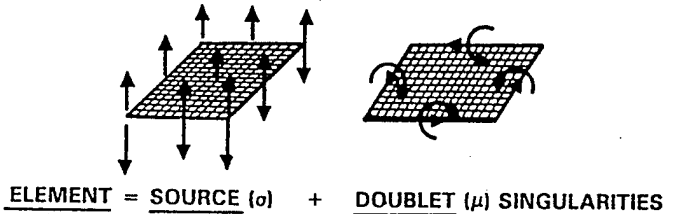
WHERE:

$$A_{ij} = v_{ij}$$

$$b_i = - \sum_{j=1}^n u_{ij} \sigma_j$$

$$\text{WITH } \sigma_j = -\vec{V}_\infty \cdot \hat{n} + v_{\text{NORM}}$$

$u_{ij}, v_{ij}$  ARE SOURCE AND DOUBLET INFLUENCE  
COEFFICIENTS  
 $\sigma_j, \mu_j$  ARE SOURCE AND DOUBLET STRENGTHS  
 $v_{\text{NORM}}$  IS THE PRESCRIBED NORMAL VELOCITY



EQUATIONS OF MOTION:

FOR MACH = 0

$$\vec{V} = \vec{V}_\infty + \vec{v}$$

$$\Phi = \Phi_\infty + \varphi \quad \text{WHERE} \quad \nabla \varphi = \vec{v}$$

$$\nabla \Phi_\infty = \vec{V}_\infty$$

IN FLUID:

$$\nabla^2 \varphi = 0 \quad (\text{LAPLACE EQN.})$$

ON SURFACE:

$$\frac{\partial \varphi}{\partial n} = -\vec{V}_\infty \cdot \hat{n} + v_{\text{NORM}}$$

FOR MACH  $\neq 0$

$$(1 - M_\infty^2) \frac{\partial^2 \varphi}{\partial x^2} + \frac{\partial^2 \varphi}{\partial y^2} + \frac{\partial^2 \varphi}{\partial z^2} = 0$$

(PRANDTL GLAUERT EQN.)

Figure 3-8 Formulation of QUADPAN

#### Reduction To A Linear Algebraic System

The perturbation velocity (or potential) at each control point in the potential flow is the velocity (or potential) induced at that control point by a unit strength singularity on each element, times the strength of that element, summed over all the elements on the surface. Since the normal velocity at each control point is known from the boundary conditions, the strength of the singularities on each element can be found by solving a system of linear equations.

$$[A]\{x\} = \{b\}$$

where the unknown  $\{x\}$  vector is the strength of the singularities on the elements (Fig. 3-8). The  $i,j$ -th element of the  $[A]$  matrix is the potential induced at control point  $i$  by a unit strength doublet singularity on element  $j$ . The  $[A]$  matrix is known as the aerodynamic influence coefficient (AIC) matrix.

### **Boundary Conditions**

The right-hand side vector  $\{b\}$  in the equation is determined from the desired normal velocity on the wetted surface of the body at each control point. In the following discussion, exterior refers to the region(s) occupied (or wetted) by the fluid, and interior refers to the region(s) which are not. The concept of interior and exterior regions should not be confused with the terminology of internal and external flows, which denotes whether the region of space occupied by the fluid is bounded or unbounded. QUADPAN uses the same basic mathematical formulation for internal and external flows with a slight alteration in boundary conditions.

In order to make the method relatively insensitive to the location and shape of the elements, QUADPAN employs an internal potential boundary condition that is equivalent to specifying the normal velocity on the exterior (wetted) surface of the body. By selecting the strength of the source singularities as a function of the prescribed normal velocity distribution, the doublet strength which makes the perturbation potential inside the body equal to zero automatically yields the specified normal velocity on the exterior (wetted) surface of the body.

This method is obtained by applying Green's identity to points inside and outside the body. Derivations may be found in Lamb (Ref. 14) and the Theoretical Report (Ref. 15). The technique of satisfying the boundary condition on the wetted side of the body with a boundary condition on the potential inside the body leads to the requirement that each body be closed, with a well defined exterior surface which is in contact with the fluid, and an interior surface which is not.

### **Determination of Surface Velocity, Pressure, and Forces**

Once the linear system is solved for the doublet strengths, the perturbation potential on the exterior surface of the body is known and is, in fact, equal to the doublet strength at that point. The velocity at each control point is determined from the gradient of the potential on the surface. The derivatives in the gradient are calculated by a numerical technique that uses the potential at the control points surrounding the control point where the velocity is being calculated. To do this, the program must keep track of the elements that surround each element. The effect of this on QUADPAN geometric models is discussed in a following subsection under **Discretization of Surface Geometry into Elements**.

The forces on the configuration are calculated by multiplying the area of each element by the corresponding pressure and summing over all the elements. In potential flow the only drag which can exist is induced drag. Since the drag is the result of summing large pressure forces which nearly cancel, it is typically the least accurate of the forces and moments calculated by the program.

The forces calculated on elements that have a specified nonzero normal velocity (e.g., a panel used to model an inlet face) include the momentum flux due to the fluid that passes through the surface of the element. This must be considered to correctly account for the forces on propulsion installations.

### **Velocity and Pressure Away from the Body: Survey Points**

The velocity at points away from the surface of the body can also be determined once the singularity strengths have been established. Points off the body, where flow information is desired, are called survey points. The influence of each singularity is calculated at the survey points. Multiplying each

influence by the singularity strength and summing over all the elements yields the velocity at the survey point.

Survey points should not be placed too close to the surface of the body for two reasons. First, the boundary condition is satisfied only at the control points, so the velocity elsewhere on the surface is not meaningful. Secondly, the jump in singularity strength that occurs at the edges of elements causes large, incorrect velocities to appear near singularity edges. Therefore, velocity survey points should not be closer to the body than one element length or width.

## **GENERATION OF LIFT: VORTEX WAKES**

A configuration that is to generate lift in three-dimensional flow must have a trailing vortex wake, without which there can be no circulation about the wing. A wing/fuselage geometry with a trailing vortex wake is depicted in Figure 3-9.

### **Representation of Wakes with Fixed Doublet Sheets**

A doublet element of constant strength produces the same flow as a vortex ring around the periphery of the element (see Figure 3-8). The trailing vortex wake and starting vortex needed to produce lift may therefore be simulated by a doublet sheet that extends far downstream. The strength of this sheet must be constant in the streamwise direction, and must vary in strength across the span of the lifting surface to ensure that the flow leaves the wing tangent to the trailing edge. This doublet distribution is approximated by a collection of constant strength doublet elements, with enough of them across the span of the trailing edge to capture the spanwise variation of the circulation around the lifting surface. The edge of the wake that touches the trailing edge of the lifting surface will be referred to as the shed edge. The edge opposite the shed edge represents the starting vortex, and the remaining edges represent the trailing vortices.

### **Calculation of Doublet Sheet Strength**

The strength of each strip of constant doublet strength on the wake is set by the requirement that the flow leave tangent to the trailing edge of the wing. This requirement is met by forcing the potential jump due to the wake to equal the potential jump due to the sources and doublets on the two wing surfaces that form the trailing edge. To assign the wake strength, the program must be told which elements are wake elements and it must determine which elements on the lifting surface shed the wake.



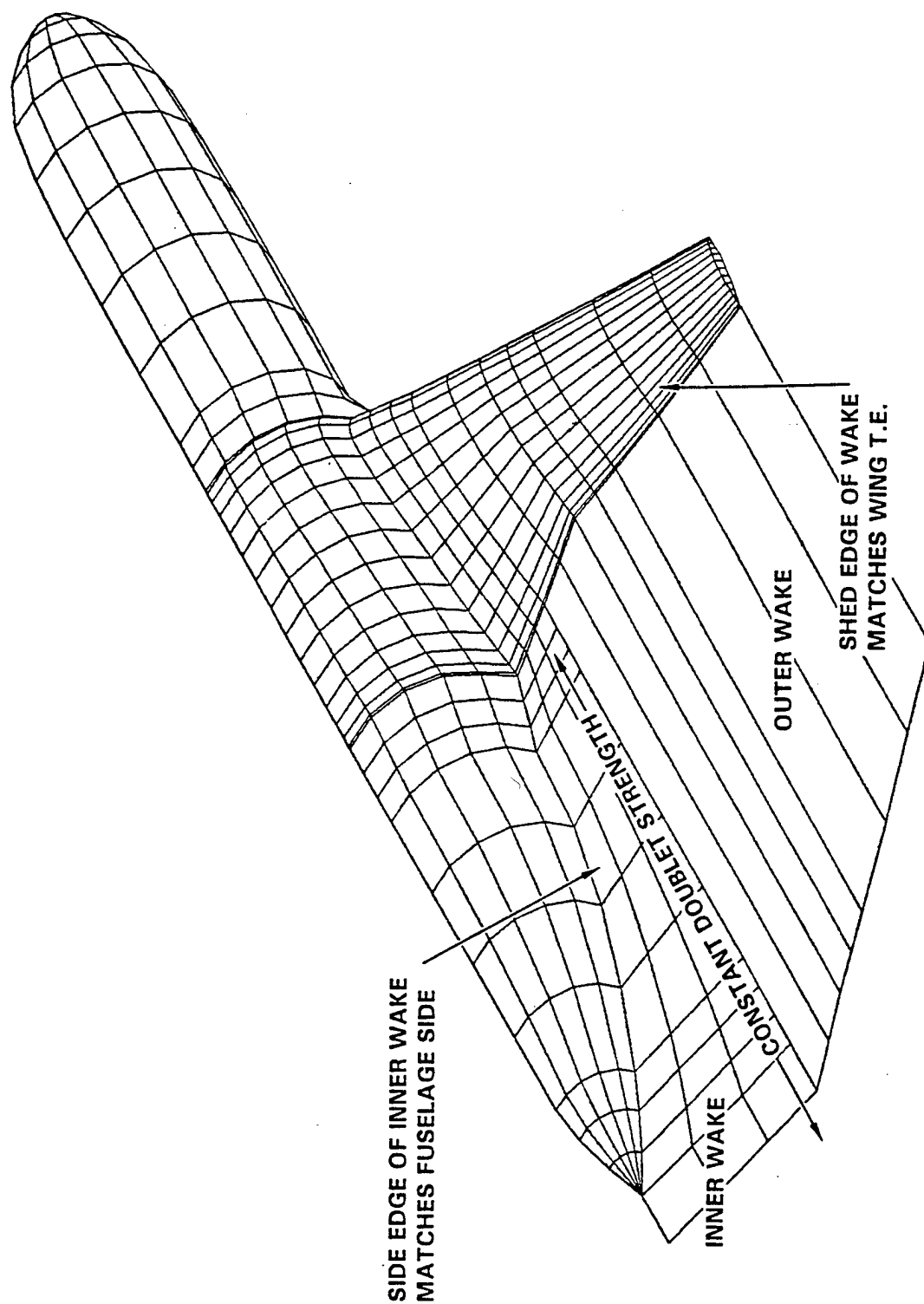


Figure 3-9 Use of Vortex Wake on Lifting Configurations

### **Location and Shape of Wake**

The theoretically correct position of the wake is where the wake is parallel to the flow and has no pressure difference across it. This condition is nonlinear and would greatly increase the difficulty of the calculation. Fortunately, the lift generated by a surface is not strongly affected by the location of its wake, so it is sufficient to put the wake in a fixed location and apply the linear relation described above to establish its strength. It is only necessary that the edge of the wake that represents the starting vortex be about 5-20 body lengths or spans downstream. When modeled this way, the wake is not a stream surface but it does not carry a load unless large spanwise flows are present.

Downstream lifting surfaces may be affected by the location of the wake. Therefore tail downwash, and canard/wing interference may not be accurately calculated, depending on the particular configuration being analyzed and the position chosen for the wake sheets.

Although most lifting surfaces are not appreciably affected by the shape of their vortex wake, there exist situations where the orientation of the wake can be significant. In particular, if the wing has significant flow parallel to the trailing edge, the approximation of a fixed location wake with a linearized Kutta condition breaks down. The spanwise flow causes a force to be induced on the trailing vortices, because they are not aligned with the local velocity. This violates the physical requirement that the wake be force-free, and appears as a mismatch in the pressures on the upper and lower surfaces at the trailing edge. This is illustrated in Figure 3-10 for a wing with a winglet, where a vortex wake has been extended straight behind the trailing edge, not aligned with the free-stream. The trailing edge pressures match well on the inboard wing, where the average spanwise flow is small, but do not match well on the winglet. This is because the dihedral combined with the angle of attack produces a large spanwise flow on the winglet. In this case, changing the wake shape by aligning it with the free-stream direction improved the pressure match at the trailing edge. Changing the wake position to accommodate different onset flow directions results in overly large computer costs in typical use.

### **Shed ("Kutta") Edge of Wake**

The edges of wakes are line vortices. This impacts the use of the program in several ways. There must be no gaps between the shed edge of the wake and the lifting surface which sheds the wake, and the wake and lifting surface elements must line up exactly. Otherwise, the line vortex will induce flow around the trailing edge of the wing, thwarting the establishment of the Kutta condition. This is so critical that the code checks the alignment of these elements. If only small misalignments are detected the code will automatically correct them. If the misalignments are larger, the code will abort the run and describe the location of the error.

The two surfaces which intersect to form the edge of the configuration that sheds the wake must have elements with similar sizes and shapes near the wake shedding edge. In other words, when a lifting surface is viewed normal to its mean surface, the elements on the upper and lower surfaces should appear to coincide. This is an additional result of applying the Kutta condition to a surface modeled with discrete singularity elements.

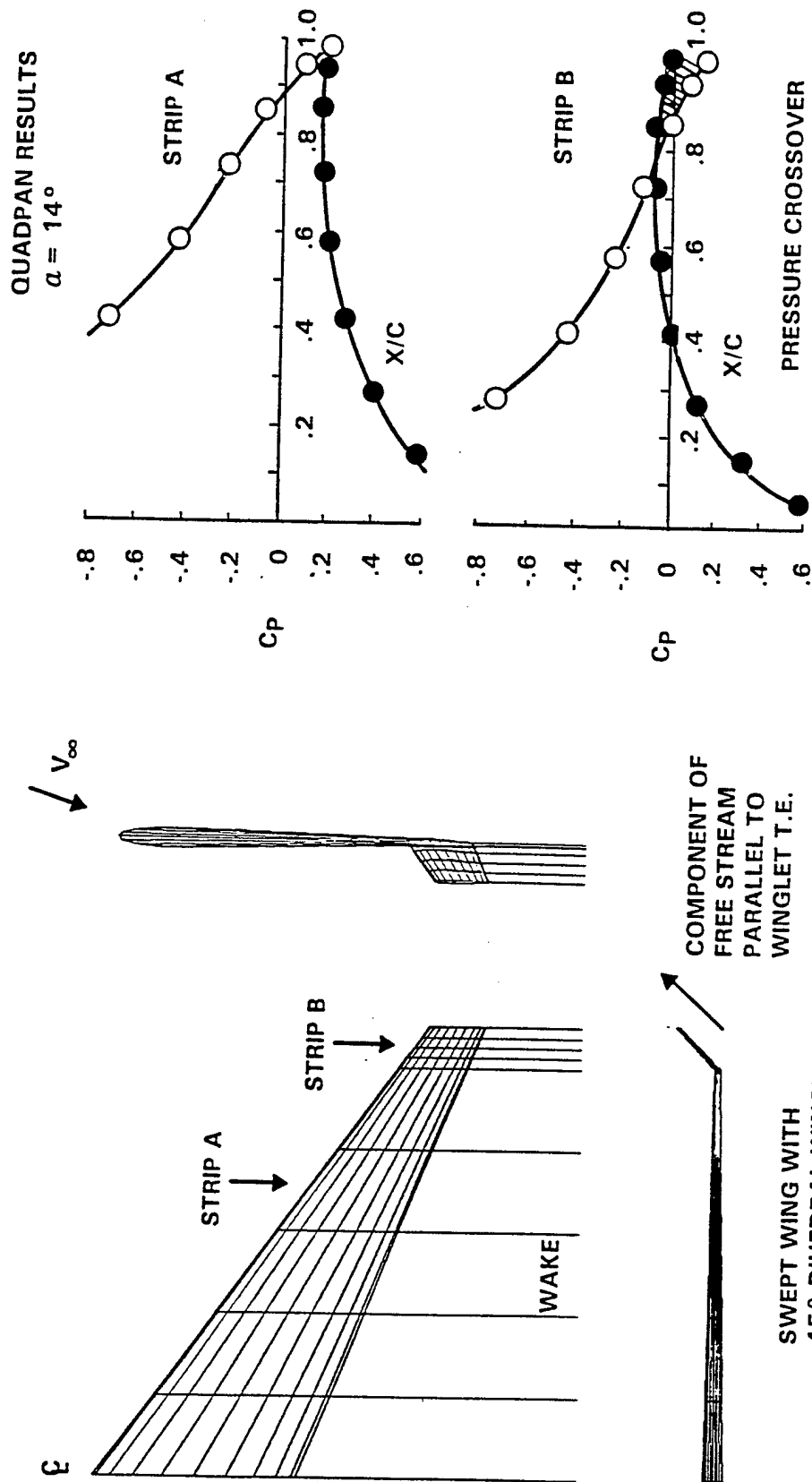


Figure 3-10 Breakdown of Kutta Condition

### Effect of Wakes on Neighboring Surfaces

Since the edges of wakes are line vortices, they must not be brought close to body element control points. Attempting to satisfy a hydrodynamic boundary condition on the body in the presence of the line vortex singularity will contaminate the solution and cause spurious pressures on neighboring surfaces. This aspect of wakes will be discussed in greater detail in 6.5.

As a result of the line vortex that is present at wake panel edges, it is almost always desirable to make the side edges of wakes conform to adjacent surfaces. This can be accomplished by breaking the wake into several elements in the stream direction as well as the cross-stream direction, as shown in Figure 3-9. To facilitate this, the program automatically lumps the wake elements together in such a way that the requirement of constant wake strength in the direction away from the wake shedding edge is satisfied.

### COMPRESSIBILITY

Compressibility effects are treated by solving the Prandtl-Glauert equation. This equation is arrived at by linearizing the compressible flow equations. The appropriate boundary conditions are also linearized. The equation and boundary conditions can be reduced to the equations for incompressible flow by stretching the coordinate system in the free stream direction. This means that the geometry which is actually used to calculate the influence coefficient matrix depends on the Mach number. Hence a unique matrix must be produced for each configuration and for each flight Mach number.

The computational cost can be reduced if the same matrix can be used for different onset (angle of attack, sideslip, etc.). Therefore QUADPAN makes the additional approximation that the coordinate stretching is done in the direction of the X-axis rather than the free stream direction. At moderate angles of attack and sideslip (typically 15 degrees or less) and slender configurations, this approximation has a negligible effect. For nonzero Mach numbers, the results will be invalid if the free-stream is greatly skewed from the X-direction, especially at the higher Mach numbers. This restriction does not apply to incompressible flows.

Another consequence of linearizing the compressible flow problem is that, for compressible flow, the exact normal velocity distribution that is prescribed is not achieved. The linearized boundary condition actually prescribes the first-order mass flux. Therefore, a body that is specified as impermeable will exhibit a leakage velocity that can be large near stagnation points. The leakage increases with Mach number and is entirely absent in incompressible flow.

### COMPUTATIONAL COST

The computational cost of using QUADPAN is made up of two major contributions:

- The cost of calculating and solving the matrix for the linear system. This includes the cost of generating the influence coefficients, constructing the linear system, and solving the set of equations. This is roughly proportional to the cube of the number of elements used to represent the geometry.
- The cost of generating a right-hand side for the equation from the specified boundary conditions, obtaining the surface velocity and pressure from the resulting solution and integrating these find the forces and moments. This is approximately proportional to the square of the number of elements.

The relative costs of these operations varies somewhat with the number of elements used to model the configuration, but for configurations with numbers of elements exceeding 600, the cost of generating and solving the linear system greatly exceeds the cost of processing the solution for a single flow condition.

### **Solution of the Linear System**

As discussed above, the bulk of the computational effort expended in calculating the flow is used to generate and solve the system of linear equations. These equations are solved by a method known as LU decomposition. In this scheme, a process similar to Gauss elimination is used to convert the matrix to triangular form, at a cost approximately proportional to the cube of the number of elements in the model. Once the matrix is triangularized into upper and lower factors, and the right hand side is specified, a solution can be obtained at a cost proportional to the square of the number of elements.

### **Multiple Flow Conditions**

Once the matrix has been decomposed, it is very inexpensive to solve for the  $\{x\}$  vector given a  $\{b\}$  vector. Recalling that the  $[A]$  matrix is determined entirely by the geometry and Mach number, and the  $\{b\}$  vector is determined by the boundary conditions, it is clear that once the computational cost of decomposing the matrix is absorbed, the solutions for additional boundary conditions can be obtained for little increase in cost.

In particular, additional angles of attack, angles of sideslip, angular rates, inlet flows, and small perturbation control surface deflections can be obtained inexpensively. The quantities which can be changed without incurring the expense of generating a new matrix decomposition relate to either the boundary conditions or the output processing. Multiple onset flows can be requested on any run.

### **Use of Configuration Symmetry**

If the geometry is symmetric, additional savings in cost are realized by solving one or two half-size systems instead of the full size system. If the geometry and boundary conditions (onset flow, deflections, and permeabilities) are symmetric, the solution will be identical on both sides of the configuration, so that the true number of unknowns is only half of the number of control points on the complete configuration. By summing the influence coefficients of elements that are symmetrically opposite each other and only considering control points on one side of the configuration, a half size system is produced. Exploiting symmetry in this case reduces the solution cost by almost a factor of eight.

Cases of antisymmetric boundary conditions will instantiate an automatic reflection of the geometry in QUADPAN across the geometric X-Z plane of symmetry and an associated asymmetric solution. This occurs, because it is likely that the resulting solution of antisymmetric boundary conditions in QUADPAN will result in asymmetric flow conditions. This is discussed further in the following paragraphs under Coordinate Systems.

## **COORDINATE SYSTEMS**

Input geometries for QUADPAN are defined in an orthogonal Cartesian coordinate system, referred to as the Global Coordinate System (GCS) with components X,Y, and Z. For conventional applications of the code, the X-axis points aft, the Z-axis points upward and the Y-axis points to starboard to form a right-handed system. This axis system corresponds to an aircraft lofting coordinate system with X,Y,Z taking the place of fuselage station, buttock line and waterline. Figure 3-11 illustrates the global reference system used in QUADPAN.

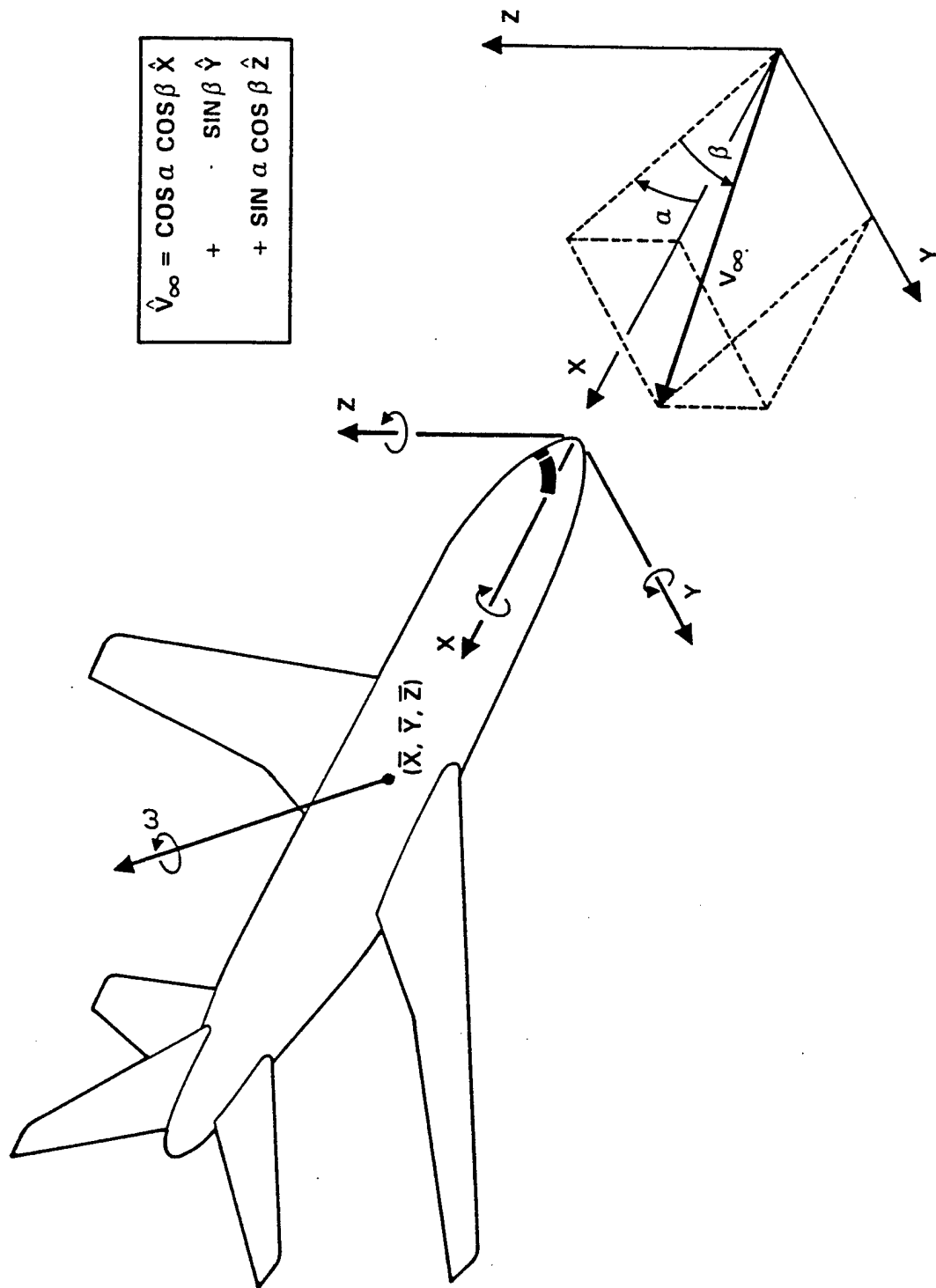


Figure 3-11 Global Coordinate System

The configuration to be analyzed may be located anywhere in the X,Y,Z system and may be made up of components that are symmetrical about the X-Z plane. QUADPAN can treat the X-Z plane as a plane of symmetry to generate an "image" half of the configuration that need not be input by the user. Since the program will achieve substantial savings in computational cost for geometries that are symmetric about this plan, it is best to locate the input geometry in the global system in such a way as to exploit lateral symmetry wherever possible.

### **Flow Direction**

The geometric definition of the configuration is independent of its translational or rotational motion. The free stream velocity vector is not fixed to the coordinate frame and is specified by an angle of attack (ALPHA) and angle of sideslip (BETA). The angle of attack is the angle made by the projection of the free stream vector into the X-Z plane with the X axis and is positive when the Z component of velocity is positive. The angle of sideslip is the angle between the free stream vector and the X-Z plane and is positive when the Y component of velocity is positive. Note that this is not the same as the angle between the X-axis and the projection of the velocity vector into the X-Y plane!

The rotational motion of the configuration may be specified by an angular velocity vector and a rotation center. The free stream vector corresponds to the X-axis when the angle of attack and sideslip are zero.

### **Compressibility Direction**

The compressibility direction (from the Prandtl-Glauert equation) is fixed to the X-axis for computational simplicity. This means that the flow vector should lie nearly along the X-axis for accurate results for compressible flows. This is not usually a problem due to the small angles of attack or sideslip required by the assumption of small perturbations for compressible flow. However, the configuration may not be arbitrarily oriented in the global system without affecting the results. This additional geometric limitation is not present for incompressible flows. For a Mach number of zero, the results are independent of orientation as long as the flow direction is also rotated to give the appropriate angles of attack and sideslip.

## **BASIC REQUIREMENTS FOR THE GEOMETRIC MODEL**

The formulation of QUADPAN places several constraints on the geometric models that are to be analyzed. An input configuration must consist of one or more closed bodies, here defined as volumes bounded by surfaces that are wetted only on one side by the exterior flow. Laterally symmetric bodies need only be defined on one side of the plane of symmetry (same side, however) and are closed by their image across the plane of symmetry. When each defined panel has an image, the program exploits symmetry to reduce the cost of the computation.

Lifting configurations must contain vortex wakes, explicitly defined by the user, that issue from the trailing edge of any lifting portion of the body. If these vortex wakes are omitted, the program will calculate the non-lifting flow about the configuration. A vortex wake is defined in much the same way as a body except that the wake is a sheet wetted on both sides by the flow and not a closed geometry. The user must define the vortex wake so that it does not lie interior to the body, and is sufficiently long (10-20 body lengths or wing spans) that the downstream end, representing the starting vortex, will not affect the upstream conditions. The code can be run on models with openings in the body, such as at a wing tip or a fuselage base, although the extent to which they will affect the results is unpredictable and it is strongly recommended that large gaps be closed in keeping with the definition of a body.

## DISCRETIZATION OF SURFACE GEOMETRY INTO ELEMENTS

The formulation of QUADPAN is based on the representation of the configuration by a mesh of quadrilateral surface singularity elements whose corner points lie on the body surface. These quadrilateral surface singularities will be referred to as ELEMENTS in keeping with the terminology of finite element techniques. An element is defined by four straight lines joining the four element corner points, making it planar or near-planar. Highly twisted elements should be avoided because QUADPAN flattens elements to calculate their induced potential or velocity. The control point, which is the point where the boundary condition is applied, is located at the geometric mean of the four element corner points.

In most applications of the code, the elements should be arranged to form a regular mesh in which neighboring elements share a complete common side and corner points. Elements arranged in this way are referred to as contiguous, and are illustrated in Figure 3-12. Constructing a model with contiguous elements ensures that there will not be any holes in the model. On non-planar surfaces, noncontiguous elements produce triangular holes as shown in the figure. The velocity calculation is more accurate when contiguous elements are used, since each element has a neighbor on each side that can be used to calculate the potential gradient. There are occasionally situations which are best handled with noncontiguous elements. These are discussed in Section 3.3.2.3. Note that contiguous elements are not required along the side edges of a wake, except where that wake edge lies adjacent to a body. This is illustrated in Figure 3-9, where the inner wake side edge near the fuselage matches the fuselage elements, but the outboard edge of the inner wake does not match the outer wake edge.

## COMPUTATION OF THE AIC MATRIX

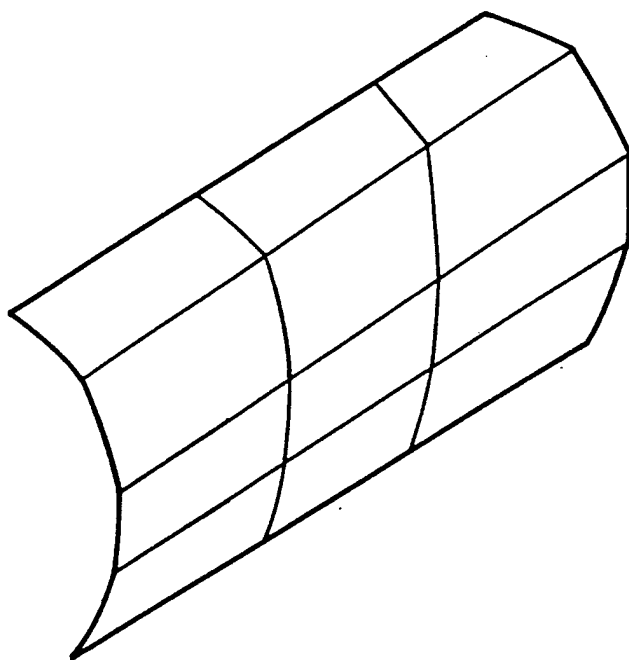
The AIC matrix measures the change in airload at one element due to a deflection of another element. It is considered as a sensitivity which is applicable to relatively small inclination changes measured from a base geometry, Mach number, and flow. QUADPAN has two methods of computation for the AIC matrix. A theoretically derived method provides AIC based on incompressible flow. A finite difference approach is available that provides for flow sensitivities with QUADPAN's base assumptions.

The AIC matrix is obtained by perturbing the angle  $\theta$  for each element and then calculating the perturbation in  $C_p$  at all elements. The program requires the solution to a linear system of equations  $Ax=b$  whose order is the same as the number of elements. The perturbation of  $\theta$  represents a change in the right hand side vector  $b$ . The finite difference approach requires as many right hand sides as elements in the model. The angle  $\theta$  is measured between the onset flow direction and the outward normal of a given element. Details of the theoretical and the finite difference approaches are described in Ref. 16.

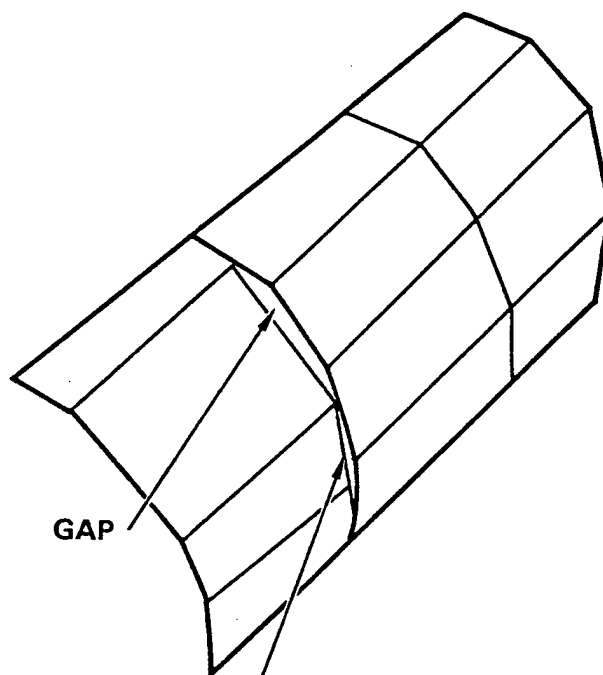
For the finite difference approach, the program operates from the initial onset condition specified by the user to compute the AIC matrix. For instance, if the user specifies an initial onset condition of  $\alpha = 9$  degrees, and requests an AIC matrix, the matrix finite difference will be computed from the three-dimensional flows at this condition. This allows QUADPAN to provide a more accurate flow field to compute local perturbations.

The program also interprets flow requests for computation of the AIC matrix and instantiates geometry based on geometric and flow symmetries. If a centerline symmetric geometry (i.e. symmetric about the X-Z plane) is present, and symmetric flows are specified through requested onset flows and control surface sweeps, QUADPAN will compute a symmetric AIC matrix. If centerline symmetric geometry is present, and an antisymmetric boundary condition is specified through requested onset flows and / or control surface sweeps, QUADPAN will instantiate a mirror image reflection in geometry and compute an asymmetric AIC. This AIC represents 2 times the number of elements as in the symmetric case. The QUADPAN user must be aware of these situations and be prepared to accept the results in terms of spline and structural models.





**CONTINUOUS ELEMENT MESH**



**GAP**

**NO WELL-DEFINED  
NEIGHBOR**

**DISCONTINUOUS ELEMENT MESH**

Figure 3-12 Contiguous and Non-Contiguous Elements

## SUMMARY OF THEORETICAL CONSIDERATIONS

An understanding of the basic limitations of QUADPAN is necessary prior to using the program. The formulation of the method requires that the user consider the following items:

1. Any body modeled with the code must be made into a collection of quadrilateral elements. This collection must be closed and free of holes with one surface entirely wetted by the flow and the other surface not exposed to the flow. Models can be constructed with small gaps, but the accuracy of the solution near the gaps will be unpredictable.
2. The user must specify to the program which side of each element is the side that is exposed to the flow. Otherwise the wrong side of the element may be forced to have a perturbation potential of zero.
3. To facilitate differentiation of the potential to obtain surface velocities and pressures, the elements should be arranged (if possible) so that neighboring quadrilateral elements have coincident corner points.
4. The boundary condition is only applied at the control points. Normal and tangential velocities are not accurate anywhere else on the elements. Velocities can be obtained at off body points if the points are located at least one element length or width away from the body.
5. Wakes should be attached to any sharp edge which will have a Kutta condition on it. Lift cannot be generated without a wake. The upper and lower surface elements at the trailing edge which sheds the wake should be nearly identical in size and shape.
6. The placement of the Kutta edge of the wake is critical to the solution. The side edges of the wake may require special treatment with adjacent body panels to avoid gaps between the edges and the body.
7. A linearized equation for compressible flow is employed. This prohibits the use of the code for transonic phenomena. The greatest accuracy occurs when the free stream is roughly in the direction of the X-axis.
8. Most of the cost of solution is in solving the matrix equations. Once the equations are solved and the results stored, the code can be restarted to solve for different onset flows and other boundary conditions related parameters at minimum expense. However, any changes in geometry or Mach number require a new matrix solution.
9. Geometric symmetry across the X-Z plane reduces the cost of the run substantially. If the flow is symmetric, the cost for symmetric geometries is approximately one-eighth of that for an asymmetric geometry (with the same total number of elements). If the geometry is symmetric and the flow conditions are asymmetric, the cost will be approximately one-fourth of that for an asymmetric geometry. Stored solutions for symmetric flows can be later extended to include asymmetric flows for a minimal increase in the cost of running asymmetric flows from the start.
10. The accuracy of solution increases with the number of elements, with diminishing improvement as the number of elements increases. The cost increases as roughly the cube of the number of elements. Additional elements in the streamwise direction on wakes do not increase the cost of solution.

### 3.3.2.3 QUADPAN Integration In ASTROS

Integration of QUADPAN allows for use of its original input packets with minor modifications. The original ASTROS paradigm of input emulated NASTRAN bulk data. The AANDE program instantiated changes that not only integrated QUADPAN but also enabled future integration of similarly fully integrated legacy codes without rework of the legacy user input. The benefit herein allows ready use of existing models in ASTROS. An overview of QUADPAN input is provided to introduce concepts and note unique additions to QUADPAN that facilitated ASTROS integration. Details of QUADPAN input are documented in Ref. 12, and a description of the ASTROS' QUADPAN module are documented in Ref. 11.

#### QUADPAN MODIFICATIONS

QUADPAN native capabilities as described in the previous subsections are preserved in ASTROS integration. SAERO Discipline input in the SOLUTION packet controls the use of QUADPAN through the METHOD=QUADPAN and the MACH=<mach> specifications as described in Section 3.1. Input for the QUADPAN model (where model denotes geometry and flow boundary conditions) is provided for ASTROS users in the original QUADPAN input format. The user isolates this input from the standard ASTROS 'BULK DATA' packet by providing a 'QUADPAN' packet. The 'BULK DATA' packet is still used for USSAERO (which is fully supported under the AANDE paradigm) and standard ASTROS input. The ASTROS packets appear to the user as following:

```
SOLUTION
  ANALYZE
    BOUNDARY
      SAERO
    END
  BEGIN QUADPAN
  .
  .
  ENDDATA
  BEGIN BULK
  .
  .
  ENDDATA
```

ASTROS will execute QUADPAN for every Mach number specified in the SOLUTION packet and store the results on the Run-time database (default) or ARCHIVED database for each case. The data is stored with MODEL name, METHOD, and MACH classification.

Modifications to the native QUADPAN included linkage to the ASTROS memory manager, creation of routines to read and pass native input to QUADPAN, and routines to write QUADPAN data to the new ASTROS database entities. Data stored consists of the MODEL group (named through the SAERO MODEL=<modelname>), the STDYGEOM group, the AIC group, and the RIGDALOD group. Other modifications included provisions for computation of control surface pressure vectors. Native QUADPAN provided for multiple onset-parameter ( $\alpha$ ,  $\beta$ ,  $P$ ,  $Q$ ,  $R$ ) solutions. The user input includes a provision for designating a set of QUADPAN panels to simulated deflections off of the original geometry. This designation remains constant for all of the onset-parameter solutions. The input to the QUADPAN suite was extended to allow the definition of control surfaces through this capacity and allow control surface sweeps for each onset-parameter solution. Figure 3-13 illustrates the looping in QUADPAN to create pressure vectors that are stored in the RIGDALOD group. As discussed in the boundary condition

description in subsection 3.3.2.2, the normal velocities on each element is modified to simulate the onset-parameter / control surface deflection combination. This capability should be used with discretion by the ASTROS user because while it allows a rapid build-up of a nonlinear database (because of three-dimensional flow), it also can create computational waste. If rate terms and sideslip terms are desired with no associated control surface sweeps, it is best to make two QUADPAN runs (one with control surface sweeps alone and one with onset parameters alone). The IMPORT, OVERLAY, and ASSEMBLE commands (discussed in Subsection 3.2.3) provide the necessary capability to combine these pressure sets for later solutions.

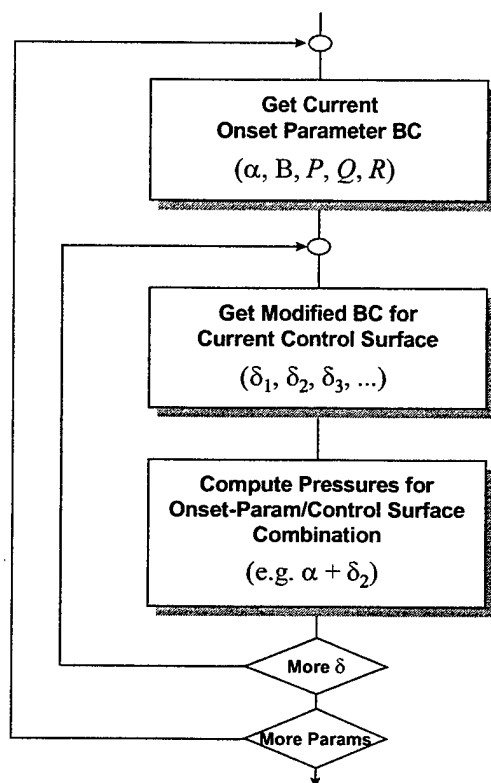


Figure 3-13 A Control Surface Sweep Computed For Each Onset Parameter

## THE QUADPAN INPUT

The QUADPAN input packet is divided into two basic sections:

1. Solution Control and Control Surface Definitions
2. Model Geometry and Connectivity

### QUADPAN Solution Control and Control Surface Definitions

Figure 3-14 illustrates the solution control data for a forward swept wing example. The packet is initiated with 'BEGIN QUADPAN'. The \* symbol denotes a comment in the deck. A title card is provided. The parameters following the title card allow a variety of controls. As will be discussed throughout the following paragraphs, the QUADPAN model is made up of PANELS comprise groups of quadrilateral elements. The ABSTOL and RELTOL terms are abutment control parameters that

QUADPAN uses to check geometric tolerances between PANELS. The user controls the accuracy of interference effects on the basis of these tolerances. QUADPAN will not run unless the user specified tolerances are met. There is more discussion on these terms in the User's Document (Ref. 12)

```
BEGIN QUADPAN
*****
FSW ASTROS QA PROBLEM
*****
*MACH  RUN   PRINT  DUMP  ABSTOL  RELTOL  RFREQ  FROUDE
0.9      1       2      1    1.0E-03  0.0100
*REFERENCE PARAMETERS
*SREF  CBAR  WSPAN  XBAR  YBAR  ZBAR  AIC  FACTOR
400.0  10.00  40.00  30.00  0      0      0.001
*FLOW CONDITIONS
*ALPHA  BETA  OMEGAX  OMEGAY  OMEGAZ  VINP
0.0      0.0
1.0      0.0
0.0      1.0
0.0      0.0      38.0      980.0
*
** CONTROL SURFACES
*
AESURF
AILERON
-1
PANELS
25  26
ANGLES
1.0
*
AESURF
FLAP
.....
PANEL
.
```

**QUADPAN Packet**  
**Problem Title**  
**Control Deck**

**Control Surface Definition**

**AESURF**  
**Surface Name**  
**Deflection Symmetry**  
**(1 - SYM, 0 - ASYM, -1 - ANTI)**  
**PANELS**  
**Panel #'s**  
**ANGLES**  
**Surface Deflection (degrees)**

Figure 3-14 Initial Data in QUADPAN Packet

The third set of parameters includes an AIC method selection. The AIC matrix can be computed by finite difference or through a theoretical approach based on incompressible flow. Finite approach is the recommended approach, and a value of 0.001 radians is the recommended value for input. A value of '0' instantiates the theoretical approach. The foundation of the AIC method is discussed in Subsection 3.3.2.2.

The flow conditions are the next specification in the QUADPAN solution control. The user may specify angle of attack, sideslip, or any of the three rigid body rate terms. These may be specified in combination or independently. In the previous discussion of QUADPAN's solution flow, the user should be careful how he specifies these flow conditions in conjunction with control surface sweeps in order to avoid long computational times and large databases. Rate terms are referenced about the QUADPAN body axes and relative to a free stream velocity (VINP) and the angular rate. These terms are important. The pressure magnitude and distribution is nonlinearly dependent on these values. These terms are stored in RIGDALOD and used later in aeroelastic solutions within ASTROS.

The final set of data in the solution control is the control surface specifications. Control surface symmetries, geometry, and distributions are determined by the input. Table 3-3 includes the keywords that are used in this data flow to define the control surfaces.

Table 3-3 Definition of Control Surfaces in QUADPAN

<option>	Description
"AESURF"	(keyword)
User Name	an 8 character (truncated from 10) surface name
Symmetry	the surface symmetry (-1, 1 or blank)
"PANELS"	(keyword) panel ids' one or more records of 1 to 8 panel ids that comprise the surface
"ANGLES"	(keyword) angular deflection, one or more records of 1 to 0 angles (in deg.) that comprise the surface sweeps.

Solutions are obtained for the flow condition with no surface input and then each surface is swept through its angles for the flow condition. This is repeated for each flow condition. Any number of control surfaces may be defined. In the example, shown in Figure 3-16, the AILERON surface referenced under an AESURF designation has PANELS 25 and 26 referenced defining its geometry. The definitions of PANELS and specification control surface hinge axes through the use of the DEFLECT entry are discussed in the following paragraphs.

#### Model Geometry and Connectivity

Geometry and connectivity input is controlled through keywords. The most used primitive words are PANEL, JSPACE, KSPACE, & SECTION. PANEL denotes a collection of elements. PANELs are quadrilateral, as are the elements inside. The normal of a PANEL and its elements is determined by the geometry defined under the keywords JSPACE and KSPACE as shown in Figure 3-15. Under JSPACE and KSPACE the user specifies options for geometry construction and element generation. In the example shown, rectangular coordinates are specified with a spacing of four elements spanwise and three elements chordwise. The orientation of the NJ and NK vectors is determined by the rectilinear coordinates specified in the input deck. The cross product of NK into NJ determines the normal of the panel being defined.

```

PANEL
23  OUTER WING UPPER
*TYPE  WET  FORCE  IMAGE
0      1    1      1
*
JSPACE
*NJ    JSPACE
4      0
KSPACE
*NK    KSPACE
3      0
*
SECTION
RECT
*X     Y     Z
19.22650 10.00000 0.00
21.72650 10.00000 0.50
24.22650 10.00000 0.50
26.72650 10.00000 0.50
*
SECTION
RECT
*X     Y     Z
13.45300 20.00000 0.00
15.95300 20.00000 0.00
18.45300 20.00000 0.00
20.95300 20.00000 0.00
*

```

- User Defines JSPACE, KSPACE & SECTION
- Code Panel Abutment Governs Interference
  - Control Points Checked
  - User Controls Tolerance

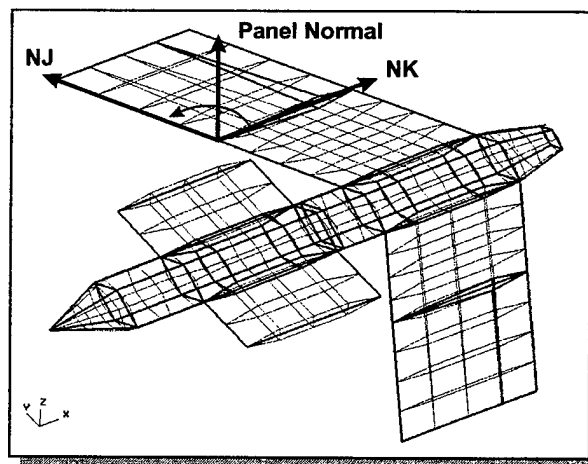


Figure 3-15 QUADPAN Geometry and Connectivity

Each PANEL has a title and control parameters. Each PANEL is checked against its neighbor to determine whether PANEL boundaries match up. The RELSTOL and ABSTOL terms in the solution control are used to determine the degree of matching.

QUADPAN PANELS can simulate geometric deflection through an application of transpiration methodology. A DEFLECT entry as shown in Figure 3-16 provides the deflection axes for both the real geometry side and the image side) in the potential case of QUADPAN instantiating an image for asymmetric flows). The axis of rotation follows the right hand rule. Note in the figure that the image side points out the span of the image as the real side axis points out the real side. Also note that the aileron is made up of an upper PANEL (25) and a lower PANEL (26) as was designated back in Figure 3-14.

```
PANEL
25  AILERON UPPER
*TYPE  WET  FORCE  IMAGE
0    1    1    1
*
DEFLECT
**XTAIL  YTAIL  ZTAIL  XHEAD  YHEAD  ZHEAD  DEFLECT
26.72650 10.0   0.0   20.95300 20.00000 0.0   0.0
26.72650 -10.0  0.0   20.95300 -20.00000 0.0   0.0
*
JSPACE
*NJ  JSPACE
4    0
KSPACE
*NK  KSPACE
1    0
*
SECTION
RECT
*X  Y  Z
26.72650 10.00000 0.50
29.22650 10.00000 0.00
*
SECTION
RECT
*X  Y  Z
20.95300 20.00000 0.00
23.45300 20.00000 0.00
*
*
```

- Transpiration Method of Deflection
- Deflection Follows Right Hand Rule

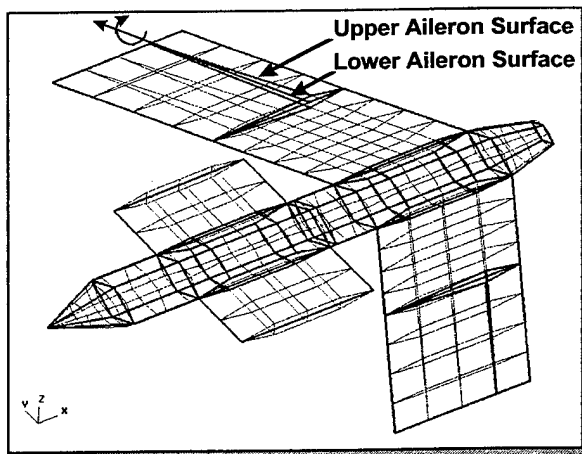


Figure 3-16 QUADPAN Control Surface Hinge Axes Definition

For further discussion on the user input refer to Ref. 12.

### 3.3.2.4 Modeling Techniques In QUADPAN

This section describes the techniques used in the generation of a QUADPAN model. This includes guidelines for establishing panel boundaries, element size and spacing within the panels, and the modeling of lifting effects with vortex wake panels. In addition, models for simulating inlet and exhaust flows are suggested. This section does not describe details of the program input; instead it is a compendium of experience derived from using the program.

#### PANEL LAYOUT

The first step in constructing a QUADPAN model is to break the entire configuration into panels and/or spacing intervals. The way this is done depends on the geometric features of the configuration, the constraints needed to keep the final element mesh from becoming highly kinked or twisted and the arrangement of vortex wakes needed to correctly represent the physics of the flow.

Since the arrangement of panels and spacing intervals on one part of the configuration can affect how other parts of the configuration are broken up, the entire paneling arrangement should be worked out before starting to define the geometry. Regarding the panel as the basic unit of input, the panel boundaries are one of the tools the user has for controlling the arrangement of the mesh. Figures 3-17 through 3-19 illustrate the arrangement of panel boundaries on the geometric model of a jet trainer configuration. The vortex wakes have been removed from this model for clarity.

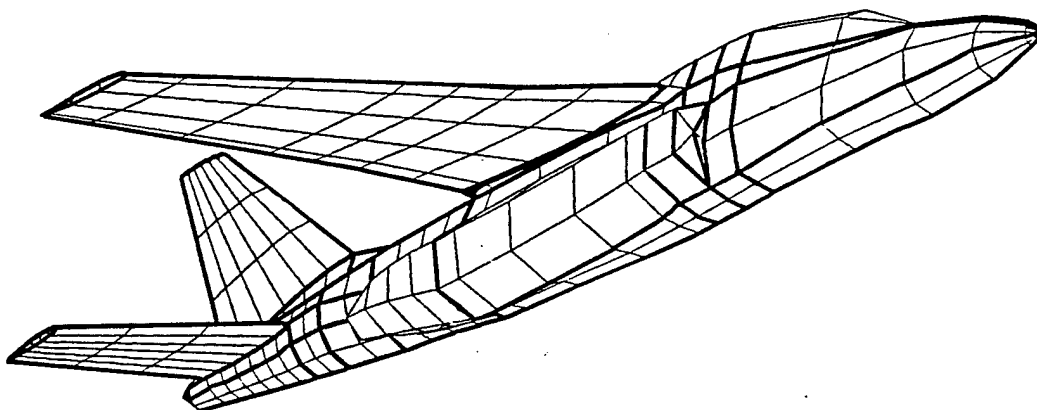


Figure 3-17 Model of Jet Aircraft - Forward Lower View



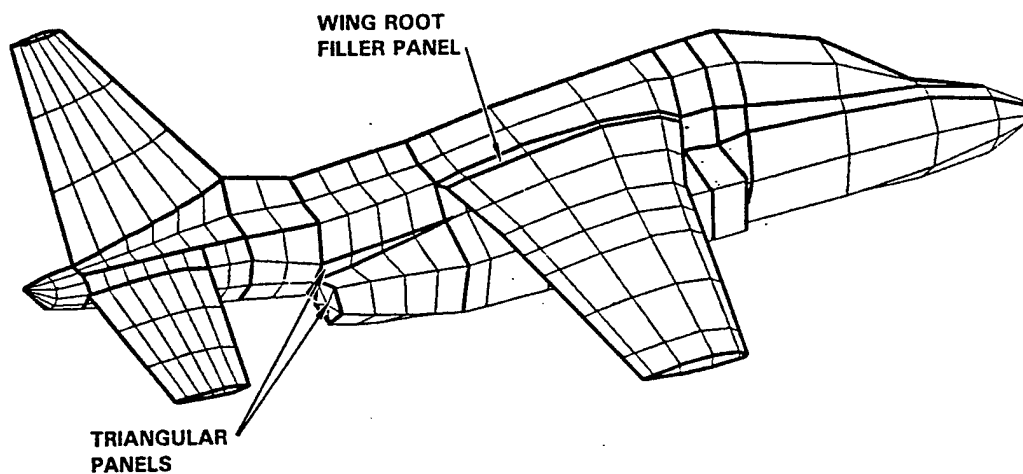


Figure 3-18 Model of Jet Aircraft - Aft Upper View

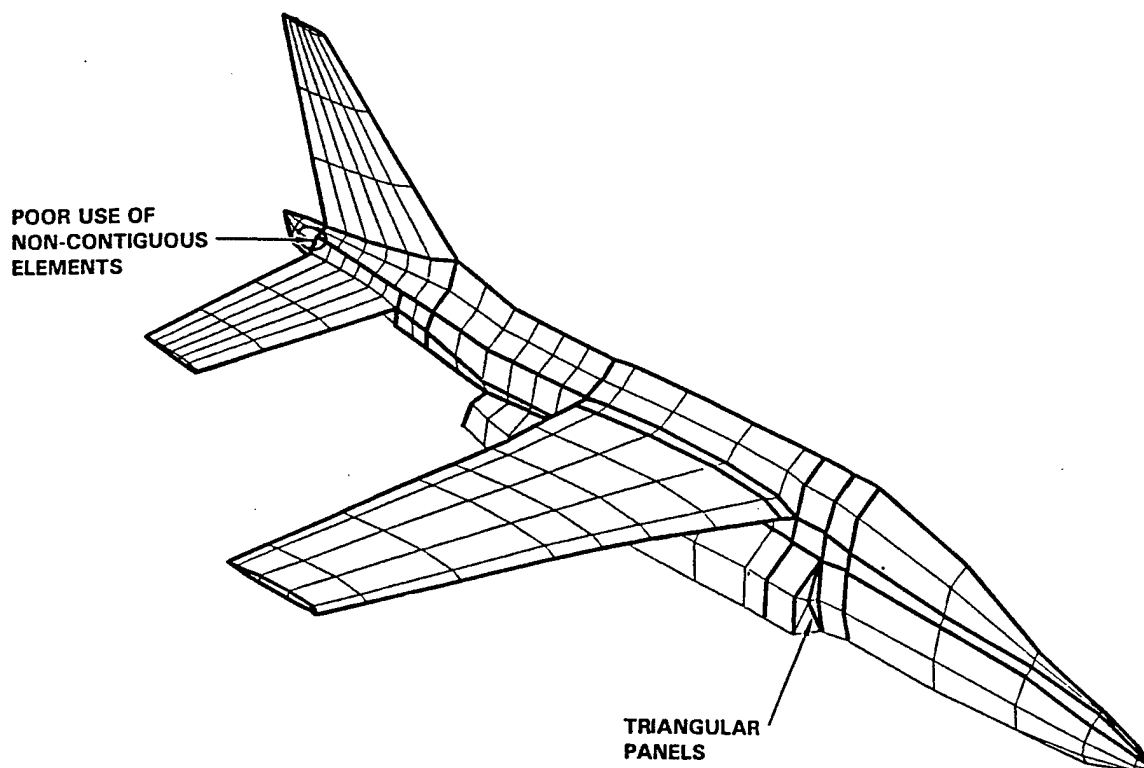


Figure 3-19 Model of Jet Aircraft - Forward Upper View

### Layout for Panel Junctions

Geometrical features such as the intersections of wings and fuselages are maintained in the lattice representation of the configuration by making them panel boundaries or spacing intervals. This forces element corner points to represent the features instead of allowing the element lattice to bridge over them. Regions of the mesh that are kinked or twisted can be straightened by employing spacing intervals or panel boundaries. This is illustrated by the wing/fuselage junction in Figure 3-20. In general, spacing intervals or panel boundaries should be placed where geometrical features are located.

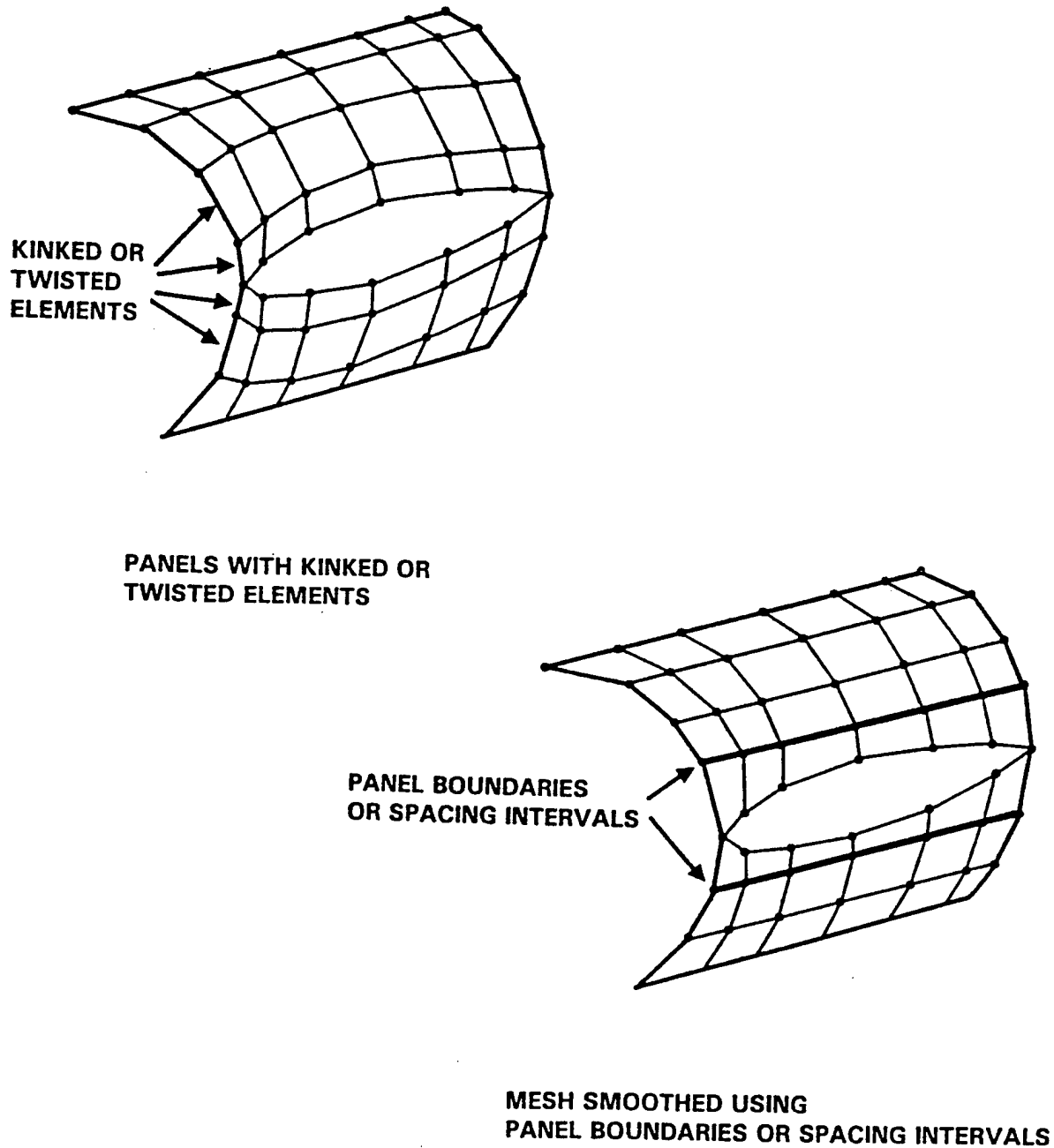


Figure 3-20 Use of Panel Boundaries or Spacing Intervals to Control Mesh

### **Layout for Boundary Conditions**

In order to utilize features such as the small perturbation representation of control surface deflections, the control surfaces must be separate panels. Vortex wake panels use different boundary conditions, and must be modeled with separate panels from the wing. The user should be especially careful with the panel layout on lifting configurations, as discussed later in this chapter.

It is sometimes handy to represent features of the configuration with separate panels in order to isolate certain output information in a run. An example is the upper and lower surface of a wing panel, where modeling the wing with separate panels enables the user to make use of the program's calculation of the fractional chord location of the control point to simplify comparison with chordwise pressure data. This separation into upper and lower panels has the disadvantage that the continuity of the spline curves used for resampling is lost at the leading edge, requiring a more detailed input definition near the leading edge. This is not a serious problem in actual practice, and normally separate panels are used.

## **NUMBER AND SPACING OF ELEMENTS**

The number of elements used in a QUADPAN model depends on the complexity of the geometry, and the need for accuracy. More complex geometries naturally require more elements. The number of elements used must at least be sufficient to produce an element lattice that is an adequate geometrical representation of the configuration.

As the number of elements increases, the accuracy improves, but the rate of improvement diminishes rapidly as the number of elements increase. Since the cost increases as nearly the cube of the number of elements, increasing the number of elements beyond a certain level will result in a large cost increase with only a small improvement in accuracy.

### **Spacing of Elements**

In order to use a given number of elements efficiently, the spacing of the elements should vary over the configuration, with elements concentrated in regions of large velocity gradients, or in regions where there is a special need to resolve details of the flow. Wings should have dense paneling at their leading and trailing edges, suggesting the use of cosine spacing. While QUADPAN is relatively insensitive to abrupt changes in spacing, elements are not used efficiently if finely spaced regions are adjacent to coarsely spaced regions. The continuously variable spacing functions are useful for smoothly increasing the element density in the areas that require additional elements.

### **Number of Elements**

It is impossible to give any definite information on the numbers of elements which are required. In addition to the rule of thumb that the lattice be sufficiently dense to represent the geometry, the following numbers may be considered a crude starting point. The upper and lower surfaces on any major lifting component should have between 8 and 20 elements chordwise with cosine spacing and between 4 and 10 equally spaced elements spanwise. Fuselages should have 5 to 10 equally spaced elements around half the periphery, and enough elements along the length so that the elements are not much more than twice as long as they are wide, on the average.

The density of elements on the transport model shown in Figure 3-21 is typical of standard applications of the code. The number of elements on the wing in this model (8, cosine spaced) should be increased to at least 12 or 15 for calculating an accurate pitching moment or to generate a detailed pressure distribution. In addition, the number of elements on the nacelles should be increased if details of that area

are required. The density of elements on the model shown in Figure 3-17 was reduced for clarity. The wing in particular contains too few elements in the chordwise direction for accurate results.

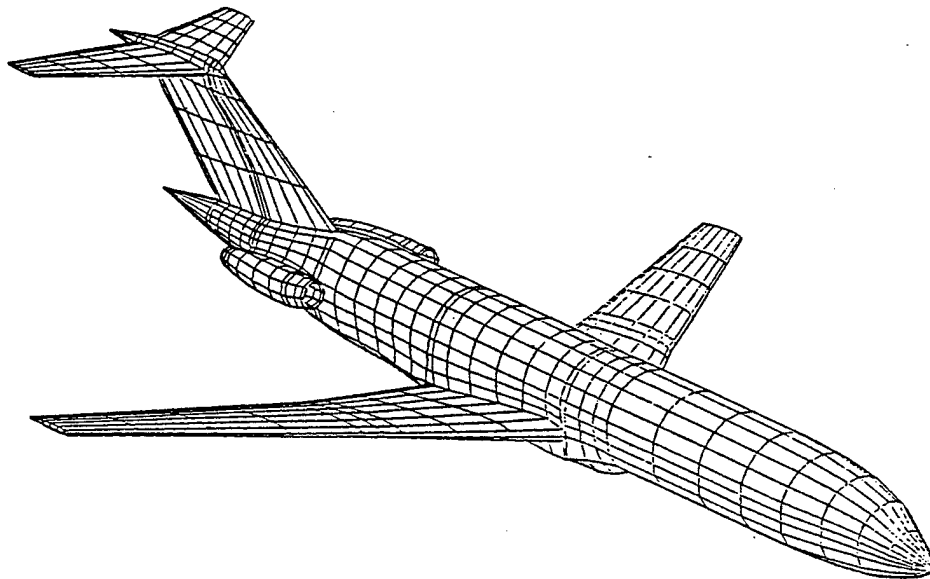


Figure 3-21 Model of Transport Aircraft

## USE OF CONTIGUOUS VS. NONCONTIGUOUS ELEMENTS

An important concept in establishing an acceptable mesh of elements on the surface is that of contiguous elements. Contiguous elements refer to those elements whose corner points on the panel edge coincide with corner points of elements on adjacent panels (See Figure 3-12). Normally contiguous elements should be used throughout a model, to ensure that there will be no triangular gaps when a curved panel edge is being represented by two different sets of line segments.

Configurations defined with contiguous elements at panel edges will give the most accurate results. This is a result of the method used to find the surface velocity at each control point, using the surface potential at several neighboring elements. Surface potential information across panel boundaries is used only when the elements at the panel edges are contiguous. The program attempts to use a three point differencing scheme to calculate the velocity wherever possible. Depending on the situation, forward, central or backward differences are used. If the panel is sufficiently isolated by noncontiguous elements that fewer than three elements are available in each direction for differencing, the accuracy of this differentiation can suffer. If only two elements are available for differentiation in a given direction, only a simple difference can be used. If only a single element is available, the derivative in that direction will be set to zero. Gradients (perturbation velocities) in this direction will not be correct in this case.

### Ensuring Contiguous Elements

The user can construct models with contiguous elements in two ways.

- By breaking up the configuration into a set of contiguous panels.
- Using spacing intervals on noncontiguous panels.

The first method requires that the user arrange the panels so that adjoining panels have identical bounding curves with identical numbers of elements and spacings. It is crucial to note that the bounding curves must be defined at the same points to ensure that the elements be contiguous. This is because the QUADPAN geometry routines first fit a spline (parameterized by arc-length) through the points which define the bounding curves. The element corner points are selected to lie on the spline at arc length intervals determined by the spacing parameters. In general, for the element corner points to be coincident, the splines must be identical which means the sets of points used to define the splines must also be identical.

If boundaries with contiguous elements could only be constructed from contiguous panels, configurations would have to be diced up into a large number of panels themselves being contiguous. This feature may be used to generate contiguous elements across a boundary that has several panels on one side and a single panel on the other side. An example is a wing consisting of separate panels for the slat, main wing, and flap abutting a fuselage consisting of a single panel. Note that the bounding curves must still consist of identical (or nearly identical) sets of points, and the spacing intervals on the fuselage must be break points so that a separate spline is established for each segment of the bounding curve.

The need to use identical bounding curves on panels to produce contiguous elements can be a problem if a complete surface definition of the configuration is unavailable, as is often the case in preliminary design applications. The vehicle in Figure 3-17 required 20 points along the chord of the wing to define the airfoil section. The fuselage was defined by only three sections normal to its axis in the region of the wing/body junction. Rather than generate the fuselage surface so that the exact intersection between the wing and the fuselage could be determined, an approximate filler panel was used. This is the narrow panel joining the wing to the body. The outer edge of the panel is defined with the same curve used to define the airfoil section. The inner edge is defined only at the points where fuselage sections were defined. While the filler panel does not have the correct section, it is sufficiently small that the geometric liberties taken in its definition will not alter the overall results. The use of the approximate filler panel saved much time in constructing the model.

A problem that frequently arises when attempting to construct a model entirely from contiguous elements is that of adjusting the distribution of elements over the surface so that elements are used efficiently. This may often be done with panels that have a degenerate edge as shown in Figure 3-18. At the aft end of the engine pod, a roughly triangular panel is used to add an additional longitudinal strip of elements to the aft fuselage. Similarly, the use of panels with degenerate edges on the inlet face, made it possible to provide additional elements to model the ducts and pods, without wasting elements (and therefore computer time) on an unnecessarily dense model of the forebody.

#### Use of Noncontiguous Elements

There are circumstances in which it is desirable to have noncontiguous elements in a model. This is sometimes the case when detailed information is needed on a specific area of a configuration, usually in the form of pressures or flow directions. A dense mesh of elements should be used in the area of interest, but maintaining that density on the entire model would unnecessarily increase the cost of the analysis. By using a dense mesh on the panels in the region of interest and a sparse mesh everywhere else, the detailed information can be obtained at a minimum cost. As long as the noncontiguous elements are kept away from the region of interest, there will be no loss in accuracy.

An example of the use of noncontiguous elements is illustrated in the P-3C model in Figure 3-22. The wing outboard of the outer nacelle has a dense mesh for a detailed calculation of the flow around the wing store. The use of a mesh this dense on the entire wing would have resulted in an unduly expensive computation. Note that the noncontiguous panel boundary is sufficiently far from the area of interest that the results are not contaminated. As long as detailed information about flow around the store is important, this exemplifies an appropriate use of noncontiguous elements.

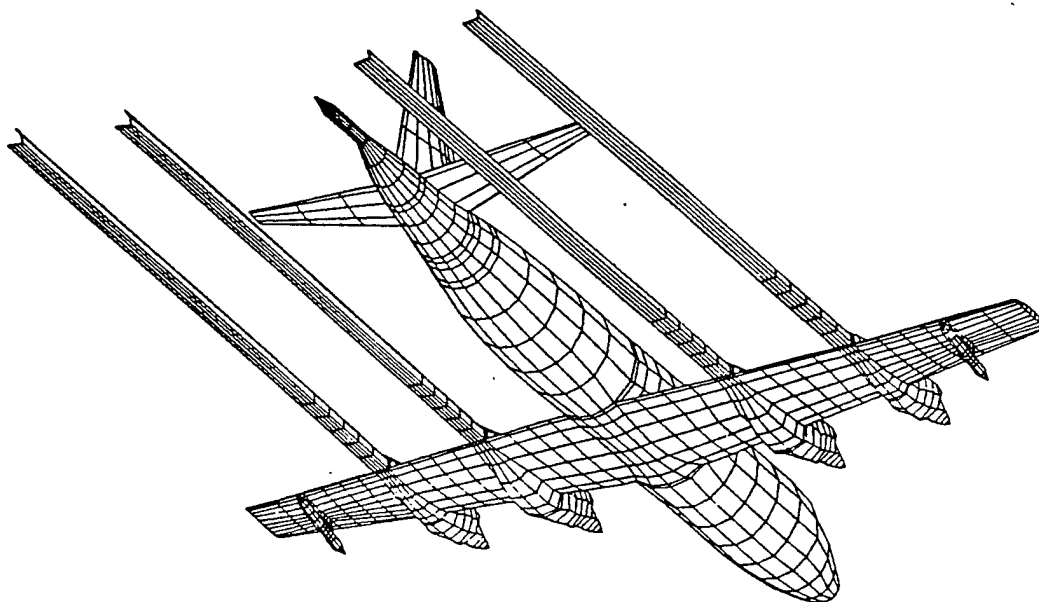


Figure 3-22 Model of P-3C With Wing Stores and Nacelle Exhaust

The model shown in Figure 3-19 employs noncontiguous elements along the side of the fuselage between the vertical and horizontal tails. This was done so that the number and distribution of elements on the vertical and horizontal surfaces could be specified independently. For example, cosine spacing could be used on the horizontal tail without wasting a band of dense elements in the middle of the vertical fin where they would not substantially improve the accuracy of the calculation. The impact of the noncontiguous boundary was minimized since it is nearly a straight line. Therefore, the usual triangular gaps produced by such boundaries do not appear. In addition, the velocity component normal to the boundary is expected to be small in the surrounding region so that differentiation in that direction is not likely to be important. In spite of this, it is almost always better to use contiguous elements at a slight sacrifice in the cost of the run, and would have been better in this example.

The noncontiguous boundary on the tailcone in Figure 3-19 is an example of a misuse of noncontiguous elements. Not only are gaps opened in the model, but with only two elements available for differentiation in the streamwise direction, the results on the tailcone would be very poor.

### MODELING VORTEX WAKES

Lifting effects are modeled in QUADPAN using vortex wakes, attached to any surface that must develop lift (usually at a sharp edge) where a well-defined Kutta condition is present. Wings, horizontal tails, and vertical fins are examples of surfaces which have well defined Kutta conditions. A round or blunt edge, such as found on an elliptical airfoil, is an example of a poorly defined Kutta condition. The actual point at which the wake is shed on such a surface is likely to change with the angle of attack, making a good approximation with a fixed wake location unlikely. Figure 3-23 illustrates the vortex wakes used on a P-3C model. Since only symmetrical flow conditions were studied, the wake from the vertical tail was not used.

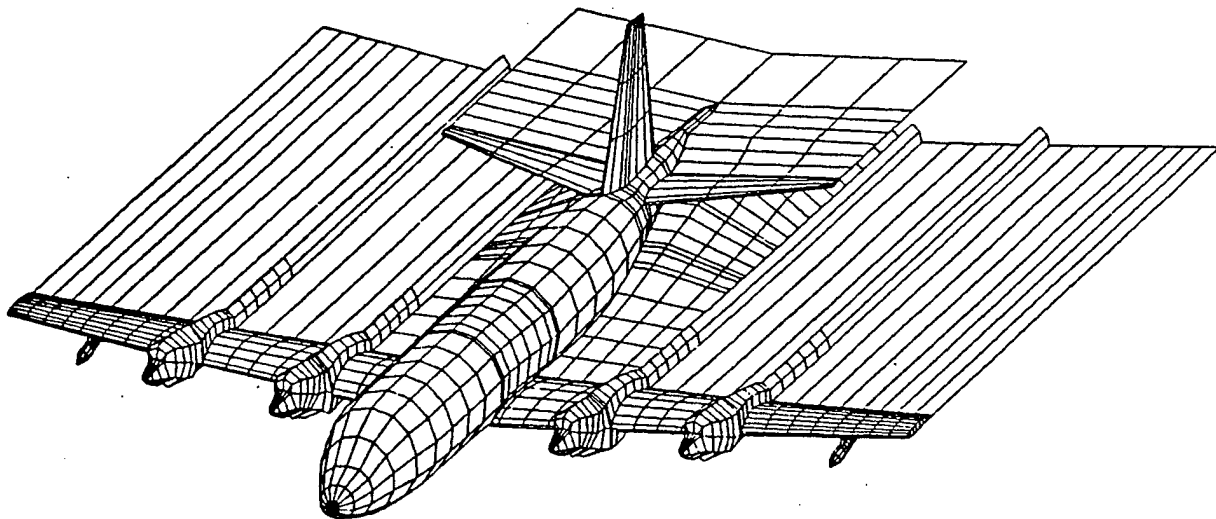


Figure 3-23 P-3C With Vortex Wakes

Wake panels are used to model the vortex sheet leaving the lifting surface at the trailing edge. These wake panels are input geometrically the same as any other panel, except that their TYPE flag (controlling the boundary condition used) specifies the edge of the wake (the shed edge) which abuts the sharp edge on the body and enforces the Kutta condition. The edge of the wake opposite the shed edge represents the starting vortex, and should be approximately ten spans or vehicle lengths downstream of the configuration.

This vortex wake behind the lifting surface can be modeled with a single panel or by a collection of several wake panels placed end to end. If a single wake panel is used, it is often necessary to use spacing intervals to generate the mesh so that it is contiguous with the elements on another panel, such as a fuselage side. If several wake panels are used, they should be placed end to end, with the "Kutta" edge of each following wake touching the end of the preceding wake. The program automatically hooks up the abutting wakes to pick up the adjacent vortex wake strength.

In general, only a single wake should be shed directly from a Kutta condition edge. The exception to this is a wake which lies on the plane of symmetry. Such wakes are needed for modeling vertical fins. In order to exploit the cost savings of geometric symmetry, each panel must have an image, including wakes. It is permissible for a wake and its image to be shed from the same edge, thereby preserving the symmetry of the model.

In most cases, the shape of the wake does not strongly affect the surface which sheds it, but does affect surfaces it passes near. Interference effects such as tail downwash are dependent on the wake location, which is input by the user and is not calculated by the code. The wake shape can effect the surface it is shed from if large spanwise flows are present. Aligning the wake with the free-stream can help in this case.

An additional consideration in modeling wakes that pass near other surfaces is that the "streamwise" edges of the elements in the wake must not pass too close to control points. The wake from the wing of the P-3C has been kept well below the tail so that the edges of the wake elements are not close to the control points on the lower surface of the tail. Some care must be taken when the wing and tail are in nearly the same plane, as in the model of Figure 3-17. The wakes have not been shown for this configuration, but the spanwise spacing of the elements on the wing wake in the neighborhood of the tail has been arranged so that the "streamwise" edges of the wake elements pass directly over the edges of the elements on the tail.

In very difficult situations, the portion of the wing wake which would interfere with the tail (if the wing wake had to pass over or under it) can be connected instead directly into the leading edge of the tail. The tail wake would then automatically combine the circulation of the tail with the circulation from the wing wake. If this is done, care must be taken to ensure that the elements are contiguous at all intersections and that all the program finds all the abutments between the wakes and the upper and lower tail surfaces. It must be remembered that any precautions taken to make sure that the edges of wake elements do not come close to surface control points do not address the basic problem of the (unknown) correct wake shape. This may preclude the accurate calculation of lifting surface interference for some configurations.

#### **Wake "Kutta" Edge**

As discussed above, the wake "Kutta" edge is the edge of the wake that actually enforces the Kutta condition. It is important that:

- The Kutta edge be contiguous with the edges of the panels (upper and lower) shedding the wake.
- The two surfaces forming the sharp edge which sheds the wake should have element spacings in the strip direction "normal" to the wake shedding line which are nearly identical in the vicinity of their wake-shedding edges.



In particular, the upper and lower surfaces on a wing should have almost identical element spacing near the trailing edge. Otherwise, a control point on one side of the shedding edge may be too close to an element edge on the other side, producing inaccurate answers. Particular care must be taken if the section is thin, since the elements near the Kutta edge on the two surfaces abutting the wake are nearly identical in shape and size, so that the meshes on the surfaces are nearly parallel when viewed in a direction normal to the wake.

It should be noted that the Kutta edge of the wake will automatically pick up the strength of any other wake panel to which it is contiguous. This allows several wake panels to be connected to form a vortex wake system.

### Wake Side Edges

If the trailing edge of the lifting surface intersects another surface such as a fuselage side, the side edge of the wake (not the shed edge) must abut this surface. If this is not done the line vortex at the edge of the wake will cause a spurious low pressure region along the adjacent surface. In the typical case of an upswept fuselage, this results in incorrect pitching moment and lift prediction (because the carryover of lift across the fuselage is not properly modeled). Correct and incorrect wake/fuselage modeling on an L-1011 wind tunnel model are illustrated in Figure 3-24. This problem would also occur for a wing with a wing tip tank, where the increase in wing span due to the presence of the tip tank will not be properly accounted for unless the wake is run along the edge of the tank.

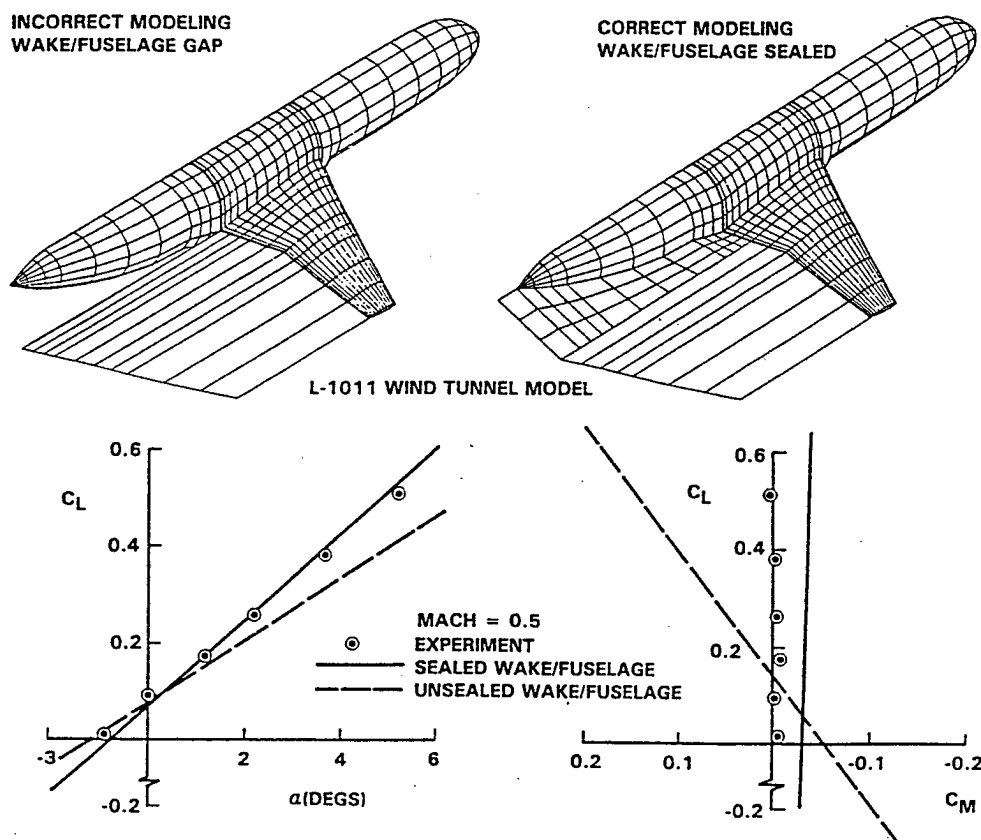


Figure 3-24 The Importance of Wake Side Edge Modeling

There is essentially no cost penalty for adding wake elements along the side edges. This is because the elements in each strip have the same singularity strength and the program associates all such elements on a wake panel with only one unknown.

Making the elements on the wake side edge contiguous with the adjacent surface panels is strongly recommended because it automatically ensures that there will be no holes between the wake and the body (as long as the same points are used to define the coincident edges of the wake and body panels). Due to the program limitations on panel abutments, the side edge of a wake can only be abutted to the edges of adjacent body panels; it may not cross the interior of other panels!

In addition, the abutting elements on a wake and its adjacent body panels should be contiguous because the potential jump due to the wake will be automatically included in calculation of the velocity on the body. This is necessary because a finite difference operation is used to find the velocity on the surface of the body. The potential jump due to the wake must be subtracted from the difference in potential between control points on opposite sides of the wake to avoid spurious velocities. The program does this automatically only if the wake abuts the surface at a panel boundary and the wake and panel elements are contiguous. If it is necessary to make the abutment with the side edge of the wake noncontiguous, then differentiation between the two body panels, across the wake, must be suppressed by restricting the abutment search. This can be done by specifying that the panel edges involved have no neighboring panels.

## MODELING INLETS AND NACELLES

For subsonic flows, inlets are modeled by using a permeable panel over the entrance to the inlet. The panel normal velocity is specified to establish the desired volume flux into the inlet. The forces calculated for the panel include the term from the momentum flux as well as the force from the pressure on the panel. The presence of the momentum flux term in the forces calculated by QUADPAN must be considered when using the results in conjunction with propulsion installation results.

In the case of supersonic flows, mach-super-inclined elements must be constructed to accommodate shock effects. A tube is constructed forward and aft of the inlet and nacelle.

### Flow-through Nacelles

Flow through nacelles can be modeled with QUADPAN. The nacelle is modeled by an outer surface and an inner surface which together form an annular body. A tubular wake shed from the trailing edge is required to generate the correct circulation. The only unusual feature of flow through nacelles is that they require relatively dense paneling to produce accurate results, due to the large velocity gradients at the throat and leading edge.

## MODELING EXHAUSTS

Exhausts can only be approximated in QUADPAN since the non-rotational nature of the code precludes accurate modeling of the jet shear layer. It is not possible to simulate an exhaust with a source panel along because the irrotational flow associated with the source panel does not resemble the free shear layer of the jet. The use of a wake to model the shear layer in conjunction with a source panel at the nozzle exit does not work. The long tubular wake and the source panel form a finite closed region with specified normal velocity, which results in an ill-posed problem, and a near-singular matrix. The flow through nacelle does not have this problem because the region inside the wake tube is connected to the rest of the flow field by way of the duct in the nacelle.

Currently, the best way to model an exhaust is to represent the exhaust plume as a force free solid body which extends from the exhaust nozzle. This approximation is satisfactory if the momentum flux of the jet is large compared to the surrounding fluid. A nonzero value of the normal velocity may be assigned to the body representing the exhaust to simulate entrainment. The exhaust should extend several diameters downstream and be closed on the aft end. Although the forces on the body simulating the exhaust plume are

not of interest, sufficient elements must be used on the exhaust tube to accurately establish the boundary conditions on the surface of the body.

Force free bodies which simulate exhaust plumes must be used carefully because the interference of the solid body used to simulate the plume with the rest of the vehicle can be large. An extreme example of this is a trailing edge with blowing. In this case the body used to simulate the jet acts like a large flap which can cause erroneous results for the lift of the wing.

## MODELING INTERNAL FLOWS

Internal flows, such as the flow in an inlet duct or a wind tunnel can be modeled with QUADPAN. The primary consideration in modeling internal flows is that it is not possible to arbitrarily specify the normal velocity on the entire surface as can be done for external flow problems. Therefore the surface which represents either the inflow or outflow region of the internal flow problem must be modeled with a panel on which the potential is specified (TYPE = -1) rather than the normal velocity.

An additional consideration is that the compressibility direction is constant throughout the flow domain. In internal flow problems it is possible that the local direction of the flow can vary in different parts of the domain (such as in a curved inlet duct). In this case, the effect of compressibility will not be calculated accurately.

### 3.3.2.5 QUADPAN Output

This subsection provides background material on the printed output from a QUADPAN run. An overview of the basic organization of the QUADPAN output is given, followed by a detailed explanation of the output data. An example printed output is included. An optional dump file for post-processing applications can also be written to punch.

## OVERVIEW OF QUADPAN OUTPUT

The printed output is subdivided into four major groups of information, as detailed below. The information printed by the program may be controlled by the user Figure 3-25.

- **Input Summary and Checking** - This section provides a summary of program resource usage, a listing of the basic parameters used for the panels, the panel edge abutment list and any warning or error messages from program checking operations.
- **Geometric Data** - Complete information on the geometry of every element is listed. The coordinates of the flow field survey points are given if a flow survey is specified.
- **Flow Condition Output Data** - This section contains the output data for the run and contains one set of output data for each flow condition. The data for each flow condition is subdivided into several output data groups, including the forces and moments in three axis systems, the flow quantities on the elements, flow field survey data, and the singularity strengths.

PRINTED OUTPUT DATA	PRINT FLAG			
	0	1	2	3
Program resource usage	X	X	X	X
Panel parameter data	X	X	X	X
Abutment check	X	X	X	X
Equation mapping information	X	X	X	X
Geometric data	X	O	O	O
Force and moments	X	X	X	X
Pressures for each element	X	X	X	O
Singularity strengths	X	X	O	O
<p>An 'X' in the column indicates output that is printed.  An 'O' indicates output that is suppressed.</p>				

Figure 3-25 Print Flag Options

## INPUT SUMMARY AND CHECKING

QUADPAN output has been modified in the integration to ASTROS. Much of the input data has been integrated into the ASTROS database and can be viewed through the ASTROS database program ICE. Still necessary data from QUADPAN processing is echoed in the ASTROS output.

This section contains a summary that may be used to check the use of program resources and the assignment of the basic panel parameters. The panel abutment list provides the user with the means to verify the geometry of the input dataset by listing the panel edge abutments found by the program. Error checking is done on wake panel Kutta edges and a consistency check is done on panel interior/exterior surfaces where panel edges abut. Finally, the number of equations required for the case is displayed.

The information provided on program resource usage is the number of panels, elements, points, and survey points used for the run. This section, together with the equation mapping section, can be used to estimate the size and cost of a QUADPAN run before actually calculating a flow solution.

A summary of the basic input parameters chosen for the panels is next provided (e.g. Figure 3-26). The following parameters are listed for each panel:

PANEL	Panel sequential index
ID	Panel identification number
NJ, NK	Number of elements in the J and K directions
IFRST	Element index of first element in panel (J=1, K=1)
TYPE	Panel type flag
FORCE	Panel force flag
WET	Panel wet flag
IMAGE	Panel image flag
VNORM	Normal velocity
Panel Title	

Image panels are not generated or listed for symmetric bodies in symmetric flow. Only the first forty-eight characters of a panel title will be printed in the output.

THE GEOMETRY IS Laterally Symmetric

PROGRAM MEMORY RESOURCE USAGE

43 PANELS  
322 ELEMENTS  
590 VERTICES

0 SURVEY POINTS  
0 SURVEY PANELS

0 MODAL POINTS  
0 MODAL PANELS

0 PROPELLERS

2 CONTROL SURFACES

386264 WORDS ALLOCATED FOR RESOURCES  
10568064 WORDS USED FOR WORK MEMORY

PANEL PARAMETER DATA

PANEL	ID	NJ	NK	IFRST	TYPE	CLASS	FORCE	WET	IMAGE	VNORM	
1	1	3	2	1	0	0	1	1	1	0.0000	UPPER NOSE
2	2	3	2	7	0	0	1	1	1	0.0000	LOWER NOSE
3	3	2	2	13	0	0	1	1	1	0.0000	UPPER FORE-BODY
4	4	2	2	17	0	0	1	1	1	0.0000	LOWER FORE-BODY
5	5	1	2	21	0	0	1	1	1	0.0000	FUSELAGE UPPER AT CANARD LEADING EDGE
6	6	1	2	23	0	0	1	1	1	0.0000	FUSELAGE LOWER AT CANARD LEADING EDGE
7	7	2	2	25	0	0	1	1	1	0.0000	BODY UPPER AT CANARD
8	8	2	2	29	0	0	1	1	1	0.0000	BODY LOWER AT CANARD
9	9	1	2	33	0	0	1	1	1	0.0000	FUSELAGE UPPER AT CANARD TRAILING EDGE
10	10	1	2	35	0	0	1	1	1	0.0000	FUSELAGE LOWER AT CANARD TRAILING EDGE
11	11	2	2	37	0	0	1	1	1	0.0000	MID-BODY UPPER
12	12	2	2	41	0	0	1	1	1	0.0000	MID-BODY LOWER
13	13	1	2	45	0	0	1	1	1	0.0000	BODY-WING LE UPPER
14	14	1	2	47	0	0	1	1	1	0.0000	BODY-WING LE LOWER
15	15	2	2	49	0	0	1	1	1	0.0000	BODY-WING UPPER
16	16	2	2	53	0	0	1	1	1	0.0000	BODY-WING LOWER
17	17	1	2	57	0	0	1	1	1	0.0000	BODY-WING TE UPPER
.	.	.	.	.	.	.	.	.	.	.	.
39	39	2	4	305	0	0	1	-1	1	0.0000	CANARD LOWER SURFACE
40	40	1	4	313	0	0	1	1	1	0.0000	CANARD CLOSURE
41	41	1	2	317	1	0	0	1	1	0.0000	CANARD WAKE
42	42	1	2	319	0	0	1	1	1	0.0000	MID-BODY FOR CANARD WAKE - UPPER
43	43	1	2	321	0	0	1	1	1	0.0000	MID-BODY FOR CANARD WAKE - LOWER

END OF PARAMETER DATA

Figure 3-26 Model Geometry Information Provided For Input Checking

*One of the first steps a user should make in verifying a geometry is to check the panel edge abutment list.* If abutments are not found for two panels that were meant to be connected, then there is a gap between them that should be corrected before making a complete run.

As shown in Figure 3-27 the panel abutment list begins with a printout of the tolerances used to determine which panels are connected to each other. This is followed by a panel-by-panel listing of the neighbors for the edges of each panel. The abutment information for each panel starts with:

Panel ID	Panel identification number
NJ, NK	Number of elements in the J and K directions
Panel title	

Abutments are listed for each panel by edge number (1-4). When QUADPAN finds that a group of elements on a panel edge abuts a group of elements on another panel edge, it prints the edge number and local J and K panel index range of elements on the panel under consideration, and the panel identification number, edge index, J and K ranges, and panel title of the abutting group of elements on the neighboring panel.

```

PANEL ABUTMENT CHECK

SEARCH PARAMETERS USED FOR ESTABLISHING PANEL EDGE ABUTMENTS
ABSTOL = 0.1000E-02 (MAXIMUM ABSOLUTE MATCHING DISTANCE BETWEEN ELEMENT EDGE MIDPOINTS)
RELTOL = 0.1000E-01 (MAXIMUM RELATIVE MATCHING DISTANCE BETWEEN ELEMENT EDGE MIDPOINTS
                     AS A FRACTION OF THE ELEMENT EDGE LENGTH)

** PANEL ABUTMENT LIST **

*-----*
ABUTMENTS FOR PANEL ID-> 1      NJ = 3      NK = 2      UPPER NOSE
EDGE  J, K TO J, K ABUTS PANEL EDGE  J, K TO J, K
1  1 1 1 2      3 3 2 1 2 2      UPPER FORE-BODY
2  1 2 3 2      2 4 1 1 3 1      LOWER NOSE
3  DEGENERATE EDGE
4  3 1 1 1      -1 4 3 1 1 1      UPPER NOSE
*-----*
ABUTMENTS FOR PANEL ID-> 2      NJ = 3      NK = 2      LOWER NOSE
.
.
.
*-----*
ABUTMENTS FOR PANEL ID-> 43     NJ = 1      NK = 2      MID-BODY FOR CANARD WAKE - LOWER
EDGE  J, K TO J, K ABUTS PANEL EDGE  J, K TO J, K
1  1 1 1 2      12 3 2 1 2 2      MID-BODY LOWER
2  1 2 1 2      -43 2 1 2 1 2      MID-BODY FOR CANARD WAKE - LOWER
3  1 2 1 1      10 1 1 2 1 1      FUSELAGE LOWER AT CANARD TRAILING EDGE
4  1 1 1 1      41 4 1 1 1 1      CANARD WAKE
4  1 1 1 1      42 2 1 2 1 2      MID-BODY FOR CANARD WAKE - UPPER
END OF PANEL ABUTMENT CHECK

```

Figure 3-27 Abutment Checks Are Critical To Model Debugging

Following the abutment list may be warning messages concerning wake Kutta edge alignment and panel interior/exterior surface assignment. Warning and error messages will be printed in the output listing if there are no abutments found for the Kutta edge of a wake panel (no shedding elements) or if abutting panels have inconsistent interior and exterior surfaces, as controlled by the panel WET flags.

The output section on equation mapping, illustrated in Figure 3-28 gives the number of equations (number of rows and columns in the matrices) that QUADPAN will use for the run. These are broken down into equations with hydrodynamic boundary conditions (corresponding to body elements), and those with wake boundary conditions (wake elements). It is important to keep in mind that each wake strip has only one equation associated with it, no matter how many elements are in the wake strip. Since there is only one

boundary condition for a wake strip, there is no computational penalty for adding extra wake elements to a strip.

```

EQUATION MAPPING

226 TOTAL EQUATION ROWS AND COLUMNS

192 NEUMANN BOUNDARY CONDITION EQUATIONS
0   DIRICHLET BOUNDARY CONDITION EQUATIONS
34  WAKE BOUNDARY CONDITION EQUATIONS
0   FREE SURFACE BOUNDARY CONDITION EQUATIONS

END OF EQUATION MAPPING

```

Figure 3-28 Equation Mapping Section Indicates Order of Matrices In The Solution

## GEOMETRIC DATA

Full geometric data is provided for each element in the configuration in the ASTROS runtime database. This information can be used for debugging the input geometry, and can be retrieved using ICE. Since complicated cases require many elements, this output section would have been quite large and therefore was removed from the standard ASTROS output. For this reason, the QUADPAN user may also output a separate geometric printout in the punch file (.pch).

The geometric data printed by QUADPAN for each element is grouped by panels and constant J strips and includes:

I	Element index
J,K	Local element indices on panel
X1/Y1/Z1	Element corner point 1
X2/Y2/Z2	Element corner point 2
X3/Y3/Z3	Element corner point 3
X4/Y4/Z4	Element corner point 4
XC/YC/ZC	Element control point
NX/NY/NZ	Normal vector components
AREA	Element area

All geometric coordinates are given in the Global Coordinate System (3.3.2.2) used for the input. The numbering of indices and corner points follows the convention explained in Ref. 12. The normals printed are the true geometric normals, regardless of any simulated deflections. The normals used in QUADPAN are outward pointing vectors, i.e., they point outward from the body into the fluid.

## FLOW CONDITION OUTPUT

The flow output information from the run is divided into several groups of data for each flow condition (angle of attack, sideslip and angular velocity combination):

- Forces and moments
- Surface pressures and velocities
- Singularity strengths

The user can control which of these groups are printed using the PRINT control flag in the input dataset.

The forces and moments are printed out for the configuration as a whole and for each panel. This data is printed in three axis systems as a convenience to the user - the BODY, STABILITY, and WIND axes, as discussed below and illustrated in Figures 3-29 through 3-31. The user should take careful note of the sign conventions used for these axis systems!

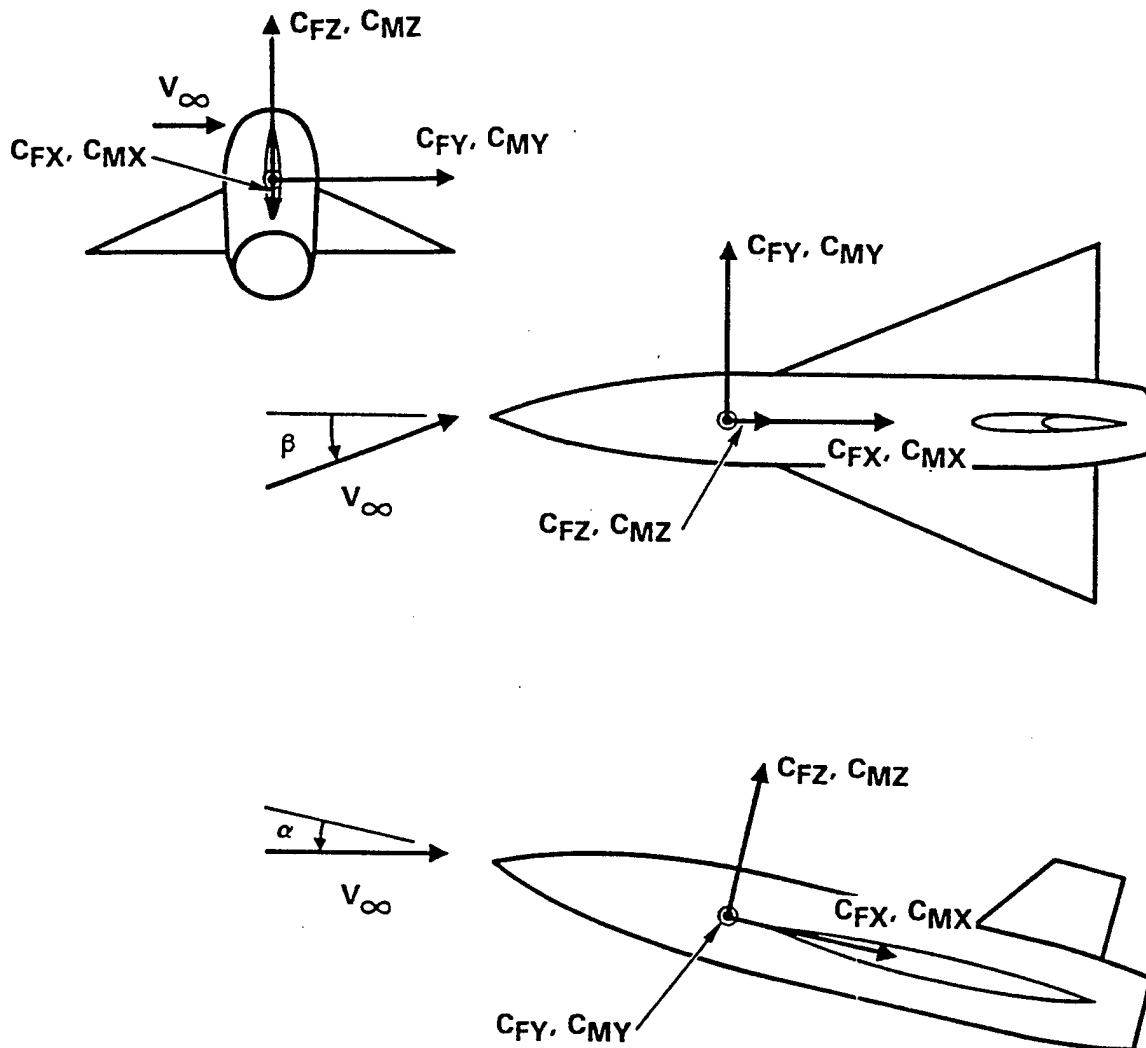


Figure 3-29 QUADPAN Body Axes



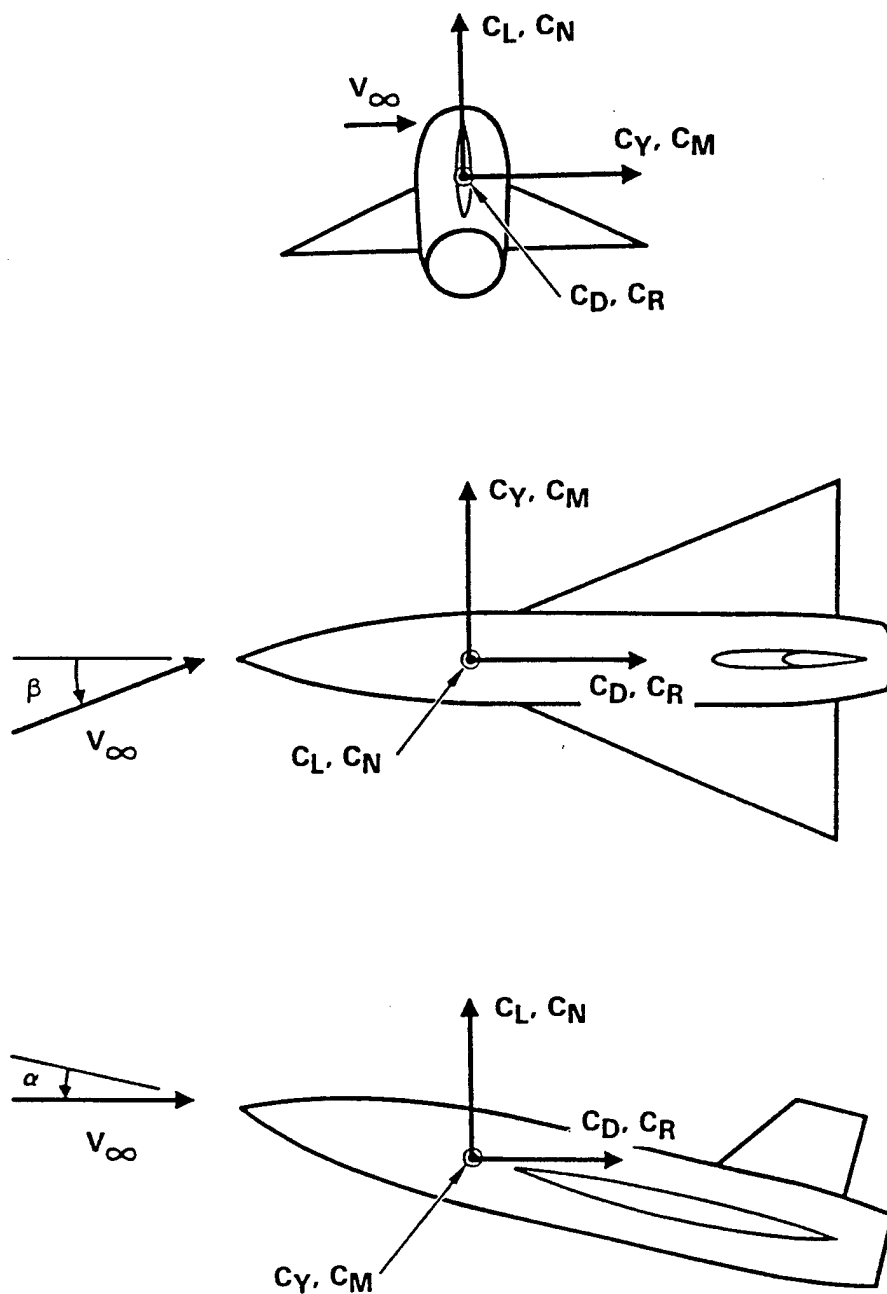


Figure 3-30 QUADPAN Stability Axes

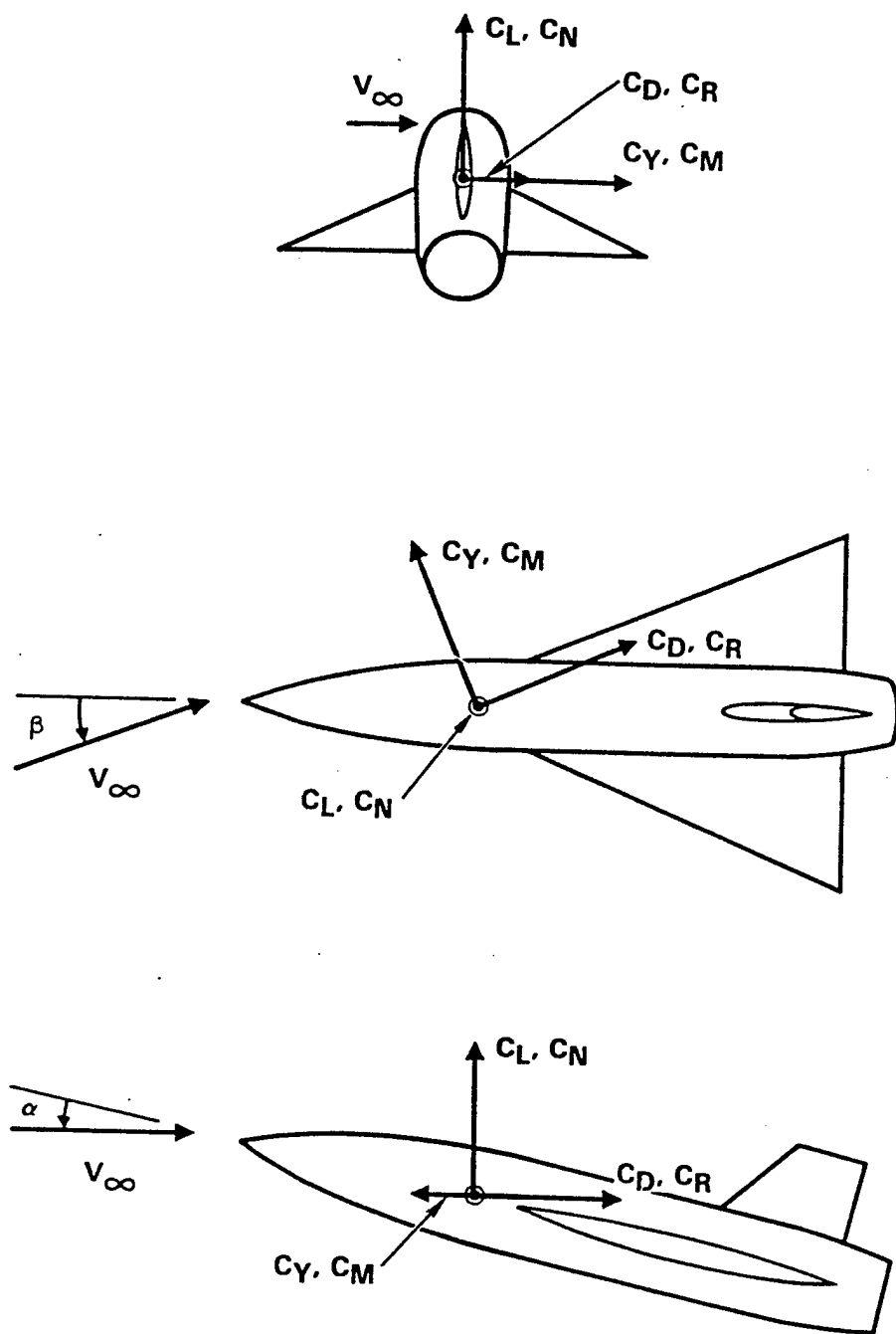


Figure 3-31 QUADPAN Wind Axes

## 1 FSW ASTROS QA PROBLEM

QUADPAN VERSION 3.5.1.18

MACH = 0.9000 ALPHA = 0.0000 DEG BETA = 0.0000 DEG RFREQ = 0.0000  
 ROLL = 0.0000 D/S PITCH = 0.0000 D/S YAW = 0.0000 D/S FROUDE = 0.0000

\*\*\*\*\*

FORCES AND MOMENTS ARE IN THE COORDINATE DIRECTIONS OF THE BODY AXES. \* BODY AXES \*  
 (MOMENTS ARE POSITIVE IN THE DIRECTION GIVEN BY THE RIGHT-HAND RULE)

ANGULAR RATES IN BODY AXES: ROLL = 0.00000 PITCH = 0.00000 YAW = 0.00000

MOMENT AND ROTATION CENTER: XBAR = 30.0000 YBAR = 0.0000 ZBAR = 0.0000  
 REFERENCE AREA AND LENGTHS: SREF = 400.00 CBAR = 10.0000 WSPAN = 40.0000

FORCES AND MOMENTS IN BODY AXES: (IMAGE PANEL ID NO.S ARE PRECEDED BY A MINUS SIGN)  
 (CFX,CFY,CFZ REFERENCED TO SREF; CMX,CMY,CMZ REFERENCED TO SREF\*CBAR)

PANEL	ID	FORCE	CFX	CFY	CFZ	CMX	CMY	CMZ	
*** TOTALS ***			0.02099	0.00000	0.00000	0.00000	0.00000	0.00000	
1	1	1	0.00067	-0.00106	-0.00177	-0.00003	-0.00518	0.00306	UPPER NOSE
2	2	1	0.00067	-0.00106	0.00177	0.00003	0.00518	0.00306	LOWER NOSE
3	3	1	0.00000	0.00150	0.00331	0.00029	0.00807	-0.00372	UPPER FORE-BODY
4	4	1	0.00000	0.00150	-0.00331	-0.00029	-0.00807	-0.00372	LOWER FORE-BODY
5	5	1	-0.00001	0.00015	0.00043	0.00003	0.00081	-0.00028	FUSELAGE UPPER AT CANARD LEADING EDGE
6	6	1	-0.00001	0.00015	-0.00043	-0.00003	-0.00081	-0.00028	FUSELAGE LOWER AT CANARD LEADING EDGE
7	7	1	0.00000	0.00175	0.00467	0.00044	0.00704	-0.00264	BODY UPPER AT CANARD
8	8	1	0.00000	0.00175	-0.00467	-0.00044	-0.00704	-0.00264	BODY LOWER AT CANARD
9	9	1	-0.00001	-0.00015	-0.00020	-0.00003	-0.00023	0.00017	FUSELAGE UPPER AT CANARD TRAILING EDGE
10	10	1	-0.00001	-0.00015	0.00020	0.00003	0.00023	0.00017	FUSELAGE LOWER AT CANARD TRAILING EDGE
11	11	1	0.00000	-0.00140	-0.00223	-0.00024	-0.00186	0.00116	MID-BODY UPPER
12	12	1	0.00000	-0.00140	0.00223	0.00024	0.00186	0.00116	MID-BODY LOWER
13	13	1	-0.00006	0.00097	0.00222	0.00020	0.00115	-0.00049	BODY-WING LE UPPER
14	14	1	-0.00006	0.00097	-0.00222	-0.00020	-0.00115	-0.00049	BODY-WING LE LOWER
15	15	1	0.00000	0.00214	0.00584	0.00054	0.00098	-0.00036	BODY-WING UPPER
16	16	1	0.00000	0.00214	-0.00584	-0.00054	-0.00098	-0.00036	BODY-WING LOWER
17	17	1	0.00005	0.00085	0.00224	0.00019	-0.00051	0.00019	BODY-WING TE UPPER
18	18	1	0.00005	0.00085	-0.00224	-0.00019	0.00051	0.00019	BODY-WING TE LOWER
19	19	1	-0.00038	-0.00096	-0.00159	-0.00011	0.00099	-0.00054	NOZZLE - UPPER
20	20	1	-0.00038	-0.00096	0.00159	0.00011	-0.00099	-0.00054	NOZZLE - LOWER
21	21	1	0.00195	0.00094	0.05545	0.03460	0.01645	-0.00076	INBOARD WING UPPER
22	22	1	0.00195	0.00094	-0.05545	-0.03460	-0.01645	-0.00076	INBOARD WING LOWER
23	23	1	-0.00051	0.00089	0.02560	0.03522	0.02144	0.00001	OUTER WING UPPER
24	24	1	-0.00051	0.00089	-0.02560	-0.03522	-0.02144	0.00001	OUTER WING LOWER
25	25	1	0.00224	0.00176	0.01876	0.02631	0.00821	-0.00357	AILERON UPPER
26	26	1	0.00224	0.00176	-0.01876	-0.02631	-0.00821	-0.00357	AILERON LOWER
27	27	0	0.00000	0.00000	0.00000	0.00000	0.00000	0.00000	INBOARD WING WAKE
28	28	0	0.00000	0.00000	0.00000	0.00000	0.00000	0.00000	OUTBOARD WING WAKE
29	29	0	0.00000	0.00000	0.00000	0.00000	0.00000	0.00000	WING WAKE INBOARD
30	30	0	0.00000	0.00000	0.00000	0.00000	0.00000	0.00000	WING WAKE OUTBOARD
31	31	0	0.00000	0.00000	0.00000	0.00000	0.00000	0.00000	WING WAKE - INBOARD
32	32	0	0.00000	0.00000	0.00000	0.00000	0.00000	0.00000	WING WAKE - OUTBOARD
33	33	0	0.00000	0.00000	0.00000	0.00000	0.00000	0.00000	WING WAKE
34	34	0	0.00000	-0.00126	-0.00251	-0.00012	0.00002	-0.00001	NOZZLE PLUME - UPPER
35	35	0	0.00000	-0.00126	0.00251	0.00012	-0.00002	-0.00001	NOZZLE PLUME - LOWER
36	36	0	-0.00002	-0.00015	-0.00027	0.00000	0.00210	-0.00114	NOZZLE PLUME CONE - UPPER
37	37	0	-0.00002	-0.00015	0.00027	0.00000	-0.00210	-0.00114	NOZZLE PLUME CONE - LOWER
38	38	1	0.00130	0.00000	0.03201	0.01559	0.04556	-0.00063	CANARD UPPER SURFACE
39	39	1	0.00130	0.00000	-0.03201	-0.01559	-0.04556	-0.00063	CANARD LOWER SURFACE
40	40	1	0.00000	0.00112	0.00000	0.00000	0.00000	-0.00186	CANARD CLOSURE
41	41	0	0.00000	0.00000	0.00000	0.00000	0.00000	0.00000	CANARD WAKE
42	42	1	0.00000	-0.00036	-0.00058	-0.00006	-0.00056	0.00035	MID-BODY FOR CANARD WAKE - UPPER
43	43	1	0.00000	-0.00036	0.00058	0.00006	0.00056	0.00035	MID-BODY FOR CANARD WAKE - LOWER

END OF FORCE AND MOMENT DATA IN BODY AXES

Figure 3-32 Forward Swept Wing Sample Forces and Moments In The Body Axis

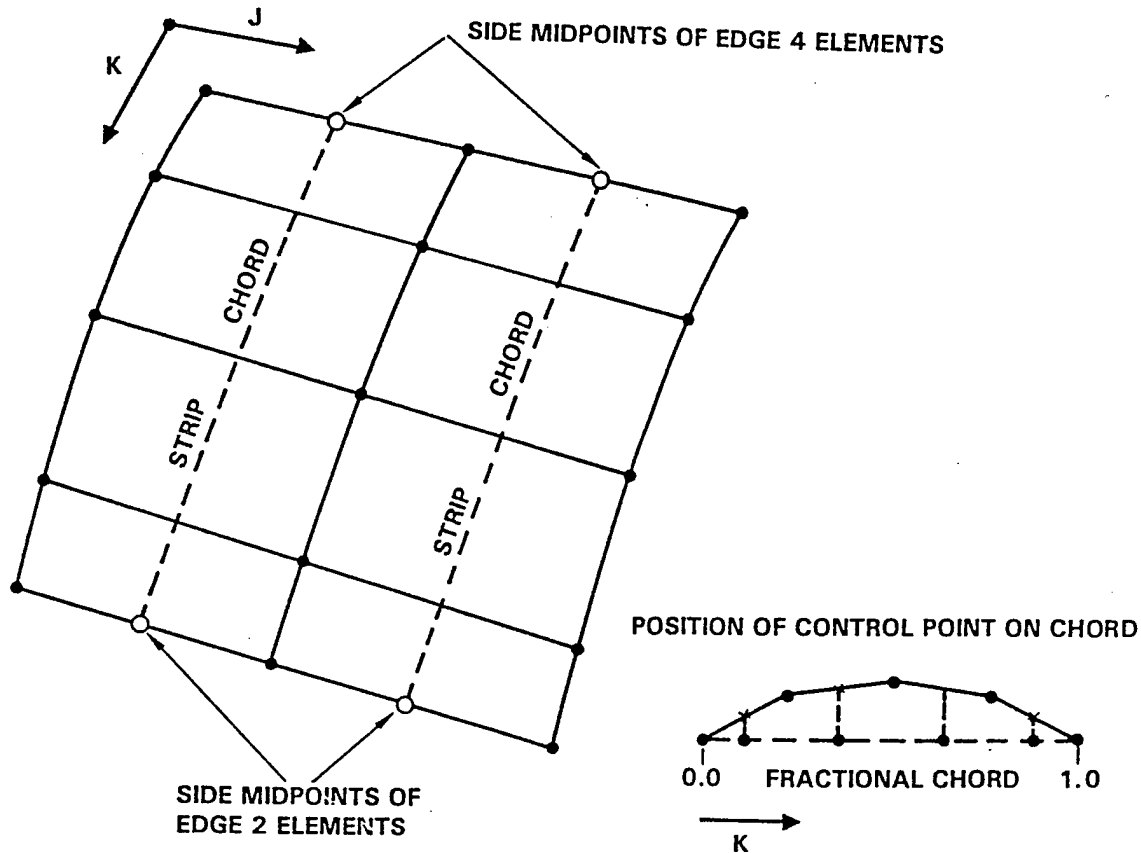


Figure 3-33 Strip Chord

### 3.3.3 Alternate Steady Aerodynamic Data

The group entity is utilized as a means of specifying *alternate* aerodynamic data for run-time solutions and archiving run-time data to user specified databases. *Alternate* Data is such data that is meant to augment an existing model and can be specified for use at run-time using the model assembly commands defined in Section 3.2. Five formalized group entity types are available to the user in the run-time model:

- STDYGEOM - steady aerodynamic model geometry
- RIGDALOD - rigid aerodynamic parameter load vectors
- AIC - AIC matrices
- SPLINE - spline matrices
- RIGDSL0D - user defined rigid structural load vectors

As discussed thoroughly in Subsection 3.2 model assembly commands are available within the solution control packet in order to assemble the run-time MODEL for each subcase. The MODEL is itself a group entity which contains the names (and database locations) of the formalized group members and additional entity names (and database locations) which will be created at run-time. Model assembly commands further allow user defined combinations of both run-time and/or alternate formalized group

entities through use of the OVERLAY command (e.g., partial set of wind tunnel rigid parameter data with run-time QUADPAN solution for parameters where wind tunnel data does not exist).

Each subcase (of type FTRIM) has associated with it a unique MODEL group which specifies the set of entities associated with the MODEL. However, members of a particular MODEL may also be members of other MODELS (i.e., the same STDYGEOM group may be used by more than one model). Recall that two formalized MODEL groups have been established as depicted in Figure 3-34. A unique SAMODEL will be established for each SAERO subcase while a unique SAEMODEL will be established for each FTRIM subcase.

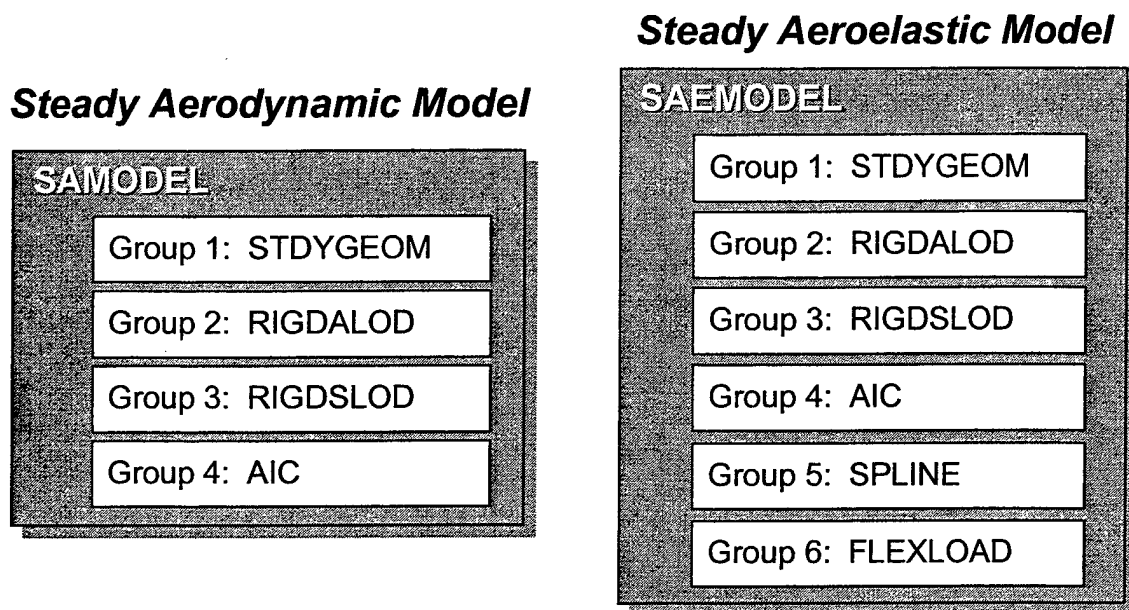


Figure 3-34 Steady Aerodynamic and Steady Aeroelastic Model Groups.

With these groups, a user may construct an alternate aerodynamic database consisting of pressure data from computation fluid dynamics solutions or even wind tunnel pressure data. Alternate data may be provided in the form of aerodynamic influence coefficient matrices (AIC group), pressure data (RIGDALOD group), geometry (STDYGEOM group), and splines (SPLINE group). The user can construct a CADDDB database using ASTROS application protocol interface routines and database entity definitions found in the ASTROS' programmer's manual (Ref. 13) and the AANDE programmer's document (Ref. 11). The aforementioned groups must be available in the database including all of the entities defined within the programmer's manual. A database does not need to contain every group within a MODEL, only the groups that are desired during the anticipated model assembly commands.

For instance, to include nonlinear pressure data from a CFD analysis, only a RIGDALOD group is required within the database. To include an aerodynamic influence coefficient matrix developed from some source outside of ASTROS, the AIC group must be included. If the aerodynamic influence coefficient theory requires a unique operation from the ASTROS paradigm for mapping aerodynamics to structures, a SPLINE group will be required as well. Otherwise, the spline theories in ASTROS can be used in acquiring an aeroelastic solution.

The only alternate aerodynamics requirement that ASTROS will check for in the AANDE modifications is compliance in order between vectors and matrices. No other checking is conceivable; therefore, the user of alternate aerodynamic patches into ASTROS must check for compliant assumptions in aerodynamic theories.

### 3.4 STEADY AERODYNAMIC SPLINES

Interconnection between the aerodynamic model and the structural finite element model is accomplished by two transformations to the basic equation for aeroelastic analysis:

$$[K - qA]u + [M]\ddot{u} = \{P\}\delta$$

-or -

[Eqn. 3-1]

$$[K - q[[G][AIC][GS]]]u + [M]\ddot{u} = [G]\{PA\}\delta$$

First, the load transformation is accomplished through a single spline matrix which transforms rigid air load at aerodynamic boxes to structural grids. Second, the aeroelastic increment transformation consists of both a load spline and a slope spline. The load spline pre-multiplies the aerodynamic influence coefficient matrix to give forces in the structural domain as a function of aerodynamic slope, while the slope spline post multiplies the resulting matrix to give forces in the structural domain as a function of structural displacements. The previous methodology did not differentiate between the two load splines used in each transformation. MAPOL structure was expanded to allow for three distinct splines; an *aerodynamic* load spline, *aeroelastic* load increment spline, and an *aeroelastic* slope increment spline. The distinction between the *aerodynamic* load spline and the *aeroelastic* load spline serve to further generalize the aeroelastic solution.

ASTROS methodology previously included three transformation options to define interconnectivity between the aerodynamic and structural models; two-dimensional surface, beam and attach spline options. Modifications to the current capability occurred in three areas. First, a three-dimensional surface spline was added to the library of spline options. The three-dimensional spline serves to maintain the improved accuracy of the three-dimensional loads (provided by the new QUADPAN aerodynamics option) between the aerodynamic and structural models. Secondly, the attach methodology was modified in order to provide more generality. Lastly, the aerodynamic load, aeroelastic load increment and aeroelastic slope increment splines is not limited solely to ASTROS library of spline options. A completely general approach was also developed to include user-specified alternate spline matrices.

The attach option maps the resultant aerodynamic load from a group of aerodynamic boxes to a single structural grid and defines the aeroelastic slope of the group of boxes to be equal to the displacement of the structural grid to which they are attached. Methodology was expanded such that the aeroelastic increment of attached boxes is either included (as is the current function) or excluded. Exclusion of aeroelastic feedback for certain groups of boxes required distinct aerodynamic load and aeroelastic load increment splines. The new attach feature is easily defined, and the reader is referred to Ref. 12 for implementation.

The baseline spline method continues to be the Harder-Desmarais infinite plate spline (Ref. 17) used by the ASTROS version 12.0 software. However implementation of the spline features has changed slightly. The spline cards now require a MODEL name since splines are associated with the Steady Aeroelastic Model. Also, new input cards have been defined (PANLST1 and PANLST2) to accommodate extension in aerodynamic modeling concepts (see Ref. 12).

Extension of the 2D surface spline to a 3D transformation is discussed in Sections 3.4.1 and 3.4.2. The new ASTROS card for this feature is denoted as a SPLINE3.

### 3.4.1 Assembly of the Three-Dimensional Force Spline

The basic 2D force spline,  $[G']$ , computes forces (perpendicular to the spline plane) at a specified set of output points for a given set of perpendicular forces at specified input points.

$$\{F\}_O = [G']\{F\}_I \quad [\text{Eqn. 3-2}]$$

where;

- $\{F\}_O$  = vector of output forces having one row for each output point.
- $[G']$  = 2D force spline matrix relating forces at input points to forces at output points. The matrix has one row for each output point and one column for each input point.
- $\{F\}_I$  = vector of input forces having one row for each output point.

Three-dimensional structural loads (i.e., xyz-component loads) can be computed by applying the 2D force spline separately to each aerodynamic component load vector.

$$\begin{aligned} \{F_X\}_S &= [G']\{F_X\}_A = [[G'][\hat{n}_X]]\{F\}_A \\ \{F_Y\}_S &= [G']\{F_Y\}_A = [[G'][\hat{n}_Y]]\{F\}_A \\ \{F_Z\}_S &= [G']\{F_Z\}_A = [[G'][\hat{n}_Z]]\{F\}_A \\ \{M_X\}_S &= 0 \\ \{M_Y\}_S &= 0 \\ \{M_Z\}_S &= 0 \end{aligned} \quad [\text{Eqn. 3-3}]$$

where the matrices  $[\hat{n}_X]$ ,  $[\hat{n}_Y]$ , and  $[\hat{n}_Z]$  are diagonal matrices containing components of the normal vectors for each of the aerodynamic panels:

$$[\hat{n}_X] = \begin{bmatrix} n_{X_1} & 0 & \cdots & 0 \\ 0 & n_{X_2} & \cdots & 0 \\ \vdots & \vdots & \ddots & \vdots \\ 0 & 0 & \cdots & n_{X_n} \end{bmatrix}, [\hat{n}_Y] = \begin{bmatrix} n_{Y_1} & 0 & \cdots & 0 \\ 0 & n_{Y_2} & \cdots & 0 \\ \vdots & \vdots & \ddots & \vdots \\ 0 & 0 & \cdots & n_{Y_n} \end{bmatrix}, \text{ and } [\hat{n}_Z] = \begin{bmatrix} n_{Z_1} & 0 & \cdots & 0 \\ 0 & n_{Z_2} & \cdots & 0 \\ \vdots & \vdots & \ddots & \vdots \\ 0 & 0 & \cdots & n_{Z_n} \end{bmatrix}.$$

A 3D force spline matrix,  $[G]$ , can be assembled from the previous set of six equations and the rows rearranged corresponding to the internal sequencing specified in the BGPDT relation.

$$\{F\}_S = \begin{Bmatrix} F_X \\ F_Y \\ F_Z \\ M_X \\ M_Y \\ M_Z \end{Bmatrix}_S = \begin{bmatrix} [G'][\hat{n}_X] \\ [G'][\hat{n}_Y] \\ [G'][\hat{n}_Z] \\ [0] \\ [0] \\ [0] \end{bmatrix} \{F\}_A = [G]\{F\}_A \quad [\text{Eqn. 3-4}]$$

### 3.4.2 Derivation of the Three-Dimensional Slope Spline

Angle of attack is defined as the angle between the panel normal and the flow stream axis. Therefore, a rotation axis is defined as the cross product of the panel normal and the flow stream axis. The change in angle of attack (measured about the panel rotation axis) for a given panel,  $i$ , can be approximated by the quantity  $-\partial W_i / \partial X_i$ , where  $W_i$  is the displacement normal to the plane defined by the panel rotation axis and the flow stream axis, and the spline plane X-axis is defined to be equal to the flow stream axis. Derivation of the slope spline matrix is presented in the following paragraphs and covers the following topics:

- computation of the local spline plane unit vectors
- computation of panel slope spline
- transformation from primary to local spline plane
- assembly of slope spline matrix

#### Computation of the Local Spline Plane Unit Vectors

The GEOMSA relation contains defining geometry for each panel in the aerodynamic model. The GEOMSA relation was expanded to contain both the panel centroid and panel control point locations. The slope spline methodology developed here computes slopes at the panel centroid while the force methodology developed in the preceding section transforms forces applied at the panel control point. The following terms are defined in order to represent the data contained in the GEOMSA relation and additionally the flow stream axis.

- $\langle \mathbf{X}_{CP} \rangle$  - location of panel control point
- $\langle \mathbf{X}_0 \rangle$  - location of panel centroid
- $\langle \hat{\mathbf{n}}_N \rangle$  - unit vector defining panel normal
- $\langle \hat{\mathbf{n}}_R \rangle$  - unit vector defining panel rotation axis
- $\langle \hat{\mathbf{n}}_{V0} \rangle$  - unit vector defining direction of flow stream

Additional terms are defined in order to represent computed data and the spline plane defining data for a given panel.

- $\langle \hat{\mathbf{n}}_V \rangle$  - unit vector defining panel X-axis
- $\langle \hat{\mathbf{n}}_{N'} \rangle$  - unit vector defining local spline plane normal
- $\langle \hat{\mathbf{n}}_{R'} \rangle$  - unit vector defining local spline plane rotation axis
- $\langle \hat{\mathbf{n}}_{V'} \rangle$  - unit vector defining local spline plane X'-axis

The slope approximation,  $Da_i = -\partial W_i / \partial X_i$ , computes positive panel slope for a positive rotation about the local Y-axis or rotation axis. Therefore, for a given panel, the local spline plane rotation axis is defined to be equal to the panel rotation axis.

$$\langle \hat{\mathbf{n}}_{R'} \rangle = \langle \hat{\mathbf{n}}_R \rangle \quad [\text{Eqn. 3-5}]$$

Since the rotation axis is normal to the flow stream by definition, the spline plane X-axis is defined to be equal to the flow stream axis.

$$\langle \hat{\mathbf{n}}_{V'} \rangle = \langle \hat{\mathbf{n}}_{V0} \rangle \quad [\text{Eqn. 3-6}]$$



Finally, since the displacements,  $W$ , are normal to the plane defined by the panel rotation axis and the flow stream, the normal to the local spline plane can be computed from the cross product as shown.

$$\langle \hat{\mathbf{n}}_{N'} \rangle = \langle \hat{\mathbf{n}}_{V0} \rangle \times \langle \hat{\mathbf{n}}_{R'} \rangle \quad [\text{Eqn. 3-7}]$$

#### Computation of Panel Slope Spline

The baseline spline method continues to be the Harder-Desmarais infinite plate spline used by the ASTROS version 12.0 software. Also, the approach continues to require definition of a primary spline plane for some group of aerodynamic panels and associated structural grids. However, a restriction was imposed which requires the primary spline plane to include the flow stream axis. This restriction allows the 2D slope spline matrix derived from displacements perpendicular to the primary spline plane to be transformed to local panel coordinates on a panel by panel basis.

All structural grids in the user defined spline set are projected to the primary spline plane and a slope spline matrix is defined as is the current ASTROS function. The resulting basic slope spline matrix,  $[\mathbf{GS}']$ , relates displacements measured perpendicular to the spline plane to panel rotations measured about the spline plane rotation axis.

$$\{\theta\} = -[\mathbf{GS}']\{\mathbf{W}_0\} \quad [\text{Eqn. 3-8}]$$

where;

$\{\theta\}$  = Vector of panel rotations measured about the spline plane rotation axis. The vector has one row for each aerodynamic panel.

$[\mathbf{GS}']$  = Basic slope spline matrix relating displacements perpendicular to the spline plane to panel rotations about the spline plane rotation axis. The matrix has a single row for each aerodynamic panel and a single column for each structural grid. Columns of the matrix are organized according the internal/external ID relationship specified in the BGPDT relation.

$\{\mathbf{W}_0\}$  = Vector of structural displacements perpendicular to the primary spline plane. The vector has one row for each structural degree of freedom.

#### Transformation from Primary to Local Spline Plane

The next step is to transform panel rotations measured about the primary spline plane rotation axis to panel rotations measured about their respective local rotation axes. The basic spline matrix approximates the values  $Dq_i = -(\partial W_0 / \partial X)_i$ , while our objective is the values  $Da_i = -\partial W_i / \partial X_i$ . Two observations are noted to facilitate the transformation. First, the X-axis in each case is identical due to the restriction imposed above (the primary spline plane must include the flow stream axis). Further, the local spline plane X-axis is always equal to the flow stream axis because the local rotation axis is defined by the cross product of the panel normal and flow stream axis. Second, the rotations in the first case are computed using displacements perpendicular to the primary spline plane while the rotations in the second case are computed using displacements perpendicular to the respective local spline planes. Therefore, the transformation consists of simply computing each panel slope separately using displacements perpendicular to the local spline plane.

$$\alpha_i = -\{\mathbf{GS}'\}_i \{\mathbf{W}\}_i \quad [\text{Eqn. 3-9}]$$

where;

$\alpha_i$  = Slope for the  $i^{\text{th}}$  aerodynamic panel.

$\{\mathbf{GS}'\}_i$  = Vector of 2D slope spline coefficients relating displacements to slopes.  
The vector has a single row and one column for each structural grid.

$\{\mathbf{W}\}_i$  = Vector of structural displacements perpendicular to the local spline plane.  
The vector has one row for each structural grid.

Extension to the 3D case implies that the structural displacement vector,  $\{\mathbf{W}\}_i$ , has been transformed to the local coordinate system of the  $i^{\text{th}}$  local spline plane. This transformation can be accomplished by multiplying each structural displacement (in the basic coordinate system) by the  $i^{\text{th}}$  local spline plane normal.

$$W_j = \langle n_{x_i}, n_{y_i}, n_{z_i}, 0, 0, 0 \rangle \bullet \langle X_j, Y_j, Z_j, \theta_{x_j}, \theta_{y_j}, \theta_{z_j} \rangle$$

-or-

$$\{\mathbf{W}\}_i = \begin{bmatrix} \langle \hat{n}_i \rangle & 0 & \cdots & 0 \\ 0 & \langle \hat{n}_i \rangle & \cdots & 0 \\ \vdots & \vdots & \ddots & \vdots \\ 0 & 0 & \cdots & \langle \hat{n}_i \rangle \end{bmatrix} \{\mathbf{U}_B\} \quad [\text{Eqn. 3-10}]$$

where;

$W_j$  = The  $j^{\text{th}}$  structural displacement perpendicular to the  $i^{\text{th}}$  spline plane.

$\langle \hat{n}_i \rangle$  = Spline plane normal vector for the  $i^{\text{th}}$  aerodynamic panel.

$\{\mathbf{U}_B\}$  = Vector of structural displacements in the basic coordinate system. The vector has one row for each structural degree of freedom.

Simplifying the notation of the previous equation we arrive at the following transformation from displacements in the basic system to displacements perpendicular to the local spline plane.

$$\{\mathbf{W}\}_i = [\hat{n}]_i \{\mathbf{U}_B\} \quad [\text{Eqn. 3-11}]$$

where;

$[\hat{n}]_i$  = Matrix of panel normal vectors for the  $i^{\text{th}}$  aerodynamic panel.

Substituting Eqn. 3-9 we can express panel slope as a function of structural displacements in the basic coordinate system.

$$\alpha_i = -\{\mathbf{GS}'\}_i [\hat{n}]_i \{\mathbf{U}_B\} \quad [\text{Eqn. 3-12}]$$

#### Assembly of Slope Spline Matrix

The 3D slope spline matrix can be assembled from the rows of Eqn. 3-12.

$$\{\alpha\} = \begin{Bmatrix} \alpha_1 \\ \alpha_2 \\ \vdots \\ \alpha_n \end{Bmatrix} = \begin{Bmatrix} -\{\mathbf{GS}'\}_1[\hat{\mathbf{n}}]_1 \\ -\{\mathbf{GS}'\}_2[\hat{\mathbf{n}}]_2 \\ \vdots \\ -\{\mathbf{GS}'\}_n[\hat{\mathbf{n}}]_n \end{Bmatrix} \{\mathbf{U}_B\} \quad [\text{Eqn. 3-13}]$$

A final transformation is required prior to returning the spline matrix to MAPOL. Eqn. 3-13 has been derived to operate on structural displacements in the basic coordinate system, while the structural displacements computed in MAPOL reside in the global coordinate system. The structural displacements can be transformed to the basic coordinate system using a coordinate system transformation matrix,  $[\mathbf{R}_{BG}]$ , assembled using the CSTM relation.

$$\{\mathbf{U}_B\} = [\mathbf{R}_{BG}]\{\mathbf{U}_G\} \quad [\text{Eqn. 3-14}]$$

where;

- $[\mathbf{R}_{BG}]$  = Transformation matrix relating displacements in the global coordinate system to displacements in the basic coordinate system. The matrix is square having one row and column for each structural degree of freedom.
- $\{\mathbf{U}_G\}$  = Vector of structural displacements in the global coordinate system. The vector has one row for each structural degree of freedom.

Substituting Eqn. 3-14 into Eqn. 3-13 yields the following equation.

$$\{\alpha\} = \begin{Bmatrix} -\{\mathbf{GS}'\}_1[\hat{\mathbf{n}}]_1 \\ -\{\mathbf{GS}'\}_2[\hat{\mathbf{n}}]_2 \\ \vdots \\ -\{\mathbf{GS}'\}_n[\hat{\mathbf{n}}]_n \end{Bmatrix} [\mathbf{R}_{BG}]\{\mathbf{U}_G\} \quad [\text{Eqn. 3-15}]$$

The final form of the slope spline matrix,  $[\mathbf{GS}]$ , is formed by performing the multiplication specified in the previous equation.

$$\{\alpha\} = [\mathbf{GS}]\{\mathbf{U}_G\} \quad [\text{Eqn. 3-16}]$$

where;

- $[\mathbf{GS}]$  = 3D slope spline matrix relating structural displacements in the global coordinate system to aerodynamic panel slopes. The matrix has one row for each aerodynamic panel and one column for each structural degree of freedom. The internal/external grid ID relationship is defined in the BGPDT relation.

### 3.5 ASSEMBLY AND SOLUTIONS OF AEROELASTIC EQUATIONS

ASTROS will perform linear steady aeroelastic analysis for both the ANALYZE and OPTIMIZE options. Under the AANDE modifications, the rigid loads and the aerodynamic influence coefficient matrices may be derived from a nonlinear basis, and these data are assumed to be piecewise linear for the basis of the aeroelastic solution. Assembly of the aeroelastic equations include development of the rigid loads in incremental format. Modifications to the ASTROS solution sequence provide for a simple

automated substructuring technique that allow for structural and aerodynamic models that have centerline symmetry about the Basic coordinate system X-Z plane. The basic steady aeroelastic equation is formed and solved to provide incremental loads and deflections for each control parameter and acceleration. Stability coefficients and maneuver trim simulations are computed, however, now in two separate modules. The maneuver trim simulation has been isolated to allow inclusion of control surface scheduling and trim optimization for redundant control effectors. As a part of the maneuver simulation, component loads are computed and made available for trim optimization. The component loads and trim optimization provide a versatile tool to include hinge moment constraints, control surface travel, and energy-type functions in maneuver simulations. Finally, some discussion is provided for efforts in integrating induced drag computations as well.

### 3.5.1 Rigid Loads

Rigid loads in the previous ASTROS paradigm only included aerodynamic loads. The AANDE enhancements generalize the rigid loads concept to include rigid body acceleration and user-defined loads in addition to the aerodynamic loads. In the current paradigm, rigid loads must be defined in both the aerodynamic and structural domains. Although the rigid body acceleration and user-defined loads do not exist in the aerodynamic domain, they are inserted in the rigid loads matrices as zero vectors to provide the necessary compatibility.

The rigid loads matrix in the aerodynamic domain (**SAROLOAD**) is created by appending the matrices containing the rigid body acceleration (**ACCELOAD**), user-defined (**UDFALOAD**), and aerodynamic loads (**AEROLOAD**), respectively.

$$\mathbf{SAROLOAD} = \mathbf{ACCELOAD} | \mathbf{UDFALOAD} | \mathbf{AEROLOAD} \quad [\text{Eqn. 3-17}]$$

The rigid loads matrix in the structural domain f-set (**PAF**) is created by appending the matrices containing the rigid body acceleration (**ACCFORCE**), user-defined (**UDFFORCX**), and aerodynamic loads ( $\bar{q}$  **AIRFORCE**), respectively.

$$\mathbf{PAF} = \mathbf{ACCFORCE} | \mathbf{UDFFORCX} | \left( \bar{q} \mathbf{AIRFORCE} \right) \quad [\text{Eqn. 3-18}]$$

The derivation of each of the component matrices is discussed in the following sections.

#### 3.5.1.1 Rigid Body Acceleration Loads

The rigid body acceleration load matrices in both the aerodynamic and structural domains (**ACCELOAD** and **ACCFORCE**, respectively) exist as null matrices with one column for each supported degree-of-freedom. The addition of rigid body acceleration terms to the rigid loads matrices allows the aeroelastic effects of these parameters to be examined separately. This approach is similar to the original ASTROS paradigm.

#### 3.5.1.2 User Defined Loads

User-defined loads are defined, and only exist, in the structural domain. User-defined loads may be mechanical, thermal, and/or gravity loads defined by bulk data entries. A new bulk entry, **SLPARM**, controls the definition of these loads. The **SLPARM** (Static Load Parameter) defines a set of loads and provides a control effector name (like the **AESURF** callout) that is used in the **TRIM** entry like any other control parameter. In addition, the loads are parameterized with respect to magnitude. For instance, if a force increment is derived at an angle of attack,  $\alpha = 12.5$  degrees, the force and the angle of 12.5 is defined in the user input. In the preface of ASTROS, a **RIGDSLOD** group will be created from **SLPARMs** (see

Subsection 3.2.1) including the force vector associated with the definition, and a parameter name and magnitude. The magnitude is used later to normalize the load as follows:

$$\mathbf{P}_{slparm\_unit} = \frac{\mathbf{P}(slparm)}{slparm_{incr}} \quad [\text{Eqn. 3-19}]$$

Similarly to acceleration loads, a user-defined null loads matrix is developed in the aerodynamic domain (**UDFALOAD**) with one column for each user-defined static load parameter identified for the current analysis. The user-defined loads matrix in the structural domain is constructed by appending g-set load vectors corresponding to the unitized value of each static load parameter required by the current analysis. The g-set matrix is reduced to the f-set to produce the **UDFFORCX** matrix. If the degree of freedom doesn't exist (at least implicitly) in the f-set, the load will not exist in the f-set.

Limitations of the user-defined loads exist in the gravity and thermal defined loads. While ASTROS in general supports design optimization for these load types, the user-defined loads are fixed with respect to the original design. These loads are defined in the ASTROS preface, and no sensitivity of these loads to ASTROS design variables is known at the creation of these loads.

### 3.5.1.3 Aerodynamic Loads

Under the AANDE ASTROS paradigm, steady aerodynamic loads are provided to ASTROS as the *actual* aerodynamic loads for the specified parameter settings including the basis vector. In order to use this data in the aeroelastic trim analysis, the aerodynamic data must be linearized about the basis configuration to produce the incremental data required by the trim algorithm. For example, the incremental aerodynamic load vector for angle-of-attack would be calculated as follows.

$$\mathbf{P}_\alpha = \frac{\mathbf{P}((\alpha_{ref} + \alpha_{incr}), \beta_{ref}, P_{ref}, Q_{ref}, R_{ref}, \delta_{ref}) - \mathbf{P}(\alpha_{ref}, \beta_{ref}, P_{ref}, Q_{ref}, R_{ref}, \delta_{ref})}{\alpha_{incr}} \quad [\text{Eqn. 3-20}]$$

where  $\mathbf{P}(\alpha_{ref}, \beta_{ref}, P_{ref}, Q_{ref}, R_{ref}, \delta_{ref}) =$  aerodynamic basis vector.

The aerodynamic load matrices are generated by appending the load vectors for the basis parameter and each non-acceleration trim parameter required by the current analysis.

### 3.5.1.4 Rigid Aerodynamic Stability Derivatives

Rigid aerodynamic stability derivatives are computed in both the aerodynamic domain (rigid-direct) and the structural domain (rigid-splined). Rigid aerodynamic stability derivatives in the structural domain are calculated in the same manner as the previous version of ASTROS. Computation of the rigid aerodynamic stability derivatives in the aerodynamic domain has been moved out of the steady aerodynamic data generation section and into the static aeroelastic analysis section. This move generalizes the stability derivative generation and allows for import of alternate steady aerodynamic data.

The rigid aerodynamic stability derivatives in the aerodynamic domain are determined by calculating the total aircraft loads per unit trim parameter.

$$\mathbf{F}_{\delta_{k_i}} = \bar{q} \text{ SAROLOAD}_{\delta_{k_i}} \{ \hat{n} \}_i \quad [\text{Eqn. 3-21}]$$

$$\begin{Bmatrix} \mathbf{F}_{\delta_k} \\ \mathbf{M}_{\delta_k} \end{Bmatrix} = \begin{Bmatrix} \sum_{i=1}^{N_{panel}} \mathbf{F}_{\delta_{ki}} \\ \sum_{i=1}^{N_{panel}} (\mathbf{R}_i \times \mathbf{F}_{\delta_{ki}}) \end{Bmatrix} = \begin{Bmatrix} \mathbf{F}_x \\ \mathbf{F}_y \\ \mathbf{F}_z \\ \mathbf{M}_x \\ \mathbf{M}_y \\ \mathbf{M}_z \end{Bmatrix}_{\delta_k} = \begin{Bmatrix} \text{Longitudinal Force} \\ \text{Lateral Force} \\ \text{Vertical Force} \\ \text{Rolling Moment} \\ \text{Pitching Moment} \\ \text{Yawing Moment} \end{Bmatrix}_{\delta_k} \quad [\text{Eqn. 3-22}]$$

where

- $\mathbf{F}_{\delta_{ki}}$  = force vector at aerodynamic panel  $i$  due to unit trim parameter  $\delta_k$
- $\bar{q}$  = dynamic pressure
- $\text{SAROLOAD}_{\delta_{ki}}$  = force per  $\bar{q}$  at aerodynamic panel  $i$  due to unit trim parameter  $\delta_k$
- $\{\hat{n}\}_i$  = unit normal vector for aerodynamic panel  $i$
- $\mathbf{F}_{\delta_k}$  = force vector due to unit trim parameter  $\delta_k$
- $\mathbf{M}_{\delta_k}$  = moment vector due to unit trim parameter  $\delta_k$
- $\mathbf{R}_i$  =  $\mathbf{P}_i - \mathbf{P}_{ref}$
- $\mathbf{P}_i$  = location of aerodynamic panel  $i$
- $\mathbf{P}_{ref}$  = location of reference point (**GREF** from **AEROS** card)

If the aerodynamic panel model is a centerline symmetric half model, the forces calculated above will be for a half aircraft. The full-span total aircraft forces per unit parameter are obtained by doubling the values calculated for the half aircraft. With the full-span total aircraft forces per unit trim parameter defined, the non-dimensional stability derivatives may be calculated for each trim parameter.

#### Non-Rate Parameters

$$C_D = \frac{\mathbf{F}_x}{\bar{q} S}$$

$$C_S = \frac{\mathbf{F}_y}{\bar{q} S}$$

$$C_L = \frac{\mathbf{F}_z}{\bar{q} S}$$

$$C_l = \frac{\mathbf{M}_x}{\bar{q} S b}$$

$$C_m = \frac{\mathbf{M}_y}{\bar{q} S c}$$

$$C_n = \frac{\mathbf{M}_z}{\bar{q} S b}$$

#### Rate Parameters

$$C_{D'} = \frac{2 \mathbf{F}_x}{\bar{q} S c}$$

$$C_{S'} = \frac{2 \mathbf{F}_y}{\bar{q} S b}$$

$$C_{L'} = \frac{2 \mathbf{F}_z}{\bar{q} S c}$$

$$C_{l'} = \frac{2 \mathbf{M}_x}{\bar{q} S b^2}$$

$$C_{m'} = \frac{2 \mathbf{M}_y}{\bar{q} S c^2}$$

$$C_{n'} = \frac{2 \mathbf{M}_z}{\bar{q} S b^2}$$

[Eqn. 3-23]

The rigid aerodynamic stability derivatives in the aerodynamic domain are stored in the STABCFA relation without any user input effectiveness values being applied. User input effectiveness factors are applied for subsequent calculations and printout.

### 3.5.2 Aeroelastic Equations With Substructuring

The asymmetric trim solution in ASTROS was developed for the general nonlinear aerodynamic conditions. If half-symmetric modeling is used, both the structural and aerodynamic simulations are expanded to the full vehicle and solved. The only efforts of code development for design optimization was performed for this feature. No new technology was required. The bulk of the coding involved bookkeeping of data. This section describes the approach taken to provide for this feature.

The assumed plane of symmetry is the X-Z plane of the Aerodynamic Coordinate System. Before any structural reflection can occur, a geometry check is made to ensure that all geometry is contained on only one side of the X-Z plane. If this condition is met and the Trim condition is asymmetric, then the structure and the aerodynamic matrices will be transformed from half symmetric to full unsymmetric. The assumption of geometric symmetry yields a relationship between the original (F set) displacement set and the expanded (X set) displacement set. This relationship is described by the pair of transformation matrices below where the superscripts  $r$  and  $i$  correspond to real and image respectively:

$$u_f^r = H_f^r u_x$$

$$u_f^i = H_f^i u_x$$

[Eqn. 3-24]

A Structural Image of the other half is created depending on Trim conditions and model definitions. The resulting transformation matrices relate the expanded system to the primary structure and image. Transformed system matrices appear as

$$M_{xx} = [H_f^r]^T M_{ff} H_f^r + [H_f^i]^T M_{ff} H_f^i$$

[Eqn. 3-25]

The aerodynamic model data must also be transformed to the expanded (Xset) displacement set. For flat plate aerodynamic methods such as USSAERO; the aerodynamic forces are produced from the symmetric and anti-symmetric AIC matrix data. The transformed AIC matrix for this case appears as:

$$\begin{aligned}
 AIC_{xx} = & \left[ H_f^r \right]^T G_{kf}^T \left[ 0.5 * (AIC_k + AAIC_k) \right] G_{kf} H_f^r \\
 & + \left[ H_f^r \right]^T G_{kf}^T \left[ 0.5 * (AIC_k - AAIC_k) \right] G_{kf} H_f^i \\
 & + \left[ H_f^i \right]^T G_{kf}^T \left[ 0.5 * (AIC_k - AAIC_k) \right] G_{kf} H_f^r \\
 & + \left[ H_f^i \right]^T G_{kf}^T \left[ 0.5 * (AIC_k + AAIC_k) \right] G_{kf} H_f^i
 \end{aligned} \quad [\text{Eqn. 3-26}]$$

The aerodynamic loads are also transformed to the structural grid, the transformation for the flat plate aerodynamic method case appears below, where *rsym* is positive for symmetric loading and negative for anti-symmetric loading:

$$PA_x = \left[ H_f^r \right]^T G_{kf}^T [PA_k] + (rsym) \left[ H_f^i \right]^T G_{kf}^T [PA_k] \quad [\text{Eqn. 3-27}]$$

An additional transformation set is required when 3-D aerodynamic methods such as QUADPAN are used. When any flow condition other than symmetric is specified, the resulting aerodynamic flowfield is asymmetric. This condition also produces an asymmetric AIC matrix from a full span aerodynamic geometry set. QUADPAN will automatically create the image aerodynamic geometry and output a full span aerodynamic model. The same assumptions of geometric symmetry about the Aerodynamic Coordinate System's X-Z plane yields an additional relationship between the input half symmetric aerodynamic (K set) displacement set and the full span expanded (denoted here as the KX set) displacement set. This relation is defined by the pair of transformation matrices below:

$$\begin{aligned}
 u_k^r &= H_k^r u_{kx} \\
 u_k^i &= H_k^i u_{kx}
 \end{aligned} \quad [\text{Eqn. 3-28}]$$

The asymmetric AIC matrix is denoted below as ASAIC, and the resulting 3-D AIC matrix transformed to the structural set appears as:

$$\begin{aligned}
 AIC_{xx} = & \left[ H_f^r \right]^T G_{kf}^T H_k^r [ASAIC_{kx}] \left[ H_k^r \right]^T G_{kf} H_f^r \\
 & + \left[ H_f^r \right]^T G_{kf}^T H_k^r [ASAIC_{kx}] \left[ H_k^i \right]^T G_{kf} H_f^i \\
 & + \left[ H_f^i \right]^T G_{kf}^T H_k^i [ASAIC_{kx}] \left[ H_k^r \right]^T G_{kf} H_f^r \\
 & + \left[ H_f^i \right]^T G_{kf}^T H_k^i [ASAIC_{kx}] \left[ H_k^i \right]^T G_{kf} H_f^i
 \end{aligned} \quad [\text{Eqn. 3-29}]$$

The aerodynamic loads must also be applied to the structural grid, the transformation for the 3-D method case appear as:

$$PA_x = \left[ H_f^r \right]^T G_{kf}^T H_k^r [PAS_{kx}] + \left[ H_f^i \right]^T G_{kf}^T H_k^i [PAS_{kx}] \quad [\text{Eqn. 3-30}]$$

At this point, the aeroelastic system can be assembled and reduced in the usual manner.



### 3.5.3 Flexible Loads

#### 3.5.3.1 Reduction To LHSA, RHSA, and Flexible Aeroelastic Stability Derivatives

The previous version of ASTROS computed flexible aeroelastic stability derivatives as unrestrained stability derivatives. Enhancements were added to compute and output restrained stability derivatives, as well. Unrestrained stability derivatives include terms associated with inertia relief effects and are values as would be measured from a "free-flying" vehicle. The unrestrained stability derivatives include the aerodynamic load, the aeroelastic increment due to structural deflections caused by the aerodynamic load, and the aeroelastic increment due to structural deflections caused by the accelerations resulting from those loads. Restrained stability derivatives do not include the terms associated with inertia relief effects and are values as would be measured from a wind tunnel model mounted on a sting. The restrained stability derivatives only include the aerodynamic load and the aeroelastic increment due to structural deflections caused by the aerodynamic load.

In order to perform the static aeroelastic analysis, the ASTROS MAPOL sequence reduces the aeroelastic stiffness and mass matrices to the following basic equation:

$$[\mathbf{K}_{22} - \mathbf{K}_{21}\mathbf{K}_{11}^{-1}\mathbf{K}_{12}]\{\mathbf{u}_2\} = [\mathbf{P}_2 - \mathbf{K}_{21}\mathbf{K}_{11}^{-1}\mathbf{P}_1]\{\delta\}$$

- or -

$$[\mathbf{LHSA}]\{\mathbf{u}_2\} = [\mathbf{RHSA}]\{\delta\}$$

[Eqn. 3-31]

where;

- $[\mathbf{LHSA}]$  = resultant aeroelastic mass reduced to the supported degrees-of-freedom (DOFs)
- $\{\mathbf{u}_2\}$  = accelerations at the supported DOFs
- $[\mathbf{RHSA}]$  = resultant aeroelastic trim forces reduced to the supported DOFs
- $\{\delta\}$  = non-acceleration trim parameter values

The unrestrained stability derivatives involve both the  $[\mathbf{LHSA}]$  and  $[\mathbf{RHSA}]$  matrices, while the restrained stability derivatives involve only the  $[\mathbf{RHSA}]$  matrix. A detailed derivation of Eqn. 3-31 can be found in Ref. 18. However, an explanation of the derivation as it relates to this discussion is provided. Once this foundation is created, the unrestrained and restrained stability derivatives are defined mathematically.

Consider Equation (9-14) of Ref. 18, which is hereby renumbered Eqn. 3-32 for discussion in this text.

$$\begin{bmatrix} \mathbf{K}_{ll}^a & \mathbf{K}_{lr}^a & \mathbf{M}_{ll}\mathbf{D} + \mathbf{M}_{lr} \\ \mathbf{D}^T\mathbf{M}_{ll} + \mathbf{M}_{rl} & \mathbf{D}^T\mathbf{M}_{lr} + \mathbf{M}_{rr} & \mathbf{0} \\ \mathbf{D}^T\mathbf{K}_{ll}^a + \mathbf{K}_{rl}^a & \mathbf{D}^T\mathbf{K}_{lr}^a + \mathbf{K}_{rr}^a & \mathbf{m}_r \end{bmatrix} \begin{Bmatrix} \mathbf{u}_l \\ \mathbf{u}_r \\ \ddot{\mathbf{u}}_r \end{Bmatrix} = \begin{bmatrix} \mathbf{P}_l^a \\ \mathbf{0} \\ \mathbf{D}^T\mathbf{P}_l^a + \mathbf{P}_r^a \end{bmatrix} \{\delta\} \quad [\text{Eqn. 3-32}]$$

This equation is derived from combining the steady aeroelastic equation (Equation (9-5) of Ref. 18) and an orthogonality criteria (Equation (9-12) of Ref. 18) of the supported and unsupported DOFs. The orthogonality criteria specifies that there are no accelerations of the unsupported DOFs (l-set) relative to the supported DOFs (r-set).

Prior to manipulation for solution, the equation was partitioned in three rows: (1) loads at the unsupported DOFs, (2) loads at the supported DOFs, and (3) the orthogonality criteria. The left hand side of the equation is partitioned by three columns for constituents operated on by: (1) unsupported DOF displacements, (2) supported DOF displacements, and (3) supported DOF accelerations. Eqn. 3-32 is formed by multiplying the first row by  $\mathbf{D}^T$ , adding it to the second row, and interchanging the new second row with the third equation.

The following set of equations lead to the forming of Eqn. 3-31 shown at the beginning of the section. By renaming the terms of Eqn. 3-32,

$$\begin{bmatrix} \mathbf{R}_{11} & \mathbf{R}_{12} & \mathbf{R}_{13} \\ \mathbf{R}_{21} & \mathbf{R}_{22} & \mathbf{R}_{23} \\ \mathbf{R}_{31} & \mathbf{R}_{32} & \mathbf{R}_{33} \end{bmatrix} \begin{Bmatrix} u_l \\ u_r \\ \ddot{u}_r \end{Bmatrix} = \begin{bmatrix} \mathbf{P}_l^a \\ \mathbf{0} \\ \mathbf{D}^T \mathbf{P}_l^a + \mathbf{P}_r^a \end{bmatrix} \{\delta\} \quad [\text{Eqn. 3-33}]$$

where;

- $\mathbf{R}_{11} = \mathbf{K}_{ll}^a$  - Aeroelastic loads at the flexible DOFs due to deflections at the flexible DOFs
- $\mathbf{R}_{12} = \mathbf{K}_{lr}^a$  - Aeroelastic loads at the flexible DOFs due to deflections at the supported DOFs
- $\mathbf{R}_{13} = \mathbf{M}_{ll} \mathbf{D} + \mathbf{M}_{lr}$  - Inertial loads at the flexible DOFs due to accelerations at the supported DOFs ( $\mathbf{M}_{ll} \mathbf{D}$  is the transformed inertial loads from deflections at the flexible DOFs,  $\mathbf{D}$  is the rigid body transformation matrix that relates the displacements of the flexible DOFs to the supported DOFs - See Equation (6-17) of Ref. 18)
- $\mathbf{R}_{21} = \mathbf{D}^T \mathbf{M}_{ll} + \mathbf{M}_{rl}$  - Inertial moments about the supported DOFs due to deflections at the flexible DOFs ( $\mathbf{D}^T \mathbf{M}_{ll}$  is the transformed inertial moment from about the flexible DOFs to about the supported DOFs)
- $\mathbf{R}_{22} = \mathbf{D}^T \mathbf{M}_{lr} + \mathbf{M}_{rr}$  - Inertial moments about the supported DOFs due to deflections at the supported DOFs ( $\mathbf{D}^T \mathbf{M}_{lr}$  is the transformed inertial moment from about the flexible DOFs to about the supported DOFs)
- $\mathbf{R}_{23} = \text{Zero}$  by definition (the principle of the orthogonality criteria of which  $\mathbf{R}_{21}$ ,  $\mathbf{R}_{22}$ , and  $\mathbf{R}_{23}$  are a part of)
- $\mathbf{R}_{31} = \mathbf{D}^T \mathbf{K}_{ll}^a + \mathbf{K}_{rl}^a$  - Aeroelastic loads at the supported DOFs due to deflections at the flexible DOFs ( $\mathbf{D}^T \mathbf{K}_{ll}^a$  is the transformed aeroelastic loads from the flexible DOFs to the supported DOFs)
- $\mathbf{R}_{32} = \mathbf{D}^T \mathbf{K}_{lr}^a + \mathbf{K}_{rr}^a$  - Aeroelastic loads at the supported DOFs to displacements at the supported DOFs ( $\mathbf{D}^T \mathbf{K}_{lr}^a$  is the transformed aeroelastic loads from the flexible DOFs to the supported DOFs)
- $\mathbf{R}_{33} = \mathbf{m}_r$  - Inertial load at the supported DOFs due to accelerations at the supported DOFs ( $\mathbf{m}_r$  is the total mass reduced and transformed to the supported DOFs)

With these definitions, the steady aeroelastic solution is reconfigured by a coordinate transformation of the flexible displacement DOFs ( $u_l$ ) in terms of the supported DOFs ( $u_r$ ). This is done by solving for ( $u_l$ ) in the first row of Eqn. 3-33. The coordinate transformation equation is displayed as follows:

$$u_l = \mathbf{R}_{11}^{-1} [\mathbf{P}_l^a \delta - \mathbf{R}_{12} u_r - \mathbf{R}_{13} \ddot{u}_r] \quad [\text{Eqn. 3-34}]$$

Substituting for  $u_l$  in the second and third rows of Eqn. 3-33, the equations can be rewritten in terms of rigid body displacements,  $u_1$ , and rigid body accelerations,  $u_2$ .

$$\begin{bmatrix} \mathbf{K}_{11} & \mathbf{K}_{12} \\ \mathbf{K}_{21} & \mathbf{K}_{22} \end{bmatrix} \begin{Bmatrix} u_1 \\ u_2 \end{Bmatrix} = \begin{bmatrix} \mathbf{P}_1 \\ \mathbf{P}_2 \end{bmatrix} \{\delta\} \quad [\text{Eqn. 3-35}]$$

where;

$$\begin{aligned} \mathbf{K}_{11} &= \mathbf{R}_{22} - \mathbf{R}_{21} \mathbf{R}_{11}^{-1} \mathbf{R}_{12} \\ \mathbf{K}_{12} &= \mathbf{R}_{23} - \mathbf{R}_{21} \mathbf{R}_{11}^{-1} \mathbf{R}_{13} \\ \mathbf{K}_{21} &= \mathbf{R}_{32} - \mathbf{R}_{31} \mathbf{R}_{11}^{-1} \mathbf{R}_{12} \\ \mathbf{K}_{22} &= \mathbf{R}_{33} - \mathbf{R}_{31} \mathbf{R}_{11}^{-1} \mathbf{R}_{13} \\ \mathbf{P}_1 &= -\mathbf{R}_{22} \mathbf{R}_{11}^{-1} \mathbf{P}_l^a \\ \mathbf{P}_2 &= \mathbf{D}^T \mathbf{P}_l^a + \mathbf{P}_r^a - \mathbf{R}_{31} \mathbf{R}_{11}^{-1} \mathbf{P}_l^a \end{aligned}$$

Solving for rigid body accelerations,  $u_2$ , Eqn. 3-35 reduces to the basic equation for static aeroelastic analysis:

$$\begin{aligned} [\mathbf{K}_{22} - \mathbf{K}_{21} \mathbf{K}_{11}^{-1} \mathbf{K}_{12}] \{u_2\} &= [\mathbf{P}_2 - \mathbf{K}_{21} \mathbf{K}_{11}^{-1} \mathbf{P}_1] \{\delta\} \\ &\text{— or —} \\ [\mathbf{LHSA}] \{u_2\} &= [\mathbf{RHSA}] \{\delta\} \end{aligned} \quad [\text{Eqn. 3-36}]$$

In essence, the steady aeroelastic solution has been reduced to an equation of the supported DOF accelerations ( $u_2$ ) and the aeroelastic trim variables ( $\delta$ ). This derivation was developed to minimize the solution time in the ASTROS' DECOMP module (non-symmetric matrix decomposition). From the computed values of the [LHSA] and [RHSA] matrices, the aeroelastic stability derivatives are derived.

The ASTROS convention for aeroelastic stability derivatives includes the mass/inertia effects. This philosophy corresponds to stability derivatives which would be measured on a "free-flying" or "unrestrained" air vehicle. In other words, a unit angle of attack would generate rigid air loads, flexible increment, and inertia relief loads for the accelerating vehicle. The inertia relief increment is coupled to the aeroelastic trim forces as shown:

$$\text{Aeroelastic} + \text{Inertia Forces} = [\mathbf{m}_r] [\mathbf{LHSA}]^{-1} [\mathbf{RHSA}] \quad [\text{Eqn. 3-37}]$$

where;

$$[\mathbf{m}_r] = \text{resultant rigid body mass reduced to the supported DOFs}$$

This equation results from using an identity matrix for  $\{\delta\}$  in Eqn. 3-36 and solving for  $\{u_2\}$ . Realizing that the  $u_2$  terms are the accelerations of the supported DOFs due to unit parameters, the forces and moments for the flexible vehicle can be found by multiplying mass,  $[\mathbf{m}_r]$ , times acceleration,  $\{u_2\}$ .

Resultant "unrestrained" loads for a unit perturbation of a trim parameter can be resolved at the supported DOFs by multiplying Eqn. 3-37 times the vector,  $\{\delta\}$ , corresponding to the set of trim parameter values. For example, resultant aeroelastic and inertia loads for a unit angle of attack are computed by

$$\begin{bmatrix} F_x \\ F_y \\ F_z \\ M_x \\ M_y \\ M_z \end{bmatrix}_{\alpha=1} = [\mathbf{m}_r] [\mathbf{LHSA}]^{-1} [\mathbf{RHSA}] \begin{bmatrix} \delta_o = 0 \\ \delta_\alpha = 1 \\ \delta_q = 0 \\ \delta_{surf} = 0 \end{bmatrix} \quad [\text{Eqn. 3-38}]$$

Unrestrained stability derivatives for supported DOFs are computed using Eqn. 3-23 and the unrestrained loads. The aeroelastic load equations for unrestrained stability derivatives do not have inertia relief stability derivatives (since the inertia relief is already imbedded). The trim equations using unrestrained stability derivatives would consist of the aeroelastic load equations shown below set equal to the rigid body mass matrix,  $[\mathbf{m}_r]$ , times the accelerations at the support point,  $\{u_2\}$ .

#### Aeroelastic Load Equations (Unrestrained Stability Derivatives)

$$\begin{aligned} \text{Drag Force} &= qS \left[ C_{D_0} + C_{D_\alpha} \alpha + C_{D_\beta} \beta + C_{D_p} \left( \frac{pb}{2V} \right) + C_{D_q} \left( \frac{qc}{2V} \right) + C_{D_r} \left( \frac{rb}{2V} \right) + \left\{ C_{D_{\delta_{surf}}} \right\} \left\{ \delta_{surf} \right\} \right] \\ \text{Side Force} &= qS \left[ C_{S_0} + C_{S_\alpha} \alpha + C_{S_\beta} \beta + C_{S_p} \left( \frac{pb}{2V} \right) + C_{S_q} \left( \frac{qc}{2V} \right) + C_{S_r} \left( \frac{rb}{2V} \right) + \left\{ C_{S_{\delta_{surf}}} \right\} \left\{ \delta_{surf} \right\} \right] \\ \text{Lift Force} &= qS \left[ C_{L_0} + C_{L_\alpha} \alpha + C_{L_\beta} \beta + C_{L_p} \left( \frac{pb}{2V} \right) + C_{L_q} \left( \frac{qc}{2V} \right) + C_{L_r} \left( \frac{rb}{2V} \right) + \left\{ C_{L_{\delta_{surf}}} \right\} \left\{ \delta_{surf} \right\} \right] \\ \text{Roll Moment} &= qSb \left[ C_{\ell_0} + C_{\ell_\alpha} \alpha + C_{\ell_\beta} \beta + C_{\ell_p} \left( \frac{pb}{2V} \right) + C_{\ell_q} \left( \frac{qc}{2V} \right) + C_{\ell_r} \left( \frac{rb}{2V} \right) + \left\{ C_{\ell_{\delta_{surf}}} \right\} \left\{ \delta_{surf} \right\} \right] \\ \text{Pitch Moment} &= qSc \left[ C_{m_0} + C_{m_\alpha} \alpha + C_{m_\beta} \beta + C_{m_p} \left( \frac{pb}{2V} \right) + C_{m_q} \left( \frac{qc}{2V} \right) + C_{m_r} \left( \frac{rb}{2V} \right) + \left\{ C_{m_{\delta_{surf}}} \right\} \left\{ \delta_{surf} \right\} \right] \\ \text{Yaw Moment} &= qSb \left[ C_{n_0} + C_{n_\alpha} \alpha + C_{n_\beta} \beta + C_{n_p} \left( \frac{pb}{2V} \right) + C_{n_q} \left( \frac{qc}{2V} \right) + C_{n_r} \left( \frac{rb}{2V} \right) + \left\{ C_{n_{\delta_{surf}}} \right\} \left\{ \delta_{surf} \right\} \right] \end{aligned} \quad [\text{Eqn. 3-39}]$$

where;

- $S$  = reference area (AEROS bulk data entry)
- $b$  = reference span (AEROS bulk data entry)
- $c$  = reference chord (AEROS bulk data entry)

The unrestrained stability derivative philosophy can be confusing and even misleading when trying to differentiate between the aeroelastic and inertia relief effects. For example, a washout configuration wing will experience roll damping relief in response to aeroelastic effects. The washout characteristic serves to provide an increased angle of attack to the negative induced angle of attack due to roll rate and consequently reduce the magnitude of the roll damping forces. Typically, the overall result is an increased steady state roll rate. One might incorrectly assume that this should be observable in the unrestrained flex-to-rigid ratio (i.e.  $F/R < 1$ ) for the roll damping derivative,  $C_{\ell_p}$ . However, the unrestrained philosophy requires that the air vehicle undergo acceleration in the direction of the roll damping forces. The resulting inertia relief generates loads which tend to cancel aeroelastic roll damping relief and drive the flex-to-rigid

ratio (F/R) back toward unity. This result is counter-intuitive, as the maximum steady state roll rate occurs at zero acceleration and therefore experiences no inertia relief.

The newly developed "restrained" air vehicle philosophy differentiates between aeroelastic and inertia relief effects. This philosophy corresponds to stability derivatives which would be measured on a sting-mounted wind tunnel model or "restrained" air vehicle. In other words, a unit angle of attack would generate rigid air loads and flexible increment. Because the air vehicle is restrained, it undergoes no acceleration and therefore does not experience inertia relief. Inertia relief stability derivatives are subsequently decoupled from the aeroelastic stability derivatives. The restrained trim loads are simply the [RHSA] matrix while the aeroelastic increment portion of the inertia relief loads are the difference between the aeroelastic mass matrix, [LHSA], and the rigid body mass matrix, [m<sub>r</sub>].

$$\begin{aligned} \text{Aeroelastic Forces} &= [\text{RHSA}] \\ \text{Aeroelastic Increment of Inertia Relief} &= [\text{LHSA}] - [\mathbf{m}_r] \end{aligned} \quad [\text{Eqn. 3-40}]$$

Resultant "restrained" loads for a unit perturbation of a trim parameter can be resolved at the supported DOFs by multiplying [RHSA] times the vector, {δ}, corresponding to the set of trim parameter values. For example, resultant restrained loads for a unit angle of attack are given by

$$\begin{bmatrix} F_x \\ F_y \\ F_z \\ M_x \\ M_y \\ M_z \end{bmatrix}_{\alpha = 1} = [\text{RHSA}] \begin{bmatrix} \delta_o = 0 \\ \delta_\alpha = 1 \\ \delta_q = 0 \\ \delta_{surf} = 0 \end{bmatrix} \quad [\text{Eqn. 3-41}]$$

Resultant "aeroelastic increment of inertia relief" loads for a unit acceleration can be resolved for the supported DOFs in a similar fashion. For example, the resultant aeroelastic increment of inertia relief loads corresponding to a unit vertical acceleration are given by

$$\begin{bmatrix} F_x \\ F_y \\ F_z \\ M_x \\ M_y \\ M_z \end{bmatrix}_{NZ = 1} = -[[\text{LHSA}] - [\mathbf{m}_r]] \begin{bmatrix} NX = 0 \\ NY = 0 \\ NZ = 1 \\ PACCEL = 0 \\ QACCEL = 0 \\ RACCEL = 0 \end{bmatrix} \quad [\text{Eqn. 3-42}]$$

In addition to the default ASTROS "unrestrained" stability derivative table, a "restrained" stability derivative table is computed and written to standard output. The aeroelastic load equations for restrained stability derivatives include the aeroelastic increment of inertia relief stability derivatives. The trim equations using restrained stability derivatives would consist of the aeroelastic load equations shown below set equal to the rigid body mass matrix, [m<sub>r</sub>], times the accelerations at the support point, {u<sub>2</sub>}.

**Aeroelastic Load Equations (Restrained Stability Derivatives)**

$$\begin{aligned}
 \text{Drag Force} &= q S \left[ C_{D_0} + C_{D_\alpha} \alpha + C_{D_\beta} \beta + C_{D_p} \left( \frac{pb}{2V} \right) + C_{D_q} \left( \frac{qc}{2V} \right) + C_{D_r} \left( \frac{rb}{2V} \right) + \left\{ C_{D_{\delta_{surf}}} \right\} \left\{ \delta_{surf} \right\} + C_{D_{NX}} NX + \right. \\
 &\quad \left. C_{D_{NY}} NY + C_{D_{NZ}} NZ + C_{D_{PACCEL}} PACCEL + C_{D_{QACCEL}} QACCEL + C_{D_{RACCEL}} RACCEL \right] \\
 \text{Side Force} &= q S \left[ C_{S_0} + C_{S_\alpha} \alpha + C_{S_\beta} \beta + C_{S_p} \left( \frac{pb}{2V} \right) + C_{S_q} \left( \frac{qc}{2V} \right) + C_{S_r} \left( \frac{rb}{2V} \right) + \left\{ C_{S_{\delta_{surf}}} \right\} \left\{ \delta_{surf} \right\} + C_{S_{NX}} NX + \right. \\
 &\quad \left. C_{S_{NY}} NY + C_{S_{NZ}} NZ + C_{S_{PACCEL}} PACCEL + C_{S_{QACCEL}} QACCEL + C_{S_{RACCEL}} RACCEL \right] \\
 \text{Lift Force} &= q S \left[ C_{L_0} + C_{L_\alpha} \alpha + C_{L_\beta} \beta + C_{L_p} \left( \frac{pb}{2V} \right) + C_{L_q} \left( \frac{qc}{2V} \right) + C_{L_r} \left( \frac{rb}{2V} \right) + \left\{ C_{L_{\delta_{surf}}} \right\} \left\{ \delta_{surf} \right\} + C_{L_{NX}} NX + \right. \\
 &\quad \left. C_{L_{NY}} NY + C_{L_{NZ}} NZ + C_{L_{PACCEL}} PACCEL + C_{L_{QACCEL}} QACCEL + C_{L_{RACCEL}} RACCEL \right] \\
 \text{Roll Moment} &= q S b \left[ C_{\ell_0} + C_{\ell_\alpha} \alpha + C_{\ell_\beta} \beta + C_{\ell_p} \left( \frac{pb}{2V} \right) + C_{\ell_q} \left( \frac{qc}{2V} \right) + C_{\ell_r} \left( \frac{rb}{2V} \right) + \left\{ C_{\ell_{\delta_{surf}}} \right\} \left\{ \delta_{surf} \right\} + C_{\ell_{NX}} NX + \right. \\
 &\quad \left. C_{\ell_{NY}} NY + C_{\ell_{NZ}} NZ + C_{\ell_{PACCEL}} PACCEL + C_{\ell_{QACCEL}} QACCEL + C_{\ell_{RACCEL}} RACCEL \right] \\
 \text{Pitch Moment} &= q S c \left[ C_{m_0} + C_{m_\alpha} \alpha + C_{m_\beta} \beta + C_{m_p} \left( \frac{pb}{2V} \right) + C_{m_q} \left( \frac{qc}{2V} \right) + C_{m_r} \left( \frac{rb}{2V} \right) + \left\{ C_{m_{\delta_{surf}}} \right\} \left\{ \delta_{surf} \right\} + C_{m_{NX}} NX + \right. \\
 &\quad \left. C_{m_{NY}} NY + C_{m_{NZ}} NZ + C_{m_{PACCEL}} PACCEL + C_{m_{QACCEL}} QACCEL + C_{m_{RACCEL}} RACCEL \right] \\
 \text{Yaw Moment} &= q S b \left[ C_{n_0} + C_{n_\alpha} \alpha + C_{n_\beta} \beta + C_{n_p} \left( \frac{pb}{2V} \right) + C_{n_q} \left( \frac{qc}{2V} \right) + C_{n_r} \left( \frac{rb}{2V} \right) + \left\{ C_{n_{\delta_{surf}}} \right\} \left\{ \delta_{surf} \right\} + C_{n_{NX}} NX + \right. \\
 &\quad \left. C_{n_{NY}} NY + C_{n_{NZ}} NZ + C_{n_{PACCEL}} PACCEL + C_{n_{QACCEL}} QACCEL + C_{n_{RACCEL}} RACCEL \right]
 \end{aligned}$$

[Eqn. 3-43]

The trim parameter stability derivatives are computed using Eqn. 3-41 and Eqn. 3-23, while Eqn. 3-41 and the following equations are required to compute the aeroelastic increment of inertia relief terms.

- Longitudinal Acceleration (NX = 1 g):

$$\begin{aligned}
 C_{D_{NX}} &= \frac{F_X}{S} & C_{S_{NX}} &= \frac{F_Y}{S} & C_{L_{NX}} &= \frac{F_Z}{S} \\
 C_{\ell_{NX}} &= \frac{M_X}{Sb} & C_{m_{NX}} &= \frac{M_Y}{Sc} & C_{n_{NX}} &= \frac{M_Z}{Sb}
 \end{aligned}$$

[Eqn. 3-44]

- Lateral Acceleration (NY = 1 g):

$$\begin{aligned}
 C_{D_{NY}} &= \frac{F_X}{S} & C_{S_{NY}} &= \frac{F_Y}{S} & C_{L_{NY}} &= \frac{F_Z}{S} \\
 C_{\ell_{NY}} &= \frac{M_X}{Sb} & C_{m_{NY}} &= \frac{M_Y}{Sc} & C_{n_{NY}} &= \frac{M_Z}{Sb}
 \end{aligned}$$

[Eqn. 3-45]

- Vertical Acceleration (NZ = 1 g):

$$\begin{aligned} C_{D_{NZ}} &= \frac{F_X}{S} & C_{S_{NZ}} &= \frac{F_Y}{S} & C_{L_{NZ}} &= \frac{F_Z}{S} \\ C_{\ell_{NZ}} &= \frac{M_X}{Sb} & C_{m_{NZ}} &= \frac{M_Y}{Sc} & C_{n_{NZ}} &= \frac{M_Z}{Sb} \end{aligned} \quad [\text{Eqn. 3-46}]$$

- Roll Acceleration (PACCEL = 1 rad/sec<sup>2</sup>):

$$\begin{aligned} C_{D_{PACCEL}} &= \frac{F_X}{S} & C_{S_{PACCEL}} &= \frac{F_Y}{S} & C_{L_{PACCEL}} &= \frac{F_Z}{S} \\ C_{\ell_{PACCEL}} &= \frac{M_X}{Sb} & C_{m_{PACCEL}} &= \frac{M_Y}{Sc} & C_{n_{PACCEL}} &= \frac{M_Z}{Sb} \end{aligned} \quad [\text{Eqn. 3-47}]$$

- Pitch Acceleration (QACCEL = 1 rad/sec<sup>2</sup>):

$$\begin{aligned} C_{D_{QACCEL}} &= \frac{F_X}{S} & C_{S_{QACCEL}} &= \frac{F_Y}{S} & C_{L_{QACCEL}} &= \frac{F_Z}{S} \\ C_{\ell_{QACCEL}} &= \frac{M_X}{Sb} & C_{m_{QACCEL}} &= \frac{M_Y}{Sc} & C_{n_{QACCEL}} &= \frac{M_Z}{Sb} \end{aligned} \quad [\text{Eqn. 3-48}]$$

- Yaw Acceleration (RACCEL = 1 rad/sec<sup>2</sup>):

$$\begin{aligned} C_{D_{RACCEL}} &= \frac{F_X}{S} & C_{S_{RACCEL}} &= \frac{F_Y}{S} & C_{L_{RACCEL}} &= \frac{F_Z}{S} \\ C_{\ell_{RACCEL}} &= \frac{M_X}{Sb} & C_{m_{RACCEL}} &= \frac{M_Y}{Sc} & C_{n_{RACCEL}} &= \frac{M_Z}{Sb} \end{aligned} \quad [\text{Eqn. 3-49}]$$

### 3.5.3.2 Flexible Loads Computation

A flexible loads set is produced for the purpose of maneuver load control in the Trim optimization and for data presentation by the BMST (Bending Moment, Shear and Torque) output. The BMST procedure is described in Section 3.5.4.

The flexible loads are derived by first solving for the elastic deformations for unit trim variables. Remembering the aeroelastic matrix equation:

$$\begin{bmatrix} \mathbf{K}_{ll}^a & \mathbf{K}_{lr}^a & \mathbf{M}_{ll}\mathbf{D} + \mathbf{M}_{lr} \\ \mathbf{K}_{rl}^a & \mathbf{K}_{rr}^a & \mathbf{M}_{rl}\mathbf{D} + \mathbf{M}_{rr} \\ \mathbf{D}^T\mathbf{M}_{ll} + \mathbf{M}_{rl} & \mathbf{D}^T\mathbf{M}_{lr} + \mathbf{M}_{rr} & \mathbf{0} \end{bmatrix} \begin{Bmatrix} u_l \\ u_r \\ \ddot{u}_r \end{Bmatrix} = \begin{bmatrix} \mathbf{P}_l^a \\ \mathbf{P}_r^a \\ \mathbf{0} \end{bmatrix} \{\delta\} \quad [\text{Eqn. 3-50}]$$

Taking the first row, using the restrained system formulation and solving for the structural deformations gives:

$$u_l = [\mathbf{K}_{ll}^a]^{-1} [\mathbf{P}_l^a \delta - \{\mathbf{M}_{ll} \mathbf{D} + \mathbf{M}_{lr}\} \ddot{u}_r] \quad [\text{Eqn. 3-51}]$$

which is saved in parts,

$$u_l^1 = [\mathbf{K}_{ll}^a]^{-1} \mathbf{P}_l^a \quad u_l^2 = [\mathbf{K}_{ll}^a]^{-1} \{\mathbf{M}_{ll} \mathbf{D} + \mathbf{M}_{lr}\} \quad [\text{Eqn. 3-52}]$$

The deformations are used to compute unit aeroelastic load distributions on the structural G-set for each trim variable by:

$$P_g^{a1} = q G_{kg}^T [AIC] G S_{kf} u_f^1 \quad [\text{Eqn. 3-53}]$$

The asymmetric trim solution requires additional transformations to yield flexible loads on the primary and image structural components. The structural deformations are recovered to the X-set. Remembering the available transformations to the F-set, the displacement vector for the first set are:

$$\begin{aligned} u_k^{r1} &= H_k^r u_x^1 \\ u_k^{i1} &= H_k^i u_x^1 \end{aligned} \quad [\text{Eqn. 3-54}]$$

and the resulting loads on the structural G-set for the 3-D aerodynamic case are:

$$\begin{aligned} P_g^{r1} &= q G_{kg}^T H_k^r [ASAIC] [H_k^r + H_k^i] G S_{kf} [H_f^r + H_f^i] u_x^1 \\ P_g^{i1} &= q G_{kg}^T H_k^i [ASAIC] [H_k^r + H_k^i] G S_{kf} [H_f^r + H_f^i] u_x^1 \end{aligned} \quad [\text{Eqn. 3-55}]$$

while for the flat plate aerodynamic case, the loads appear as:

$$\begin{aligned} P_g^{r1} &= AIC_s u_{sym}^1 + AAIC_s u_{anti}^1 \\ P_g^{i1} &= AIC_s u_{sym}^1 - AAIC_s u_{anti}^1 \end{aligned} \quad [\text{Eqn. 3-56}]$$

where the deformations are resolved into their symmetric and anti-symmetric components,

$$\begin{aligned} u_{sym}^1 &= \frac{1}{2} \{ H_f^r u_x^1 + H_f^i u_x^1 \} \\ u_{anti}^1 &= \frac{1}{2} \{ H_f^r u_x^1 - H_f^i u_x^1 \} \end{aligned} \quad [\text{Eqn. 3-57}]$$

and the symmetric and anti-symmetric AIC matrix data are each transformed to the half symmetric structural grid:

$$\begin{aligned} AIC_s &= q G_{kg}^T [AIC] G S_{kf} \\ AAIC_s &= q G_{kg}^T [AAIC] G S_{kf} \end{aligned} \quad [\text{Eqn. 3-58}]$$

This approach results in the flexible loads data defined in the convention of the primary component.

### 3.5.4 BMST Component Load Computations

Bending Moment, Shear, and Torque (BMST) component load computations are instigated by the existence of user-defined BMST components in the bulk data input. A BMST component is defined for use in the FTRIM discipline by a label, reference location, reference coordinate system, structural grid list, and aerodynamic panel list.



The unit parameter BMST component loads are calculated by summing the forces and moments per unit parameter at the aerodynamic panels and structural grids comprising the component and then transforming the resulting loads to the BMST reference coordinate system (CS).

$$\begin{aligned} \left( \mathbf{F}'_{BMST_j} \right)_{\delta_k} &= \mathbf{T}_{BMST_j}^T \left( \sum_{i=1}^{N_{BMST_j}} \mathbf{F}_{j(i)} \right) \\ \left( \mathbf{M}'_{BMST_j} \right)_{\delta_k} &= \mathbf{T}_{BMST_j}^T \left( \sum_{i=1}^{N_{BMST_j}} \left[ (\mathbf{R} \times \mathbf{F}_{j(i)}) + \mathbf{M}_{j(i)} \right] \right) \end{aligned} \quad [\text{Eqn. 3-59}]$$

where

$$\begin{aligned} \left( \mathbf{F}'_{BMST_j} \right)_{\delta_k} &= \text{force on BMST component } j \text{ per unit parameter } \delta_k \text{ in reference CS} \\ \left( \mathbf{M}'_{BMST_j} \right)_{\delta_k} &= \text{moment on BMST component } j \text{ per unit parameter } \delta_k \text{ in reference CS} \\ \mathbf{T}_{BMST_j}^T &= \text{transpose of reference CS transformation matrix for BMST component } j \\ N_{BMST_j} &= \text{number of panels or grids comprising BMST component } j \\ \mathbf{F}_{j(i)} &= \text{force on } i^{\text{th}} \text{ panel or grid comprising BMST component } j \text{ in basic CS} \\ \mathbf{M}_{j(i)} &= \text{moment on } i^{\text{th}} \text{ panel or grid comprising BMST component } j \text{ in basic CS} \\ \mathbf{R} &= \mathbf{P}_{j(i)} - \mathbf{P}_{BMST_j} \\ \mathbf{P}_{j(i)} &= \text{location of } i^{\text{th}} \text{ panel control point or grid comprising BMST component } j \\ &\quad \text{in basic CS} \\ \mathbf{P}_{BMST_j} &= \text{reference location of BMST component } j \text{ in basic CS} \end{aligned}$$

Unit parameter BMST component loads are calculated for each trim parameter using rigid-direct, rigid-splined and flexible forces.

$$\begin{Bmatrix} \mathbf{F} \\ \mathbf{M} \end{Bmatrix}_{j(i) \text{ rigid-direct}} = \begin{Bmatrix} \bar{q} \text{ SAROLOAD}_{j(i)} \{ \hat{\mathbf{n}} \}_{j(i)} \\ \mathbf{0} \end{Bmatrix} \quad [\text{Eqn. 3-60}]$$

$$\begin{Bmatrix} \mathbf{F} \\ \mathbf{M} \end{Bmatrix}_{\text{rigid-splined}} = \bar{q} \mathbf{GP}_{kg}^T \text{ SAROLOAD} = \mathbf{PAG} \quad [\text{Eqn. 3-61}]$$

$$\begin{Bmatrix} \mathbf{F} \\ \mathbf{M} \end{Bmatrix}_{\text{flexible}} = \mathbf{FLXFRC} \quad [\text{Eqn. 3-62}]$$

where

$$\begin{aligned} \bar{q} &= \text{dynamic pressure} \\ \text{SAROLOAD} &= \text{rigid-direct (aerodynamic domain) loads matrix} \\ \{ \hat{\mathbf{n}} \} &= \text{aerodynamic panel unit normal vector} \\ \mathbf{GP}_{kg}^T &= \text{transpose of aerodynamic force spline matrix} \\ \mathbf{PAG} &= \text{g-set rigid-splined (structural domain) loads matrix} \end{aligned}$$

**FLXFRC** = g-set flexible (structural domain) loads matrix

### Image Side Processing for Substructuring

In the case of substructuring with a centerline symmetric half model, BMST component loads are calculated for the image side as well as the real side. The image side loads described below are substituted into Eqn. 3-59 directly.

The image side rigid-direct and rigid-splined loads are calculated using equal load for symmetric trim parameters and equal and opposite load for antisymmetric trim parameters. If structural substructuring has occurred, the **FLXFRC** matrix will contain two columns for each trim parameter: the first for the real side, and the second for the image side.

In the case of QUADPAN instantiating a full aerodynamic model from a centerline symmetric half aerodynamic model, the **SAROLOAD** matrix will contain the rigid-direct loads for the full model. In this case, the top half of the matrix contains the real side and the lower half contains the image side. These partitions are used to create real and image side **PAG** matrices.

### Trimmed BMST Results

Upon completion of a trim solution, the trimmed BMST results can be calculated by superposition using the rigid-direct, rigid-splined, and flexible unit parameter BMST component loads.

$$\begin{aligned} \mathbf{F}'_{BMST_j} &= \left[ \left( \mathbf{F}'_{BMST_j} \right)_{\delta_1} \quad \cdots \quad \left( \mathbf{F}'_{BMST_j} \right)_{\delta_N} \right] \begin{Bmatrix} \delta_1 \\ \vdots \\ \delta_N \end{Bmatrix} \\ \mathbf{M}'_{BMST_j} &= \left[ \left( \mathbf{M}'_{BMST_j} \right)_{\delta_1} \quad \cdots \quad \left( \mathbf{M}'_{BMST_j} \right)_{\delta_N} \right] \begin{Bmatrix} \delta_1 \\ \vdots \\ \delta_N \end{Bmatrix} \end{aligned} \quad [\text{Eqn. 3-63}]$$

where

$$\begin{Bmatrix} \delta_1 \\ \vdots \\ \delta_N \end{Bmatrix} = \begin{Bmatrix} u_2 \\ \delta \end{Bmatrix}$$

### **3.5.5 Generalized Trim**

Drawing from Section 9.1 of Ref. 18, the basic equation for static aeroelastic analysis can be written as :

$$\mathbf{L} u_2 = \mathbf{R} \delta \quad [\text{Eqn. 3-64}]$$

where

$$\mathbf{L} = \mathbf{K}_{22} - \mathbf{K}_{21} \mathbf{K}_{11}^{-1} \mathbf{K}_{12} \quad [\text{Eqn. 3-65}]$$

$$\mathbf{R} = \mathbf{P}_2 - \mathbf{K}_{21} \mathbf{K}_{11}^{-1} \mathbf{P}_1 \quad [\text{Eqn. 3-66}]$$

for flexible trim, and

$$\mathbf{L} = \mathbf{R}_{33} = \mathbf{m}_r \quad [\text{Eqn. 3-67}]$$

$$\mathbf{R} = \overline{\mathbf{P}}_2 = \mathbf{D}^T \mathbf{P}_l^a + \mathbf{P}_r^a \quad [\text{Eqn. 3-68}]$$

for rigid trim.

There is one equation in Eqn. 3-64 for each rigid body degree of freedom. In general, then,  $nr$  unknowns can be determined from these equations. The  $\mathbf{u}_2$  vector is the vector of structural accelerations at the support point (in the global coordinate system) and the  $\delta$  vector is a vector of non-acceleration trim parameters. The user is free to pick any number of **fixed** values of  $\mathbf{u}_2$  or  $\delta$  rows and exactly  $nr$  **free** values to be determined by the solution of Eqn. 3-64.

If Eqn. 3-64 is partitioned into free and known values, then

$$\begin{bmatrix} \mathbf{L}_{ff} & \mathbf{L}_{fk} \\ \mathbf{L}_{kf} & \mathbf{L}_{kk} \end{bmatrix} \begin{Bmatrix} \mathbf{u}_{2f} \\ \mathbf{u}_{2k} \end{Bmatrix} = \begin{bmatrix} \mathbf{R}_{fu} & \mathbf{R}_{fs} \\ \mathbf{R}_{ku} & \mathbf{R}_{ks} \end{bmatrix} \begin{Bmatrix} \delta_u \\ \delta_s \end{Bmatrix} \quad [\text{Eqn. 3-69}]$$

where the  $f$  and  $u$  subscripts denote **free** (or **unknown**) values and the  $k$  and  $s$  subscripts denote **known** (or **set**) values of acceleration and non-acceleration trim parameters, respectively. Rearranging to place free values at the left:

$$\begin{bmatrix} \mathbf{L}_{ff} & -\mathbf{R}_{fu} \\ \mathbf{L}_{kf} & -\mathbf{R}_{ku} \end{bmatrix} \begin{Bmatrix} \mathbf{u}_{2f} \\ \delta_u \end{Bmatrix} = \begin{bmatrix} -\mathbf{L}_{fk} & \mathbf{R}_{fs} \\ -\mathbf{L}_{kk} & \mathbf{R}_{ks} \end{bmatrix} \begin{Bmatrix} \mathbf{u}_{2k} \\ \delta_s \end{Bmatrix} \quad [\text{Eqn. 3-70}]$$

The set of values that can participate in Eqn. 3-70 is a function of ASTROS and the user's model. There are six rigid body accelerations, which in ASTROS have been given the names

$$\mathbf{u}_2 \in \left\{ \begin{array}{l} \mathbf{NX} - \text{longitudinal acceleration} \\ \mathbf{NY} - \text{lateral acceleration} \\ \mathbf{NZ} - \text{vertical acceleration} \\ \mathbf{PACCEL} - \text{roll acceleration} \\ \mathbf{QACCEL} - \text{pitch acceleration} \\ \mathbf{RACCEL} - \text{yaw acceleration} \end{array} \right\}$$

The  $\delta$  vector has a number of predefined components and the user can add components by defining control surfaces. Thus,  $\delta$  can be viewed as:

$$\delta \in \left\{ \begin{array}{l} \text{"BASE"} - \text{reference state} \\ \mathbf{ALPHA} - \text{angle of attack} \\ \mathbf{BETA} - \text{yaw angle} \\ \mathbf{PRATE} - \text{roll rate} \\ \mathbf{QRATE} - \text{pitch rate} \\ \mathbf{RRATE} - \text{yaw rate} \\ \left\{ \delta_{sym} \right\} - \text{symmetric surfaces} \\ \left\{ \delta_{anti} \right\} - \text{antisymmetric surfaces} \\ \left\{ \delta_{asym} \right\} - \text{asymmetric surfaces} \end{array} \right\}$$

Note that the “*BASE*” parameter generalizes the **THKCAM** parameter used in the USSAERO aerodynamic method. This parameter represents the reference state from which the other trim parameter aerodynamic increments are derived. While this term is generally given a fixed value of 1.0, any value may be assigned or this term may be solved for in the trim analysis. The “*BASE*” parameter is defined as **THKCAM** for USSAERO-generated steady aerodynamic data, **BASE** for QUADPAN-generated steady aerodynamic data, and a user-defined name for imported alternate steady aerodynamic data.

Note also that asymmetric control surfaces may be defined for full span aerodynamic models (user-defined or QUADPAN-instantiated) and used for asymmetric trim solutions. While asymmetric control surfaces are restricted to asymmetric trim solutions, symmetric and antisymmetric control surfaces may be used for asymmetric trim solutions with aerodynamic data generated using a centerline symmetric aerodynamic model.

For the trim analysis, Eqn. 3-70 is solved for  $u_{2f}$  and  $\delta_u$ . The  $u_{2f}$  and  $\delta_u$  vectors have between them as many terms as there are in the  $r$ -set ( $nr$ ).  $u_2$  and  $\delta$  are then obtained by merging the known values with the computed values.

The user is free to select any combination of  $nr$  free  $u_2$  and  $\delta$  components that form a solvable trim problem. Other than requiring that any free acceleration have the corresponding degree-of-freedom (DOF) supported, the program does not restrict the user in the selection of free parameters. It is up to the user to construct a well-posed trim problem. The user also has the option of selecting no free parameters (0-DOF trim) and having any resulting forces reacted at the support point.

The following guidelines should be followed to ensure a solvable trim problem. This table may be interpreted by using the following statement.

To insure the ability to balance forces in the ‘**DOF**’ degrees-of-freedom, ‘**Number of Free Parameters**’ of the following trim parameters must be free and the others must be fixed: ‘**Available Parameters**.’

DOF	Number of Free Parameters	Available Parameters
0	0	All
1	1	NX, Throttle
3, 5	2	ALPHA, Pitch Control Surface, QRATE, QACCEL, NZ
2, 6	2	BETA, Yaw Control Surface, RRATE, RACCEL, NY
4	1	Roll Control Surface, PRATE, PACCEL
3	1	ALPHA, NZ (Imbalance in DOF 5)
2	1	BETA, NY (Imbalance in DOF 6)

User-defined load parameters may be used in place of some of these parameters if the user-defined load is in the corresponding degree-of-freedom.

### 3.5.6 Control Surface Scheduling

The values of user-defined control surface parameters, or any other valid trim parameter, may be defined through user-defined schedules. A schedule, as implemented in **ASTROS**, is simply a table of values as a function of other trim parameter values. In order to use a schedule in a trim problem, each parameter to be scheduled is flagged with the character string **SCHD** on the **TRIM** card in bulk data. A **SCHEDULE** card with the same set ID as the **TRIM** card is also defined in bulk data. The schedule values and corresponding reference trim parameter values are defined through **AEFACT** cards.

Before the trim solution, the value of each schedule is calculated for the current trim state using a table lookup and interpolation scheme. The trim solver uses these values as the fixed values for the scheduled parameters. After the trim solution, the schedule values are checked for convergence with the previous values. If the schedule has not converged, the trim solution and convergence check is repeated.

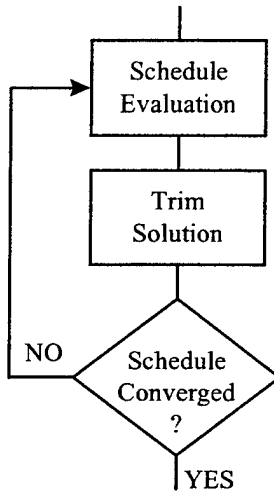


Figure 3-35 Control Surface Scheduling Flowchart

### 3.5.7 Trim Optimization

Aeroelastic trim was expanded to provide a trim optimization option. Previous methodology required that the number of free trim parameters be equal to the number of free trim degrees of freedom. The enhanced methodology allows specification of redundant control surfaces, a user defined objective function and user defined trim constraints. The trim objective function and constraints provide the opportunity to minimize, maximize, or apply limits to control parameters ( $\alpha$ ,  $\beta$ ,  $r$ ,  $p$ ,  $N_z$ , etc.), control surface travel, component loads, and trimmed aerodynamic drag. The solution algorithm provides the optimal trim parameter settings to satisfy the user defined objective function subject to the user defined trim constraints.

The trim optimization module assembles a Taylor series first order approximation of the trim equations of motion, assembles the information for MICRO-DOT, and examines the trim state to assure convergence. Trim optimization is available for both linear trim and nonlinear trim. The module utilizes redundant control effectors (control surfaces, thrust, user defined controllers (e.g. smart structures), and trim parameters (e.g.  $\alpha$ ,  $\beta$ )) to drive the trim state to a constrained minimum for the objectives and constraints defined by the user. The design variables are the control effectors. The design constraints and objectives are control effector limits, integrated maneuver loads, and maneuver performance (e.g. roll rate). Drag will be classified as a maneuver performance attribute. Although it could be considered an integrated maneuver load, the semi-empirical method described in Section 3.5.8 was not extended under this scope to provide applied loads. However, drag maneuver loads were enabled through three-dimensional aerodynamics and through this means may be considered as a performance measure simultaneous to loads.

The trim optimization problem can be specified as:

Find the set of design variables,  $v$ , which will minimize an objective function

$$F(v) \quad [\text{Eqn. 3-71}]$$

Subject to:

$$g_j(v) \leq 0.0 \quad j = 1, \dots, ncon \quad [\text{Eqn. 3-72}]$$

$$v_i^{lower} \leq v_i \leq v_i^{upper} \quad i = 1, \dots, ndv \quad [\text{Eqn. 3-73}]$$

where Eqn. 3-72 specifies the  $ncon$  inequality constraints and Eqn. 3-73 specifies upper and lower bounds (side constraints) on each of the design variables.

For trim optimization, any valid trim parameter (including rigid body accelerations) may be a design variable,  $v_i$ . The set of design variables must include each "FREE" trim parameter. "FIXED" trim parameters may be design variables, as well. Any "FIXED" trim parameter design variables must be constrained to their required values. Trim optimization performance improvements have been observed when all non-zero "FIXED" trim parameters are included in the set of design variables and included in the objective function.

The objective function,  $F(v)$ , may be a trim parameter, a component load, drag, or a linear combination of these. If a linear combination of functions is used as the objective function, it is important to weight each term appropriately to achieve the desired result. If the functions are to be weighted evenly, the weighting factors should cause the functions to be of the same order of magnitude. For example, to evenly weight vertical load factor, NZ, in ft/sec<sup>2</sup> and roll rate, PRATE, in rad/sec, PRATE should be multiplied by 10<sup>2</sup> or NZ should be multiplied by 10<sup>-2</sup>.

The basic equation for static aeroelastic analysis, Eqn. 3-64, is incorporated in the trim optimization problem as a set of constraints enforcing equilibrium. The first  $(2 \times nr)$  constraints, where  $nr$  is the number of rigid body degrees-of-freedom (DOF), are used to specify a balanced load condition. In other words, the imbalance of forces and moments at the support point must be less than a specified tolerance. This can be written as follows:

$$\begin{aligned} \begin{Bmatrix} g_1 \\ \vdots \\ g_{nr} \end{Bmatrix} &= (\mathbf{L} u_2 - \mathbf{R} \delta) - \begin{Bmatrix} 1 \\ \vdots \\ 1 \end{Bmatrix} \text{tolerance} \\ \begin{Bmatrix} g_{(nr+1)} \\ \vdots \\ g_{(2 \times nr)} \end{Bmatrix} &= (\mathbf{R} \delta - \mathbf{L} u_2) - \begin{Bmatrix} 1 \\ \vdots \\ 1 \end{Bmatrix} \text{tolerance} \end{aligned} \quad [\text{Eqn. 3-74}]$$

where  $\mathbf{L}$  and  $\mathbf{R}$  are defined in Eqn. 3-65 and Eqn. 3-66, respectively, for flexible trim, and in Eqn. 3-67 and Eqn. 3-68, respectively, for rigid trim.

Note that two equations are used for each DOF. This prevents a discontinuity at zero imbalance, which would occur if the absolute value of the imbalance were used. This formulation also avoids the added complexity of using the square of the imbalance. The constraints specifying a balanced load condition are generated internally by the trim optimization routine. The remaining constraints are those specified by the user. User-defined constraints may include trim parameters, component loads, drag, or linear combinations of these.

The user-defined trim optimization constraints are calculated using

$$g = a + b\epsilon \quad [\text{Eqn. 3-75}]$$

where  $\epsilon$  is the value of the bounded function. The  $a$  and  $b$  coefficients are listed in Table 3-4 for upper and lower bound constraints and bounding values ( $\epsilon_{req}$ ) that are positive, negative, or zero.

Table 3-4 Trim Optimization Constraint Coefficients

SIGN OF $\epsilon_{req}$	CONSTRAINT TYPE			
	UPPER		LOWER	
	$a$	$b$	$a$	$b$
POS	-1.0	$\frac{1}{\epsilon_{req}}$	1.0	$-\frac{1}{\epsilon_{req}}$
NEG	1.0	$-\frac{1}{\epsilon_{req}}$	-1.0	$\frac{1}{\epsilon_{req}}$
ZERO	0.0	1.0	0.0	-1.0

Mathematical programming approaches to the solution of Eqn. 3-71 through Eqn. 3-73 require the gradients of the objective and the constraints with respect to the design variables. That is:

$$\begin{aligned} \frac{\partial F}{\partial v_i} \quad i = 1, \dots ndv \\ \frac{\partial g_j}{\partial v_i} \quad j = 1, \dots ncon ; i = 1, \dots ndv \end{aligned} \quad [\text{Eqn. 3-76}]$$

The computation of objective and constraint functions and gradients are performed analytically by the trim optimization routine. Since the objective and constraints are linear functions of the design variables, the evaluation of functions and gradients are relatively straightforward. In fact, the gradients need only be evaluated once since they are invariant with respect to the design variables. This is also the case when using nonlinear aerodynamic data since each trim convergence iteration will be performed with linearized data.

In order to permit efficient processing by the **MICRO-DOT** algorithm, it is necessary to scale the constraints such that they are of the same order of magnitude. This is accomplished by using the absolute value of the initial value of the constraint as the scaling factor at the beginning of each iteration. If the initial value of the constraint is less than 1.0, 1.0 is used as the scaling factor. In this manner, the initial constraint values supplied to **MICRO-DOT** are between +1.0 and -1.0. If **MICRO-DOT** fails to produce a balanced trim solution within the specified tolerance, the constraints are re-scaled by their current values, and process is repeated. Generally, extra iterations are only required if the optimization has been started in infeasible space.

#### Trim Parameter Function and Gradient Evaluation

Trim parameters in the trim optimization module are either design variables or fixed values. The initial values of the design variables are specified by the **TODVPRM** card in bulk data and may be a user-defined value or the result of a standard trim solution. After initialization, the values of the design variables are defined by the **MICRO-DOT** algorithm. The gradients of trim parameters are simply:

$$\frac{\partial \delta_k}{\partial v_i} = \begin{cases} 0 & \text{if } \delta_k \neq v_i \\ 1 & \text{if } \delta_k = v_i \end{cases} \quad [\text{Eqn. 3-77}]$$

### Equilibrium Condition Function and Gradient Evaluation

If the equilibrium condition specified by Eqn. 3-74 is partitioned into free and known values and rearranged to place free values at the left, then

$$\begin{aligned} \begin{Bmatrix} g_1 \\ \vdots \\ g_{nr} \end{Bmatrix} &= \begin{bmatrix} \mathbf{L}_{ff} & -\mathbf{R}_{fu} \\ \mathbf{L}_{kf} & -\mathbf{R}_{ku} \end{bmatrix} \begin{Bmatrix} u_{2f} \\ \delta_u \end{Bmatrix} - \begin{bmatrix} -\mathbf{L}_{fk} & \mathbf{R}_{fs} \\ -\mathbf{L}_{kk} & \mathbf{R}_{ks} \end{bmatrix} \begin{Bmatrix} u_{2k} \\ \delta_s \end{Bmatrix} - \begin{Bmatrix} 1 \\ \vdots \\ 1 \end{Bmatrix} \text{tolerance} \\ \begin{Bmatrix} g_{(nr+1)} \\ \vdots \\ g_{(2 \times nr)} \end{Bmatrix} &= \begin{bmatrix} -\mathbf{L}_{fk} & \mathbf{R}_{fs} \\ -\mathbf{L}_{kk} & \mathbf{R}_{ks} \end{bmatrix} \begin{Bmatrix} u_{2k} \\ \delta_s \end{Bmatrix} - \begin{bmatrix} \mathbf{L}_{ff} & -\mathbf{R}_{fu} \\ \mathbf{L}_{kf} & -\mathbf{R}_{ku} \end{bmatrix} \begin{Bmatrix} u_{2f} \\ \delta_u \end{Bmatrix} - \begin{Bmatrix} 1 \\ \vdots \\ 1 \end{Bmatrix} \text{tolerance} \end{aligned} \quad [\text{Eqn. 3-78}]$$

where the *f* and *u* subscripts denote **free** (or **unknown**) values and the *k* and *s* subscripts denote **known** (or **set**) values of the acceleration and non-acceleration trim parameters, respectively. The set of **free** / **unknown** parameters are the trim optimization design variables and the set of **known** / **set** values are all the other trim parameters. Eqn. 3-78 may be used to calculate the equilibrium condition constraints using the values of the trim parameters as discussed above.

The gradients of the equilibrium condition function are simply the terms of the matrix equations above corresponding to each trim parameter design variable.

$$\begin{aligned} \begin{Bmatrix} \frac{\partial g_1}{\partial v_1} & \dots & \frac{\partial g_1}{\partial v_{ndv}} \\ \vdots & \ddots & \vdots \\ \frac{\partial g_{nr}}{\partial v_1} & \dots & \frac{\partial g_{nr}}{\partial v_{ndv}} \end{Bmatrix} &= \begin{bmatrix} \mathbf{L}_{ff} & -\mathbf{R}_{fu} \\ \mathbf{L}_{kf} & -\mathbf{R}_{ku} \end{bmatrix} \\ \begin{Bmatrix} \frac{\partial g_{(nr+1)}}{\partial v_1} & \dots & \frac{\partial g_{(nr+1)}}{\partial v_{ndv}} \\ \vdots & \ddots & \vdots \\ \frac{\partial g_{(2 \times nr)}}{\partial v_1} & \dots & \frac{\partial g_{(2 \times nr)}}{\partial v_{ndv}} \end{Bmatrix} &= \begin{bmatrix} -\mathbf{L}_{fk} & \mathbf{R}_{fs} \\ -\mathbf{L}_{kk} & \mathbf{R}_{ks} \end{bmatrix} \end{aligned} \quad [\text{Eqn. 3-79}]$$

### BMST Component Load Function and Gradient Evaluation

BMST component loads are calculated using Eqn. 3-63 with the current values of the trim parameters as discussed above. The gradients of the BMST component loads are simply the unit parameter BMST component loads defined by Eqn. 3-59 where

$$\frac{\partial \begin{Bmatrix} \mathbf{F}'_{BMST_j} \\ \mathbf{M}'_{BMST_j} \end{Bmatrix}}{\partial v_i} = \begin{Bmatrix} \left( \mathbf{F}'_{BMST_j} \right)_{\delta_k} \\ \left( \mathbf{M}'_{BMST_j} \right)_{\delta_k} \end{Bmatrix} \quad \text{where } \delta_k = v_i \quad [\text{Eqn. 3-80}]$$



### Drag Function and Gradient Evaluation

Although the semi-empirical method for drag computation was not implemented the computational equations and coding was developed in the trim optimization modules. Drag is calculated at the trim state determined by the standard trim solution. Additionally, the drag contribution due to each individual trim parameter is available. The drag gradients are determined by linearizing the parameterized drag contributions about the trim state. This can be expressed as:

$$\frac{\partial F_{DRAG}}{\partial v_i} = \frac{F_{DRAG}(\delta_k)}{\delta_k} \quad \text{where } \delta_k = v_i \quad [\text{Eqn. 3-81}]$$

A value for drag at any trim state required by the optimization algorithm may be determined by superposition using the gradients defined above and the values of the trim parameters.

### Combination Function and Gradient Evaluation

Trim optimization objective functions and constraints may be linear combinations of trim parameters, BMST component loads, and drag. The evaluation of function and constraint values are determined for the individual components as described above with the addition of a user-defined weighting factor.

$$F = \sum_{j=1}^N w_j F_j$$
$$\frac{\partial F}{\partial v_i} = \sum_{j=1}^N w_j \frac{\partial F_j}{\partial v_i} \quad [\text{Eqn. 3-82}]$$

where

$$F_j = \delta_k \quad \text{or} \quad \left\{ \begin{matrix} \mathbf{F}'_{BMST_j} \\ \mathbf{M}'_{BMST_j} \end{matrix} \right\} \quad \text{or} \quad F_{DRAG}$$

$w_j = \text{scalar weighting factor}$

### Trim Optimization Within Structural Optimization

The trim optimization option provides for coupling trim optimization and structural optimization. In this case, the process provides a sequence of trim optimization followed by structural optimization as shown in Figure 3-36. The process loops on itself until structural convergence is achieved. Conceptually, unit aeroelastic solutions are obtained implicitly as a default in the FTRIM discipline. These solutions provide the necessary database to create sensitivity information of the control effectors as well as to create integrated loads for the constraints and objectives. The initial trim provides the starting point for the constrained optimization problem. Sensitivities, constraints and the trim design objective functions are formulated and assembled in first order Taylor series format. Integrated loads are developed from superposition of the unit conditions developed above. Integrated force and moment coefficients from the unit conditions provide basis for the change in trim state, and drag and drag sensitivities are derived from the semi-empirical methods of the TSO-Drag subroutine. These equations are then submitted to MICRODOT and the results post-processed in preparation for structural optimization. This post-processing includes formulation of static aeroelastic constraints and sensitivities as well as the loads to be included in the structural design problem.

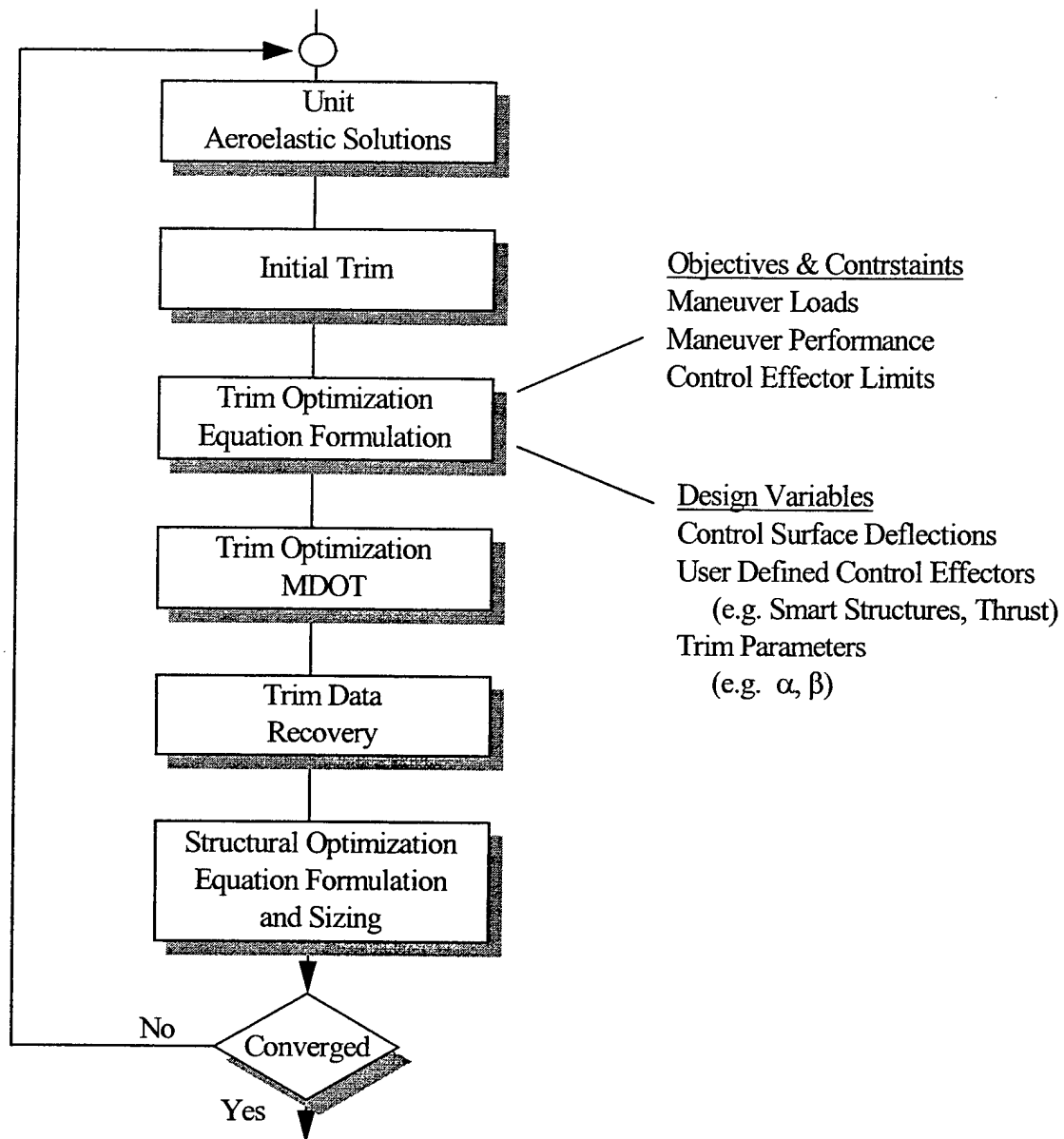


Figure 3-36 Structural Optimization Sequential To Trim Optimization.

In this case of trim optimization with linear trim analysis, the DRAG module (Section 3.5.8) was intended for use in drag state and sensitivity analysis. If the aerodynamic model for trim analysis is three-dimensional, then trimmed drag loads may differ from the predictions from the DRAG module. The DRAG module is not intended for predicting drag loads for structural resizing, and this contract was not scoped to expand the DRAG module to provide this capability. If a flat panel aerodynamic model is used, no drag loads will be computed by definition (flat panel models only produce loads normal to the free stream aerodynamics).

Finally, if three-dimensional aerodynamics is used in the simulation, drag computation may be obtained through a BMST analysis. Trim optimization with BMST was presented earlier in this section.

### 3.5.8 Drag Analysis

Trim optimization problems utilizing minimum drag criteria require computation of trimmed aerodynamic drag and also sensitivity to change in each trim parameter level. A drag module was initiated employing a semi-empirical approach based on linear theory and wind tunnel correlation factors. This module was to compute drag for the flexible trimmed flight condition or provide sensitivities to the trim optimization module for determination of optimum control surface settings when redundant control parameters are specified. As perceived in the initial design, the trim optimization module would a) perform an initial trim based on the initial user specified blend for the redundant control surfaces, b) call the drag module to compute drag using the trimmed flexible lift as well as compute sensitivities of drag to change in each of the trim parameters, c) minimize the trimmed flight condition drag by computing the optimum blend with respect to drag sensitivity data, d) recomputes flexible trim and e) repeats steps "b" through "d" until convergence is satisfied. This drag module would provide the user opportunity to tune the aerodynamic drag used in the trim optimization problem with correction factors. The vehicle flexible trim balance is achieved using the uncorrected drag load components, however, thereby maintaining balanced structural load.

The subroutine DRAG from the Wing Aeroelastic Synthesis Procedure (TSO - Ref. 19) was adapted and modified to meet the following computational requirements in the ASTROS domain:

- (1) Predict the shape of the lift curve and drag polar of the input configuration as a function of angle of attack, wing camber and control deflections.
- (2) Determine the sensitivity of drag to panel camber, control surface deflections and aeroelastic effects at a ( $C_L$ ,  $C_D$ ) design point.

The logic for predicting the drag polar shape from input AIC matrices is present in the subroutine DRAG. Adaptation included replacing existing scratch I/O with CADDDB framework. The routine's basis is focused on the Carmichael aerodynamic code, and no modifications were made to adapt the routine to other linear codes. The methods for specifying leading edge panels and other panels to monitor for separation in predicting the polar break lift coefficient and the polar shape of the break did not require modification.

New user input was developed specific to this module, and conforms to the established Bulk data formats for the reasons that this data accompanies trim data already in the format of Bulk data. User input includes calibration variables, baseline polars to calibrate to, and requested drag sensitivities. Calibration parameters include percent vacuum achieved prior to onset of leading edge separation, percent leading edge suction, and panel numbers of the panels to be monitored for flow separation. The algorithms in subroutine DRAG require information derived in trim and trim optimization such as specification for use of redundant control surfaces, flight conditions for which drag information is requested, and trim constraints/objectives reliant of DRAG analysis.

The routine was not implemented because of some unresolved issues. The algorithm with the drag routine performs a nonlinear trim computation in the aerodynamic domain necessitating computation of inertial relief terms (currently ignored). The stability coefficients used for trim are computed with estimated flow separation characteristics thus establishing the nonlinearity. In the cases of redundant control surfaces, the need for restricting assumptions arise in order to reduce the number of independent controllers to compute the drag routine case for a symmetrical pull-up (two degrees of freedom). The routine computed an entire drag polar that is a parametric function of  $C_L$ . Therefore, an open question arises: What is the trimmed state to compute drag & sensitivities since the trim optimization procedure is performing a trim for a linear aeroelastic solution?

## 4. INTEGRATED TESTS AND APPLICATIONS

Testing performed under this contract includes unit testing on new software modules, integrated testing with a class of small scale applications, and representative application studies. Unit testing was performed for each new module. In the case of QUADPAN, an extensive study was performed with aerodynamic methods to develop fundamental candidate models for the application studies (see Section 0). Integrated testing was performed in key areas and is presented in the remaining sections.

A summary of the integrated testing is presented in Tables 4-1 through 4-3. These tables illustrate the software paths of capabilities tested with various models. The capabilities are listed vertically in the matrix while the model are listed across the matrix. Capabilities were tested in the ANALYZE and / or OPTIMIZE modes of ASTROS and are thus denoted by an A or an O accordingly. Major categories presented in Table 4-1 include aerodynamic model assembly, use of aerodynamic models, and use of structural models. Table 4-2 displays areas tested for spline methods, user-defined loads, and parameter component loads. Shown in Table 4-3 are the areas tested for generalized trim and trim optimization. Results and comments are provided in the following subsections.

Table 4-1 Multi-Database, Aerodynamic Modeling, and Structural Modeling Capabilities Tested

	A - Analysis O - Optimization	Small Scale Applications	F-16 Half Model	F-16 Full Model	VAT Model
<b>Multiple Databases -</b>					
<b>Aerodynamic Model Assembly</b>					
Run time database		A / O	A	A	A
Alternate database		A	A / O	A	A
Combination of alternate + run-time		A	A	A	A
<b>Aerodynamics Models</b>					
<b>Flat Panel Aerodynamics</b>					
USSAERO		A / O			
Alternate Linear Aerodynamics			A / O	A	A
<b>3-D Panel Aerodynamics</b>					
QUADPAN		A	A	A	A
Alternate Linear Aerodynamics					
<b>Alternate Pressure Data Sets</b>					
Overlaying Pressures		A	A		
<b>Structures Models</b>					
Centerline - Half Span Models		A / O	A / O		
Full Span (Tip to Tip) Models		A		A	
Non-Centerline Models					A
Substructuring		A / O	A / O		

Table 4-2 Static Aeroelastic Component Capabilities Tested

A - Analysis O - Optimization	Small Scale Applications	F-16 Half Model	F-16 Full Model	VAT Model
<b>Static Aeroelastic Analysis</b>				
<b>Spline Methods</b>				
Flat Plane Infinite Plate Spline	A / O	A / O		
3-D Infinite Plate Spline	A	A	A	A
Alternate Spline Methods				
Flexible Attach	A / O	A / O	A	
Rigid Attach	A / O	A / O	A	A
<b>User Defined Loads</b>				
Mechanical	A	A		A
Inertia Loads				
Thermal				
<b>Parameter Component Loads (BMST)</b>				
Air Loads	A / O	A / O		
Inertia Loads	A / O	A / O		
User Defined Loads				

Table 4-3 Maneuver Trim Simulation Capabilities Tested

A - Analysis O - Optimization	Small Scale Applications	F-16 Half Model	F-16 Full Model	VAT Model
<b>Generalized Trim Analysis</b>				
<b>Linear Trim</b>				
1 DOF	A			A
2 DOF	A / O	A / O	A	
3 DOF	A / O	A / O		
4 DOF				
5 DOF			A	
6 DOF				
<b>Control Surface Scheduling</b>				
Maneuver Response Settings				
Airload Control Surfaces Settings	A	A / O		
User-Defined Control Surface Settings	A			
<b>Trim Optimization</b>				
<b>Objective Functions</b>				
Minimum Component Loads	A / O	A / O		
Maximum Maneuver Response	A			
Multiple Objective Function	A	A / O		
<b>Constraint Functions</b>				
Component Loads	A / O	A / O		
Maneuver Response	A	A		
Control Surface Limits	A / O	A / O		
<b>Design Variables</b>				
Maneuver Response Parameters	A	A		
Airload Control Surface Settings	A / O	A / O		
User Defined Controller Settings				

## 4.1 AERODYNAMIC MODELING

Benchmarking of aerodynamic codes was performed to gain perspective on QUADPAN's capabilities. Three linear panel methods were compared with experimental data over a range of conditions and models. The purpose was to assess their suitability for loads generation. In this section, the capabilities and limitations of the three codes will be presented before giving the results of the comparisons. The results provide guidance for choosing the most appropriate method for a given problem. They also show some of the limitations of linear aerodynamic methods.

### 4.1.1 Theory

The aerodynamic codes used in this study are all based on linear aerodynamic theory. Specifically, they rely on solutions to the Prandtl-Glauert equation to describe the flowfield around a body. The Prandtl-Glauert equation is derived from the full Navier-Stokes equations (conservation of mass, momentum, and energy) by making various approximations until a linear, partial differential equation with one dependent variable is obtained. These approximations limit the range of applicability of the resulting methods.

The main approximations used to derive the Prandtl-Glauert equation are the elimination of time dependent and viscous terms, the assumption of irrotational (isentropic) flow, and the neglect of higher order (non-linear) terms. The neglect of time dependent and viscous terms obviously means that the results are good only for steady flowfields that are dominated by inviscid forces. Regions where viscous forces are important, such as separations, cannot be modeled by these methods. The assumption of irrotational flow implies that the flow is also isentropic. Isentropic flows will not have the shocks normally seen at transonic and supersonic conditions. Free vortices, like those normally seen off a strake or wing tip, will also be absent. Since the wing vortices are required for lift generation, these must be placed outside the regions where the Prandtl-Glauert equation is applied. The neglect of non-linear terms means that the results will be less valid as the Mach number approaches unity or goes to very high values. It also means that the flow perturbations made by the body must be small at any Mach number other than zero.

To solve the Prandtl-Glauert equation, the methods used in this study divide the body into a large number of quadrilateral geometric regions called panels. One or more surface functions are applied on each panel. These functions yield a flowfield that satisfies the Prandtl-Glauert equation everywhere. Since the governing equation is linear, the contributions of all the functions can be added to yield a flowfield that also satisfies the equation. To get a specific flowfield the magnitudes of the functions are adjusted to make the flow tangent to all the panels. Once the function magnitudes are known, the forces on the body can be determined.

The surface functions used to satisfy the Prandtl-Glauert equation are often called singularities since all the useful ones have a singular point somewhere within the panel. Different types of singularities result in different flowfields. Sources can be used to model thickness since they displace the flow away from the panel. Doublets and vortices can be used to give the flow a direction change. This is critical, since the flow must be aligned with the trailing edge to generate lift. This is known as enforcing the Kutta condition; it would normally happen as a result of viscosity.

#### 4.1.2 Aerodynamic Codes

The three aerodynamic codes compared in this study were Vorlax (Ref. 20), Carmichael (Ref. 21), and QUADPAN (Ref. 9). All three methods solve the Prandtl-Glauert equations by using singularities whose strength is constant across a panel. They differ in their choice of singularities and the way the geometry is modeled. The Carmichael and QUADPAN codes use a distribution of sources and doublets to align the flow with the aircraft surfaces. The Vorlax code uses a set of horseshoe vortices to accomplish this. Both Vorlax and Carmichael assume that every surface is a lifting surface, i.e., the Kutta condition is applied on the trailing edge. QUADPAN allows non-lifting surfaces. Vorlax uses a flattened representation of the aircraft that is capable of modeling camber, twist, and dihedral. The Carmichael code uses a similar model, but can also add a thickness envelope around the parts. The QUADPAN code uses a full 3D geometry to model the aircraft. This allows thick parts, like the fuselage, to be handled more accurately. Both Vorlax and QUADPAN can model asymmetric configurations, but Carmichael is limited to symmetric and antisymmetric models.

Please note that the foregoing descriptions of code capability include only the features used for this study. Additional capabilities are available in Vorlax and Carmichael that could, in theory, make the results better. In the case of Vorlax, we used the version inside HASC (Ref. 22), so not all of its geometry capabilities were available. For instance, it can model fuselages by using a series of concentric vortex sheets, but the inputs to actuate that capability are not in HASC. In any case, the concentric sheet model is not as convenient as the true 3D capability in QUADPAN. The same can be said of Vorlax's capability to model wing thickness using parallel vortex sheets. It is much less convenient than the procedures in Carmichael or QUADPAN. The Carmichael code has a capability to model a body of revolution fuselage, but there are some geometry and force integration limitations, so this was never used in this study.

Because of the limitations of linear theory, the results are usually not used directly. The results are discarded at high angles of attack and empirical adjustments are made at lower ones. The most common adjustments are to the leading edge forces. Leading edge suction is frequently added for subsonic cases. This models the forward axial force due to the low pressure on the leading edge. In HASC these can be included or left out, or rotated 90° in accordance with the Polhamus suction analogy. These adjustments were left out of all the codes in this study since they do not change the pressures used to calculate loads.

While it is difficult to assess all linear aerodynamic codes, it is believed that these codes encompass many of the characteristics that will be found in panel methods. Another study (Ref. 10) entails comparison of a broader set of aerodynamic panel codes, and also makes a good case for the choice of QUADPAN in ASTROS.

#### 4.1.3 Models

The most extensive code comparisons were accomplished using the Aeroelastic Tailoring Wind Tunnel Model. This model was the result of a program conducted from 1977 to 1981 to demonstrate the benefits of aeroelastic tailoring (Ref. 23). Aeroelastic tailoring is the modification of structural properties to give beneficial aerodynamic effects under load. In this program, three flexible wings were tested. The first one was designed to achieve lower drag during turns by increasing the camber and negative twist (washout). The second one tried to achieve higher lift when under load by increasing camber and twist (washin). The third wing was untailored in order to simulate the behavior of a typical flexible wing. A fourth wing was made of steel like a regular rigid wind tunnel model. The wings were tested at AEDC from Mach 0.6 to Mach 1.2 at various dynamic pressures. Force and moment data were taken at all conditions and pressure data was obtained for all the flexible wings. This model was selected because of its wide array of data available for comparison in integrated testing of the ASTROS spline, QUADPAN, and the basic trim modules. Comparisons of flexible pressure data with the rigid linear aerodynamic pressure data are

made in the interest of qualitative assessments. During the integrated testing, further comparisons will be acquired with flexible linear aeroelastic analyses at the same conditions shown in the following discussion.

Top and side views of the Aeroelastic Tailoring model and part of its sting are shown in Figure 4-1. The lines on the figure represent the QUADPAN model's grid, the panel boundaries. The model has a body of revolution fuselage with a blunt base. The radius variation is similar to that of the F-16 fuselage. The wing planform shape is also similar to that of an F-16. The leading edge sweep is  $40^\circ$ , and there is a strake on the inboard portion. Unlike the F-16, the wing has no camber or twist, the wing-body intersection is not filleted, and there is no tail. The wing profile is based on the NACA 64A004 airfoil. The thickness ratio varies from 3.47% at the root to 4% at the tip. The strake is a sharp bi-convex airfoil that blends into the main wing at its maximum thickness point. The sting was included in some of the models, but the length was limited to half of the body length. In the 3D QUADPAN models, the blunt base was faired over; linear methods cannot model the separation that would normally occur there.

The other model used for data comparisons was an F-16XL. A planform view of the Carmichael grid is shown in Figure 4-2. An extensive pressure database was available on a 1/9th scale model tested from Mach 0.6 to Mach 1.2. The corresponding forces were not available, but subsonic results at Mach 0.2 were used. This model was added to the matrix to get results on a more complex wing and to get more reliable pressure data. (The deformation of the aeroelastic wings would have affected their pressures.) One deficiency with the F-16XL model was the absence of the wing tip launcher and missile that were on the wind tunnel pressure model.

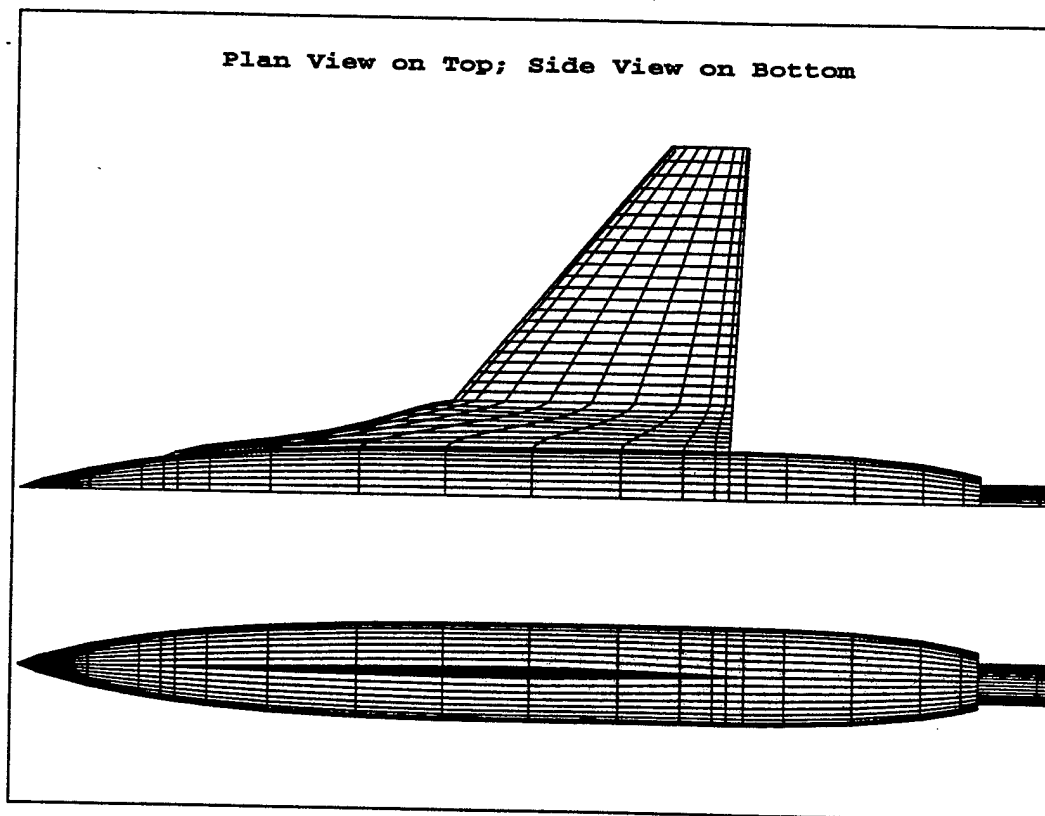


Figure 4-1 Aeroelastic Tailoring Model (QUADPAN Grid)



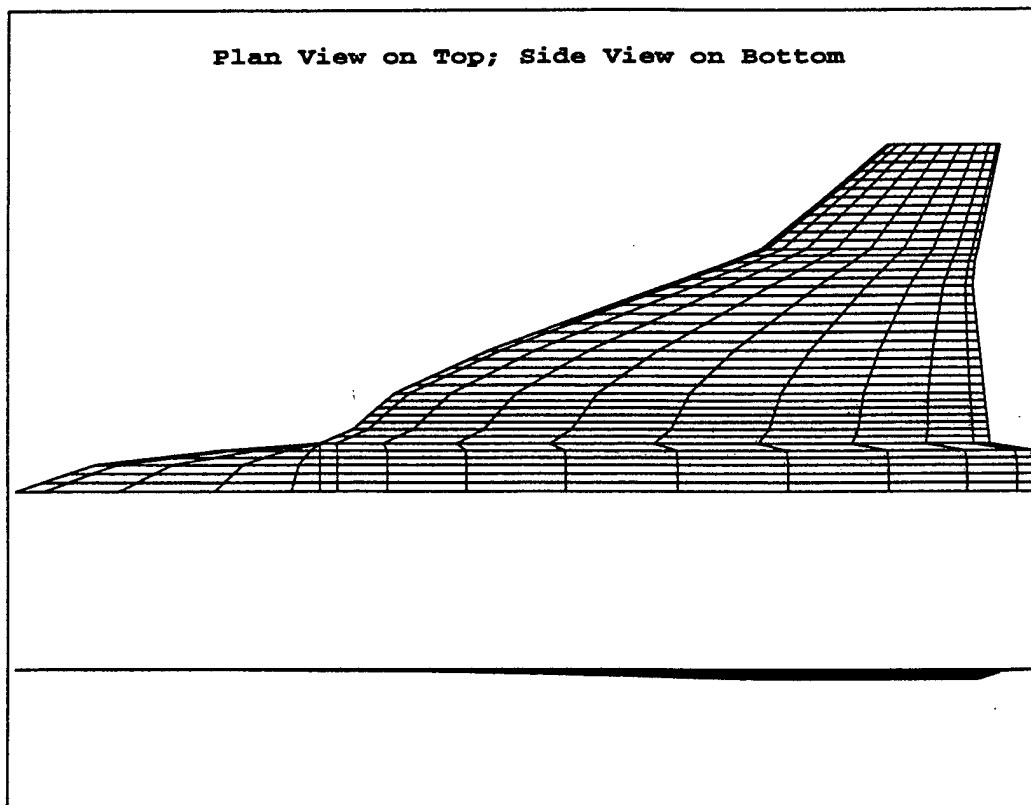


Figure 4-2 F-16XL Model (Carmichael Grid)

#### 4.1.4 Matrix Cases

Because the aerodynamic codes have different capabilities, we decided to make two types of comparisons. One comparison was made on a simplified "flat" model that all the codes were capable of representing. The other comparison used models that had as many features as the codes were capable of representing. These were referred to as the "test" models since they were designed to represent the parts present during the wind tunnel test. The results were compared at a subsonic, transonic, and supersonic Mach number. In addition to these basic comparisons, the sensitivity of each method to grid spacing was examined at subsonic conditions. This was done by doubling the number of panels in the chordwise and spanwise directions, individually.

The table below summarizes the matrix of codes and models that were compared. Note that there was no F-16XL QUADPAN model. Highlights of the code comparisons will be presented in the following sections followed by conclusions and recommendations.

Table 4-4 Selected Cases to Evaluate Aerodynamic Cases

Model\Code	HASC (Vorlax)	Carmichael	QUADPAN
Aeroelastic Tailoring Model (flat version)	Mach 0.6	Mach 0.6	Mach 0.6
Aeroelastic Tailoring Model (test version)	Mach 0.6, 0.9	Mach 0.6, 0.9, 1.2	Mach 0.6, 0.9, 1.2
F-16XL Model (flat version)	Mach 0.6, 0.9	Mach 0.6, 0.9, 1.2	

#### 4.1.5 Aeroelastic Model Comparisons - Flat Models

The baseline Vorlax grid for the flat model is shown in Figure 4-3. The flat model has no thickness or sting. The grid shows a "cosine" pattern of axial clustering with many points clustered at the leading and trailing edges. The spanwise spacing was fairly uniform. There were 988 total panels. This model was the source for the flat Carmichael and QUADPAN models. In the case of Carmichael, the only difference was the exclusion of the left side of the model. This was also true for the QUADPAN model, but additional modifications were required since QUADPAN cannot analyze a one-surface model. The upper and lower surface of the model had to be separated by a small amount while leaving the endpoints joined. They were only separated by 0.003 inches for this study, but this doubled the number of cells and significantly increased the run time.

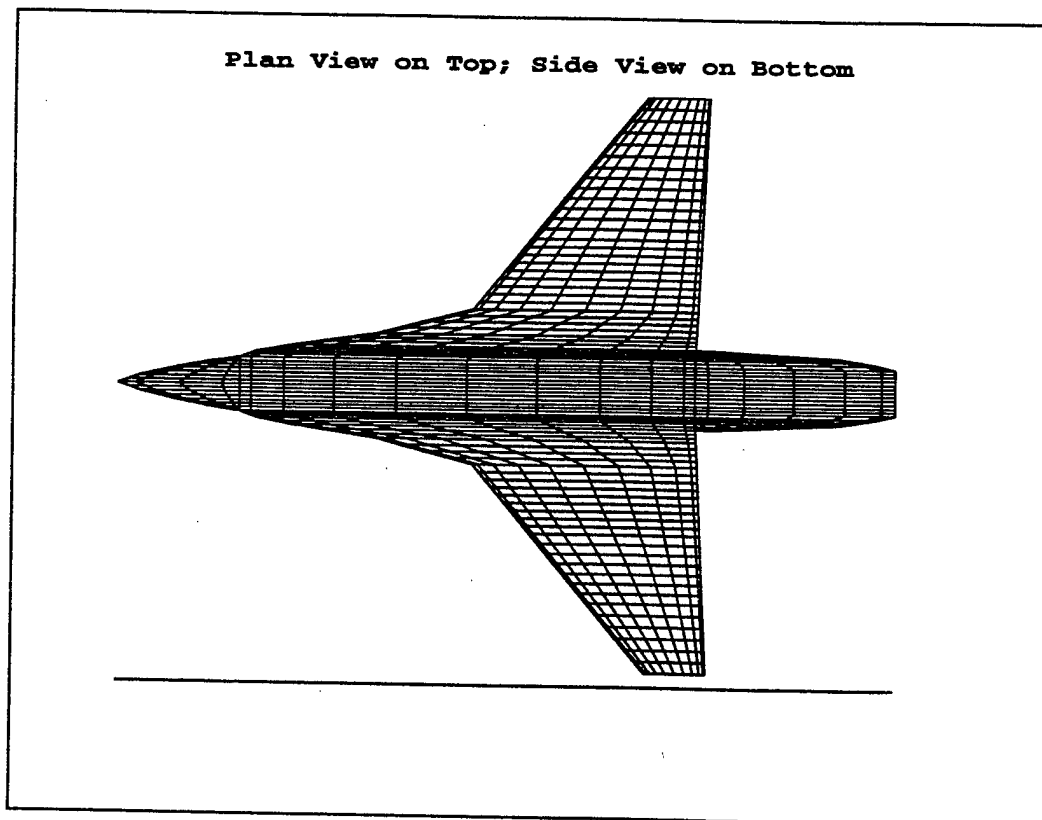


Figure 4-3 Aeroelastic Tailoring Model (Vorlax Grid)

The coefficient of lift (CL) versus angle of attack ( $\alpha$ ) comparison at Mach 0.6 is shown in Figure 4-4. The agreement between the codes and with the data is very good below  $16^\circ$   $\alpha$ . Above that, the data indicates separation and the resulting wing stall. The Vorlax CL also trails off from the others at high  $\alpha$ .

The sensitivity to the number of chordwise and spanwise panels was studied by doubling the number of panels in each direction. The sensitivity to the chordwise paneling was small and is not shown. Figure 4-5 shows the sensitivity for span panels. Carmichael and QUADPAN gave essentially the same answers they gave with the coarse grid, but the Vorlax CL trailed off farther from those results. This issue with Vorlax needs further investigation, but the difference is too small to decide that any of the results should be discounted.

The coefficient of lift (CL) versus coefficient of moment ( $C_m$ ) comparison is shown in Figure 4-6. The axes are oriented so that a positive slope of the line is stable. Positive moment is nose up. Here the

difference between the codes was much larger, but as the number of chord panels was doubled, the results moved closer together, as shown in Figure 4-7. The Vorlax results did not change much, but Carmichael became less stable, and QUADPAN became more stable. Some of the reasons for this will be discussed when the pressure results are presented. The sensitivity to the spanwise paneling was much smaller and is not plotted.

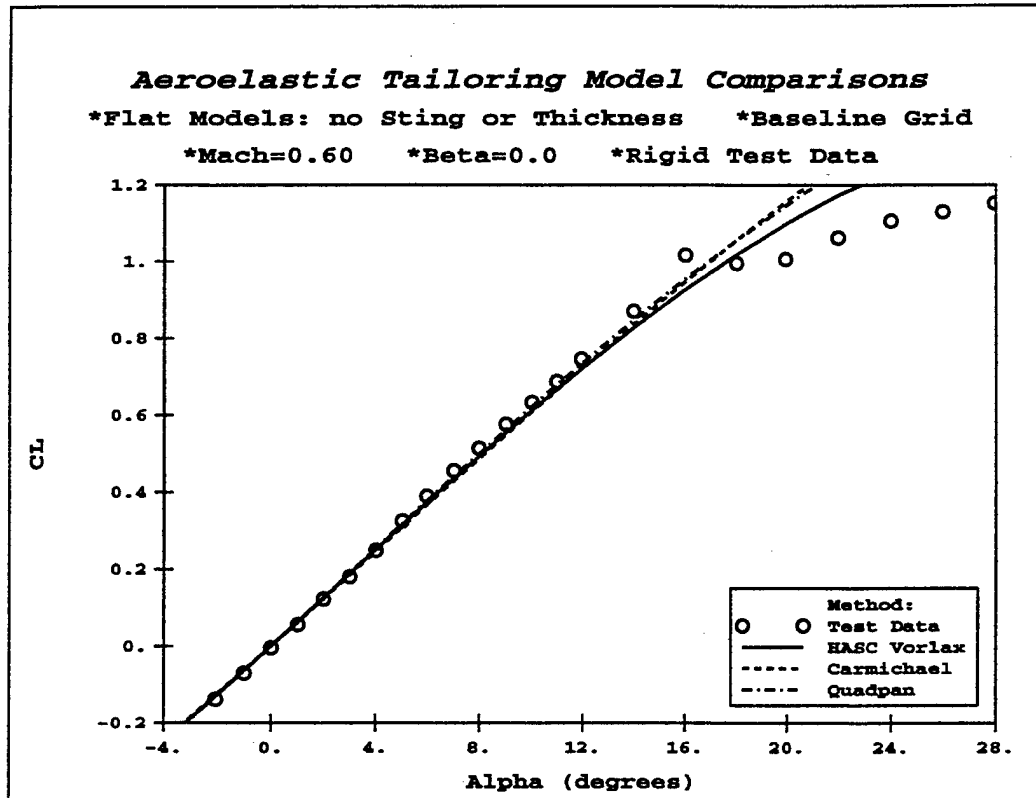


Figure 4-4 CL vs Alpha on Flat Aeroelastic Model - Mach 0.6 - Baseline Grid

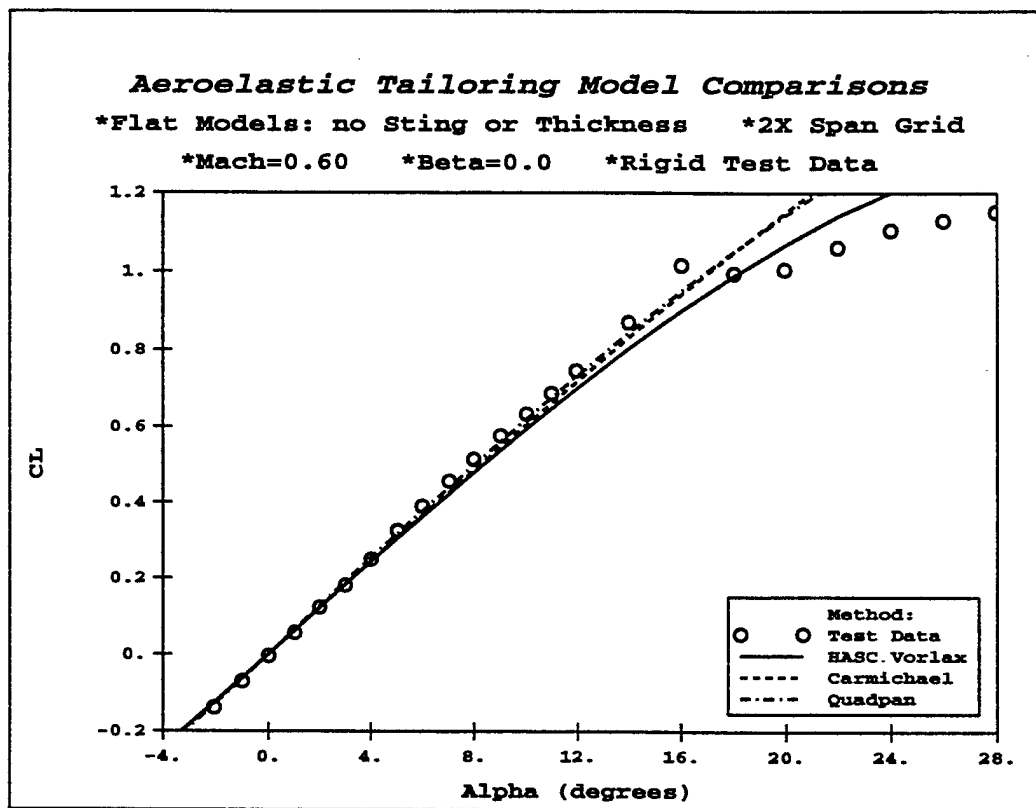


Figure 4-5 CL vs Alpha on Flat Aeroelastic Model - Mach 0.6 - Fine Span Grid

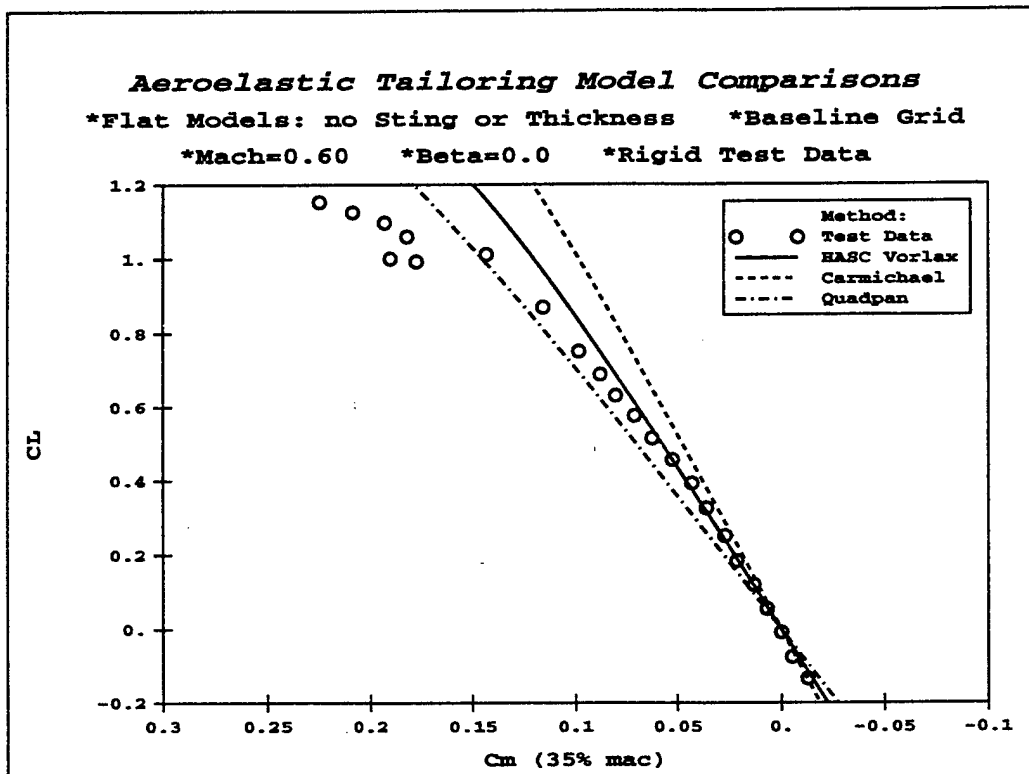


Figure 4-6 CL vs CM on Flat Aeroelastic Model - Mach 0.6 - Baseline Grid

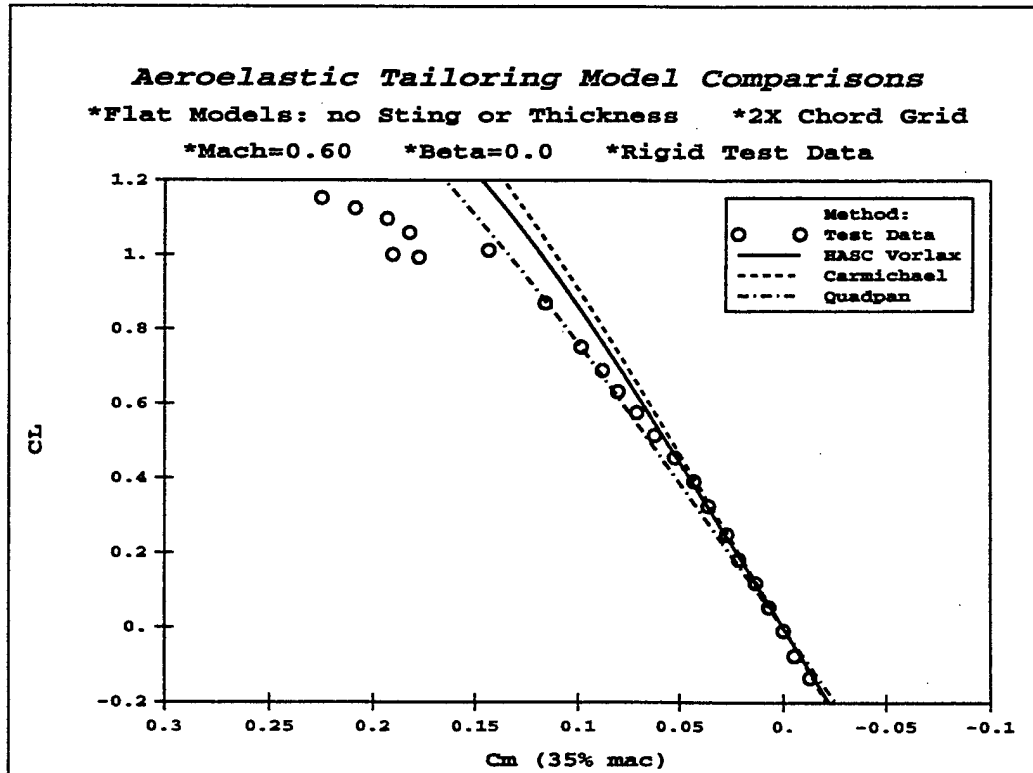


Figure 4-7 CL vs CM on Flat Aeroelastic Model - Mach 0.6 - Fine Chord Grid

The coefficient of lift (CL) versus coefficient of drag (CD) comparison is shown in Figure 4-8. The methods agree fairly well and were not especially sensitive to the number of chordwise and spanwise panels. Note that the minimum drag subtracted from the experimental data to make the comparison. This was done to eliminate the friction drag that the linear methods do not predict. The agreement with data could probably be improved at low alpha by using the leading edge suction adjustments that are usually made.

The coefficient of pressure (Cp) results were compared at four span locations on the model. The comparisons were made near the model centerline (1.3% span), on the strake (17.1%), near the mid-span of the wing (59.8%), and near the tip of the wing (88.9%). All but the centerline location had experimental data to compare with, but mid-span location proved to be the most useful for making comparisons. The tip tended to separate at moderate angles of attack leading to poor agreement with predictions, and the strake location did not have a full row of pressure taps. Accordingly, in the pressure comparisons that follow, only the mid-span location is discussed. It is representative of the types of results obtained elsewhere on the wing. The results are compared at an angle of attack that gave an overall CL of 0.7 for the rigid wing. The data from the flexible wings was taken at the angle of attack that had this CL.

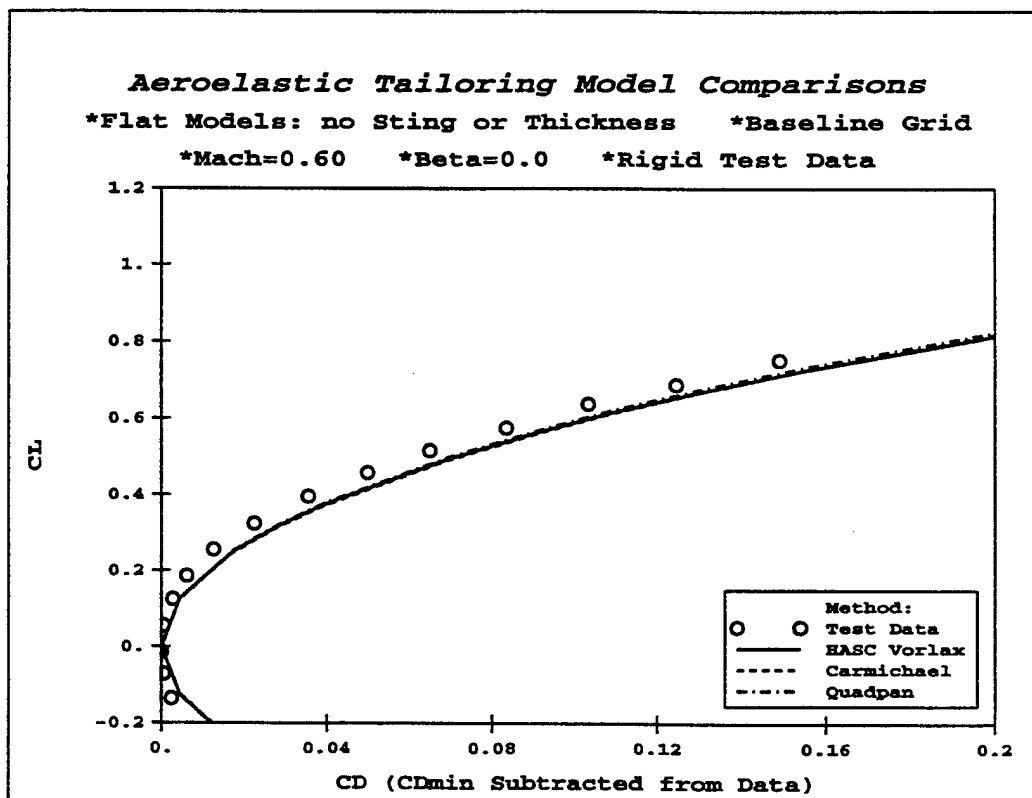


Figure 4-8 CL vs CD on Flat Aeroelastic Model - Mach 0.6 - Baseline Grid

Before comparing the methods to each other, we should note some differences in code assumptions that affected the way the comparisons were made. Each code enforces its flow tangency condition at a control point within each panel. The Vorlax control point varies from 25% of the chord at the front of the wing to 75% of the chord at the rear of the wing. The QUADPAN control point is at 50% of the chord for subsonic cases. The Carmichael control point is at 95% of the chord, but the moment is computed using a point at 50% of the chord. The moment point was used to plot the data. This prevented the Carmichael data from appearing shifted relative to the others.

Figure 4-9 shows the pressure comparison at the mid-span location. Figure 4-10 is the same plot on a different scale to highlight the leading edge region. These plots are repeated for the case with more chord panels in Figures 4-11 and 4-12. The pressure patterns are typical of linear aerodynamic codes. They give extreme pressure differences at the leading edge because the flow has to immediately turn from the freestream direction to align itself with the plate. A sharp leading edge is a singular point in linear aerodynamic theory; the pressures will keep diverging as we refine the grid. Even if the leading edge was blunt, linear theory would have problems there at non-zero Mach numbers because of the small perturbation assumption. In real life, the pressure would never fall below vacuum pressure ( $C_p$  of -3.97 for this Mach number) or exceed the isentropic stagnation pressure ( $C_p$  of 1.09).

The codes show large differences at the leading edge. QUADPAN predicts the largest pressure difference followed by Vorlax and Carmichael. The fact that the Vorlax control point is farther forward than Carmichael's may explain its higher pressures. In the case of QUADPAN, a higher order formula is used to calculate the pressures, instead of the linear  $C_p$  formula, and this may explain why it is larger. QUADPAN also uses information from neighboring panels in the pressure computation. This tends to average the results at the leading and trailing edge and make the results non-symmetric, as they will be for real flows. Apart from the leading edge regions, the methods agree relatively well with each other, but they do not match the data.

The limitation of linear theory at the leading edge is part of the reason the agreement with the data is poor. High loadings there have to be offset by low loadings elsewhere. However, we also have to remember that the data is from a flexible wing and may have developed some camber that is not modeled in the predictions.

Some of the moment sensitivity to chordwise grid resolution can also be explained by the leading edge singularity. The pressures there changed substantially when the grid was refined. The way Carmichael uses one location to enforce the boundary conditions and another to compute the moments could also have a detrimental effect.

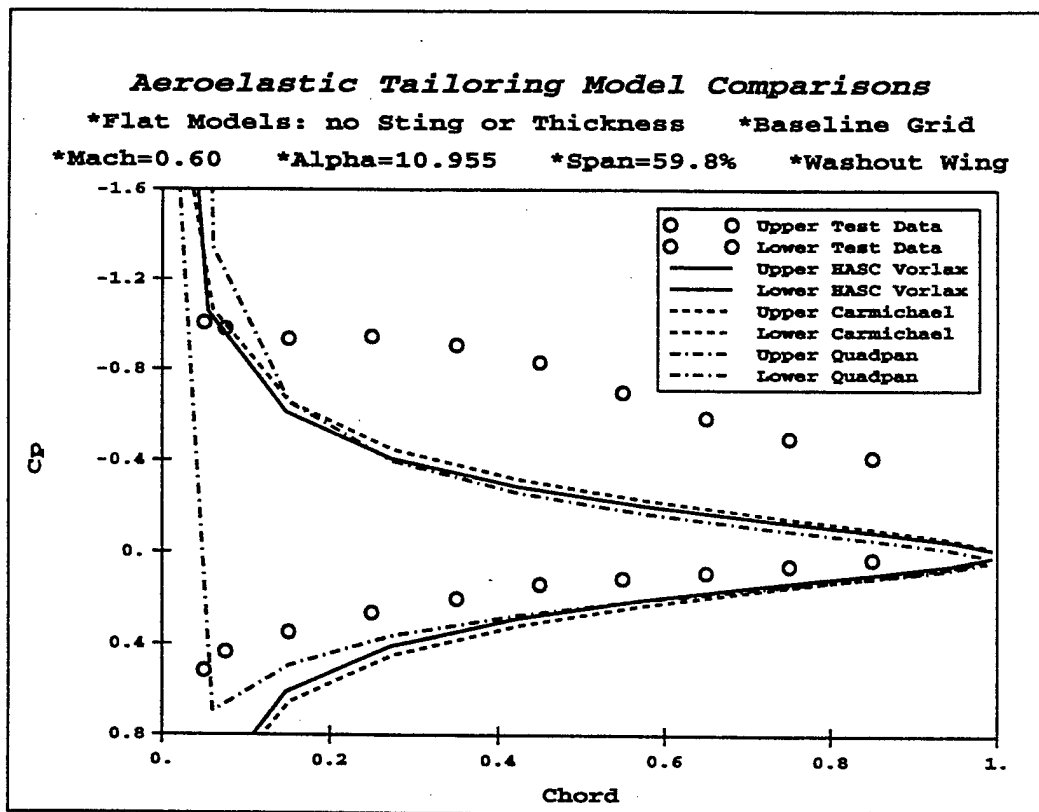


Figure 4-9 Mid-Span Cp on Flat Aeroelastic Model - Mach 0.6 - Baseline Grid

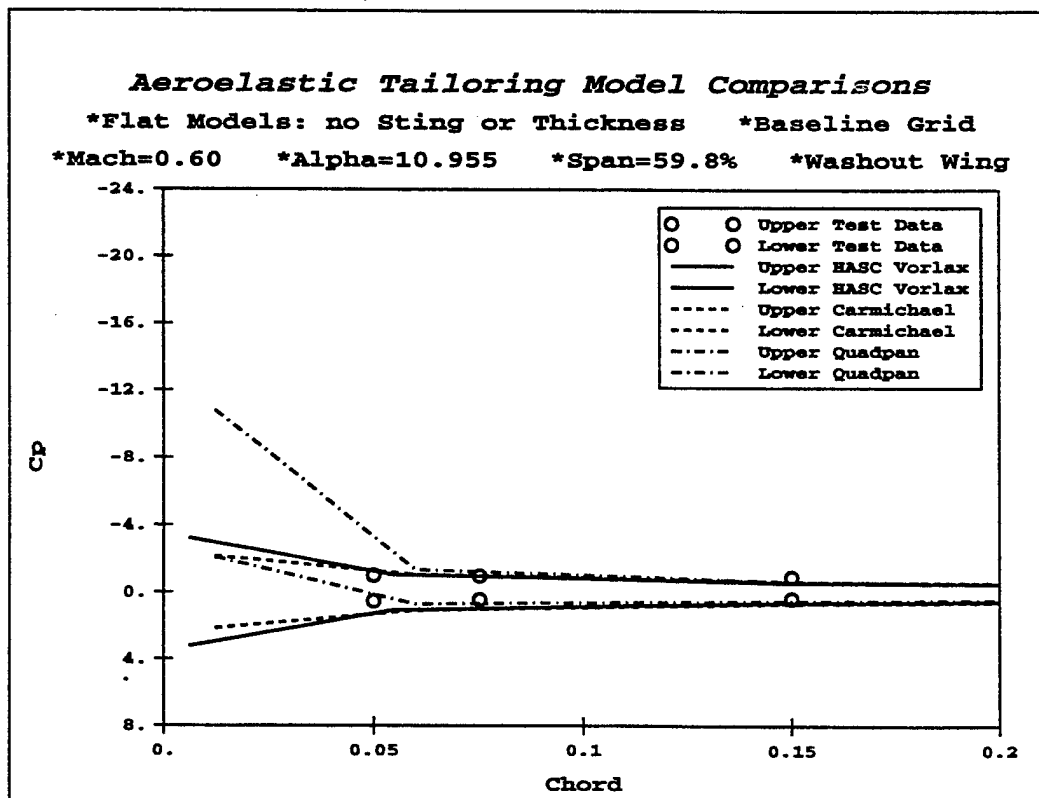


Figure 4-10 Mid-Span Cp on Flat Aeroelastic Model - Mach 0.6 - Baseline Grid



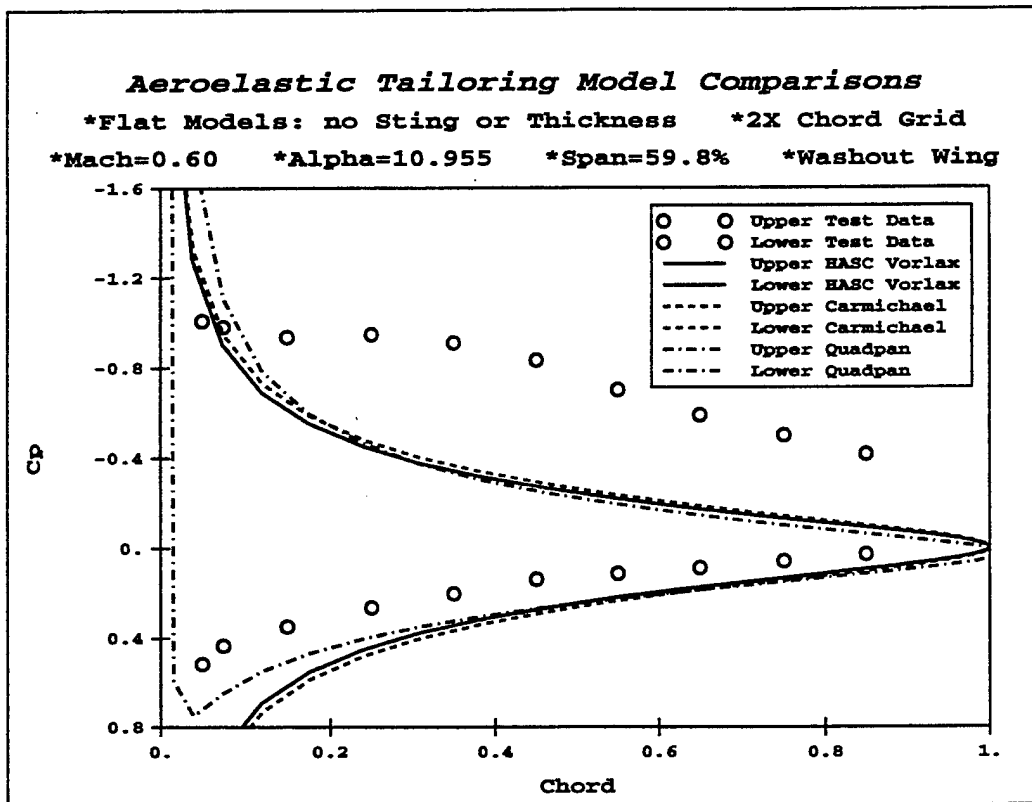


Figure 4-11 Mid-Span Cp on Flat Aeroelastic Model - Mach 0.6 - Fine Chord Grid

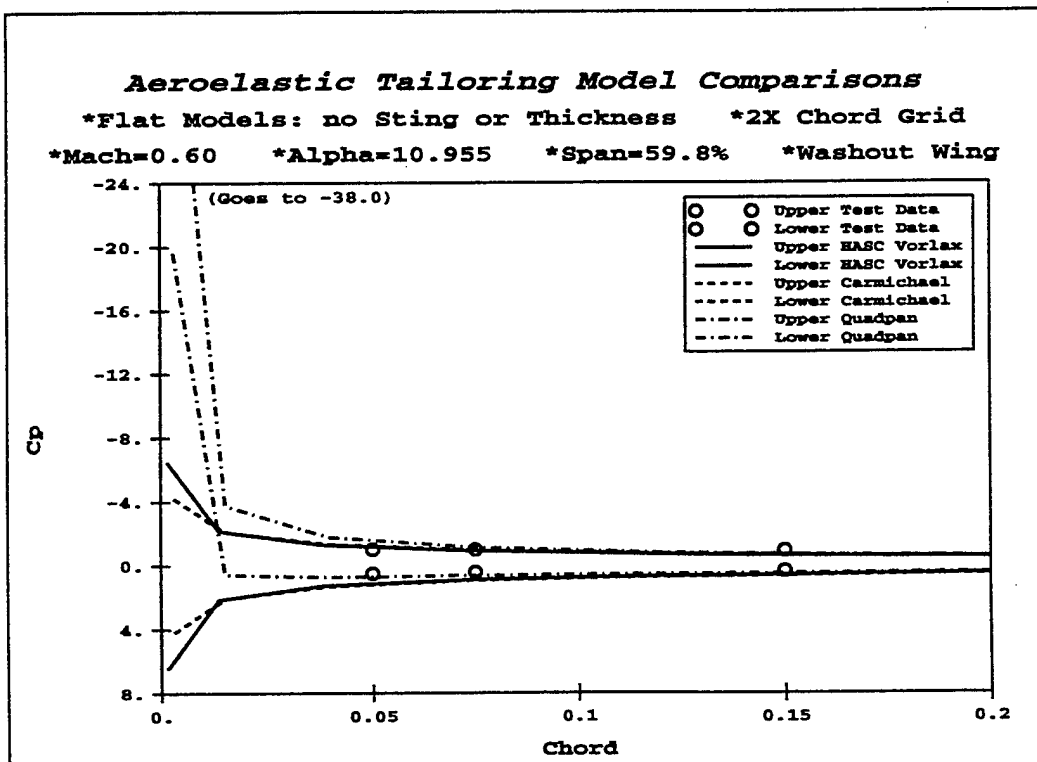


Figure 4-12 Mid-Span Cp on Flat Aeroelastic Model - Mach 0.6 - Fine Chord Grid

#### **4.1.6 Aeroelastic Model Comparisons - Test Models**

The test models were different for each code since they were designed to use all the geometric capabilities of the individual code. For the test Vorlax model, only a flat surface representing the sting was added. The rest of the grid was left the same as the flat model, and the sting forces were not included in the results. The same was done for the test Carmichael model, but the thickness slopes were also added for each panel. The test QUADPAN model was identical to that shown in figure 4-1, except that the base region was faired over. (When the base was not faired over, it developed large pressures that affected the aft fuselage enough to change the integrated axial force.)

The same comparisons and sensitivity studies done for the flat models were also done for the test models at Mach 0.6. In addition, a comparison was made at transonic conditions (Mach 0.9) and attempted at supersonic conditions (Mach 1.2). The results are summarized in the following paragraphs.

The test Vorlax model generally gave the same results as the flat model; the sting had very little effect. The addition of thickness to the Carmichael model did not change the lift and moment significantly, but did cause a slight zero alpha drag. (The base probably should have been faired like the QUADPAN model.) The biggest force changes were seen in the QUADPAN moment and drag results. The CL versus CM comparison is shown in Figure 4-13, and CL versus CD is in Figure 4-14. Compared to Figure 4-6, the QUADPAN results are much more stable and agree better with the data at low alphas. This could be due to the more accurate representation of the body geometry or the reduced leading edge pressures that will be shown later. Compared to Figure 4-8, the new QUADPAN results have a much more optimistic drag polar than the flat model. The last line of the plot shows that it is also very sensitive to chordwise resolution.

QUADPAN's reduced drag is due to leading edge suction. The traditional panel methods that used flat wings had to add this separately since there was no forward facing area to apply it to. With QUADPAN, there is no way to keep it out of the results. A new method will have to be found to adjust the results since the suction is unrealistically high due to the leading edge singularity. Incidentally, the Carmichael results with the thick wing should have shown this effect, but the use of the linearized  $C_p$  formula eliminates most of it.

Figures 4-15 and 4-16 are updated pressure comparison at the mid-span location. They can be compared with Figures 4-9 and 4-10. The Vorlax results did not change, but the Carmichael and QUADPAN results are shifted up due to thickness. QUADPAN also shows lower peak pressures around the leading edge since it is easier for the flow to make the turn around a blunt leading edge.

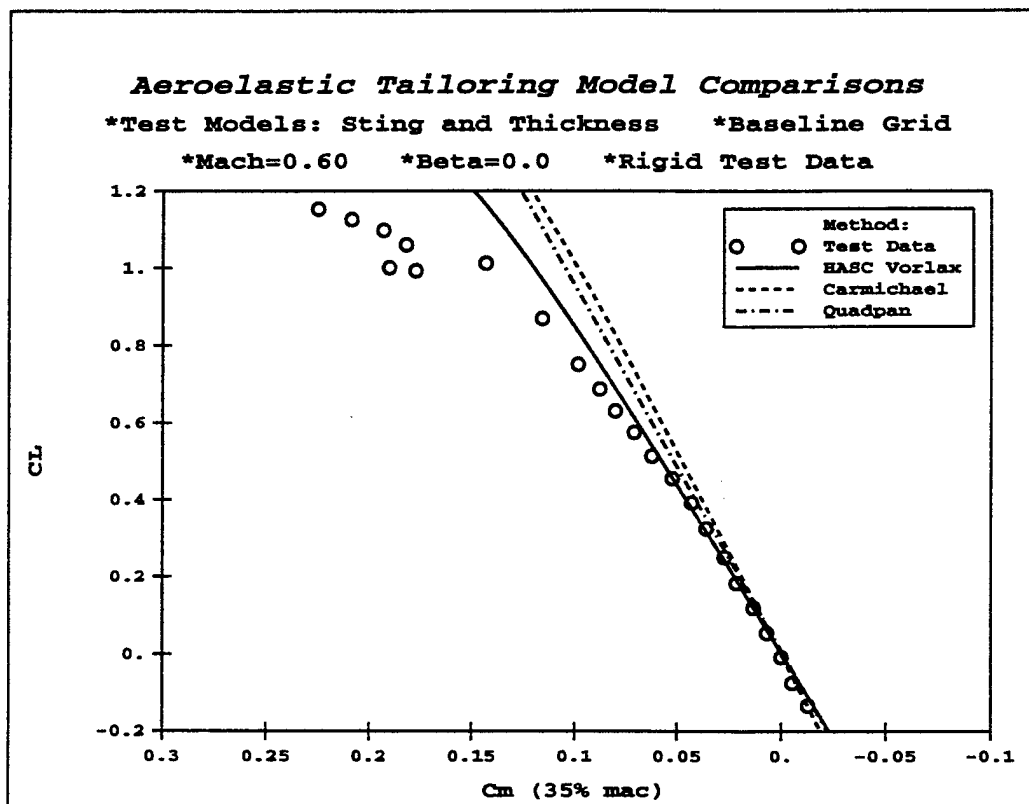


Figure 4-13 CL vs CM on Test Aeroelastic Model - Mach 0.6 - Baseline Grid

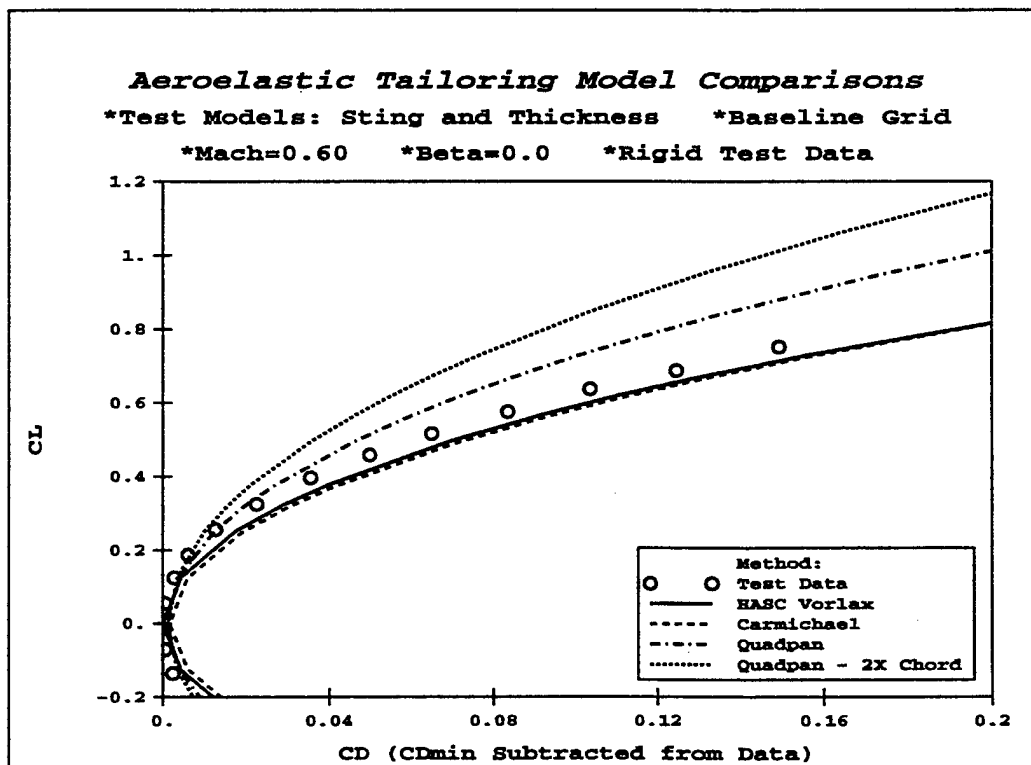


Figure 4-14 CL vs CD on Test Aeroelastic Model - Mach 0.6 - Baseline Grid

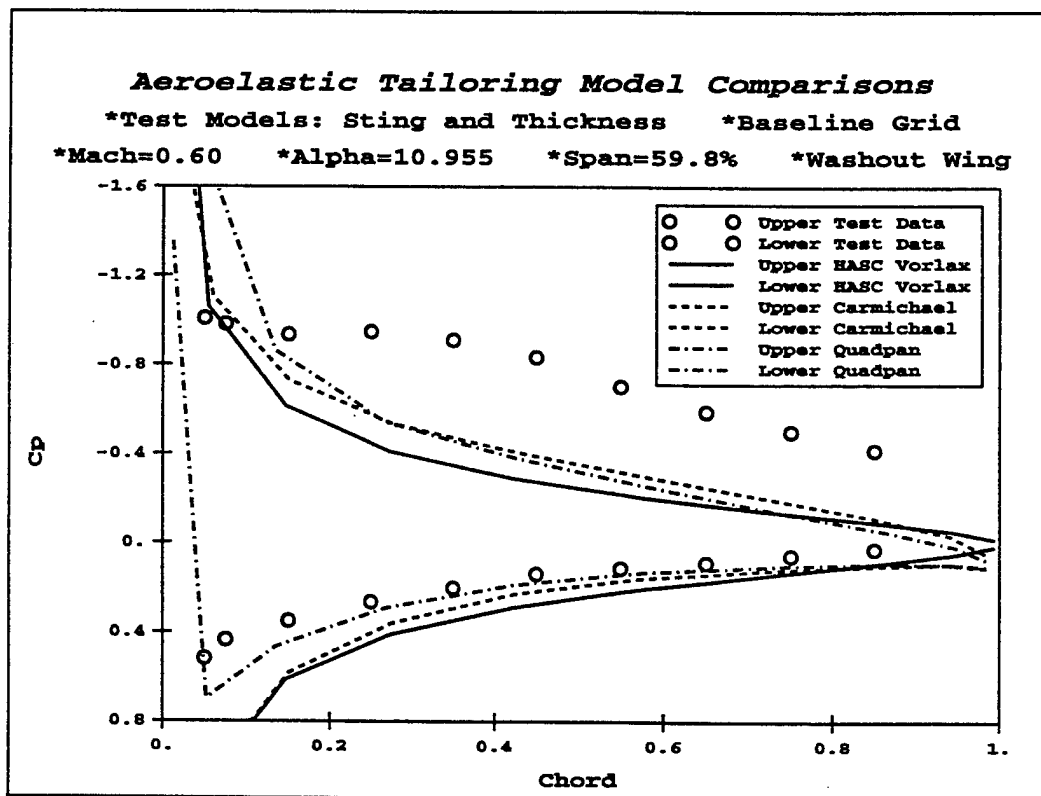


Figure 4-15 Mid-Span Cp on Test Aeroelastic Model - Mach 0.6 - Baseline Grid

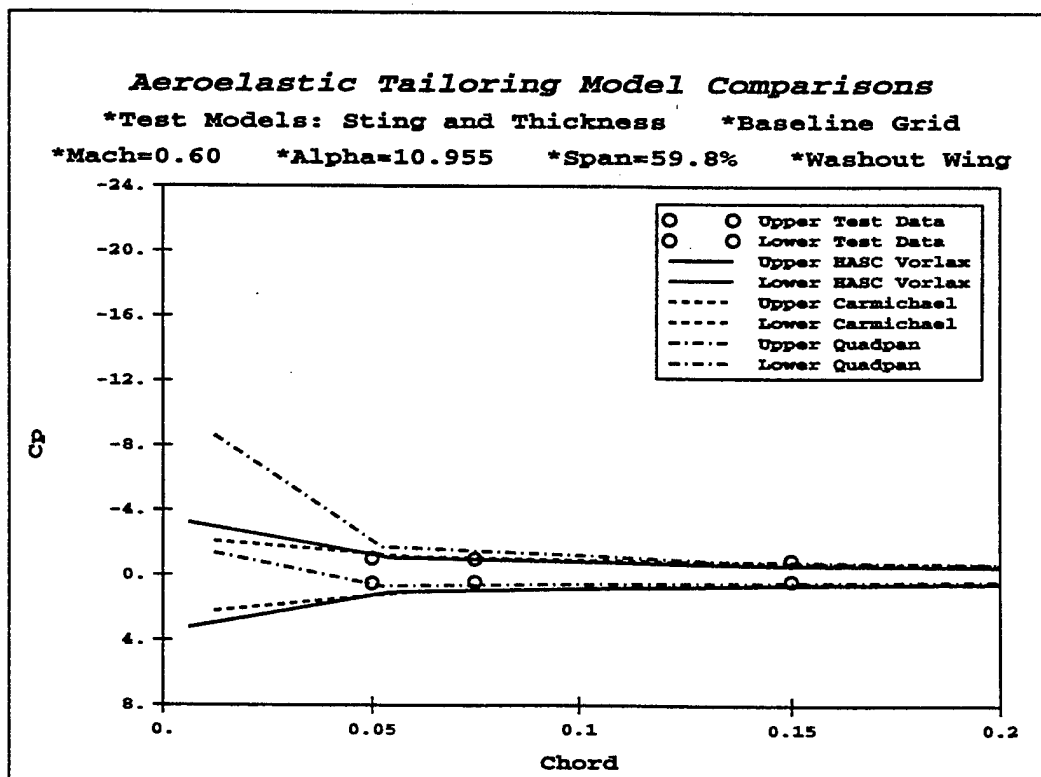


Figure 4-16 Mid-Span Cp on Test Aeroelastic Model - Mach 0.6 - Baseline Grid

All three codes were compared with experimental results at Mach 0.9. Since only small perturbations are allowed as we approach Mach 1.0, linear theory was not expected to do well at transonic conditions. Accordingly, the CL and CM predictions shown in Figures 4-17 and 4-18 agree with data only at low angles of attack. Above  $5^\circ$  alpha, the data develops non-linearities due to shock formation that cannot be modeled by these methods. Nevertheless, the predictions are still useful at this Mach number. The trends between the methods did not change from the subsonic results, so no additional comparisons are shown.

A supersonic case was attempted with all three methods. At the time of writing, only solutions from Carmichael and QUADPAN had been achieved. The CL versus alpha and CL versus CM plots for these cases are shown in Figures 4-19 and 4-20. The agreement of Carmichael with data is quite good, but the data only went up to  $6^\circ$  alpha. The QUADPAN moment results don't agree well with data, and no explanation for this problem is apparent from the investigations made.

Since linear theory should be capable of predicting the wave (thickness) drag, the drag data in the CL versus CD plot, Figure 4-21, was handled differently from the other drag data. The minimum CD value from the Mach 0.9 data, 0.011625, was subtracted from the Mach 1.2 data to remove the effect of friction drag. The plot shows that the wave drag computed by QUADPAN was very close to the data, but Carmichael's drag was much higher than measured. The most likely explanation lies in the way Carmichael uses the thickness inputs. The thickness envelope is applied in a 2D manner. This is adequate on the wings, but on the edge of the fuselage it overstates the slopes and leads to very high pressures. A new way of calculating the thickness envelope could probably be devised to eliminate this problem.

Figure 4-22 shows the supersonic pressure comparison at the mid-span location. QUADPAN shows less lift on the aft part of the wing. This is consistent with the moment results. For Carmichael, the agreement with data is much better than that of the subsonic cases since the leading edge singularity does not exist for supersonic flows. The leading edge pressures are mainly determined by the slope on the top and bottom of the wing. Because of the small perturbation assumption, the flow at the blunt part of the leading edge will still be wrong, but this is only a small region for this wing. Because of the blunt leading edge, an empirical leading edge pressure, rather than a suction, would probably be needed to get the most reliable drag values from either method.

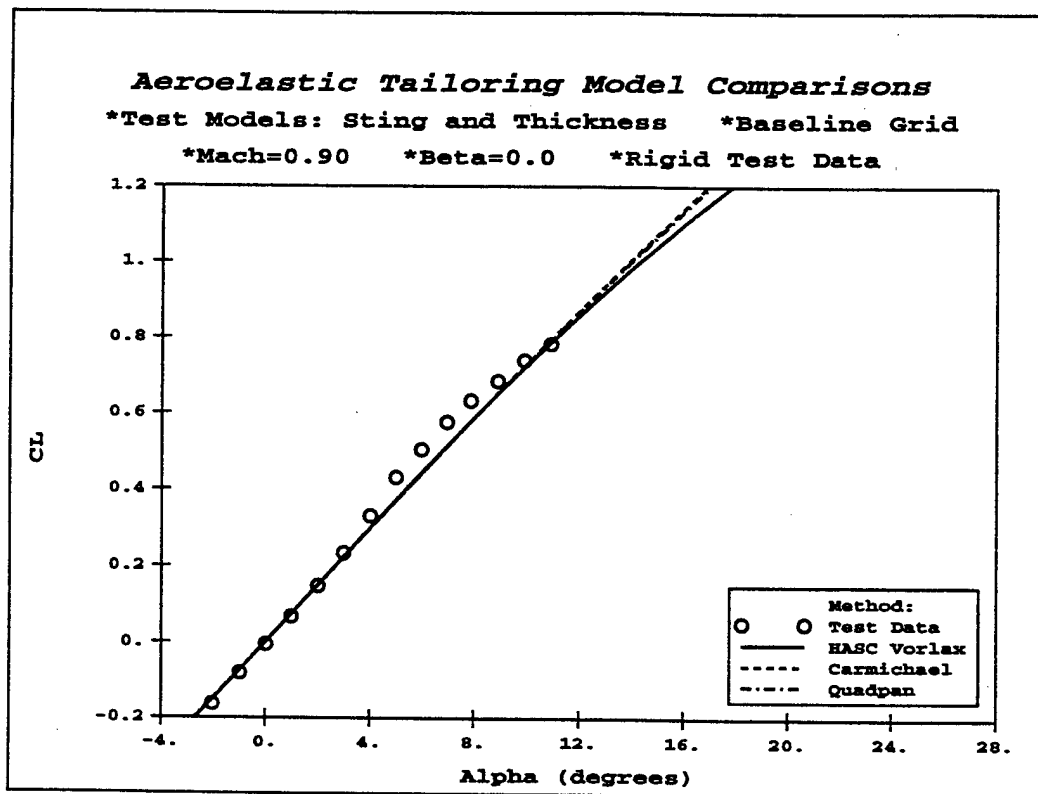


Figure 4-17 CL vs alpha on Test Aeroelastic Model - Mach 0.9 - Baseline Grid

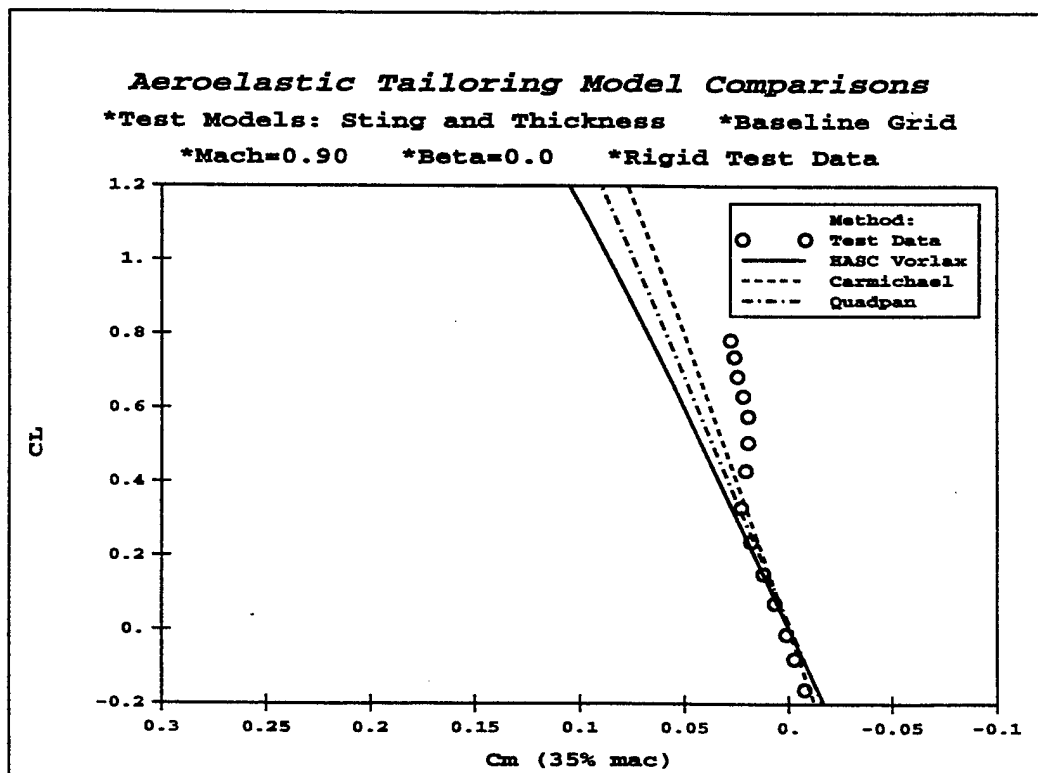


Figure 4-18 CL vs CM on Test Aeroelastic Model - Mach 0.9 - Baseline Grid

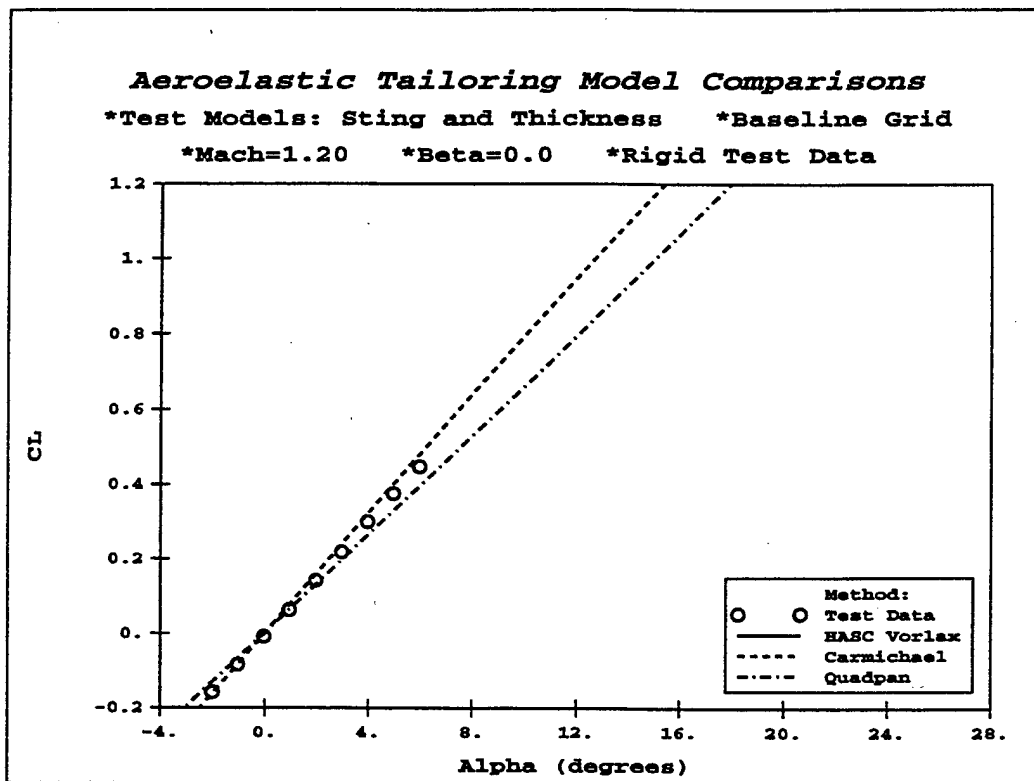


Figure 4-19 CL vs alpha on Test Aeroelastic Model - Mach 1.2 - Baseline Grid

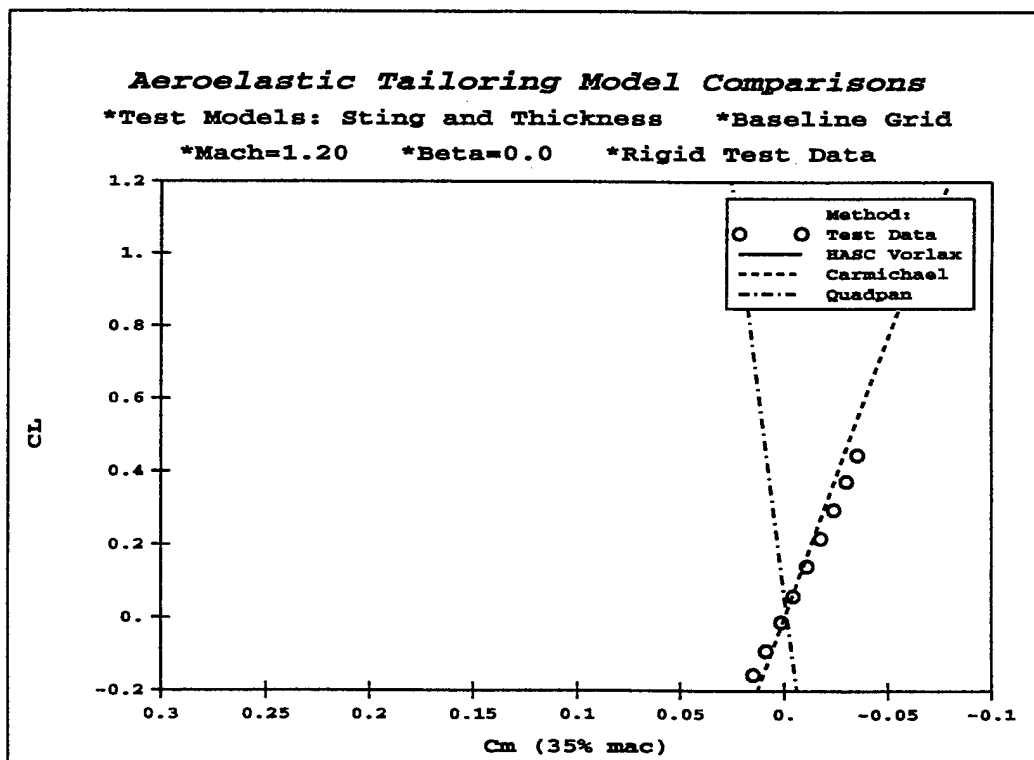


Figure 4-20 CL vs CM on Test Aeroelastic Model - Mach 1.2 - Baseline Grid

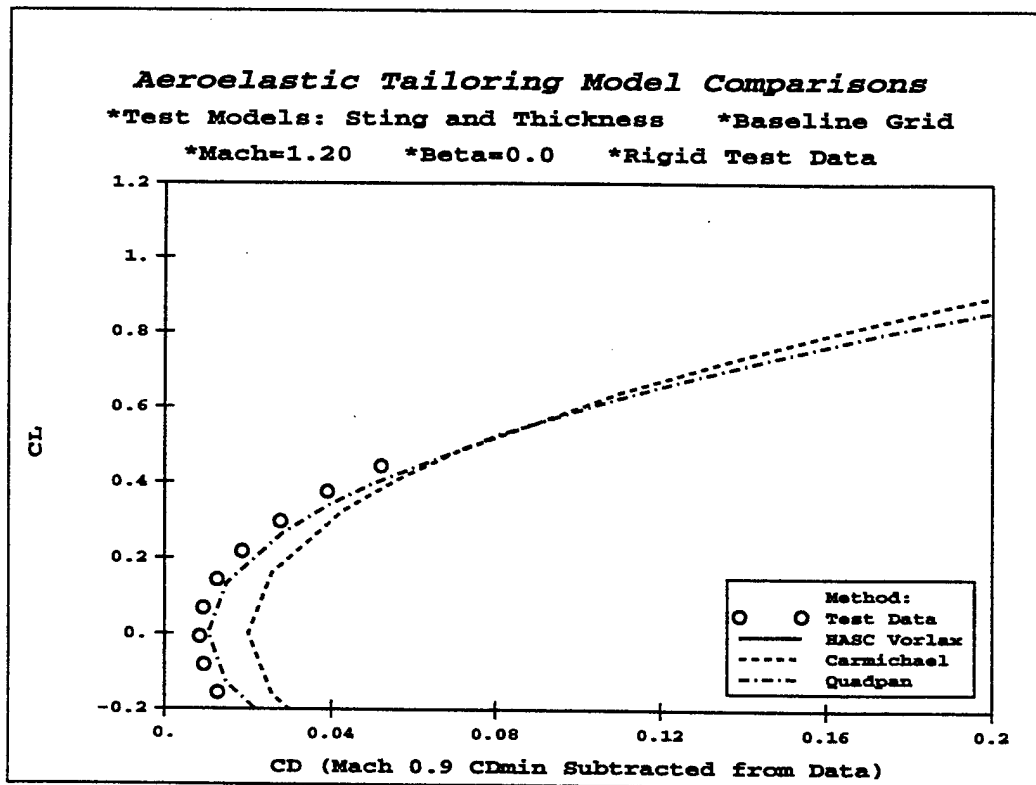


Figure 4-21 CL vs CD on Test Aeroelastic Model - Mach 1.2 - Baseline Grid

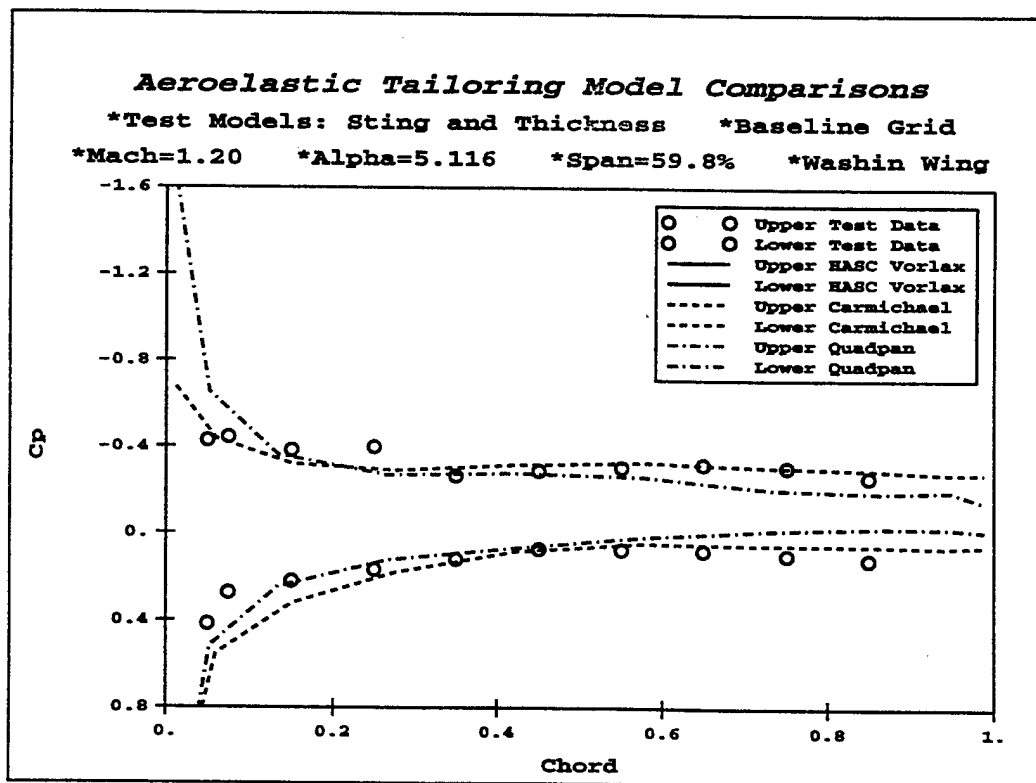


Figure 4-22 Mid-Span Cp on Test Aeroelastic Model - Mach 1.2 - Baseline Grid



#### **4.1.7 F-16XL Comparisons - Flat Models**

The baseline Carmichael grid for the F-16XL model is shown in Figure 4-2. Its construction was similar to that of the flat Aeroelastic Tailoring model. There was no thickness or sting, but the wing now has camber and twist. The number of chordwise wing points and their distribution was the same as earlier. The initial model had a 0.56 inch waterline gap between the wing and fuselage. We later realized that this made the results very sensitive to spanwise grid resolution. The gap was eliminated for all the final models.

The CL versus alpha comparison at Mach 0.6 is shown in Figure 4-23. The data is for Mach 0.2, but that should not matter at this Mach number. The agreement between the codes was similar to that seen with the Aeroelastic Tailoring model cases, but the sensitivity to spanwise resolution seen in Vorlax was not as great here. The agreement with data was only good up to 8° alpha. After that, the data shows evidence of vortex lift that cannot be modeled by the linear panel methods.

The Cp results were compared at four span locations on the model. The comparisons were made just outboard of the strake (35.5% span), before and after the wing break (67.4% and 73.0%), and near the wing tip (96.2%). The tip comparisons were not very good since the wing tip missile was not modeled. The subsonic comparisons near the wing break were similar in appearance to those on the Aeroelastic Tailoring model. No new conclusions were drawn so the plots are not presented in this report. The subsonic comparison just outside the strake is shown in Figure 4-24. Evidence of the vortex can be seen in the pressure peak on the upper surface. The supersonic comparisons at all the span stations were generally worse than those of the Aeroelastic Tailoring model since thickness was not modeled. The delta Cp agreement was probably still adequate for loads work, however.

#### **4.1.8 Conclusions and Recommendations**

The purpose of this comparison was to develop the models and data necessary for integrated testing of the feature enhancements to ASTROS under this contract, and in turn, assess the suitability of the three linear panel methods for loads work in the ASTROS program. For loads calculations, the most important quantity is the pressure difference across the wing plane. Accordingly, the most relevant comparisons are with lift, moment, and delta Cp. Drag has less effect on the loads, but it can be important if a wing camber and twist optimization is being performed. In addition to matching data, the codes must be capable of modeling all the configurations of interest and be economical to run.

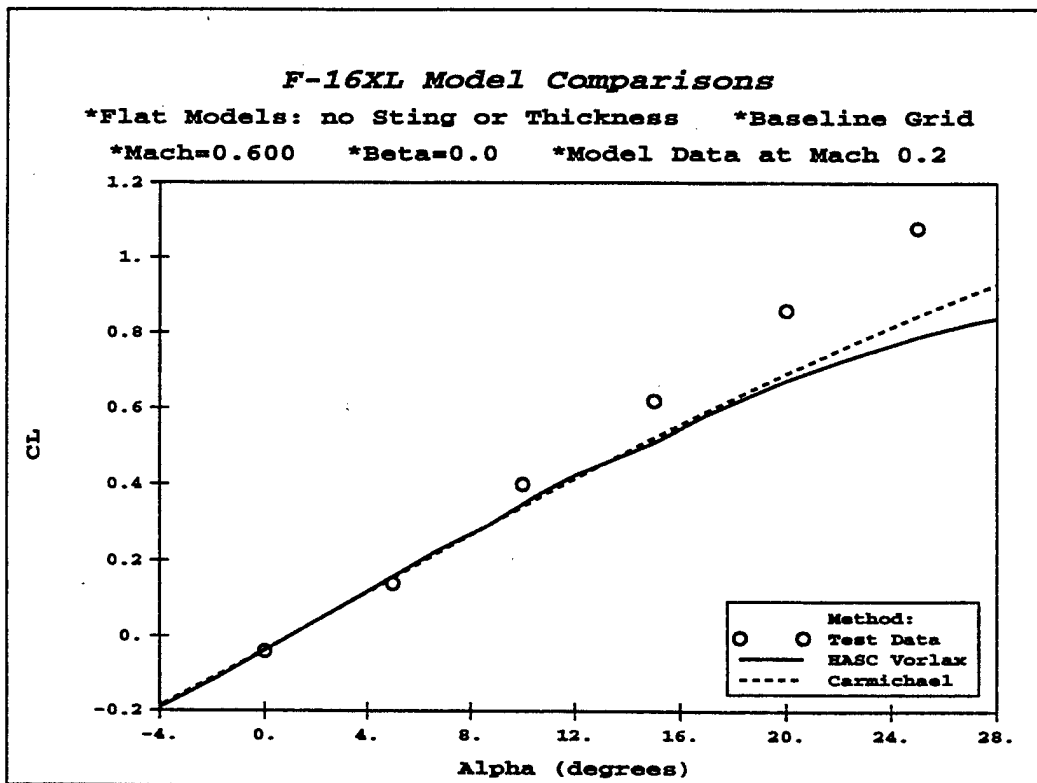


Figure 4-23 CL vs alpha on Flat F-16XL Model - Mach 0.6 - Baseline Grid

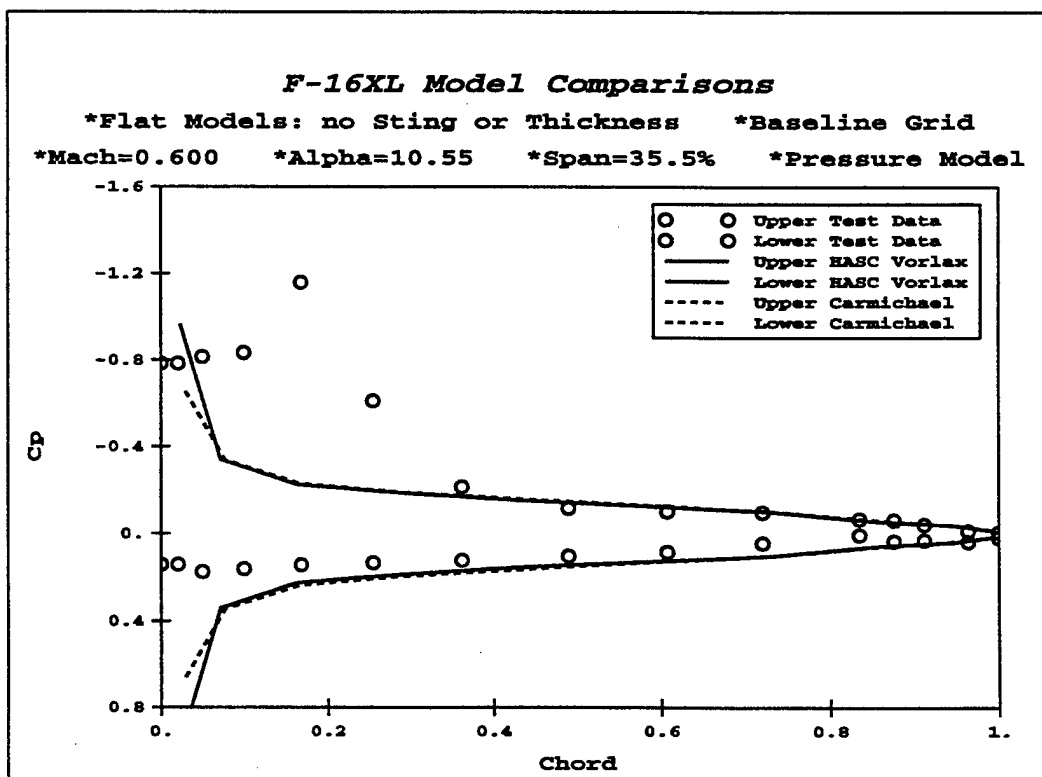


Figure 4-24 Near Strake Cp on Flat F-16XL Model - Mach 0.6 - Baseline Grid

In terms of data agreement on typical models, none of the codes stood out as being clearly superior. This should have been anticipated since they were all based on the same governing equation. The results on the flat Aeroelastic Tailoring model showed that the codes gave very similar results on a common geometry. The pressure differences between Vorlax and Carmichael on that model were negligible. The QUADPAN pressures were different on the leading and trailing edges because of its tendency to average neighboring panels, but the integrated results from the three codes were not significantly different. All of them did exhibit some sensitivity to grid resolution in either lift or moment, however.

When all the geometric modeling capabilities of the individual codes were tested, larger differences emerged. The addition of thickness to the Carmichael results improved the agreement of  $C_p$  with data. The delta  $C_p$ , lift, and moment were not affected, however. The drag was different at supersonic conditions, but the results are suspect until an improved procedure for handling fuselage thickness is devised. The 3D QUADPAN results benefited from the addition of thickness and the ability to handle the fuselage as a rounded body instead of a wing. The QUADPAN drag results will require some adjustments to the leading edge suction before they can be trusted. Currently, the most serious limit on the usefulness of Vorlax and QUADPAN is their questionable performance in supersonic flows.

From the standpoint of geometric modeling capability, QUADPAN was clearly the most powerful code in this study. Its 3D geometry capability allows it to run almost any configuration of interest. Carmichael cannot handle asymmetric configurations or the 3D effect of the fuselage. Vorlax does not have a convenient capability for thickness or fuselage effects. QUADPAN also has additional boundary conditions that the other codes do not. These allow it to model inlets, wind tunnel inflow planes, and propellers. The only drawbacks of QUADPAN are that it takes longer to set up and longer to run since it must use twice as many panels for a given problem.

This study has raised various issues that need further investigation. For Vorlax, the sensitivity to the number of span panels needs to be investigated. The supersonic capability also needs to be fixed. For Carmichael, the procedure for including thickness effects needs to be reviewed. The sensitivity of moments to the number of chord panels needs to be investigated, and the pressure calculations need to be compared with those in QUADPAN. For QUADPAN, a better method of handling the leading edge suction is desirable. It is believed that much of the areas in QUADPAN can be addressed through better modeling.

## 4.2 SMALL SCALE APPLICATIONS

Two of the ASTROS quality assurance models, the rectangular wing and forward swept wing, were modified and used throughout the AANDE program in unit tests and integrated testing. These models are depicted in Figure 4-25. The rectangular wing is shown at the upper left of the figure. The aerodynamic model is USSAERO, and the structural and aerodynamic geometry are defined as centerline symmetric. This model was used in developing the substructuring integration for both aerodynamics and structural models. The figure at the upper right depicts the forward swept wing model for USSAERO aerodynamics. It was used as centerline symmetric geometry in the development of the trim modules and trim optimization modules. The figure at the bottom depicts the forward swept wing application with QUADPAN aerodynamics. These models were used in centerline symmetric models and full tip-to-tip simulations as shown. The USSAERO aerodynamic models and the structural models are fully documented in the ASTROS Applications document (Ref. 24). Presented in this section discussions concerning use of substructuring, asymmetric QUADPAN with a symmetric aerodynamic model and full structural model, user-defined loads simulating adaptive structures, and trim optimization with response parameters.

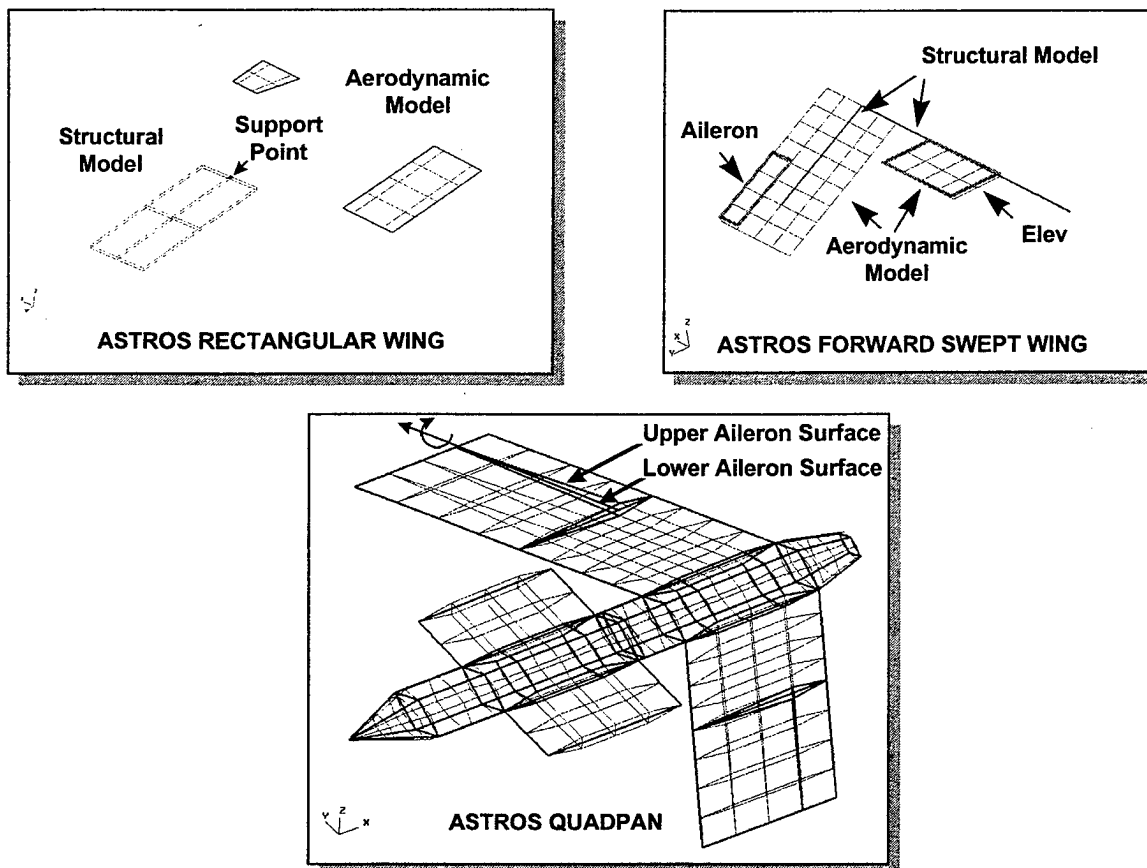


Figure 4-25 Small Scale Application Models Used in Unit and Integrated Testing

#### 4.2.1 Use of Substructuring

The rectangular wing is used to illustrate the user preparations for performing asymmetric trim simulations using USSAERO ("flat panel" aerodynamics). Also, aspects of asymmetric trim with substructuring are discussed. Substructuring is invoked in ASTROS provided the following conditions are met:

1. Centerline symmetrical structural and aerodynamic models (with respect to X-Z plane) have been defined and an asymmetric FTRIM discipline has been requested.
2. A centerline symmetrical structural model (with respect to X-Z plane) has been defined and a full three-dimensional aerodynamic model has been defined (e.g. QUADPAN).

To prepare input for use of substructuring, the user need only to provide input for the structural model. All provisions for the aerodynamic modeling are handled automatically. Invoking substructuring leads to two solution matrices; one describing the 'real' geometric structure and aerodynamics and one describing the 'image.'

To prepare the models for substructuring, degrees of freedom on the centerline of the structural model must be free for joining the real and image sides. The rectangular wing box as depicted in the upper left Figure 4-25 has multi-point constraints on the upper and lower surface nodes along the model centerline. These constraints allow the box to be rigidly linked to the support point shown in the figure. The constraints provide that the wing box root will rotate and translate in a rigid body sense with the

support point. In the case of substructuring, it is desired that the upper surface and lower surface wing root degrees of freedom join with the mirrored box. This is done through the new ASTROS bulk data 'RELES.'

Figure 4-26 illustrates a case for a simple asymmetric trim simulation. For a rolling pullout asymmetric trim using USSAERO, three structural degrees of freedom are specified at the support point - plunge, roll, and pitch (3,4, and 5). In the SOLUTION packet, BOUNDARY specifies a RELESID=666. This points to the degrees of freedom in the Bulk data that must be released to enable substructuring.

```

ASSIGN DATABASE ALEQ SHAZAM NEW
SOLUTION
TITLE = SIMPLIFIED WING STRUCTURE DESIGN
SUBTITLE = AEROELASTIC DESIGN
LABEL = OPTIMIZE FOR AILERON EFFECTIVENESS ONLY
ANALYZE
BOUNDARY MPC=600,SPC=30, SUPPORT=102, RELESID=666
LABEL = ANALYZE FOR ASYMMETRIC TRIM
SAERO (METHOD=USSAERO, MACH=0.8, MODEL=STEADY)
FTRIM ASYM(TRIM = 300, MODEL=STEADY)
PRINT TRIM, DISP = ALL
END
BEGIN BULK
SPC1 30 126 20
SPC1 30 456 1 14 8 2 13 7
MPC 600 7 3 1.0 20 3 -1.0
MPC 600 7 1 1.0 20 5 -0.5
MPC 600 8 3 1.0 20 3 -1.0
MPC 600 8 1 1.0 20 5 0.5
MPC, 600, 1, 2, 1.0, 20, 4, 0.5, ,+MPC1A
+MPC1A, ,20, 6, 10.0
MPC, 600, 2, 2, 1.0, 20, 4, -0.5, ,+MPC1A
+MPC1A, ,20, 6, 10.0
MPC, 600, 13, 2, 1.0, 20, 4, 0.5, ,+MPC1A
+MPC1A, ,20, 6, -10.0
MPC, 600, 14, 2, 1.0, 20, 4, -0.5, ,+MPC1A
+MPC1A, ,20, 6, -10.0
MPC 600 7 2 1.0 20 4 0.5
MPC 600 8 2 1.0 20 4 -0.5
SUPORT, 102, 20, 345
$-----
RELES, 666, RECT1, 7, 1, 7, 3
RELES, 666, RECT1, 8, 1, 8, 3
RELES, 666, RECT1, 1, 2, 2, 2
RELES, 666, RECT1, 7, 2, 8, 2
RELES, 666, RECT1, 13, 2, 14, 2
CORD2R, 999, , 1.0, 0.0, 0.0, 1.0, 0.0, 1.0, 2.0, 0.0, 0.0
$-----
TRIM, 300, 0.8, 6.5, , , 9864, , , +TR1
+TR1, NZ, 8.0, QRATE, 274, ALPHA, FREE, ELEV, FREE, +TR2
+TR2, THKCAM, 1., AILERON, 1., PRATE, FREE
GRID 1 10.0 0.0 0.5

```

Figure 4-26 Example of Rectangular Wing With Substructuring

The MPC equations define the "real" structure boundary conditions allowing that the stiffness matrix is fully defined at the support point in the degrees of freedom 3, 4, and 5. Grids 7 and 8 which are the points directly above and below the support point are then released in degrees of freedom 1,2, and 3. The 4, 5, and 6 degrees of freedom are SPC'd because of the element modeling assumptions. The stiffnesses of grids 7 and 8 in the 1, 2, and 3 directions are then fully defined by the real and image structural stiffnesses being joined. Gridpoints 1, 2, 13, and 14 are fore and aft of the support point, and therefore, the 2 degree of freedom is released since it was defined in the MPC.

Other areas of note in this example concern the asymmetric trim analysis itself. The logic for using USSAERO assumes from SAERO that it needs both symmetric and antisymmetric aerodynamic data unless either a symmetric and antisymmetric SAERO is specified. The TRIM card (at the bottom of the figure) declares three FREE variables (ALPHA, ELEV, and PRATE) coinciding with the SUPORT card (near the top of the figure) declaring three rigid body accelerations.

The aeroelastic solution output has been slightly reformatted. The addition of restrained stability derivative coefficients and asymmetric solutions is illustrated in Figures 4-27 and 4-28. In the printout, the unrestrained derivatives are printed first followed by the restrained derivatives. Recall that the unrestrained

derivatives include aeroelastic effects from inertial accelerations. The restrained derivatives include the aeroelastic effects from inertial relief in the rigid body acceleration parameters (e.g. Nz). Within these two stability derivative definitions, the longitudinal derivatives are printed first followed by the lateral derivatives. Forces and moments are printed for all parameters. In an asymmetric case, a parameter may have nonzero longitudinal or lateral components of load.

NONDIMENSIONAL LONGITUDINAL STABILITY DERIVATIVES COMPUTED AT THE AERODYNAMIC REFERENCE GRID AND INCLUDING ANY CONTROL EFFECTIVENESS										
TRIM IDENTIFICATION = 300			REFERENCE GRID = 20							
REFERENCE AREA = 2.4000E+03			REFERENCE CHORD = 2.0000E+01							
PARAMETER	LABEL	<<< DRAG >>>			<<< LIFT >>>			<<< PITCHING MOMENT >>>		
		RIGID DIRECT	RIGID SPLINED	FLEXIBLE	RIGID DIRECT	RIGID SPLINED	FLEXIBLE	RIGID DIRECT	RIGID SPLINED	FLEXIBLE
BASE PARAMETER	"THKCAM "	0.0000	N/A	N/A	0.0099	0.0099	0.0159	0.0057	0.0057	0.0051
PITCH RATE	"QRATE " S/DEG	0.0000	N/A	N/A	0.0940	0.0940	0.0952	-0.2024	-0.2002	-0.1899
PITCH RATE	"QRATE " S/RAD	0.0000	N/A	N/A	5.3839	5.3839	5.4534	-11.5977	-11.4719	-10.8784
ANGLE OF ATTACK	"ALPHA " 1/DEG	0.0000	N/A	N/A	0.1173	0.1173	0.1752	-0.0062	-0.0053	-0.0071
ANGLE OF ATTACK	"ALPHA " 1/RAD	0.0000	N/A	N/A	6.7224	6.7224	10.0359	-0.3552	-0.3025	-0.4071
CONTROL SURFACE	"ELEV " 1/DEG	0.0000	N/A	N/A	0.0118	0.0118	0.0107	-0.0431	-0.0431	-0.0398
CONTROL SURFACE	"ELEV " 1/RAD	0.0000	N/A	N/A	0.6781	0.6781	0.6123	-2.4702	-2.4699	-2.2796
CONTROL SURFACE	"AILERON " 1/DEG	0.0000	N/A	N/A	0.0000	0.0000	0.0000	0.0000	0.0000	0.0000
CONTROL SURFACE	"AILERON " 1/RAD	0.0000	N/A	N/A	0.0000	0.0000	0.0000	0.0000	0.0000	0.0000
ROLL RATE	"PRATE " S/DEG	0.0000	N/A	N/A	0.0000	0.0000	0.0000	0.0000	0.0000	0.0000
ROLL RATE	"PRATE " S/RAD	0.0000	N/A	N/A	0.0000	0.0000	0.0000	0.0000	0.0000	0.0000
COMPUTED DRAG VALUES ARE INCLUDED FOR COMPLETENESS AND MODEL CHECK-OUT ONLY USE CAUTION IN INTERPRETING THEIR PHYSICAL VALIDITY VALUES MARKED "N/A" CANNOT BE COMPUTED UNLESS THE CORRESPONDING DOF IS SUPPORTED										
NONDIMENSIONAL LATERAL STABILITY DERIVATIVES COMPUTED AT THE AERODYNAMIC REFERENCE GRID AND INCLUDING ANY CONTROL EFFECTIVENESS										
TRIM IDENTIFICATION = 300			REFERENCE GRID = 20							
REFERENCE AREA = 2.4000E+03			REFERENCE SPAN = 6.0000E+01							
PARAMETER	LABEL	<<< SIDE FORCE >>>			<<< ROLLING MOMENT >>>			<<< YAWING MOMENT >>>		
		RIGID DIRECT	RIGID SPLINED	FLEXIBLE	RIGID DIRECT	RIGID SPLINED	FLEXIBLE	RIGID DIRECT	RIGID SPLINED	FLEXIBLE
BASE PARAMETER	"THKCAM "	0.0000	N/A	N/A	0.0000	0.0000	0.0000	0.0000	N/A	N/A
PITCH RATE	"QRATE " S/DEG	0.0000	N/A	N/A	0.0000	0.0000	0.0000	0.0000	N/A	N/A
PITCH RATE	"QRATE " S/RAD	0.0000	N/A	N/A	0.0000	0.0000	0.0000	0.0000	N/A	N/A
ANGLE OF ATTACK	"ALPHA " 1/DEG	0.0000	N/A	N/A	0.0000	0.0000	0.0000	0.0000	N/A	N/A
ANGLE OF ATTACK	"ALPHA " 1/RAD	0.0000	N/A	N/A	0.0000	0.0000	0.0000	0.0000	N/A	N/A
CONTROL SURFACE	"ELEV " 1/DEG	0.0000	N/A	N/A	0.0000	0.0000	0.0000	0.0000	N/A	N/A
CONTROL SURFACE	"ELEV " 1/RAD	0.0000	N/A	N/A	0.0000	0.0000	0.0000	0.0000	N/A	N/A
CONTROL SURFACE	"AILERON " 1/DEG	0.0000	N/A	N/A	0.0166	0.0166	0.0163	0.0000	N/A	N/A
CONTROL SURFACE	"AILERON " 1/RAD	0.0000	N/A	N/A	0.9508	0.9508	0.9335	0.0000	N/A	N/A
ROLL RATE	"PRATE " S/DEG	0.0000	N/A	N/A	-0.0418	-0.0418	-0.0476	0.0000	N/A	N/A
ROLL RATE	"PRATE " S/RAD	0.0000	N/A	N/A	-2.3954	-2.3954	-2.7266	0.0000	N/A	N/A
VALUES MARKED "N/A" CANNOT BE COMPUTED UNLESS THE CORRESPONDING DOF IS SUPPORTED										

Figure 4-27 Rectangular Wing Unrestrained Longitudinal and Lateral Stability Derivatives

*****													
RESTRAINED STABILITY DERIVATIVES													
BOUNDARY: 1 MACH: 0.80													
*****													
SUPPORT GRID = 20 DOF = 345 X = 20.00 Y = 0.00 Z = 0.00													
RESTRAINED STABILITY DERIVATIVES:													
MACH = 0.800 LONGITUDINAL													
REFERENCE PARAMETERS: AREA = 2400.00 CHORD = 20.00 SPAN = 60.00													
MOMENT REFERENCE: XREF = 20.00 YREF = 0.00 ZREF = 0.00													
C.G. (FROM GPWG ENTRY): X CG = 0.00 Y CG = 0.00 Z CG = 0.00													

Figure 4-28 Rectangular Wing Restrained Longitudinal and Lateral Stability Derivatives

The trim printout has been updated including the parameters and values of the basis vector. Recall (see Subsection 3.3.1.1) that aerodynamic pressure vectors are stored in RIGDALOD as actual pressure vectors. In formulating the rigid incremental load vectors, the actual pressures are referenced to a basis

vector (e.g. reference angle of attack). The ASTROS maneuver simulation then computes the value of the trim parameters in a local linear space. After computing the linear aeroelastic trim, the reference values associated with the basis vector are added into the trim parameters to provide an absolute solution. The example in Section 4.3 utilizes this feature. Figure 4-29 displays the results from this run.

TRIM RESULTS FOR TRIM SET 300 OF TYPE				
MACH NUMBER		8.00000E-01		
DYNAMIC PRESSURE		6.50000E+00		
VELOCITY		9.86400E+03		
BASE PARAMETER : "THKCAM "				
BASE STATE : "ALPHA "		= 0.00000E+00 DEG		
"BETA "		= 0.00000E+00 DEG		
"PRATE "		= 0.00000E+00 DEG/S		
"QRATE "		= 0.00000E+00 DEG/S		
"RRATE "		= 0.00000E+00 DEG/S		
TRIM PARAMETERS:				
DEFINITION	LABEL	FLEXIBLE	RIGID	
LOAD FACTOR	"NZ "	3.09119E+03	3.09119E+03	(USER INPUT)
PITCH RATE	"QRATE "	1.56990E+01	1.56990E+01 DEG/S	(USER INPUT)
ANGLE OF ATTACK	"ALPHA "	1.53442E+00	2.34934E+00 DEG	(COMPUTED)
CONTROL SURFACE ROTATION	"ELEV "	-2.85815E+00	-2.66063E+00 DEG	(COMPUTED)
THICKNESS/CAMBER	"THKCAM "	1.00000E+00	1.00000E+00	(USER INPUT)
CONTROL SURFACE ROTATION	"AILERON "	1.00000E+00	1.00000E+00 DEG	(USER INPUT)
ROLL RATE	"PRATE "	1.12578E+02	1.30510E+02 DEG/S	(COMPUTED)
NOTE: THE TRIM RESULTS INCLUDE THE VALUES OF THE BASE STATE PARAMETERS SCALED BY THE VALUE OF THE BASE PARAMETER				

Figure 4-29 Asymmetric Trim Solution for Rectangular Wing

#### 4.2.2 Instantiation of QUADPAN-Image For Centerline Symmetric Structure and Asymmetric Analysis

As discussed in Subsection 3.3.2, QUADPAN automatically instantiates centerline symmetric geometry (about the X-Z plane) to a full tip-to-tip geometry in the cases of asymmetric analysis. This occurs in the presence of combined symmetric and antisymmetric boundary conditions. The case presented herein provides user requirements in the case of a full structural model and a half QUADPAN model (that will be instantiated to full). Figure 4-25 shows a QUADPAN geometry created from such a case. In the case of a half structural model, the ASTROS logic will perform substructuring operations on the structural and aerodynamic models (see Subsection 3.5.2) automatically as discussed in the previous.

For this case of a full structural model the ASTROS user must specify the spline for the image side of the structure in addition to the spline for the real structure. The three-dimensional transformation, SPLINE3, was used to map structure and aerodynamics in all QUADPAN related analyses. The MACROID field in the SPLINE entries requires the PANEL id from QUADPAN. To specify the image side SPLINE for QUADPAN, a negative PANEL id corresponding to the positive real side PANEL id is placed in the MACROID field of the SPLINE entry.

When QUADPAN instantiates an image side, the image element numbers are the same as the real side, and the image PANEL numbers are the negative of the real side. The ASTROS logic accommodates this input and creates spline transformations to operate on the real and image structures and the real and image QUADPAN aerodynamics.



### 4.2.3 User-Defined Loads Simulating Adaptive Structures

Figure 4-30 illustrates the use of Static Load Parameters (SPARM) in user-defined loads. The forward swept wing model is adapted as a full structural model and the QUADPAN geometrically symmetric aerodynamic model is instantiated to a full tip-to-tip model for the asymmetric steady roll analysis. Equal and opposite static forces are applied to the wing spar to cause an antisymmetric twist in the spar. In this case, the sum of the roll moment and forces about the airplane centerline are zero. The aeroelastic increment causes the airplane to roll.

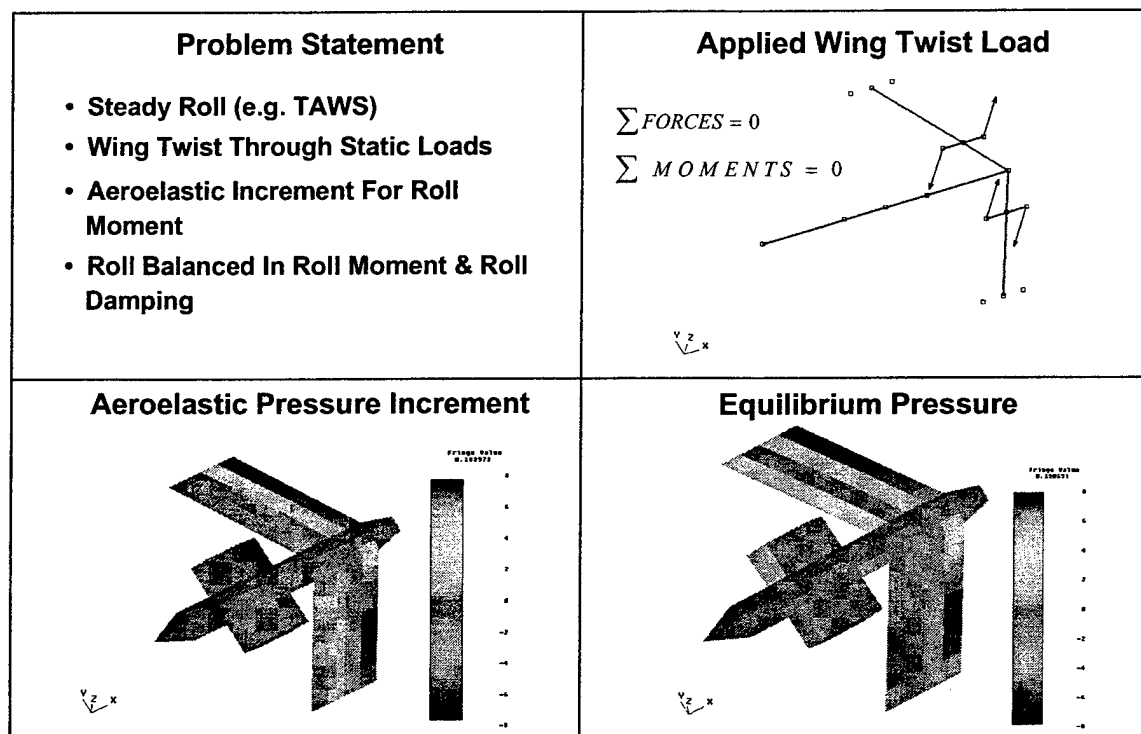


Figure 4-30 Static Load Parameters Used To Simulate Adaptive Structures

The SLPARM is described in the following cards:

SLPARM	TWIWING	1.0				ASYM	MECH	+TWIWING1
+TWIWING1	1.0	42						
FORCE	42	111	10000.	0.0	0.0	1.0		
FORCE	42	112	-10000.	0.0	0.0	1.0		
FORCE	42	1111	-10000.	0.0	0.0	1.0		
FORCE	42	1112	10000.	0.0	0.0	1.0		
TRIM	21	0.9	1200.	ROLL	980.			+TR1
+TR1	TWIWING	1.	PRATE	FREE				

Figure 4-31 Input for Torsion Actuation On FSW Wing Spar

The SLPARM card defines a user-defined parameter with the name TWIWING, a parameter magnitude of 1.0, a parameter symmetry of asymmetric, and a loadtype of Mechanical. FORCE cards are used to define the mechanical loadset. The TRIM card calls out the parameter TWIWING with a fixed input of 1.0. The PRATE solution is sought. Figure 4-32 shows the trim results. Note that the RIGID trim roll rate is 0 degrees/sec and the FLEXIBLE roll rate is almost 5 degrees/sec. The flexible roll rate is being derived from the aeroelastic increment.

TRIM RESULTS FOR TRIM SET 21 OF TYPE ROLL				
MACH NUMBER	9.00000E-01			
DYNAMIC PRESSURE	1.20000E+03			
VELOCITY	9.80000E+02			
BASE PARAMETER : "BASE "				
BASE STATE : "ALPHA "	= 0.00000E+00 DEG			
"BETA "	= 0.00000E+00 DEG			
"PRATE "	= 0.00000E+00 DEG/S			
"QRATE "	= 0.00000E+00 DEG/S			
"RRATE "	= 0.00000E+00 DEG/S			
TRIM PARAMETERS:				
DEFINITION	LABEL	FLEXIBLE	RIGID	
CONTROL SURFACE ROTATION	"TWIWING "	1.00000E+00	1.00000E+00 DEG	(USER INPUT)
ROLL RATE	"PRATE "	4.97238E+00	3.36942E-14 DEG/S	(COMPUTED)
NOTE: THE TRIM RESULTS INCLUDE THE VALUES OF THE BASE STATE PARAMETERS SCALED BY THE VALUE OF THE BASE PARAMETER				

Figure 4-32 Trim Solution for TWIWING = 1.0

#### 4.2.4 Trim Optimization With Response Parameters

The QUADPAN aerodynamic model and full structural model of the forward swept wing was used to test the functional trim optimization capability. A combined function of normal acceleration,  $N_z$ , was combined with roll rate, PRATE, to achieve a maneuver trim at both conditions simultaneously. The following trim optimization problem was posed within the new ASTROS bulk data:

Minimize: - ( $N_z + 100 \times \text{PRATE}$ )  
Subject to: Vehicle Imbalance  
Lift < 1 lb,  
Pitch < 1 in-lb  
Roll < 1 in-lb  
 $N_z$  < 10g's  
PRATE < 286 deg/sec  
Design Variables:  $N_z$ , Alpha, Elev,  
PRATE, Aileron

The necessary bulk data is shown in Figure 4-33. The TRIMOPT set ID is 29 corresponding to the TRIM set ID. The trim is set for a determinant simulation (i.e. number of FREE parameters equals the number of SUPORT degrees of freedom). The TRIMOPT card specifies that this function will be maximized, that the objective is a function, that 290 is the set ID for the function, that 101 is the set ID for the trim constraints, and that 103 is the set ID for the trim design variables. Side constraints are invoked on the trim design variables. Note that the maneuver response variables that are part of the objective function are also declared as design variables. Otherwise the objective function would be indeterminant. This problem converges to a trim solution in 30 function evaluations and 7 gradients from feasible space and in 182 function evaluations and 32 gradients from infeasible space.

```

$
$ TRIM SPECIFICATION - ASYMMETRIC BOUNDARY CONDITION
$
TRIM 29 0.9 1200. 980. +TR1
+TR1 AILERON 1. PRATE FREE ALPHA FREE ELEV FREE +TR2
+TR2 BASE 1. NZ 1.0
$
TRIMOPT 29 MAX FUNC 290 101 103
TFUNC 290 PARM NZ 1.0 +TF1
+TF1 PARM PRATE 100.
TCONTRM 101 NZ UPPER 9.0
TCONTRM 101 ALPHA UPPER 10.0
TCONTRM 101 PRATE UPPER 5.0
TCONTRM 101 PRATE LOWER -5.0
TODVPRM 103 1001 NZ -3.0 9.0 1.0
TODVPRM 103 1002 ALPHA -45.0 45.0 TRIM
TODVPRM 103 1003 ELEV -45.0 45.0 TRIM
TODVPRM 103 1004 AILERON -45.0 45.0 1.0
TODVPRM 103 1005 PRATE -5.0 5.0 TRIM

```

Figure 4-33 Input For Function Based Trim Optimization

### 4.3 VALIDATION OF AEROELASTIC TAILORING

Figure 4-34 provides an overview of an case study using data from the Validation of Aeroelastic tailoring program. This program involved wind tunnel testing of static aeroelastic models (Ref. 22). A test condition for one of the models, a washout composite tailored concept, was simulated.

- **1 DOF Trim**
  - SUPORT Fixed With SLPARM
  - Wing Root Clamped
- **3 QUADPAN Aero Models**
  - Basis Vector @  $\alpha = 0.0$  deg.,  
 $\alpha$  Inc. Vector = 1.0 deg.
  - Basis Vector @  $\alpha = 0.0$  deg.,  
☐  $\alpha$  Inc. Vector = 8.89 deg.
  - Basis Vector @  $\alpha = 8.89$  deg.,  
☐  $\alpha$  Inc. Vector = 0.0 deg.
- **Comparison to Wind Tunnel Data**

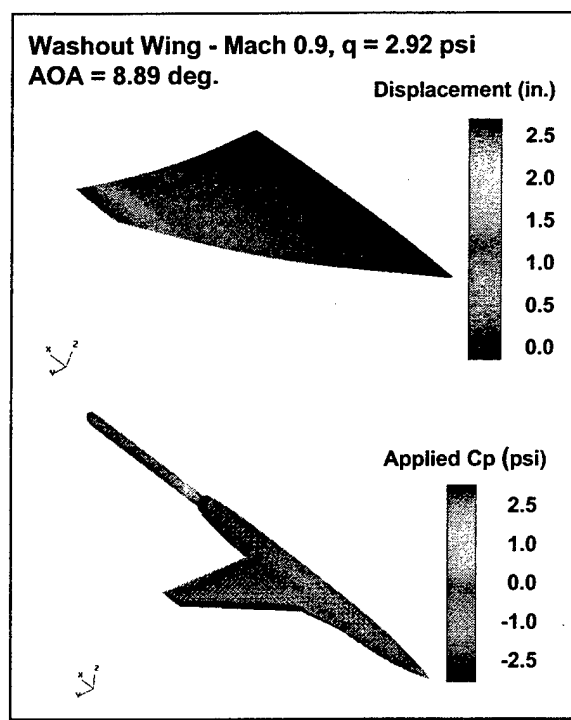


Figure 4-34 QUADPAN Used In Evaluation of Basis Vector Concept

Two new features are illustrated in this application. The user-defined load, SLPARM, capability was used to provide a fixed boundary condition at the SUPORT point. The aerodynamic basis vector concept was used to import three-dimensional aerodynamics computed at three unique reference conditions to arrive at the trim condition of  $\alpha=8.89$  degrees. The first condition evaluated used QUADPAN to derive the aerodynamic influence coefficient matrix about a reference angle  $\alpha=0.0$  degrees and an  $\alpha$  rigid pressure vector of 1.0 degrees. The second condition used QUADPAN to derive the aerodynamic influence

coefficient matrix about a reference angle  $\alpha=0.0$  degrees and an  $\alpha$  rigid pressure vector of 8.89 degrees. The third condition used QUADPAN to derive the aerodynamic influence coefficient matrix about a reference angle  $\alpha=8.89$  degrees and an  $\alpha$  rigid pressure vector of 1.0 degrees off of the reference angle or 9.89 degrees.

The structural finite element model is a "built-up" wing model with membrane, shear, and rod elements. It extends to the centerline as depicted the figure, and has 980 free degrees of freedom. The QUADPAN model was discussed in subsection 4.1.6 and consists of 1903 elements. SPLINE3 entries combined with PANLST2 entries are used to formulate the spline to 292 grids. The total solution time on a 250MHz SGI R4400 is approximately 25 CPU minutes. This time includes construction of the QUADPAN aerodynamic influence coefficient matrix and the nonsymmetric decomposition within ASTROS.

Through use of the user-defined loads capability, a fixed boundary condition can be simulated. In concept, a concentrated mass is applied at the SUPORT point. A static load (SLPARM) is applied at the SUPORT point in the desired degree of freedoms the user wishes to cancel and in the opposite direction of the acceleration that will be applied at the SUPORT point. The static load will need to cancel out the magnitude of the product of the concentrated mass and its corresponding acceleration.

The modeling for SLPARM on the VAT model for the first aerodynamic condition discussed is shown in Figure 4-35. The SPLARM entries define a symmetric control parameter using a mechanical load. The load and the size of the CONM entry are identical, and both are applied at the SUPORT point 9999. The TRIM entry includes the new parameter, WTFIX. All parameters are fixed except Nz. The normal acceleration will balance the concentrated mass and the static force because they are much larger than the applied aerodynamic loads. The Base parameter is fixed at 1.0 and Alpha is fixed at 8.9 degrees. The resulting displacement at the SUPORT point for all of the solutions was approximately  $-9 \times 10^{-6}$  inches.

SLPARM	WTFIX	1.0			SYM	MECH		+WTFIX1
+WTFIX1	1.0	42						
FORCE	42	9999	100000.	0.0	0.0	1.0		
\$								
CONM2	9999	9999	100000.					
\$								
GRID	9999	34.404	0.0	0.0		12456		
\$								
\$	*** DEFINE THE TRIM CONDITION ***							
\$								
TRIM	1	0.90	2.929	LIFT				+TR
+TR	ALPHA	8.9	WTFIX	1.0	NZ	FREE	BASE	1.0

Figure 4-35 Modeling For Fixed Boundary Condition

Figure 4-36 shows excerpts from the ASTROS run where the QUADPAN reference angle in the basis pressure vector was 8.9 degrees. The TRIM input is in the top half of the figure, while the output is in the bottom half. The TRIM input requires that the user be aware of the reference conditions in the basis vector. In this case, BASE is set to 1.0 and ALPHA is set to 0.0. The aeroelastic increment for only the BASE aerodynamic vector will be used in the final trim solution. Note that the reference condition lists the reference parameter values, and that ALPHA = 8.9 degrees. Note that in the final trim angle listing, ALPHA = 8.9 degrees. ASTROS combines the results from the linear aeroelastic trim with the reference values from the BASE vector.

```

$ *** DEFINE THE TRIM CONDITION ***
$
TRIM      1      0.90 2.929 LIFT
+TR      ALPHA 0.0 WTFIX 1.0  NZ  FREE  BASE  1.0
+TR

```

TRIM RESULTS FOR TRIM SET 1 OF TYPE LIFT

---

```

MACH NUMBER      9.00000E-01
DYNAMIC PRESSURE 2.92900E+00

```

BASE PARAMETER : "BASE "

```

BASE STATE  : "ALPHA "      = 8.90000E+00 DEG
              "BETA  "      = 0.00000E+00 DEG
              "PRATE "      = 0.00000E+00 DEG/S
              "QRATE "      = 0.00000E+00 DEG/S
              "RRATE "      = 0.00000E+00 DEG/S

```

TRIM PARAMETERS:

DEFINITION	LABEL	FLEXIBLE	RIGID	
ANGLE OF ATTACK	"ALPHA "	8.90000E+00	8.90000E+00	DEG (USER INPUT)
CONTROL SURFACE ROTATION	"WTFIX "	1.00000E+00	1.00000E+00	DEG (USER INPUT)
LOAD FACTOR	"NZ "	1.00491E+00	1.00574E+00	(COMPUTED)
BASE PARAMETER	"BASE "	1.00000E+00	1.00000E+00	(USER INPUT)

NOTE: THE TRIM RESULTS INCLUDE THE VALUES OF THE BASE STATE PARAMETERS  
 SCALED BY THE VALUE OF THE BASE PARAMETER

Figure 4-36 Modeling and Results for QUADPAN Reference = 8.9 Degrees

This example demonstrates the new feature of ASTROS performing a linear trim solution with nonlinear aerodynamic data. The solution is locally piece-wise linear incorporating the nonlinear aerodynamics at a reference condition. As discussed in subsection 3.3.1.2, the aerodynamic concepts developed under AANDE provide for eventual extension to nonlinear iterative trim analysis utilizing the concept of piece-wise linear aeroelastic trim solutions. Under this concept, a nonlinear iterative trim algorithm would use the most recent computed trim state to acquire new aerodynamic data from a populated nonlinear database and new linear aeroelastic solution would be computed. The process would continue until convergence between the aerodynamic data and the trim state.

#### 4.4 F-16 WITH QUADPAN AERODYNAMICS

Aeroelastic solutions were acquired for an F-16 simulation using the models shown in Figure 4-37. The structural model is extensively documented in Ref. 4. The centerline symmetric QUADPAN model (as it is shown) consists of 38 Panels and 3422 elements including wake elements. The total number of equations mapped is 2974. For the asymmetric solutions where the image side is instantiated, the total number of elements and equations are doubled. Aerodynamic databases were created for the QUADPAN models and imported later in aeroelastic solutions. This was accomplished by specifying BOUNDARY (no parameters needed) and SAERO in the Solution Control Packet. (Solution times for the following cases are quoted for an SGI 196MHz R10000 class machine.) The solution time is 82 CPU minutes for acquiring a symmetric aerodynamic influence coefficient matrix and 12 rigid load pressure vectors (e.g.  $P_\infty$ ,  $P_{\delta f}$ , ...). The database size is 600 Mbytes. It is believed that a tighter integration of QUADPAN into ASTROS can halve the database size. For an asymmetric aerodynamic influence coefficient matrix and 21 rigid load pressure vectors, the solution time is 540 CPU minutes. The database size is 3.2 Gbytes.

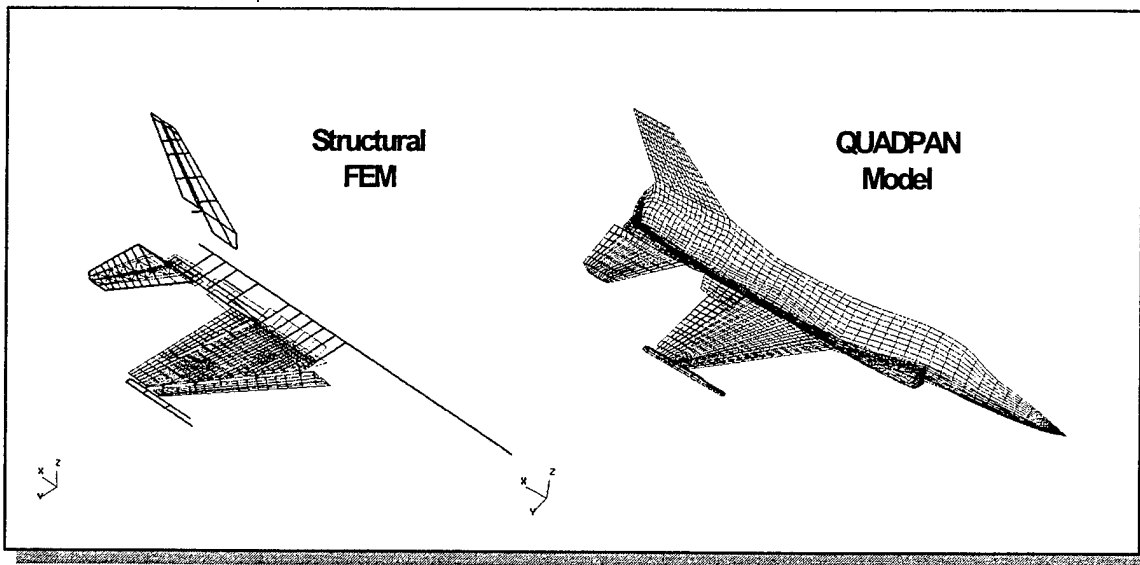


Figure 4-37 F-16 Structural and Aerodynamic Models Used in QUADPAN Based Simulations

The QUADPAN model is defined with unique PANELS for the all of the control surfaces including separate upper and lower surface PANELS. This practice is recommended to facilitate spline definition. Also, the SPLINE3 three-dimensional spline theory is limited in that it will not handle cases where a surface wraps under itself. QUADPAN will allow the user to create surfaces that wrap 360 degrees. For the purposes of these applications, the wing, elevon, and vertical tail surfaces are splined to the structure with the SPLINE3 option. The fuselage surfaces are ATTACHED with the FLEXIBLE attach option at several nodes along the fuselage. For the wing and empennage surfaces, a total of 882 structural points. This number is relatively small compared to the anticipation of splining to a built-up fuselage model (versus the stick model). The number of structural degrees of freedom in the spline influences directly the decomposition time of the aeroelastic stiffness matrix and thus the aeroelastic solution time. The user should carefully consider the number and location of points in using a three-dimensional aerodynamic theory.

The application cases presented illustrate various trim options and model assembly commands. The first application includes use of control surface scheduling to emulate the leading edge flap scheduling on the F-16. The second application illustrates the process of developing alternate rigid pressure data. The third application shows implementation and results of a five degree of freedom solution using QUADPAN aerodynamics.

#### 4.4.1 QUADPAN With Control Surface Scheduling

Redundant control surfaces are control parameters that, in total number, exceed the number of parameters required to achieve equilibrium in the course of an aircraft maneuver. For instance, in a symmetrical pull-up maneuver, two degrees of freedom, plunge and pitch, are typically satisfied by some angle of attack,  $\alpha$ , and a pitch trim surface angle,  $\delta_e$ . Given that a leading edge flap and a flaperon are available to influence  $\alpha$  and  $\delta_e$ , the total set is redundant for the symmetrical pull-up. One method of reducing the number of free surfaces to two basic parameters is to schedule the leading edge flap and flaperon to deflect in some geared ratio to one of the primary parameters. On the F-16, the leading edge flap is scheduled with angle of attack, Mach number, and altitude.

Figure 4-38 illustrates the utility of scheduling where altitude and Mach number are combined in a function of dynamic pressure. The table relates the desired deflection of the leading edge flap to ALPHA across three dynamic pressure values. The TRIM card declares the LEF as SCHD (scheduled). A

SCHEDULE card is key-named LEF and points to an AEFACT card that contains the scheduled leading flap angles (dependent values) grouped as found in columns in the table. The SCHEDULE card also refers to two other AEFACT cards that identify the independent values ALPHA and QDP.

	QDP = 500 psf	QDP = 1000 psf	QDP = 1500 psf
ALPHA = 0°	40°	25°	10°
ALPHA = 10°	35°	20°	5°
ALPHA = 20°	30°	15°	0°

The bulk data entries defining the trim and schedule would appear as :

TRIM	101	0.95	6.410			12276.0			+TR
+TR	NZ	9.0	ALPHA	FREE	FLAP	0.0	LEF	SCHD	+TR
+TR	ELEV	FREE	BASE	1.0					
SCHEDULE	101	LEF			103				+ABC
+ABC	ALPHA	105	QDP	107					
AEFACT	103	40.	35.	30.	25.	20.	15.	10.	SCH1
+CH1	5.	0.							
AEFACT	105	0.	10.	20.					
AEFACT	107	500.	1000.	1500.					

Figure 4-38 LEF Schedules As Function of ALPHA And QDP

A similar approach was used in the F-16 case, however, actual values were used in the schedule tables. The schedule algorithm assumes a scheduled value of zero for the first trim solution. Based on the first trim, the table is used to look up a scheduled value. The trim is solved again with the scheduled value, and the scheduled value is updated from the table. The process continues until the scheduled value does not need to be updated.

Figure 4-39 shows results from this application. The trim with scheduled leading edge flap was achieved in 4 iterations through the table look-up. In the printed output, the LEF parameter is denoted as SCHEDULE while the other parameters are either USER INPUT or COMPUTED. By the 4<sup>th</sup> iteration, the LEF is the correct value, and the trim parameters balance the model in equilibrium. Note that as the LEF increases in negative deflection, dumping wing load, the vehicle must go to a higher angle of attack, a to achieve enough lift for the desired 9g symmetrical pull-up.

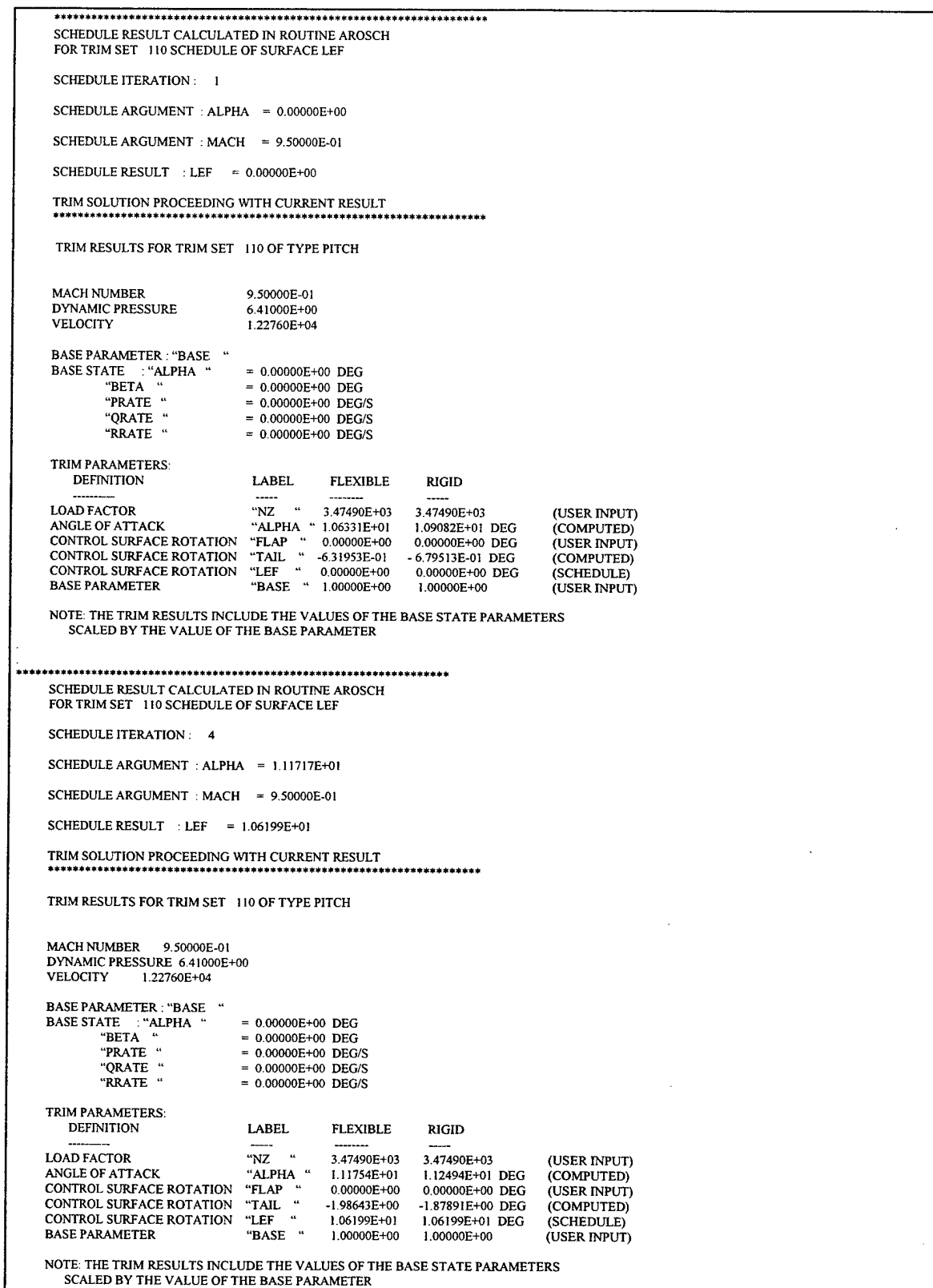


Figure 4-39 Sample Results from The F-16 QUADPAN Application



#### 4.4.2 QUADPAN Augmented With Nonlinear Aerodynamic Pressure Data

The Loads engineer acquires model inputs from many sources. With AANDE, rigid pressure data can be used from a variety of sources. In this application wind tunnel pressure data and computational fluid dynamics data were transformed to the loads aerodynamics model (a QUADPAN model) in order to use data more representative of the transonic regime. Separate aerodynamic databases were constructed, one for the wind tunnel data and one for the SplitFlow data. Both conditions were similar to the case of interest for the aeroelastic solution. A 9g pull-up at Mach 0.95 and 10K feet was simulated. An angle of attack,  $\alpha$ , close to 10 degrees with a leading edge flap deflection close to 10 degrees was desired.

A wind tunnel pressure condition from an F-16 loads pressure model test was used to create a RIGDALOD group (depicted in Figure 4-40). The test pressures were mapped to the QUADPAN model through in-house surface fit routines. A program was written to build the database. The program incorporates ASTROS modules and relations in the version 12.0 Programmer's Document (Ref. 13) and the AANDE modules and relations (Ref. 11). The program reads the pressure data and associated attributes from a flat file and creates a RIGDALOD group in a CADDDB database. The only requirement of the RIGDALOD group is that the attributes of the group be full, and that AIRFRC single-column matrix named in the RIGDALOD group and associated PARAM1 of the group be compliant with the aerodynamic model targeted for use.

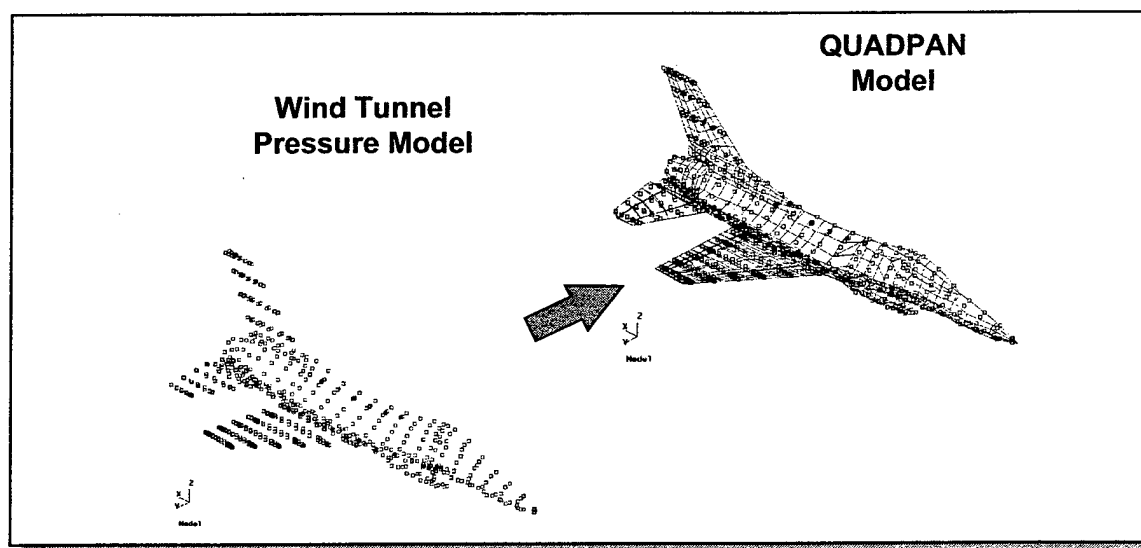


Figure 4-40 Wind Tunnel Pressures Were Transformed To The QUADPAN Model

Note that no tip missile or launcher is shown in Figure 4-40. Wind tunnel force increment data was acquired for the tip missile, and SLPARM and SCHEDULE options were used to link the tip missile force data to ALPHA in the TRIM card.

As depicted in Figure 4-41, Euler computation fluid dynamics data was acquired and fit to the QUADPAN model. A second database was created. The fit of the CFD data was much simpler than the wind tunnel data because of the grid density of the CFD model. The figure shows the facets of the CFD model since SplitFlow is an unstructured grid code. Fit of the data simply involved finding the closest match of a centroid of the triangular facets to the centroid of the QUADPAN model. The program created to transcribe the wind tunnel data was used to create a RIGDALOD group for the SplitFlow results.

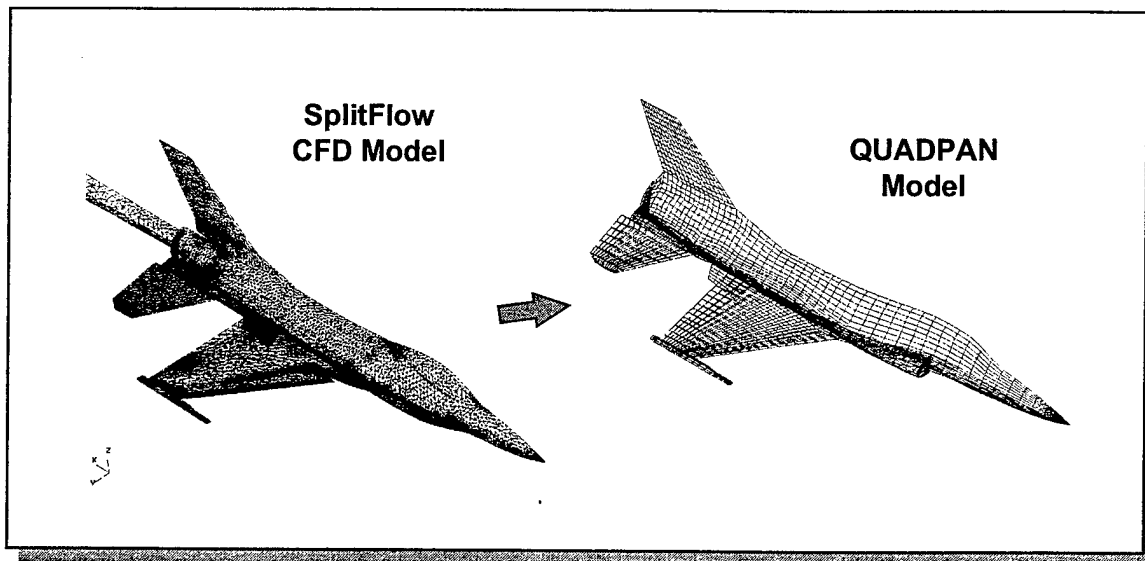


Figure 4-41 Euler Computation Fluid Dynamics Pressures Were Transformed To The QUADPAN Model

Once the RIGDALOD groups and CADDDB databases are created, MODEL ASSEMBLY commands are used to IMPORT, OVERLAY, and ASSEMBLE the aerodynamic model for aeroelastic analyses. Figure 4-42 illustrates the SOLUTION control commands to perform these tasks. As mentioned in the previous paragraphs, the wind tunnel pressure model did not include the wing tip missile pressures. The SLPARM and SCHEDULE features developed under AANDE were used to incorporate wind tunnel force data. This data is grouped in the RIGDSLOD group and declared in the MODEL RGDSLD. The figure actually shows the model assembly language for the wind tunnel case. The SAERO command is removed for the case of the CFD data overlay.

Generate Static Load  
Parameter For Tip  
Missile Forces

QUADPAN DB  
Wind Tunnel Data  
or SplitFlow CFD Data

Overlay Steady  
Aerodynamic Data

Assemble Steady  
Aerodynamic Model

Trim Solution

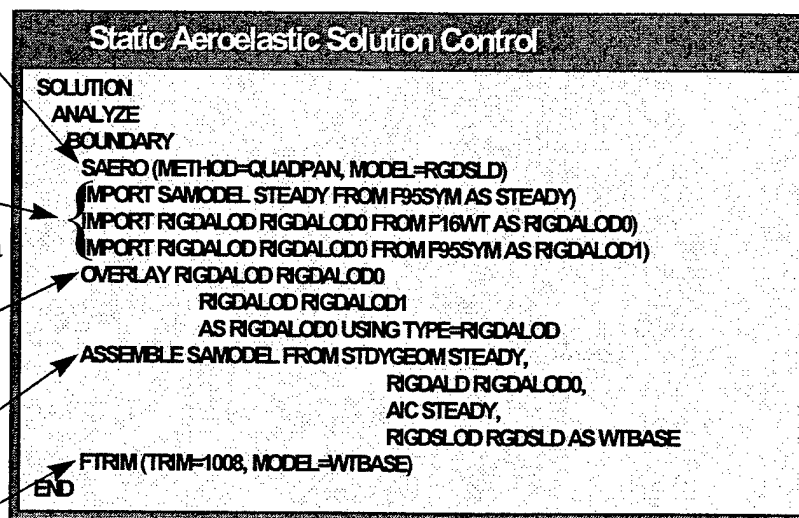


Figure 4-42 Solution Control For RIGDALOD Import

The results of the two augmented QUADPAN aeroelastic analyses are shown for comparison in figure 4-43 along side an analysis with QUADPAN linear aeroelastic analysis alone. In the top of the figure are the applied pressure data for the trim solution. The trimmed angle of attack for each of these cases range from 11.5 degrees to 14.3 degrees because of the distribution of pressure on the wing and some losses in fitting the wind tunnel data ( $\alpha=14.3$  degrees). Interestingly, the Euler case trim angle of attack was right on the production F-16 flight loads value for this condition. However, the wing tip deflection for the Euler case (shown in the bottom half of the figure) was 50% higher than the production analysis deflection. The QUADPAN and the QUADPAN+Wind Tunnel cases provided wing tip deflections very close the production analysis (as do the calculated bending moments). Noting the aerodynamic pressure in the figures, high suction loads are overpredicted by the Euler theory. It is important to model the separation effects. The linear theory misses the wing torsion, but captures the spanwise distribution as well as the wind tunnel case and better than the Euler case. *Other planforms, however, would not be so forgiving to linear methods.*

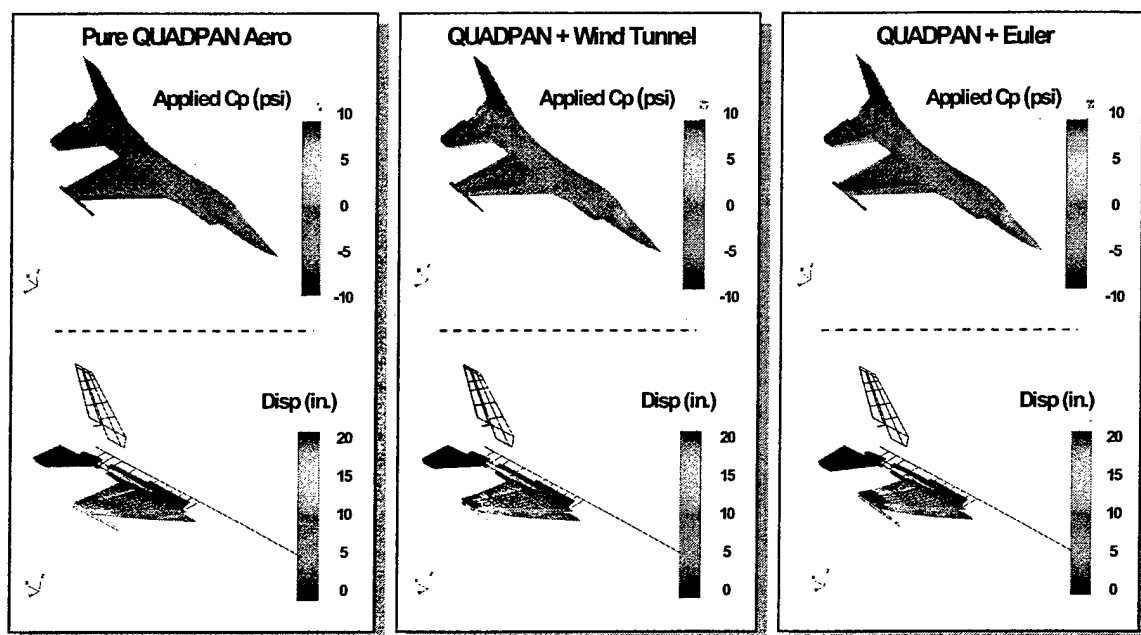


Figure 4-43 Comparison of Pure QUADPAN and Two Alternate Nonlinear Aerodynamic Cases

#### 4.4.3 QUADPAN Five Degree of Freedom Trim

Using a tip-to-tip structural finite element models and an asymmetric QUADPAN aerodynamic model, a five degree of freedom trim solution was executed in the AANDE version. The TRIM card is shown in Figure 4-44. Five accelerations are specified, four at 0.0 and  $N_z$  as  $5.86g's$ . A roll rate equivalent to about 120 degrees/sec is specified. ALPHA, AILERON, ELEVATOR, RUDDER, and BETA are the free degrees of freedom, and the leading edge flap, LEF, is scheduled.

TRIM	112	0.95	6.410			12276.0		+TR
+TR	NY	0.00	NZ	5.86	PACCEL	0.0	QACCEL	0.0+TR
+TR	RACCEL	0.0	ALPHA	FREE	AILERON	FREE	LEF	SCHD+TR
+TR	ELEVATOR	FREE	BASE	1.0	RUDDER	FREE	PRATE	2.094+TR
+TR	BETA	FREE	QRATE	0.0	RRATE	0.0		

Figure 4-44 TRIM Specification for Five Degree of Freedom Rolling Pull-Out Maneuver

Figure 4-45 displays the resulting trim conditions. The trimmed angle of attack is 7.28 degrees. The case reported in subsection 4.4.1 used the same input for scheduling, however, the trim request was for 9g's and not 5.86g's as in this case. Therefore, the final LEF deflection is less ( $\alpha=11.6$ ,  $\delta_{LEF}=10.6$  to  $\alpha=7.3$ ,  $\delta_{LEF}=4.1$ ). There is a slight yaw angle and a slight rudder reversal. The aileron deflection is antisymmetric in this case. QUADPAN can be used to develop asymmetric rigid load vectors such as a right aileron and a left aileron. It remains to the users of the AANDE enhancements to do so.

TRIM RESULTS FOR TRIM SET 112 OF TYPE					
-----					
MACH NUMBER	9.50000E-01				
DYNAMIC PRESSURE	6.41000E+00				
VELOCITY	1.22760E+04				
BASE PARAMETER :	"BASE "				
BASE STATE :	"ALPHA "	= 0.00000E+00	DEG		
	"BETA "	= 0.00000E+00	DEG		
	"PRATE "	= 0.00000E+00	DEG/S		
	"QRATE "	= 0.00000E+00	DEG/S		
	"RRATE "	= 0.00000E+00	DEG/S		
TRIM PARAMETERS:					
DEFINITION	LABEL	FLEXIBLE	RIGID		
SIDE-SLIP ACCELERATION	"NY "	0.00000E+00	0.00000E+00		(USER INPUT)
LOAD FACTOR	"NZ "	2.26255E+03	2.26255E+03		(USER INPUT)
ROLL ACCELERATION	"PACCEL "	0.00000E+00	0.00000E+00	RAD/S/S	(USER INPUT)
PITCH ACCELERATION	"QACCEL "	0.00000E+00	0.00000E+00	RAD/S/S	(USER INPUT)
YAW ACCELERATION	"RACCEL "	0.00000E+00	0.00000E+00	RAD/S/S	(USER INPUT)
ANGLE OF ATTACK	"ALPHA "	7.28123E+00	7.20878E+00	DEG	(COMPUTED)
CONTROL SURFACE ROTATION	"AILERON "	6.51333E+00	3.20970E+00	DEG	(COMPUTED)
CONTROL SURFACE ROTATION	"LEF "	4.09323E+00	4.09323E+00	DEG	(SCHEDULE)
CONTROL SURFACE ROTATION	"ELEVATOR "	-1.95517E+00	-2.06204E+00	DEG	(COMPUTED)
BASE PARAMETER	"BASE "	1.00000E+00	1.00000E+00		(USER INPUT)
CONTROL SURFACE ROTATION	"RUDDER "	2.58018E+00	3.96762E+00	DEG	(COMPUTED)
ROLL RATE	"PRATE "	1.19977E+02	1.19977E+02	DEG/S	(USER INPUT)
YAW ANGLE	"BETA "	-1.23006E+00	-1.17478E+00	DEG	(COMPUTED)
PITCH RATE	"QRATE "	0.00000E+00	0.00000E+00	DEG/S	(USER INPUT)
YAW RATE	"RRATE "	0.00000E+00	0.00000E+00	DEG/S	(USER INPUT)
NOTE: THE TRIM RESULTS INCLUDE THE VALUES OF THE BASE STATE PARAMETERS SCALED BY THE VALUE OF THE BASE PARAMETER					

Figure 4-45 Trim Results

The displacements and applied pressures for this solution are shown in Figure 4-46. Several observations are noteworthy. From the trim results in the previous figure, the deflection of the horizontal tail is almost -2 degrees, thus causing a negative load. The equilibrium elastic deflection of the tail is asymmetric as seen in Figure 4-46. While it is difficult to see in this figure, the wing deflection is also asymmetric. The applied pressures, however, can be noted on the wing as asymmetric. The QUADPAN based aeroelastic solution seems to be reasonable.

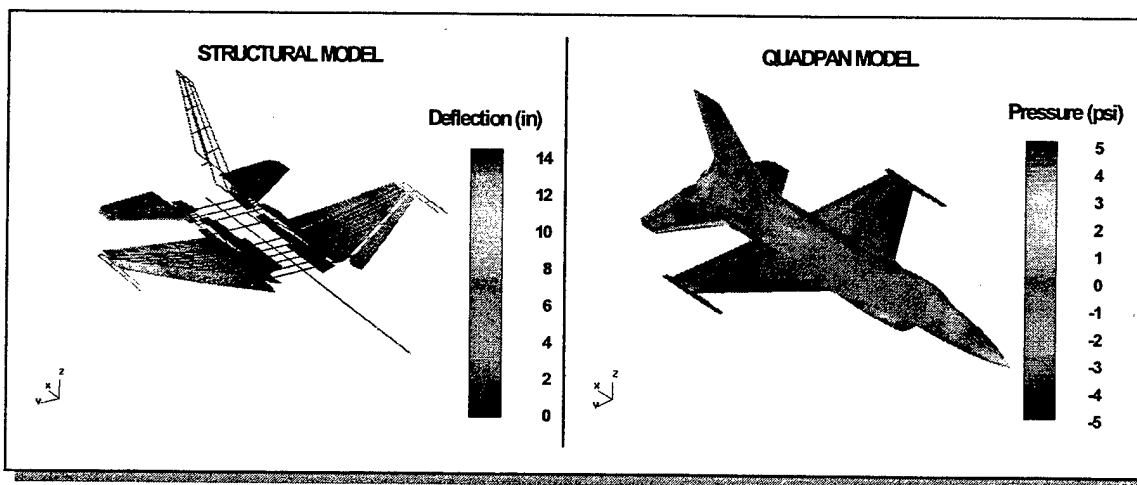


Figure 4-46 Behavioral Results for Rolling Pull-Out Case

## 4.5 DESIGN OPTIMIZATION WITH ALTERNATE LINEAR AERODYNAMICS

Design optimization runs were conducted with the centerline symmetric F-16 structural finite element model and an alternate flat panel aerodynamics model using the Carmichael code (Ref. 21). Using the program mentioned in subsection 4.4.2, an alternate aerodynamic database was created housing pressure data, aerodynamic influence coefficient data, and geometry in the AIC, RIGDALOD, and STDYGEOM groups accordingly. Figure 4-47 illustrates the data and models utilized in these optimization runs. The aerodynamics model includes 395 elements and provides symmetric and antisymmetric data. The design model for the runs is described thoroughly in Ref. 4.

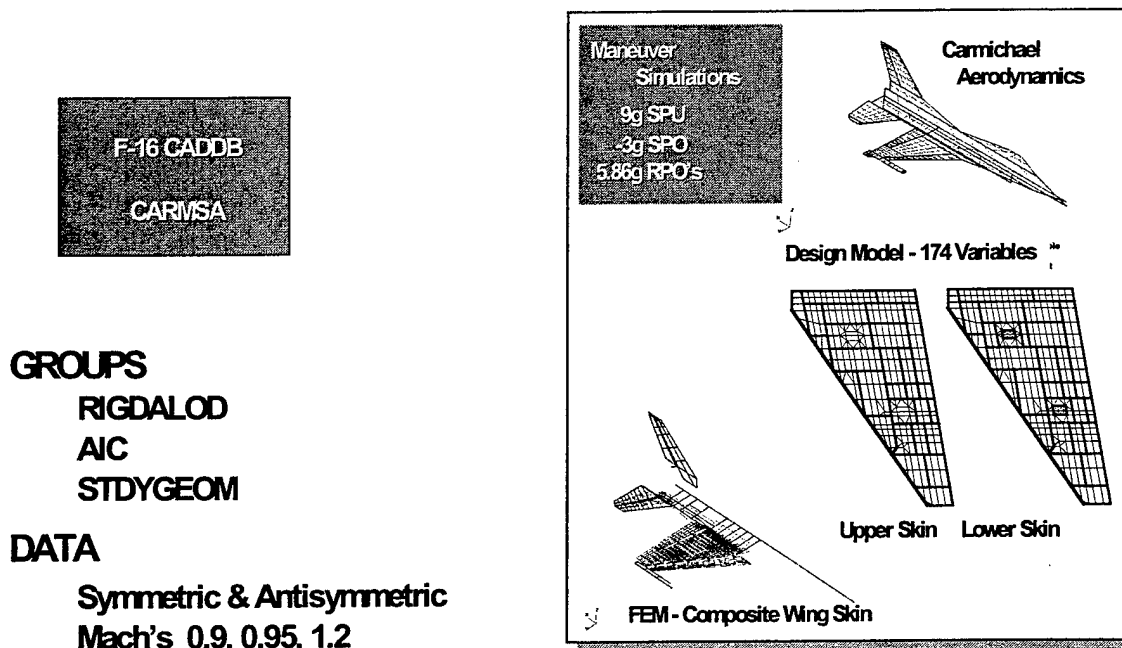


Figure 4-47 Design Optimization Studies Performed With Alternate Linear Aerodynamics Data

Four maneuver simulations were selected for the runs. Subsonic and a supersonic 5.86g rolling pull-out maneuvers were simulated in 3 degree of freedom trims. A subsonic 9g symmetric pull-up and a -3g push-over were also simulated. Figure 4-48 shows the solution control, and the extent of this alternate aerodynamic database. Three aerodynamic models resided in this database (SAMODEL000, SAMODEL001, SAMODEL002). Each model happened to have the same geometry, however, the geometry for each could have been unique. Each model had symmetric and antisymmetric aerodynamic influence coefficient matrices. SAMODEL002 was IMPORTed once and used in multiple BOUNDARY conditions. The asymmetric solutions invoked substructuring automatically.

3 Aerodynamic Models  
1 Database (CARMSA)

Asymmetry Infers  
Substructuring

1 Model Contains  
Symmetric &  
Antisymmetric  
Aerodynamic Data

```

Static Aeroelastic Solution Control

SOLUTION
OPTIMIZE
BOUNDARY SPC=109, MPC=999, SUPORT=1009, RELESID=345
IMPORT SAMODEL SAMODEL001 FROM CARMSA AS ALTAERO
FTRIM ASYM (TRIM=110, MODEL=ALTAERO)
LABEL=ASYMMETRIC RPO, M=0.95, 10K, 5.86g
PRINT TRIM, DISP=ALL
BOUNDARY SPC=109, MPC=999, SUPORT=1009, RELESID=345
IMPORT SAMODEL SAMODEL002 FROM CARMSA AS ALTAER1
FTRIM ASYM (TRIM=112, MODEL=ALTAER1)
PRINT TRIM, DISP=ALL
LABEL=ASYMMETRIC RPO, M=1.2, SL, 5.86g
BOUNDARY SPC=107, MPC=999, SUPORT=1007, RELESID=345
FTRIM ASYM (TRIM=111, MODEL=ALTAER1)
LABEL=SPO, M=1.2, SL, -3.0g
PRINT TRIM, DISP=ALL
BOUNDARY SPC=107, MPC=999, SUPORT=1007, RELESID=345
IMPORT SAMODEL SAMODEL000 FROM CARMSA AS ALTAER3
FTRIM ASYM (TRIM=113, MODEL=ALTAER3)
LABEL=SPU, M=0.9, SL, 9.0g
PRINT TRIM, DISP=ALL
END

```

Figure 4-48 Solution Control With Alternate Aerodynamic Database

One design optimization run was completed satisfactorily with this model and aeroelastic simulation. The run consisted of a strength optimization. The strength constraints were composite fiber strains over the wing box skin (Ref 4). Figure 4-49 shows the convergence of this run.

A design optimization with trim optimization in the structural optimization loop was attempted but not completed at the time of this documentation. However, the problem set-up is described herein to provide intent of the capability. Figure 4-50 shows the cards necessary for subsonic rolling pull-out problem. The TRIMOPT card has a set ID that matches the TRIM ID in the SOLUTION Control. A function is called out to be minimized. The function points to a TFUNC card where a simple sum of the real and image side BMST named WROOT is defined. The negative sign on the component 4 in the second line of the TFUNC designates that the image of the substructure is used. A positive sign designates that the real side is used. The TRIMOPT card points to the design variables of the trim optimization, TODVPRM. Note also that trim constraints, TCONTRM, are pointed to in TRIMOPT for the trim parameters ALPHA, FLAP, LEF, and TAIL\_S. Also, hinge moment constraints are also defined for the BMST components named FLAP and LEF. These components are defined in BMST cards (not shown) like WROOT. In the TCONBMST, the 4 refers to the local coordinate system defined on the BMST card and not to the traditional Basic coordinate system.

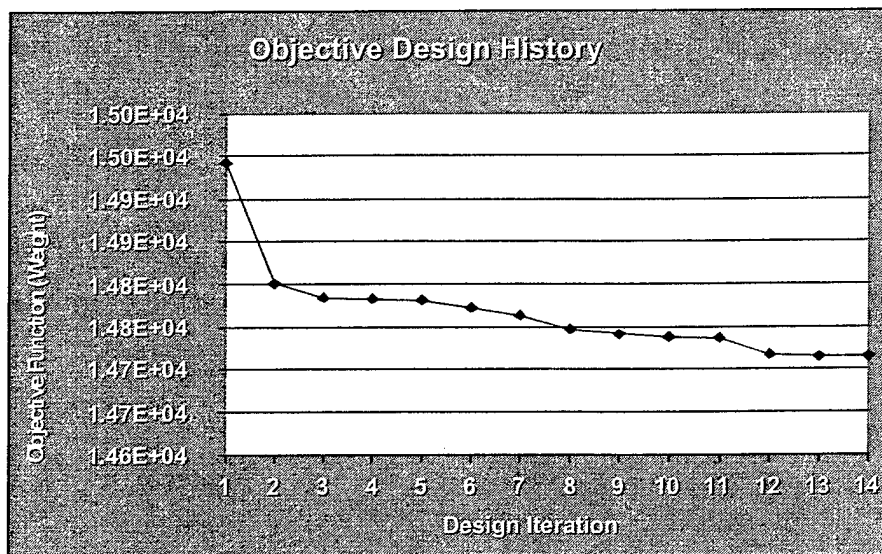


Figure 4-49 Weight History For Strength Optimization

```

$
$ TRIMOPT for TRIM CASE 110 Mach 0.95 RPO
$
TRIMOPT 110 MIN FUNC 101 101 103 +TOPT
+TOPT
TCONTRM 101 ALPHA UPPER 30.0
TCONTRM 101 ALPHA LOWER -10.0
TCONTRM 101 FLAP UPPER 30.0
TCONTRM 101 FLAP LOWER -30.0
TCONTRM 101 LEF UPPER 5.0
TCONTRM 101 LEF LOWER -30.0
TCONTRM 101 TAIL S UPPER 30.0
TCONTRM 101 TAIL S LOWER -30.0
TODVPRM 103 1002 ALPHA -45.0 45.0 TRIM
TODVPRM 103 1003 FLAP -45.0 45.0 0.0
TODVPRM 103 1004 LEF -45.0 5.0 -25.
TODVPRM 103 1005 TAIL S -45.0 45.0 TRIM
TODVPRM 103 1006 AILERON -45.0 45.0 TRIM
$
TFUNC 101 BMST WROOT 4 1.0 +BMST
+BMST BMST WROOT -4 1.0
BMST WROOT 2077 501 503
TCONBMST 101 FLAP 4 UPPER 1.9E05
TCONBMST 101 FLAP 4 LOWER -1.9E05
TCONBMST 101 LEF 4 UPPER 3.0E05
TCONBMST 101 LEF 4 LOWER -3.0E05
$

```

Figure 4-50 Problem Set-Up For Trim Optimization With BMST Constraints

## 5. REFERENCES

1. Johnson, E.H. and Venkayya, V.B. "Automated Structural Optimization System (ASTROS), Theoretical Manual, "AFWAL-TR-88-3028, Vol. 1 December 1988.
2. Love, M.H., "Software Design Document for The Aerodynamic Analysis for the Design Environment," FZM 8399, 17 June 1996.
3. Barker and M.H. Love, "An ASTROS Application With Path Dependent Results," Proceedings of the AIAA/USAF /NASA/ISSMO Multidisciplinary Analysis and Optimization, September 4-6, 1996.
4. Love, M.H., Barker, D.K., and Bohlmann, J.D, "An Aircraft Design Application Using ASTROS," WL-TR-93-3037, June 1993.
5. Bohlmann, J.D, Love, M.H., Barker, D.K., Rogers, W.A., and Paul, B.K., "Application of Analytical and Design Tools for Fighter Wing Aeroelastic Tailoring," AGARD Printed Report 784, Integrated Design Analysis and Optimisation of Aircraft Structures, Feb. 1992.
6. Striz, A.G. and Lee, W.T., "Multidisciplinary Optimization of a Transport Aircraft Wing," Paper No. 94-4410-CP, Proceedings of the AIAA/USAF /NASA/ISSMO Multidisciplinary Analysis and Optimization, September 7-9, 1994.
7. Yurkovich, R., "Optimum Wing Shape for an Active Aeroelastic Wing," Proceedings of 36th AIAA/ASME/ASCE/AHS/ASC Structures, Structural Dynamics, and Materials Conference, April 10-13, 1995.
8. Volk, J. and Ausman, J., "Integration of a Generic Flight Control System into ASTROS," AIAA Paper No. 96-1335, Proceedings of 36th AIAA/ASME /ASCE/AHS/ASC Structures, Structural Dynamics, and Materials Conference, April 15-17, 1996.
9. Youngren, H.H., et al., "Quadrilateral Element Panel Method (QUADPAN)," User's Manual, Lockheed Report LR 29671, July 1983.
10. Strang, W.Z., et al., "Evaluation of Four Aerodynamic Prediction Methods (MCAERO, Pan Air, Quadpan, and VSAERO), AIAA Paper No. 85-4092, AIAA 3rd Applied Aerodynamics Conference, October 14-16, 1985.
11. Love, M.H., "Aerodynamic Analysis for the Design Environment Programmer's Document," FZM-8537, 24 July 1998.
12. Love, M.H., "Aerodynamic Analysis for the Design Environment User's Document," FZM-8538, 24 July 1998.
13. Neill, D.J., Herendeen, D.L., Venkayya, V.B., "ASTROS Enhancements, Volume II - ASTROS Programmer's Manual," WL-TR-95-3006, May 1995. Lamb, H., Hydrodynamics, Cambridge University Press, 1932.
14. Lamb, H., Hydrodynamics, Cambridge University Press, 1932.
15. Coopersmith, R.M., Quadrilateral Panel Method (QUADPAN) For Aerodynamics Theoretical Documentation, LASC Report No. LG 90ER0072.
16. Coopersmith, R.M., Computation of Aerodynamic Influence Coefficients (AIC) Matrix for QUADPAN Panel Method (QUADPAN), January 1990, LR 31744.
17. Harder, R. L. and Desmarais, R. N., "Interpolation Using Surface Splines," *Journal of Aircraft*, Vol. 9, No. 2, 1972, pp. 189-191.
18. Neill, D.J., Herendeen, D.L., Venkayya, V.B., "ASTROS Enhancements, Volume III - ASTROS Theoretical Manual," WL-TR-95-3006, May 1995.



19. Lynch, R.W., Rogers, W.A., and Braymen, W.W., "Aeroelastic Tailoring of Advanced Composite Structures for Military Aircraft," AFFDL-TR-76-100, April 1977.
20. Miranda, L.R., Elliott, R.D., and Baker, W.M., A Generalized Vortex Lattice Method for Subsonic and Supersonic Flow Applications, NASA CR-2865, December 1977.
21. Carmichael, R.L., Castellano, C.R., and Chen, F.C., "The Use of Finite Element Methods for Predicting the Aerodynamics of Wing-Body Combinations", Symposium on Analytical Methods in Aircraft Aerodynamics, Ames Research Center, NASA SP-228, October 1969.
22. Adler, C.O., and Dixon, C.J, High Angle of Attack Stability and Control - Prediction Methods and Code, Air Force Report, WL-TR-92-3050, October 1992.
23. Rogers, W.A., Braymen, W.W., Murphy, A.C., Graham, D.C. and Love, M.H.. "Validation of Aeroelastic Tailoring by Static Aeroelastic and Flutter Tests - Volumes I-V," AFFDL-TR-81-3160, September 1982.
24. Johnson, E.H. and Neill, D.J., Automated Structural Optimization System (ASTROS), Volume III - Applications Manual, December 1988, AFWAL-TR-88-3028.